Universidad Autónoma de Madrid

Facultad de Ciencias

Departamento de Química Orgánica

SENSORES SÓLIDOS FLUORESCENTES OBTENIDOS POR FUNCIONALIZACIÓN CON DERIVADOS DE 1,8-NAFTALIMIDA DE COPOLÍMEROS DE ETILENO-ACRILATO DE BUTILO Y DE MEMBRANAS ACRÍLICAS FOTOENTRECRUZADAS

Sabela Fernández Alonso

Consejo Superior de Investigaciones Científicas

Instituto de Ciencia y Tecnología de Polímeros

Departamento de Química Macromolecular Aplicada

Grupo de Fotoquímica de Polímeros

Madrid, 2018

TESIS DOCTORAL

SENSORES SÓLIDOS FLUORESCENTES OBTENIDOS POR FUNCIONALIZACIÓN CON DERIVADOS DE 1,8-NAFTALIMIDA DE COPOLÍMEROS DE ETILENO-ACRILATO DE BUTILO Y DE MEMBRANAS ACRÍLICAS FOTOENTRECRUZADAS

SABELA FERNÁNDEZ ALONSO

Directores:

Dr. Fernando Catalina Lapuente (CSIC)

Dra. Teresa Corrales Viscasillas (CSIC)

La presente Tesis Doctoral, titulada "SENSORES SÓLIDOS FLUORESCENTES OBTENIDOS POR FUNCIONALIZACIÓN CON DERIVADOS DE 1,8-NAFTALIMIDA DE COPOLÍMEROS DE ETILENO-ACRILATO DE BUTILO Y DE MEMBRANAS ACRÍLICAS FOTOENTRECRUZADAS", ha sido llevada a cabo en el Departamento de Química Macromolecular Aplicada del Instituto de Ciencia y Tecnología de Polímeros del Consejo Superior de Investigaciones Científicas (CSIC), bajo la dirección del Doctor Fernando Catalina Lapuente y de la Doctora Teresa Corrales Viscasillas, para optar al grado de Doctor en Química.

La financiación de este trabajo de investigación ha sido aportada por el Ministerio de Economía, Industria y Competitividad (MINECO): beca de Formación de Personal Investigador (FPI) BES-2013-066624 asociada al Proyecto de Investigación MAT2012-31709.

De acuerdo con el informe correspondiente autorizado por los Directores de Tesis y el Órgano Responsable del Programa de Doctorado, se presenta como un compendio de tres trabajos previamente publicados. La contribución de la autora ha sido uniforme en las tres publicaciones y ha consistido en la realización de la parte experimental: síntesis y caracterización de todos los compuestos, preparación, tratamiento y caracterización de los nuevos materiales sintetizados, estudio de sus propiedades fotofísicas y superficiales. Las referencias completas de los artículos que constituyen el Trabajo de la Tesis son las siguientes:

- S. Fernández-Alonso, T. Corrales, J. L. Pablos, F. Catalina, "Surface modification of poly(ethylene-butyl acrylate) copolymers by microwave methodology and functionalization with 4-dimethylamino-N-(2-hydroxyethyl)-1,8-naphthalimide for acidity sensing", Reactive and Functional Polymers 107 (2016) 78-86. Índice de impacto: 3.151.

- S. Fernández-Alonso, T. Corrales, J. L. Pablos, F. Catalina, "Solid fluorescence sensors obtained by functionalization of photocrosslinked water-swollen acrylic membranes with 4-piperazine naphthalimide derivatives", Polymer 124 (2017) 139-150. Índice de impacto: 3.684.

- S. Fernández-Alonso, T. Corrales, J. L. Pablos, F. Catalina, "A Switchable fluorescence solid sensor for Hg^{2+} detection in aqueous media based in a photocrosslinked membrane functionalized with (benzimidazolyl)methyl-piperazine derivative of 1,8-naphthalimide" Sensors and Actuators: B. Chemical 270 (2018) 256-262. Índice de impacto: 5.401.

“Hay una fuerza motriz más poderosa que el vapor, la electricidad y la energía atómica: la voluntad”

Albert Einstein

AGRADECIMIENTOS

Son muchas las personas que me han apoyado durante la realización de esta Tesis, y a todas ellas les quiero expresar mi más sincero y profundo agradecimiento.

En primer lugar, a mis directores de Tesis, el Dr. Fernando Catalina y la Dra. Teresa Corrales, por vuestra completa dedicación e inestimable ayuda, por vuestro apoyo, por guiarme en el mundo de la investigación, por el trabajo en equipo y las muchas horas de reuniones.

A Jesús, sin duda un pilar fundamental en esta Tesis. Gracias por estar ahí, por tu apoyo constante y por compartir conmigo tus conocimientos y experiencias, y sobre todo por tu actitud siempre positiva y hacer todo un poco más fácil.

A mis compañeros de laboratorio, Levi y Sandra, por su compañía y ayuda. A Andrés, por la buena amistad que hemos entablado y por los buenos momentos compartidos, aunque su paso por el laboratorio haya sido breve. A Carmela y Enrique, por hacer más amenos los días de trabajo y más entretenidas las comidas.

A mis compañeros de otros laboratorios, los Albertos, Marta, Rosa, Albanelly, Francisco, Valentina, Alicia, Fabio, Patricia, gracias por vuestra ayuda siempre que la he necesitado, por los cafés y por los momentos de diversión.

A la Dra. Paula Bosch, por sus consejos y ayuda.

A todo el equipo de caracterización del ICTP por su enorme dedicación, y al grupo de resonancia, en especial a la Dra. Elisa García, gracias por compartir tus conocimientos conmigo y estar siempre dispuesta a ayudarme.

A todos mis amigos del máster y de la facultad.

A mis amigos de Galicia. Gracias por vuestro apoyo, por arroparme, por hacerme reír, por las experiencias vividas. Gracias por comprender mis ausencias.

A toda a miña familia, por crer en min.

A Juanjo, por estar sempre o meu lado, porque estes anos pasaron tanto por él como por min. Por ser o meu compañeiro de viaxe.

GLOSARIO DE ABREVIATURAS

Abs	Absorbancia
A_0	Absorbancia inicial
AFM	Microscopía de fuerza atómica
BA	Acrilato de butilo
CA	Ángulo de contacto
CRS	Espectroscopía Raman Confocal
γ	Energía superficial
γ^d	Componente dispersiva de la energía superficial
γ^p	Componente polar de la energía superficial
DMAN	4-dimetilamino-N-(2-hidroxietil)-1,8-naphtalimida
DSC	Calorimetría diferencial de barrido
$\Delta\nu$	Desplazamiento de Stokes
EBA	Copolímero de etileno-acrilato de butilo
EBA-DMAN	Copolímero EBA funcionalizado con derivado de DMAN
EBA-pl-DMAN	Copolímero EBA funcionalizado con derivado de DMAN tratado con plasma
EGDMMA	Dimetacrilato de etilenglicol
$E_T(30)$	Parámetro de polaridad de disolvente
ε	Coeficiente de extinción molar
F_{50}	Resistencia al impacto
FE	Factor de aumento de la fluorescencia
HDPE	Polietileno de alta densidad
Hg-MBZN	Complejo formado por el mercurio y MBZN
HOMO	Orbital molecular ocupado de más alta energía
ICT	Transferencia de carga intramolecular
I_F	Intensidad de fluorescencia
I_{F0}	Intensidad de fluorescencia inicial
I2959	Irgacure 2959
LDPE	Polietileno de baja densidad
LLDPE	Polietileno lineal de baja densidad
LOD	Límites de detección
LUMO	Orbital molecular no ocupado de más baja energía
λ	Longitud de onda
MACl	Cloruro de metacriloilo
MBZN	N-(2-hidroxietil)-4-(4-(1H-benzo[d]imidazol-2-il)metil)piperazina-1-il)-1,8-naftalimida
M-MBZN	Membrana funcionalizada con derivado de MBZN
MCl	Membrana con sustituyente cloruro de ácido
PE	Polietileno
PP	Polipropileno
PET	Transferencia electrónica fotoinducida
pK_a	Constante de acidez
pK_a*	Constante de acidez en el estado excitado
ϕ_F	Rendimiento cuántico de fluorescencia
R_a	Rugosidad media
SD	Grado de hinchamiento
TGA	Análisis termogravimétrico
TGA-MS	Análisis termogravimétrico acoplado a masas
T_g	Temperatura de transición vítrea
T_m	Temperatura de fusión
T_5	Temperatura a la que se produce el 5% de pérdida de peso

T_{10}	Temperatura a la que se produce el 10% de pérdida de peso
VP	Vinilpirrolidona
W_d	Peso de membrana en seco
W_s	Peso de membrana en mojado
X_{Hg2+}	Fracción molar de mercurio
X_{MBZN}	Fracción molar de MBZN

RESUMEN

La detección y cuantificación de especies químicas o analitos son algunos de los desafíos clave en la investigación química, especialmente en el área medioambiental, donde la detección de contaminantes mediante técnicas sencillas, rápidas y económicas siempre ha sido de gran importancia.

Si bien las técnicas analíticas tradicionales permiten la detección y cuantificación selectiva y precisa de las especies químicas, estas técnicas consumen mucho tiempo, y además requieren equipos sofisticados y costosos. Como alternativa de gran interés, los sensores químicos, en particular los sensores fluorescentes, han adquirido gran popularidad en los últimos años.

Para que las aplicaciones prácticas del sensor sean óptimas surge la necesidad de incorporarlo a un soporte sólido. Los materiales polímeros reúnen una serie de características que hacen que sean adecuados para ser empleados como soportes sólidos de las moléculas sensores.

La modificación química o física de polímeros constituye en la actualidad un campo de investigación de enorme importancia para obtener nuevos materiales y que presenta un gran interés desde el punto de vista tecnológico y económico. La modificación y funcionalización de polímeros es una vía alternativa a la síntesis directa que permite obtener polímeros para aplicaciones específicas.

El objetivo de la presente Tesis Doctoral ha sido la preparación de nuevos materiales poliméricos de alto valor añadido como sensores sólidos fluorescentes. Para ello se han empleado dos metodologías. En el Capítulo 2, se ha llevado a cabo la modificación superficial del copolímero de etileno-acrilato de butilo (EBA) a través de una secuencia de reacciones en fase heterogénea mediante radiación microondas. El sustrato modificado contiene grupos reactivos para su posterior funcionalización. En los Capítulos 3 y 4, se han preparado hidrogeles por fotopolimerización-fotoentrecruzamiento con características de hinchamiento en agua controladas (30%) y también portadores de grupos reactivos.

Se ha sintetizado una serie de sensores fluorescentes basados en derivados de 1,8-naftalimidas portadores de grupos adecuados para la reacción con los sustratos poliméricos. Estos derivados se han sintetizado mediante radiación microondas, obteniéndose mejores rendimientos y a tiempos de reacción más cortos, en comparación con la metodología de calentamiento convencional.

A continuación se procedió a la funcionalización de los polímeros reactivos en estado sólido con los derivados de 1,8-naftalimida, obteniéndose materiales de buenas propiedades ópticas y mecánicas.

El material funcionalizado EBA, ha sido tratado con plasma de oxígeno para mejorar sus propiedades de hidrofilia y conseguir así un comportamiento adecuado en medios acuosos.

Los sensores sólidos fluorescentes se estudiaron en medios acuosos y se caracterizaron de forma comparativa con respecto a los fluoróforos libres en disolución. Se han obtenido así sensores sólidos

reversibles de pH (en superficie y en bloque) y un sensor de coordinación, también reversible, para la detección de mercurio en agua.

ÍNDICE

OBJETIVOS

El objetivo de la presente Tesis Doctoral es la preparación de nuevos materiales poliméricos de alto valor añadido para su aplicación como sensores fluorescentes sólidos, a partir de copolímeros de etileno-acrilato de butilo (EBA) comerciales y de membranas hidrofílicas fotoentrecruzadas sintetizadas en este Trabajo.

Para ello se plantean como objetivos concretos:

- Modificación estructural o de superficie de polímeros y formulaciones, mediante las técnicas de Radiación Microondas, y Tratamiento con Plasma de Radiofrecuencia.

- Síntesis y caracterización de nuevas estructuras de fluoróforos derivadas de la 1,8-naftalimida con sustituyentes adecuados para la funcionalización.

- Estudio fotofísico de los fluoróforos en disolución en diferentes medios.

- Obtención de polímeros sensores con posibilidades de aplicación para la detección y/o seguimiento reversible por fluorescencia de ácidos, metales, contaminantes, etc.

En definitiva, con los objetivos propuestos se pretende el desarrollo de nuevos materiales con propiedades avanzadas de interés medioambiental.

CAPÍTULO 1

Introducción.

1 Introducción

1.1 Modificación de polímeros

La modificación química o física de polímeros constituye en la actualidad una vía alternativa a la síntesis directa para obtener nuevos polímeros y presenta una alta viabilidad desde el punto de vista tecnológico y económico. Se ha hecho un gran esfuerzo en llevar a cabo las reacciones de modificación de polímeros en condiciones respetuosas con el medio ambiente, por ejemplo libres de disolventes como es el caso de las reacciones en estado fundido o en condiciones suaves como son las reacciones en fase heterogénea que se realizan a baja temperatura. Sin embargo, el área de la modificación de polímeros es mucho más amplia que estas reacciones mencionadas y puede realizarse en forma superficial o en el polímero en bloque tanto en fundido como en disolución[1].

La reacción de modificación de polímeros más difundida y clásica es la de entrecruzamiento o vulcanización con la que se transforma un material a veces inservible en uno con propiedades excelentes. Con las reacciones de entrecruzamiento de polímeros se consiguen materiales con propiedades importantes como son la estabilidad dimensional, la resistencia al calor y a disolventes, así como una mejora drástica en las propiedades mecánicas. Actualmente, la modificación de polímeros representa un área de investigación muy activa y que se orienta a transformaciones muy diversas como pueden ser reacciones de polimerización, funcionalización por injerto, obtención de copolímeros, degradaciones controladas, etc. En todos los procesos de modificación de polímeros el objetivo es conseguir dotar al material inicial de propiedades específicas y de alto valor añadido. Pueden mencionarse como áreas de especial relevancia dentro de la modificación de polímeros la obtención de nuevos materiales para aplicaciones biomédicas y farmacéuticas, también polímeros con procesabilidad o reciclabilidad mejorada, de estructura controlada con funcionalidades superficiales, terminales de cadena o en bloque, siempre con el objetivo de obtener materiales con propiedades avanzadas.

Se puede clasificar en dos grandes grupos la funcionalización de los materiales poliméricos:

- Funcionalización química en bloque (en disolución, en fase heterogénea y en fundido) o en superficie (en estado sólido). Las reacciones de funcionalización se pueden llevar a cabo durante el proceso de polimerización si uno de los monómeros que interviene está funcionalizado (polimerización directa). En ocasiones la funcionalización directa no es posible debido a que cierta funcionalidad puede interferir en la polimerización. En este caso, la funcionalización post-polimerización es un método preferible y ampliamente utilizado, donde el copolímero es portador de un comonómero que contiene grupos reactivos para la

[1] S. Mane, "Functional polymers: a review" Can. Chem. Trans. 4 (2016) 316-327.

funcionalización. Cuando es difícil obtener el material deseado por cualquiera de los dos métodos anteriores, se recurre a la funcionalización mediante reacciones de injerto.

- Funcionalización empleando tratamientos físicos, generalmente en superficie. Entre estos tratamientos cabe destacar plasma, radiación-γ, UV, ionización a la llama y corona, haces de electrones. Después del tratamiento físico puede tener lugar una funcionalización covalente o no covalente (adsorción).

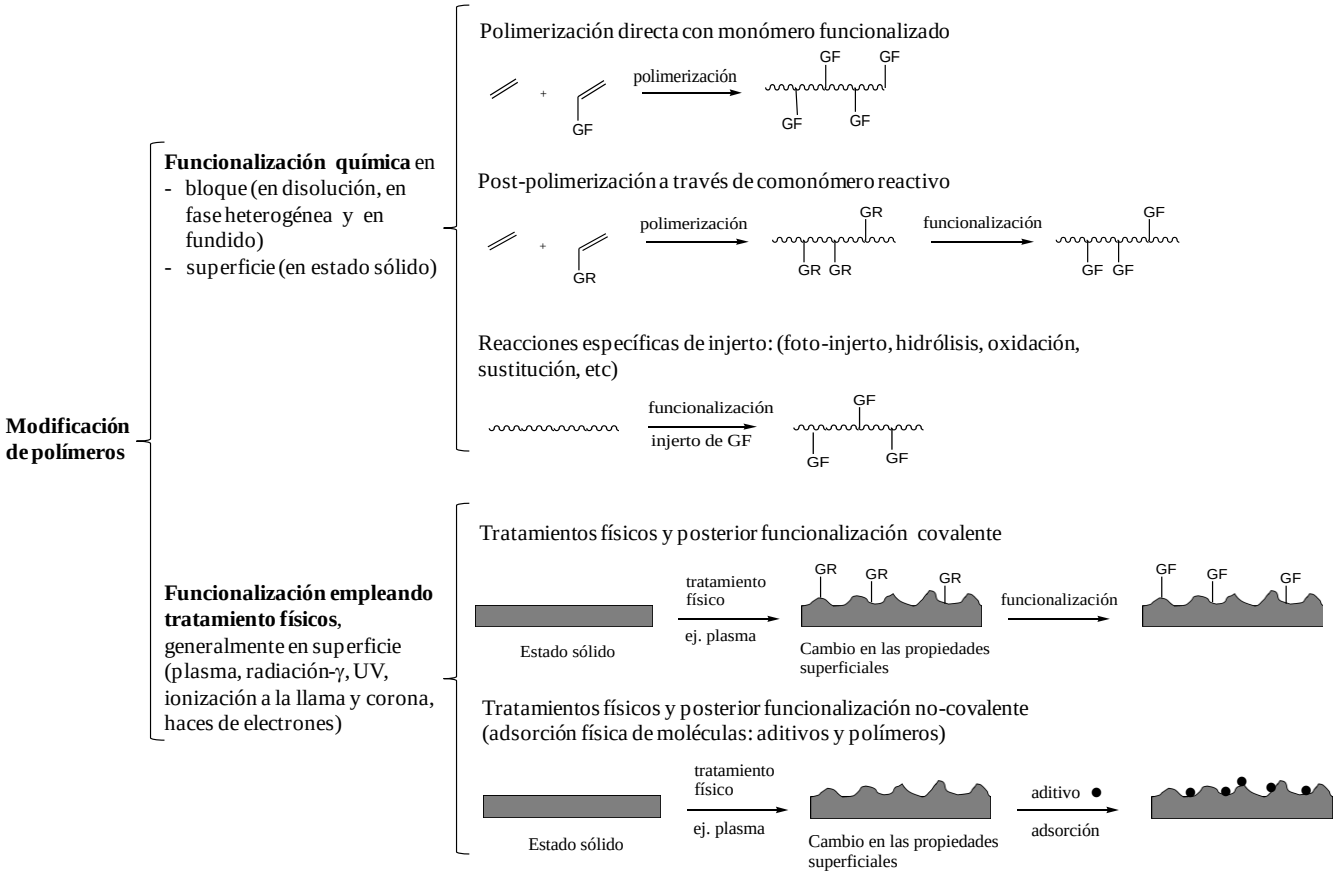

Figura 1. Esquema general de las diferentes vías de funcionalización de polímeros.
(GR–grupo reactivo, GF–grupo funcional)

En este Trabajo, se ha llevado a cabo la modificación superficial del copolímero comercial de etileno-acrilato de butilo (EBA) con una sonda fluorescente derivada de la naftalimida mediante la realización de una secuencia de reacciones químicas y posterior tratamiento con plasma para mejorar sus propiedades en medios acuosos. Este trabajo ha dado lugar a la primera publicación. En la segunda y

tercera publicaciones se han sintetizado membranas poliméricas fotoentrecruzadas a partir de una combinación de monómeros, hidrófilo, hidrófobo y difuncional, que incluye además un comonómero reactivo que permite la posterior funcionalización. En estos dos trabajos de la presente Tesis las membranas fotoentrecruzadas se han funcionalizado con nuevas sondas fluorescentes derivadas de 1,8-naftalimidas previamente sintetizadas. La síntesis de los derivados de naftalimida ha constituido una parte importante de la presente Tesis, habiéndose abordado la síntesis de los productos orgánicos tanto por métodos convencionales como empleando radiación microondas.

1.2 Poliolefinas

1.2.1 Introducción

Las poliolefinas, principalmente el polietileno (PE), el polipropileno (PP) y sus copolímeros, representan casi la mitad de los polímeros comerciales producidos en el mundo[2]. Estos polímeros termoplásticos combinan una serie de propiedades como baja densidad, estabilidad química, resistencia mecánica, facilidad de procesado y reciclado, lo que hace que se hayan introducido en una gran diversidad de aplicaciones.

El polietileno, que fue descubierto fortuitamente en Reino Unido en 1933, es la poliolefina más sencilla desde el punto de vista de su estructura química, pero es muy complejo debido a la variedad estructural y por tanto de propiedades a las que puede dar lugar según sus procesos de obtención.

En función del contenido en ramificaciones, se pueden clasificar los tipos de polietileno en tres grandes grupos:

- Polietileno de alta densidad (HDPE - *High Density Polyethylene*). Formado por cadenas lineales que presentan un grado de ramificación bajo, 0.5-2.5 ramificaciones por cada 1000 carbonos, contribuyendo a una cristalinidad elevada. Su densidad se encuentra entre 0.94 y 0.97 g/cm^3. Este tipo de polietileno se obtiene mediante procesos de polimerización a bajas presiones, utilizando catalizadores de coordinación, proceso Ziegler-Natta o mediante procesos de polimerización a presiones medias, con catalizadores de óxidos metálicos, proceso Phillips.
- Polietileno de baja densidad (LDPE - *Low Density Polyethylene*). Estos polietilenos presentan 20-30 ramificaciones de distintas longitudes por cada 1000 carbonos, lo que dificulta la

[2] www.plasticseurope.org

cristalización. La densidad de estos polímeros oscila entre 0.90 y 0.94 g/cm^3. Se obtiene por procesos de polimerización a alta presión empleando peróxidos, proceso ICI.

- Polietileno lineal de baja densidad (LLDPE – *Linear Low Density Polyethylene*). Las cadenas lineales presentan ramificaciones cortas. Su densidad está comprendida entre 0.90 y 0.94 g/cm^3. Estos polietilenos se pueden obtener empleando catalizadores Ziegler-Natta mediante copolimerización de etileno con α-olefinas, especialmente con 1-buteno, 1-hexeno y 1-octeno.

A principios de la década de 1980, el descubrimiento de catalizadores de metaloceno[3,4] proporcionó una nueva era en la industria de las poliolefinas, así como una nueva oportunidad para desarrollar nuevas estructuras de poliolefinas. Además de sus actividades catalíticas superiores, la principal ventaja del catalizador de metaloceno es su centro activo único, bien definido y el mecanismo de reacción asociado y bien controlado. Varios copolímeros de PE y PP que contienen comonómeros grandes se prepararon eficazmente con alto peso molecular, una amplia gama de composiciones de copolímeros, y distribuciones de peso molecular y composición estrechas[5].

El polietileno es un polímero semicristalino. Parte de sus macromoléculas son capaces de empaquetarse para dar lugar a una red tridimensional ordenada. Por otro lado, las largas cadenas junto con la presencia de ramificaciones laterales, conduce a ovillamientos moleculares que restringen dicho ordenamiento cristalino. De este modo, cuanto mayor sea el número de ramificaciones y/o defectos estructurales, así como el contenido de comonómero en los copolímeros de etileno menor será la cristalinidad del polímero resultante.

El polietileno tiene una temperatura de fusión relativamente baja, que varía en función de las condiciones de cristalización, el peso molecular y el grado de ramificación. La temperatura de fusión de los polietilenos de alta densidad se encuentra entre 130-135 ºC, mientras que en el caso de los polímeros de baja densidad se encuentra entre 106-115 ºC.

Los copolímeros de etileno de mayor interés son los que se obtienen con monómeros polares o con poliolefinas. Debido a su excelente procesabilidad, flexibilidad y compatibilidad con otros polímeros, aditivos y cargas, en este Trabajo se ha seleccionado el copolímero con acrilato de butilo (EBA) con un 7% de contenido de acrilato de butilo. Dichas propiedades hacen que estos copolímeros sean adecuados como filmes para envasado y cubiertas de invernadero, cables, o espumas microcelulares, entre otros.

[3] H. Sinn, W. Kaminsky, "Zieggler-Natta catalysis" Adv. Organomet. Chem. 18 (1980) 99-149.
[4] E. T. Kiesewetter, S. Randall, M. Radlauer, R. M. Waymouth, "Stereospecific octahedral group 4 bis(phenolate) ether complexes for olefin polymerization" J. Am. Chem. Soc. 132 (2010) 5566-5567.
[5] M. Chung, "Functionalization of polypropylene by the combination of metallocene catalysts and reactive comonomers" Macromol. React. Eng. 8 (2014) 69-80.

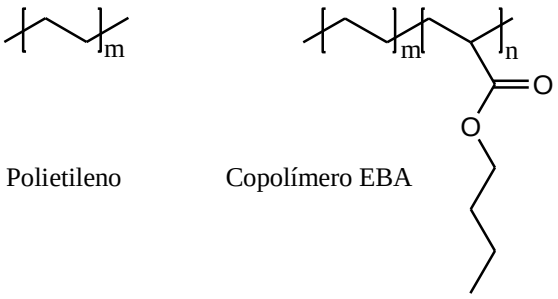

Polietileno Copolímero EBA

Figura 2. Estructuras químicas de polietileno y copolímero etileno-acrilato de butilo.

Estos materiales de EBA pueden ser procesados en un intervalo de temperatura más amplio que el de otras poliolefinas, debido a la excelente estabilidad térmica que presentan (pueden ser procesados a temperaturas de hasta 200 ºC). Además, tienen mejores propiedades ópticas y son más resistentes a la luz UV comparado con el LDPE.

En la Tabla 1, se muestran algunas propiedades del LDPE y del EBA empleado en este Trabajo[6].

[6] Especificaciones técnicas suministradas por Repsol: www.quimica.repsol.com

Tabla 1. Características generales del polietileno de baja densidad y del copolímero etileno-acrilato de butilo empleados en este Trabajo.

Propiedades generales	**Unidad**	**LDPE**	**EBA 7%**	**Método**
Indice de fluidez (190°C 2.16 Kg)	g/10 min	0.3	0.5	ISO 1133
Densidad a 23°C	Kg m^{-3}	921	924	ISO 1183
Temperatura de fusión (T_m)	°C	110	105	ISO 306
Filme				
Espesor	µm	200	125	Interno
Resistencia al impacto (F_{50})	g	900	>850	ISO 7765-1
Resistencia al rasgado (DM/DT)	N	750/1100	750/850	ISO 6483-2
Resistencia a la tracción en rotura	MPa	19/20	24/25	ISO 527-3
Alargamiento en el punto de rotura	%	650/730	680/710	ISO 527-3

DM (dirección máquina en el sentido de salida de la boquilla); DT (dirección transversal)

1.2.2 Funcionalización química

La naturaleza inerte de las poliolefinas ha hecho que su funcionalización sea un tema de investigación muy importante tanto a nivel académico como industrial[7,8]. Con la condición de conservar sus propiedades térmicas y mecánicas, la funcionalización de las poliolefinas permite la introducción de grupos funcionales mejorando sus prestaciones.

Como ya se ha comentado, existen tres métodos para abordar el desafío de funcionalización en los polímeros, que son: polimerización directa con monómero funcional, post-polimerización a través de comonómero reactivo que puede prepararse eficazmente y luego convertirse selectivamente en grupos funcionales bajo condiciones de reacción suaves, y reacciones específicas de injerto.

[7] T. C. Chung, "Synthesis of polyalcohols via Ziegler-Natta polymerization" Macromolecules 21 (1988) 865-869.
[8] M. J. Yanjarappa, S. Sivaram, "Recent developments in the synthesis of functional poly(olefin)s" Prog. Polym. Sci. 27 (2002) 1347.

El método de funcionalización más directo y sencillo es la copolimerización. Sin embargo, este proceso [9] tiene industrialmente inconvenientes por la alteración que supone la presencia de un comonómero en la eficiencia catalítica de la síntesis de poliolefinas. En la industria, la producción de copolímeros tradicionales poliolefinicos está muy optimizada y los productores son reacios a introducir en sus procesos monómeros específicos que serían los interesantes para su posterior funcionalización.

Como alternativa a la copolimerización directa, el método de funcionalización post-polimerización a través de comonómero reactivo permite obtener de una manera eficaz poliolefinas funcionalizadas[10] tras la transformación química de los grupos reactivos en grupos funcionales. El comonómero reactivo debe tener una reactividad comparable a la del monómero principal y el grupo reactivo debe reaccionar fácilmente bajo condiciones suaves de reacción. Sin embargo, si se trabaja con altas concentraciones de grupos funcionales, se producirá la pérdida de las propiedades iniciales de las poliolefinas, tales como, punto de fusión y cristalinidad.

El método de funcionalización mediante reacciones de injerto[11,12] consiste en la unión covalente de grupos funcionales sobre la cadena macromolecular de la poliolefina, mediante su empleo puede alcanzarse un alto grado de funcionalización y, simultáneamente, mantener propiedades inherentes de las poliolefinas.

1.2.3 Funcionalización mediante tratamientos físicos. Modificación superficial inducida por plasma

En general, la mayoría de las superficies poliméricas son de naturaleza inerte e hidrófoba, y usualmente tienen una baja energía de superficie. Por lo tanto, no poseen las propiedades de superficie específicas necesarias en diversas aplicaciones, y sus superficies deben tratarse para lograr este fin.

Los tratamientos físicos en general se emplean para diferentes aplicaciones, como son, la funcionalización, la limpieza, el grabado y el recubrimiento sobre la superficie. La funcionalización de

[9] A. Nakamura, S. Ito, K. Nozaki, "Coordination-insertion copolymerization of fundamental polar monomers" Chem. Rev. 109 (2009) 5215-5244.
[10] B. C. Peoples, V. N. Dougnac, G. B. Galland, F. M. Rabagliati, R. Quijada, "Preparation of poly(ethylene-co-dicyclopentadiene) copolymers and a study on their post-polymerization epoxidation" Polym. Bull. 70 (2013) 117-129.
[11] A. Oromiehie, H. Ebadi-Dehaghani, S. Mirbagheri, "Chemical modification of polypropylene by maleic anhydride:melt grafting, characterization and mechanism" Inter. J. Chem. Eng. Appl. 5 (2014) 117-122.
[12] J. H. Lee, S. C. Hong, "Study on the controlled preparation of polyolefin based block or graft copolymers" Elastomers and Composites 48 (2013) 30-38.

la superficie se utiliza para modificar la capa superficial de un polímero insertando algunos grupos funcionales con el fin de mejorar su humectabilidad, sellabilidad, capacidad de impresión, absorción del tinte, su resistencia a la cristalización o adhesión a otros polímeros o metales, mientras mantiene las deseables propiedades del seno del material[13,14]. La funcionalización de la superficie también se puede usar para mejorar las propiedades barrera de los polímeros y para impartir a los polímeros algunas propiedades antimicrobianas[15].

Aunque la modificación superficial de los polímeros se puede realizar mediante métodos químicos o físicos, los métodos físicos ofrecen algunas ventajas sobre los métodos químicos. La primera ventaja notable de los métodos físicos es la capacidad de proporcionar una modificación de superficie más precisa sin el requisito de un control riguroso del proceso. Además, permiten la introducción de gran variedad de grupos funcionales en un solo paso, son métodos sencillos y limpios. Entre las desventajas que conllevan hay que destacar que estos tratamientos requieren equipos costosos, y que las propiedades ópticas de los materiales poliméricos pueden verse afectadas.

Mientras los métodos físicos son los más aplicados en la industria por su buena relación precio-eficacia, desde el punto de vista académico son más interesantes los métodos químicos porque se obtienen resultados más uniformes y mejor definidos.

Los métodos físicos de modificación de la superficie más usados son:

- Plasma[16]
- Radiación γ[17]
- Radiación UV[18]
- Ionización a la llama[19]
- Descarga en corona[20]

[13] E. M. Liston, L. Martinu, M. R. Wertheimer, "Plasma surface modification of polymers for improved adhesion: a critical review" J. Adhesion Sci. Technol. 7 (1993) 1091–1127.
[14] N. J. Chou, C. A. Chang, Surface modification of polymers. In: H. M. Tong, S. P. Kowalczyk, R. Saraf, N. J. Chou, Eds., Characterization of Polymers, Butterworth-Heinemann Inc., Boston, (1994) 169–197.
[15] S. K. Pankaj, C. Bueno-Ferrer, N. N. Misra, V. Milosavljević, C. P. O´Donnell, P. Bourke, K. M. Keener, P. J. Cullen, "Applications of cold plasma technology in food packaging" Trends Food Sci. Technol. 35 (2014) 5–17.
[16] I. L. Punga, G. Borcia, "Surface modification and stability of polymers treated by atmospheric-pressure, helium plasma" J. Adv. Res. Phys. 4 (2013) 1-5.
[17] L. Xing, L. Liu, Y. Huang, D. Jiang, B. Jiang, J. He, "Enhanced interfacial properties of domestic aramid fiber-12 via high energy gamma ray irradiation" Composites Part B 69 (2015) 50-57.
[18] F. Kessler, D. Steffens, G. A. Lando, P. Pranke, D. E. Weibel, "Wettability and cell spreading enhancement in poly(sulfone) and polyurethane surfaces by UV-assisted treatment for tissue engineering purposes" J. Tissue Eng. Regen. Med. 11 (2014) 23-31.
[19] I. S. Bayer, A. J. Davis, A. Biswas, "A robust superhydrophobic surfaces from small diffusion flame treatment of hydrophobic polymers" RSC Adv. 4 (2014) 264-268.
[20] A. Popelka, P. N. Khanam, M. A. Almaadeed, "Surface modification of polyethylene/grapheme composite using corona discharge" J. Phys. D Appl. Phys. 51 (2018) 105302.

- Haces de electrones[21]

La modificación superficial de los materiales orgánicos por exposición al plasma ha sido de gran interés desde finales de 1950 y principios de 1960[22]. Un plasma es un estado gaseoso complejo de materia constituido por radicales libres, electrones, iones, etc., y formado cuando un gas inerte o reactivo que se encuentra a presión reducida se somete a la acción de descargas eléctricas, oscilaciones electromagnéticas de frecuencia elevada, ondas de choque, radiaciones de alta energía, etc.

Las funcionalidades que aparecen en los materiales polímeros después del tratamiento con plasma pueden variar en función de los parámetros de operación, como la naturaleza y el caudal de flujo del gas precursor, la presión y la temperatura dentro de la cámara, la potencia y el tiempo de exposición de la muestra[23]. Pero sobre todo los gases precursores seleccionados en los tratamientos con plasma son el factor determinante para la funcionalización del material. A continuación, se muestran algunos ejemplos:

- Destrucción de impurezas de la superficie de un polímero. Para ello, se utiliza un gas inerte como el argón o el neón.
- Introducción de grupos funcionales en la superficie del polímero. En este caso, se usan gases reactivos. Por ejemplo, los plasmas de aire, oxígeno y vapor de agua introducen grupos funcionales que contienen oxígeno (carboxilo, -COOH e hidroxilo, -OH). Los plasmas de nitrógeno o amoníaco se usan para introducir grupos que contienen nitrógeno (amina, $-NH_2$).
- Deposición de recubrimientos poliméricos delgados sobre la superficie de otro polímero[24]. Para ello, el plasma debe ser generado a partir de monómeros orgánicos gaseosos, los cuales se depositan en la superficie y polimerizan formando una capa uniforme y resistente.

Una de las principales ventajas que ofrece el plasma frente a los métodos químicos húmedos es que no implica la utilización de disolventes tóxicos o corrosivos, en consecuencia, el interés industrial en el plasma continúa en aumento ya que es un tratamiento respetuoso con el medio ambiente[25,26]. Además,

[21] I. V. Puhova, K. V. Rubtsov, I. A. Kurzina, A. V. Kazakov, A. V. Medovnik, "Modification of polymer materials by electron beam treatment" Key Eng. Mater. 670 (2016) 118-125.
[22] G. D. Cooper, M. Prober, "The action of oxygen corona and of ozone on polyethylene" J. Polym. Sci. 44 (1960) 397-409.
[23] I. Djordjevic, L. G. Britcher, S. Kumar, "Morphological and surface compositional changes in poly(lactide-co-glycolide) tissue engineering scaffolds upon ratio frequency glow discharge plasma treatment" Appl. Surf. Sci., 254 (2008) 1929–1935.
[24] G. Mishra, C. D. Easton, G. J. S. Fowler, S. L. McArthur, "Spontaneously reactive plasma polymer micropatterns" Polymer 52 (2011) 1882–1890.
[25] S. Duan, Y. Wang, X. Liu, D. Shao, T. Hayat, A. Alsaedi, J. Li, "Removal of UV(VI) from aqueous solution by amino functionalized flake graphite prepared by plasma treatment" ACS Sustainable Chem. Eng. 5 (2017) 4073-4085.
[26] J. Lai, B. Sunderland, J. Xue, S. Yan, W. Zhao, M. Folkard, B. D. Michael, Y. Wang, "Study on hydrophilicity of polymer surfaces improved by plasma treatment" Appl. Surf. Sci., 252 (2006) 3375–3379.

el plasma permite modificar la superficie de un polímero con menor rugosidad y degradación superficial[27].

Sin embargo, en los tratamientos con plasma preocupa especialmente el efecto de envejecimiento superficial. Los grupos funcionales generados no son estables con el tiempo ya que la superficie del polímero tratado con plasma de alta energía tiende a "relajarse" y volver a su estado no tratado. Los principales procesos responsables del envejecimiento superficial son la reorientación de los grupos polares en la superficie y la movilidad de pequeños fragmentos de polímero por migración en la matriz del polímero. Otros factores que influyen en el envejecimiento son las condiciones de almacenamiento, la humedad, la temperatura, etc.

Hay que señalar que la limpieza exhaustiva de la cámara del plasma después de su uso es muy importante, especialmente si se cambia el gas precursor, para evitar procesos contaminantes[28].

En cuanto a la caracterización de las superficies tratadas con plasma, las medidas de ángulo de contacto (CA) empleando agua como líquido de contacto proporcionan información sobre las propiedades hidrofílicas de la superficie del material. Las técnicas basadas en espectroscopía de electrones y de iones son más adecuadas para establecer la morfología superficial y determinar la composición y la distribución espacial de los componentes. Entre estas técnicas destacan: espectroscopía infrarroja de transformada de Fourier en combinación con la reflexión total atenuada (ATR-FTIR) que da información acerca de la naturaleza de las especies formadas tras el tratamiento con plasma, espectroscopía fotoelectrónica de rayos X (XPS) y espectroscopía de masas de ión secundario estático (SIMS). Las técnicas de imágenes son también de especial interés en el análisis de superficies, como la microscopía electrónica de barrido (SEM) que proporciona imágenes de alta resolución de la superficie y la microscopía de fuerza atómica (AFM) que aporta información sobre la topografía y rugosidad del material.

En este Trabajo, los filmes de EBA ya funcionalizados han sido sometidos a tratamiento de plasma de oxígeno para mejorar las propiedades hidrofílicas de la superficie del filme.

[27] D. Caschera, A. Mezzi, L. Cerri, T. de Caro, C. Riccucci, G. M. Ingo, G. Padeletti, M. Biasiucci, G. Gigli, B. Cortese, “Effects of plasma treatments for improving extreme wettability behavior of cotton fabrics” Cellulose 21 (2014) 741–756.
[28] J. M. Goddard, J. H. Hotchkiss, “Polymer surface modification for the attachment of bioactive compounds” Prog. Polym. Sci., 32 (2007) 698–725.

1.3 Redes poliméricas fotoentrecruzadas

1.3.1 Introducción

Los geles poliméricos consisten en un conjunto de cadenas de polímeros entrecruzadas entre sí formando redes tridimensionales y una fase líquida que hincha la red (agua o disolventes orgánicos). Los geles poliméricos poseen tanto las propiedades cohesivas de los sólidos, como las propiedades de transporte difusivo de los líquidos. Los geles son blandos, desde el punto de vista elástico y altamente activos, desde el punto de vista osmótico. Esta dualidad es la que confiere a los geles sus interesantes propiedades de absorción y reológicas que son la base de numerosas aplicaciones importantes.

Los geles poliméricos se pueden clasificar en función del tipo de entrecruzamiento que crea la red tridimensional (geles físicos o químicos). En los geles químicos las conexiones tienen lugar mediante enlaces covalentes, mientras que en los geles físicos la unión entre cadenas tiene lugar mediante interacciones de van der Waals. También se pueden clasificar en función de la naturaleza del polímero (geles de biopolímeros o de polímeros sintéticos), en función de la forma y tamaño de la configuración del gel (macro y microgeles) y en función del tipo de disolvente.

De interés particular son los hidrogeles, es decir, geles poliméricos que se hinchan extensivamente en agua[29]. Estos materiales poseen muchas propiedades específicas que los hacen atractivos para una amplia gama de aplicaciones. Su capacidad de contener agua, estabilidad en medios acuosos y suavidad, hace que los hidrogeles sean compatibles con sistemas biológicos y así se propusieron para diferentes aplicaciones biomédicas tales como ingeniería de tejidos, adhesión celular o liberación controlada de fármacos[30,31,32,33,34]. También es muy conocida su utilización como soporte para moléculas activas, geles para el cabello o los modernos desarrollos de sistemas inteligentes que responden a diferentes tipos de estímulos.

En el presente Trabajo se han preparado unos hidrogeles acrílicos de grado de hinchamiento controlado al objeto de que los materiales hinchados en agua mantuvieran una estabilidad dimensional adecuada para permitir su empleo como sensores ópticos. La estructura química de los hidrogeles

[29] J. F. Kuenzler, Hydrogels. In Encyclopedia of Polymer Science and Technology, 3rd ed.; Mark, H.F., Ed.; Wiley-Interscience: New York, NY, USA, 2 (2004) 691–722.
[30] G. D. Nicodemus, S. J. Bryant, "Cell encapsulation in biodegradable hydrogels for tissue engineering applications" Tissue Eng. Part B-Rev. 14 (2008) 149–165.
[31] M. S. Shoichet, "Polymer scaffolds for biomaterials applications" Macromolecules 43 (2010) 581–591.
[32] M. Hamidi, A. Azadi, P. Rafiei, "Hydrogel nanoparticles in drug delivery" Adv. Drug Deliver. Rev. 60 (2008) 1638–1649.
[33] T. R. Hoare, D. S. Kohane, "Hydrogels in drug delivery: Progress and challenges" Polymer 49 (2008) 1993–2007.
[34] O. H. Kwon, A. Kikuchi, M. Yamato, Y. Sakurai, T. Okano, "Rapid cell sheet detachment from poly(N-isopropylacrylamide)-grafted porous cell culture membranes" J. Biomed. Mater. Res. 50 (2000) 82–89.

poliméricos así como la de los preparados en este Trabajo se diseña a partir de los siguientes componentes:

- Monómero hidrófilo: Es el bloque de construcción dominante de la estructura del polímero y puede diferir sustancialmente, en particular, entre los hidrogeles de origen biológico y sintético. Los polímeros típicos de origen biológico son polipéptidos, polinucleótidos y polisacáridos. En los hidrogeles sintéticos, una gran fracción se basa en derivados de vinilo con dobles enlaces olefínicos que pueden experimentar polimerización por radicales para formar la cadena principal del polímero. Algunos ejemplos característicos son poli(ácido acrílico) o poli(ácido metacrílico), poliacrilatos o polimetacrilatos, poliacrilamidas o polimetacrilamidas, polialcohol vinílico, polivinilpirrolidona y sus copolímeros correspondientes. Otros ejemplos de tipos de polímeros sintéticos para hidrogeles son poliéteres, poliuretanos y polietilén glicol. En el presente Trabajo se ha empleado como monómero principal la polivinilpirrolidona.
- Comonómero hidrófobo: En los casos en que se requiere un control del grado de hinchamiento de los hidrogeles en agua, se emplea un segundo comonómero hidrofóbico al objeto de obtener un balance de propiedades hidrófilo-hidrófobo. En el presente Trabajo se ha empleado el acrilato de butilo.
- Entrecruzante: El entrecruzante o agente de reticulación se define como la entidad molecular a la que se pueden unir tres o más cadenas para formar un punto de reticulación y convertir el polímero en una red. El contenido y naturaleza del agente de reticulación en la composición del hidrogel tiene una gran influencia en las propiedades mecánicas y en el grado de hinchamiento del material. Algunos ejemplos de entrecruzantes son dimetacrilato de etilenglicol, dimetacrilato de 1,6-hexanodiol o N, N'-metilenbisacrilamida. En este Trabajo se ha empleado el dimetacrilato de etilenglicol.
- Monómero reactivo: También en la estructura del hidrogel se pueden incorporar monómeros con grupos funcionales, que poseen propiedades específicas para permitir una modificación química posterior del hidrogel o proporcionar a la red propiedades funcionales adicionales. Algunos ejemplos de grupos funcionales son grupos ácido carboxílico, amino e hidroxilo, que son intrínsecamente parte del polímero o pueden introducirse posteriormente en el hidrogel después de la formación de la red. En el presente Trabajo se ha empleado como comonómero reactivo el cloruro de metacriloílo.

Aunque los hidrogeles pueden prepararse por métodos de polimerización convencionales (calor, interacción iónica y redox), la fotopolimerización-fotoentrecruzamiento constituye un procedimiento alternativo de gran interés aplicado[35,36].

En la Figura 3 se muestra un esquema de la preparación de una red tridimensional por fotopolimerización-fotoentrecruzamiento constituido por los diferentes monómeros comentados anteriormente y de estructura genérica similar a los preparados en esta Tesis.

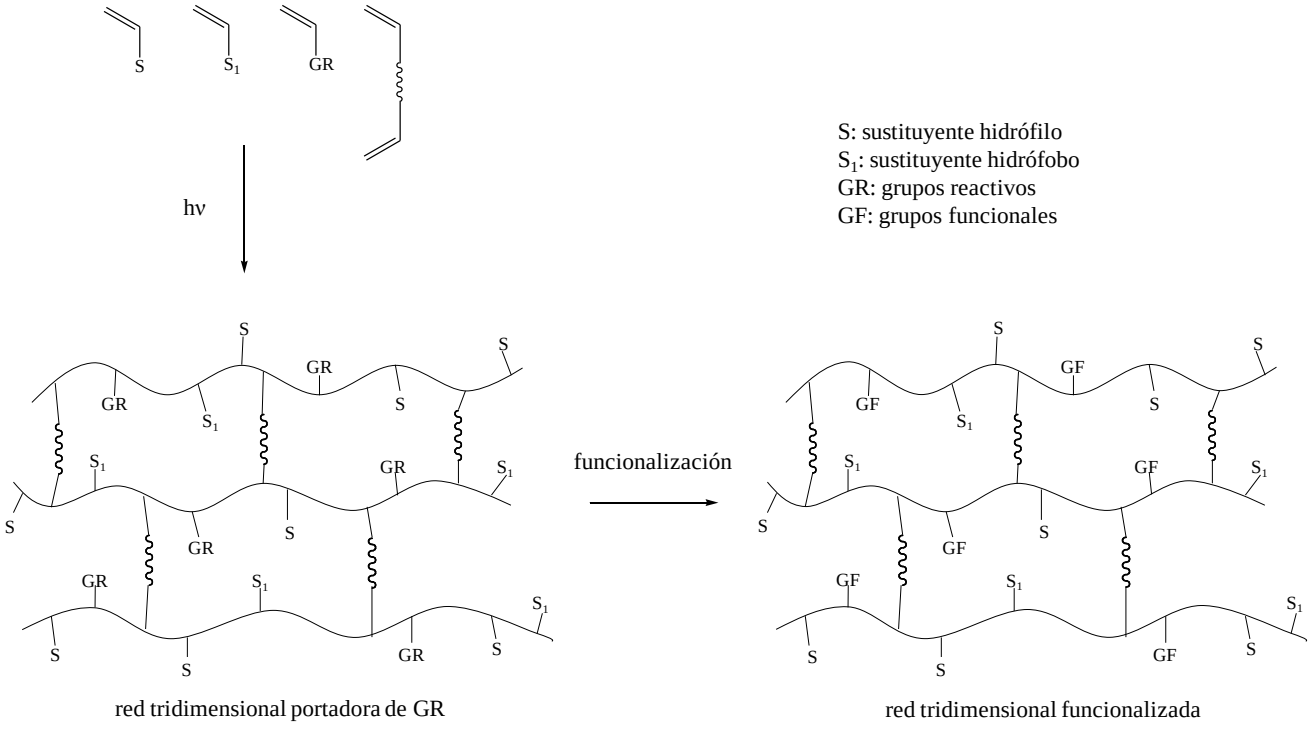

Figura 3. Síntesis fotoquímica de red tridimensional entrecruzada a partir de una composición específica de monómeros y posterior funcionalización.

[35] J. L. Drury, D. J. Mooney, "Hydrogels for tissue engineering: scaffold design variables and applications" Biomaterials 24 (2003) 4337–51.
[36] K. T. Nguyen, J. L. West, "Photopolymerizable hydrogels for tissue engineering applications" Biomaterials 23 (2002) 4307–4314.

1.3.2 Polimerización radical fotoiniciada. Obtención de redes poliméricas para posterior funcionalización

En comparación con los métodos de polimerización convencionales, las reacciones de fotopolimerización presentan numerosas ventajas[37], que incluyen:

- rápida cinética de reacción.
- control espacio-temporal sobre el proceso de polimerización.
- procesabilidad a temperatura ambiente, sin necesidad de grandes requerimientos de energía.
- utilización de sistemas que no necesitan disolventes.
- tiene lugar en un solo paso.
- los requerimientos de pureza son menores.

Por todo ello, la fotopolimerización tiene una gran implantación industrial[38], y sus aplicaciones en uso cumplen una amplia gama de sectores de actividad, tales como Electricidad y Electrónica (fabricación de circuitos impresos e integrados), Artes gráficas (planchas de impresión, tintas de fotosecado rápido), Óptica (lentes de contacto), Medicina (empaste dentales y prótesis), Recubrimientos (barnices, lacas y pinturas).

La polimerización radical fotoiniciada es una reacción en cadena iniciada mediante irradiación directa de una molécula denominada fotoiniciador, creándose un estado excitado a partir del cual se desencadena la rotura de enlaces y la formación de radicales primarios. Los radicales formados reaccionan con las moléculas de monómero, generando macrorradicales cuyo crecimiento termina mediante reacciones de combinación o desproporción en la etapa final de polimerización, dando lugar a cadenas de polímero terminadas[39].

Cuando se diseña un sistema de fotopolimerización la elección del fotoiniciador es fundamental para la eficiencia de polimerización. En su elección hay que considerar que el espectro de absorción del fotoiniciador debe solapar con el espectro de emisión de la fuente de luz utilizada y que su eficiencia en la generación de radicales libres sea elevada en el medio y condiciones de reacción. La concentración del fotoiniciador y su absorción en el espesor de material a fotopolimerizar o camino óptico (ley de Lamber-beer) son también consideraciones fundamentales para las aplicaciones.

[37] K. Dietlicker in Chemistry and Technology of UV and EB Formulations for Coatings, Inks and Paints, Vol. III, "Photoinitiators for Free radical and Cationic Polymerisation", Ed. P. K. T. Oldring, SITA Technology Ltd., (1991).
[38] N. S. Allen, (Ed) "Photochemistry and Photophysics of Polymer Materials" Chapters: 10-14th, Wiley, Koboken, New Jersey, USA, 2010.
[39] G. Odian, Principles of Polymerization. 4th ed.; John Wiley & Sons: New Jersey, (2004).

De acuerdo con los mecanismos de generación radical, los fotoiniciadores radicales se pueden dividir en dos categorías[40]: fotoiniciadores de fragmentación (Tipo I) y sistema de fotoiniciación bimolecular (Tipo II). En el caso de los fotoiniciadores de Tipo I (Fig. 4(a)), se producen radicales por ruptura homolítica del enlace, por lo que es necesario que el enlace sea débil y que su energía de disociación sea inferior a la energía del estado excitado reactivo, aunque lo suficientemente alta para que el producto sea estable térmicamente. Ejemplos de fotoiniciadores de fragmentación[41] empleados en hidrogeles son la benzoina y sus derivados, los bencilacetales, acetofenonas, etc.

El mecanismo de iniciación de los sistemas de Tipo II es más complejo (Fig. 4(b)) dado que la reacción es bimolecular. El fotoiniciador bimolecular no tiene la capacidad de generar radicales por sí mismo, solo absorbe la luz y es su estado excitado el que reacciona con una segunda molécula (co-iniciador) para formar los radicales primarios mediante transferencia electrónica o captura de hidrógeno (generalmente de un co-iniciador anima o alcohol). Ejemplos de sistemas bimoleculares son los sistemas formados por cetonas aromáticas como benzofenonas, y aminas, alcoholes o tioles que actúan como donadores de hidrógeno.

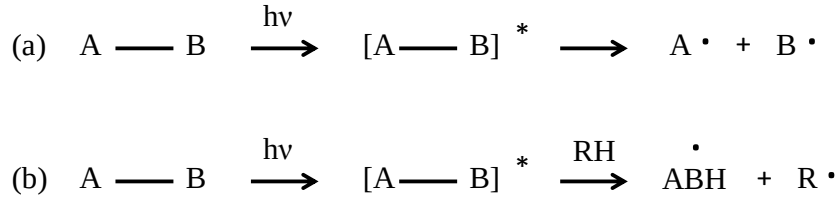

Figura 4. Mecanismo de generación de radicales de los fotoiniciadores Tipo I (a) y Tipo II (b).

En este Trabajo se ha empleado el fotoiniciador Irgacure 2959 de Tipo I. En la siguiente figura se muestra su estructura (2-Hidroxi-4′-(2-hidroxietoxi)-2-metilpropiofenona) y su fotofragmentación.

[40] N. S. Allen, F. Catalina, P. N. Green, W. A. Green, "Photochemistry of carbonyl photoinitiators" Eur. Polym. J. 22 (1986) 49-56.
[41] X-H. Qin, A. Ovsianikov, J. Stampfl, R. Liska, "Additive manufacturing of photosensitive hydrogels for tissue engineering applications" Bionanomaterials 15 (2014) 49-70.

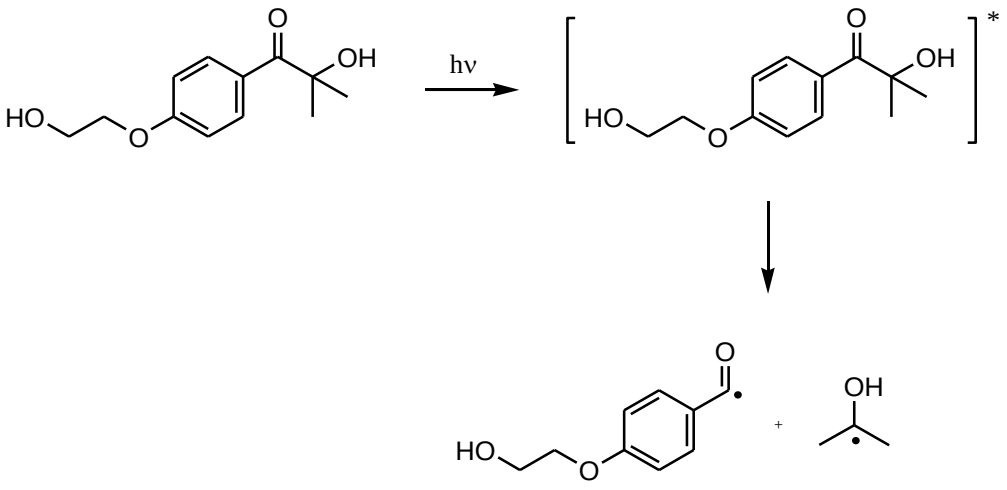

Figura 5. Mecanismo de fotofragmentación del fotoiniciador Irgacure 2959.

En las fotopolimerizaciones realizadas en esta Tesis se ha empleado el fotoiniciador I2959 a una concentración de 1 % en peso con respecto a los monómeros y manteniendo en todos los casos las mismas condiciones de atmósfera de argón y empleando un sistema de irradiación de tubos fluorescentes con emisión centrada en 365 nm. El espesor de las membranas obtenidas con el sistema diseñado en nuestros laboratorios se encuentra dentro del intervalo de 40-180 micras (empleando separadores), con ello se ha asegurado una transmisión de la luz en todo el camino óptico y una fotopolimerización homogénea en todo el espesor de la membrana. Los detalles se encuentran recogidos en la parte experimental de las publicaciones.

1.4 Modificación química de polímeros con radiación microondas

El uso de la radiación microondas (MW) para la síntesis y modificación de polímeros como alternativa al calentamiento convencional está adquiriendo cada vez mayor popularidad puesto que ofrece una serie de ventajas[42], entre las que cabe destacar la rapidez y la homogeneidad de las reacciones, así como los altos rendimientos de los productos obtenidos.

Las MW son ondas del espectro electromagnético con frecuencias comprendidas entre 300 GHz y 300 MHz. Las longitudes de onda correspondientes abarcan un rango de 1 mm a 1 m, que muestra la

[42] C. O. Kappe, "Controlled Microwave Heating in Modern Organic Synthesis" Angew. Chem. Int. Ed. 43 (2004) 6250–6284.

posición media de las microondas entre las ondas de infrarrojos y de radio. Sin embargo, la mayor parte de los aparatos de microondas comerciales trabajan con una frecuencia de 2 450 MHz para evitar interferencias con dispositivos de telecomunicación.

El calentamiento por MW se basa en la calefacción microondas dieléctrica, es decir, las moléculas que tienen un momento dipolar permanente intentarán alinearse con el campo electromagnético aplicado, lo que provocará rotación, fricción y colisión de las moléculas y, por tanto, generación de calor. Como resultado, la eficacia del calentamiento por MW depende fundamentalmente de las propiedades dieléctricas y de los tiempos de relajación de la mezcla de reacción, por lo que el uso de buenos disolventes absorbentes de MW da como resultado un calentamiento muy rápido[43].

La radiación MW también se puede considerar como una forma de excitación selectiva de las moléculas, por lo que sólo se van a activar algunas de ellas. Esto hace que se reduzcan las reacciones secundarias, obteniéndose productos más puros con mayores rendimientos y más fácilmente aislables. Por tanto, las mejoras que ofrece el MW frente al método térmico convencional son debidas a la combinación de esta excitación selectiva y de las altas temperaturas alcanzadas que disminuyen los tiempos de reacción.

Otra ventaja importante que ofrece el empleo de MW es la síntesis a altas presiones, que se puede llevar a cabo en los viales de reacción cerrados, y que permite el reemplazo de disolventes con alto punto de ebullición por disolventes con bajos puntos de ebullición. Además, el empleo de estos viales cerrados permite un control preciso de la presión debido al arqueamiento del cierre septum y de la temperatura dentro del vial, detectado por un sensor IR dirigido hacia las paredes de vidrio del vial.

El desarrollo de los reactores de microondas comerciales ha mejorado significativamente en los últimos años, y por tanto también los resultados obtenidos en las síntesis como se refleja en el número de publicaciones sobre síntesis y modificación de polímeros llevadas a cabo en microondas durante los últimos años[44,45,46,47,48].

[43] C. Gabriel, S. Gabriel, E. H. Grant, B. S. J. Halstead, D. M. P. Mingos, "Dielectric parameters relevant to microwave dielectric heating" Chem. Soc. Rev. 27 **(**1998**)** 213-224.
[44] L. J. Schwarz, M. K. Potdar, B. Danylec, R. I. Boysen, M. T. H. Hearn, "Microwave-assisted synthesis of resveratrol imprinted polymers with enhanced selectivity" Anal. Methods 7 (2015) 150-154.
[45]B. Govindaraj, M. Sarojadevi, "Microwave-assisted synthesis and characterization of polyimide/functionalized MWCNT nanocomposites containing quinolyl moiety" 37 Polym. Compos. (2016) 2417-2424.
[46] M. Kang, M. Cho, S. Kim, J. H. Youk, "Microwave-assisted one-step synthesis of poly(2-isopropyl-2-oxazoline) block copolymers using a dual initiator for CROP and RAFT polymerization" Fibers and polymers 18 (2017) 1215-1220.
[47] A. Biswas, S. Kim, A. Gómez, M. Buttrum, V. Boddu, H. N. Cheng, "Microwave-assisted synthesis of sucrose polyurethanes and their semi-interpenetrating polymer networks with polycaprolactone and soybean oil" Ind. Eng. Chem. Res. 57 (2018) 3227-3234.
[48] K. Kempe, C. R. Becer, U. S. Schubert, "Microwave-assisted polymerizations: recent status and future perspectives" Macromolecules 44 (2011) 5825-5842.

En esta Tesis, las reacciones de modificación y funcionalización del copolímero EBA se han llevado a cabo con radiación microondas en fase heterogénea empleándose una cámara CCD para visualizar que los filmes de EBA se mantuvieran en estado sólido durante el transcurso de las reacciones. También se ha empleado la metodología microondas para la síntesis de sondas fluorescentes. De forma comparativa con la metodología de calentamiento convencional, en estas reacciones se han obtenido mejores rendimientos y en tiempos más cortos de reacción.

1.5 Fluorescencia. Aspectos básicos.

La luminiscencia se puede definir como la emisión de radiación desde un estado excitado de una molécula a un estado fundamental tras la absorción de un fotón de luz.

Los procesos de absorción y emisión de luz y su evolución en los niveles electrónicos y vibracionales de una molécula se representan por el denominado diagrama de Jablonski[49] (Figura 6).

[49] A. M. Braun, M. T. Maurette, E. Oliveros, Photochemical Technology, Ed. J. W. Sons (1991) Chichester, Sussex, UK.

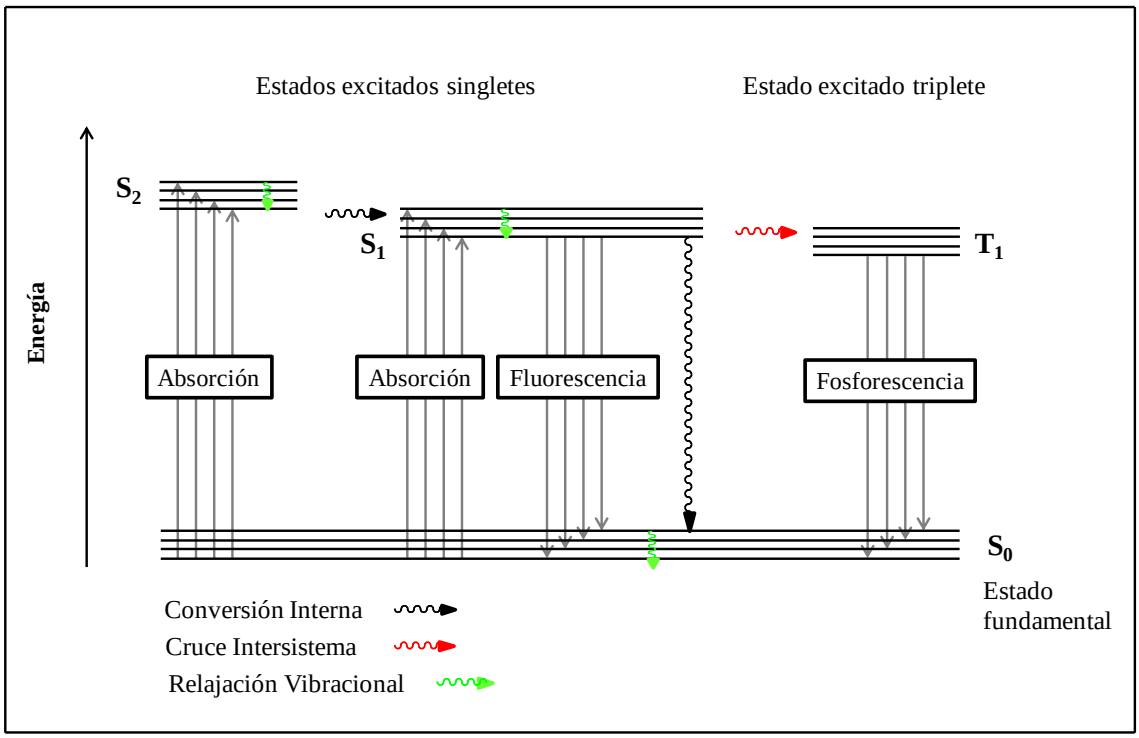

Figura 6. Diagrama de Jablonski que ilustra los procesos probables de excitación y relajación.

Si una especie que se encuentra en su estado electrónico fundamental (S_0) absorbe un fotón de luz, aumenta su energía y un electrón puede promocionar a un estado excitado singlete de mayor energía (S_1, S_2…). Por lo general, el tiempo de vida media de una especie excitada es breve porque hay diversas formas en las cuales puede liberar su exceso de energía y relajarse a su estado fundamental. Dos de los procesos de relajación o desactivación más importantes son:

- procesos de desactivación radiativos (que implica los procesos de fluorescencia y fosforescencia). La fluorescencia, es un proceso de relajación desde el estado electrónico excitado (S_1) al estado fundamental (S_0). Ambos estados presentan la misma multiplicidad de spín. En cambio, la fosforescencia tiene lugar desde el estado excitado triplete (T_1), de distinta multiplicidad que el estado fundamental.
- procesos de desactivación no radiativos (relajación vibracional, conversión interna, cruce intersistema y quenching):
    - Relajación vibracional. La relajación vibracional implica la disipación de energía entre niveles vibracionales dentro del mismo estado electrónico excitado.
    - Conversión interna. La relajación tiene lugar entre dos estados electrónicos de la misma multiplicidad.
    - Cruce intersistema. La desactivación de energía tiene lugar entre dos estados electrónicos excitados con diferente multiplicidad de spin. Las transiciones entre

estados electrónicos con diferente multiplicidad de spín están en principio prohibidas, sin embargo, pueden ocurrir debido al proceso conocido como acoplamiento spin-orbital.

- Desactivación bimolecular o quenching. En este proceso la especie excitada se desactiva al interaccionar con otra especie llamada quencher o inhibidor de fluorescencia.

Dado que la conversión interna y el cruce intersistema competirán con la fluorescencia en la desactivación del estado excitado de menor energía, no todas las moléculas van a volver al estado fundamental mediante la emisión de fluorescencia. La fracción de moléculas excitadas que fluorescen es lo que se conoce como rendimiento cuántico de fluorescencia (ϕ_F) y es una constante física que depende de la temperatura y el entorno de las especies moleculares excitadas.

Las bandas de fluorescencia por lo regular se observan a longitudes de onda más largas, y por tanto a energías menores, que la banda de radiación responsable de su excitación (o banda de absorción). Este desplazamiento hacia longitudes de onda mayores se llama desplazamiento de Stokes.

La espectroscopia de fluorescencia[50] ha adquirido gran popularidad en el estudio de cambios a nivel molecular en todo tipo de sistemas. Esto es debido a las ventajas que ofrece esta técnica en comparación con otras técnicas convencionales[51,52]:

- Presenta alta selectividad y sensibilidad.
- Los tiempos de respuesta son muy cortos (alrededor de 10^{-9}s).
- No destruye la muestra.
- No se requieren grandes cantidades de muestra.
- Los procesos que tienen lugar en diferentes escalas de tiempo podrían estudiarse en tiempo real.

[50] J.C. Scaiano (Ed.).”Handbook of Organic Photochemistry” Vol I and II, CRC-Press, Inc., Boca Raton, Florida, USA, 1989 .
[51] W. Retting, B. Strehmel, S. Schrader, H. Seifert, “Applied Fluorescence in Chemistry, Biology and Medicine” Springer Berlin, (1999).
[52] A. Sharma, S. G. Schulman, “Introduction to Fluorescence Spectroscopy” John Wiley & Sons, Ltd. New York, (1999).

1.6 Sensores

La detección y cuantificación de especies químicas o analitos son algunos de los desafíos clave en la investigación química, especialmente en el área medioambiental, donde la detección de contaminantes mediante técnicas sencillas, rápidas y económicas siempre ha sido de gran importancia.

Si bien las técnicas analíticas tradicionales, como la espectroscopia de absorción atómica (AAS), la espectrometría de masas con plasma acoplado inductivamente (ICP-MS), la cromatografía líquida de alta resolución (HPLC) y la electroquímica, permiten la detección y cuantificación selectiva y precisa de las especies químicas, estas técnicas consumen mucho tiempo, y además requieren equipos sofisticados y costosos. Como alternativa de gran interés, los sensores químicos han adquirido gran popularidad en los últimos años[53].

Los sensores químicos son moléculas que generalmente se componen de dos subunidades: una subunidad emisora de la señal analítica y una subunidad coordinante[54]. La capacidad de interactuar selectivamente, o incluso reaccionar, con el analito de interés es competencia de la subunidad coordinante y ésta se diseña teniendo en cuenta principios de coordinación y de química supramolecular, mientras que el fenómeno de detección, que surge de variaciones en las propiedades macroscópicas, depende de la infraestructura de señalización.

Los sensores químicos más ampliamente utilizados son aquellos que responden ante las variaciones de color y/o fluorescencia o en las propiedades redox cuando se produce la interacción con el analito, denominándose sensores ópticos (cromogénicos y/o fluorogénicos) y electroquímicos, respectivamente. Los sensores ópticos[55] son especialmente interesantes porque la presencia del analito puede detectarse a simple vista o usando un espectrofotómetro, evitando así utilizar equipos caros y sofisticados.

Las interacciones entre la subunidad coordinante y el analito son reversibles, y dependiendo del tipo de unión entre las subunidades emisora y coordinante, pueden actuar mediante: (a) mecanismo subunidad coordinante-subunidad emisora, en el que ambas están unidas covalentemente y (b) mecanismo de desplazamiento, en el que existe una interacción débil entre ambas unidades.

En el primer caso, las dos subunidades se encuentran unidas covalentemente ya sea directamente o a través de un espaciador (Figura 7(a)). La subunidad coordinante interactúa reversiblemente con el analito por medio de interacciones débiles: enlaces de hidrógeno, interacciones electrostáticas e

[53] E. V. Anslyn, "Supramolecular analytical chemistry" J. Org. Chem., 72 (2007) 687-699.
[54] J. Wu, B. Kwon, W. Liu, E. V. Anslyn, P. Wang, J. S. Kim, "Chromogenic/fluorogenic ensemble chemosensing systems" Chem. Rev. 115 (2015) 7893-7943.
[55] J. M. García, F. C. García, F. Serna, J. L. de la Peña, "Fluorogenic and chromogenic polymer chemosensors" Polymer Reviews 51 (2011) 341-390.

interacciones metal-analito, lo que provoca cambios en las propiedades de la subunidad emisora, generalmente de la absorción (color) o modificación de su fluorescencia. Este mecanismo es el más ampliamente utilizado[56,57,58,59].

En el segundo caso, al no existir interacción covalente entre ambas subunidades, la interacción entre el analito y la subunidad coordinante provoca el desplazamiento de la subunidad emisora y su liberación al medio, de manera que sus propiedades espectroscópicas se modifican (Figura 7(b)). Este proceso es reversible y existen en la literatura numerosos trabajos en los que se utiliza como método de detección[60,61].

Por último, existe otra posibilidad para el diseño de sensores químicos: el dosímetro químico[62,63]. Se basa en reacciones selectivas de la molécula sensor con el analito para dar lugar a una molécula diferente que muestra propiedades cromogénicas o de fluorescencia diferentes a su precursora (Figura 7(c)). La eficiencia de la molécula sensor se basa en la selectividad de la reacción química entre el analito y la molécula sensor. Este tipo de detección no puede clasificarse estrictamente como sensor químico debido a la irreversibilidad general de las reacciones, sino que debe emplearse el término dosímetro químico[64].

[56] M. Alfonso, A. Sola, A. Caballero, A. Tárraga, P. Molina, "Heteroditopic ligands based on ferrocenyl benzimidazoles fused to an additional diaza heterocyclic ring system" Dalton Trans. 43 (2009) 9653-9658.
[57] S. K. Kim, D. H. Lee, J. Hong, J. Yoon, "Chemosensors for pyrophosphate" Acc. Chem. Res. 42 (2009) 23-31.
[58] T. Gunnlaugsson, H. D. P. Ali, M. Glynn, P. E. Kruger, G. M. Hussey, F. M. Pfeffer, C. M. G. dos Santos, J. Tierney, "Fluorescent photoinduced electron transfer (PET) sensors for anions; from design to potential application" J. Fluoresc. 15 (2005) 287-299.
[59] A. P. de Silva, T. S. Moody, G. D. Wright, "Fluorescent PET (photoinduced electron transfer) sensors as potent analytical tools" Analyst 134 (2009) 2385-2393.
[60] P. A. Gale, L. J. Twyman, C. I. Handlin, J. L. Sessler, "A colourimetric calix[4]pyrrole–4-nitrophenolate based anion sensor" Chem. Commun. 18 (1999) 1851-1852.
[61] S. L. Wiskur, H. Ait-Haddou, J. J. Lavigne, E. V. Anslyn, "Teaching old indicators new tricks" Acc. Chem. Res. 34 (2001) 963–972.
[62] V. Dujols, F. Ford, A. W. Czarnik, "A long-wavelength fluorescent chemodosimeter selective for Cu(II) ion in water" J. Am. Chem. Soc. 119 (1997) 7386-7687.
[63] S. Y. Kim, J. I. Hong, "Chromogenic and fluorescent chemodosimeter for detection of fluoride in aqueous solution" Org. Lett. 9 (2007) 3109-3112.
[64] M. Y. Chae, A. W. Czarnik, "Fluorometric chemodosimetry-mercury(II) and silver(I) indication in water via enhanced fluorescence signaling" J. Am. Chem. Soc. 114 (1992) 9704–9705.

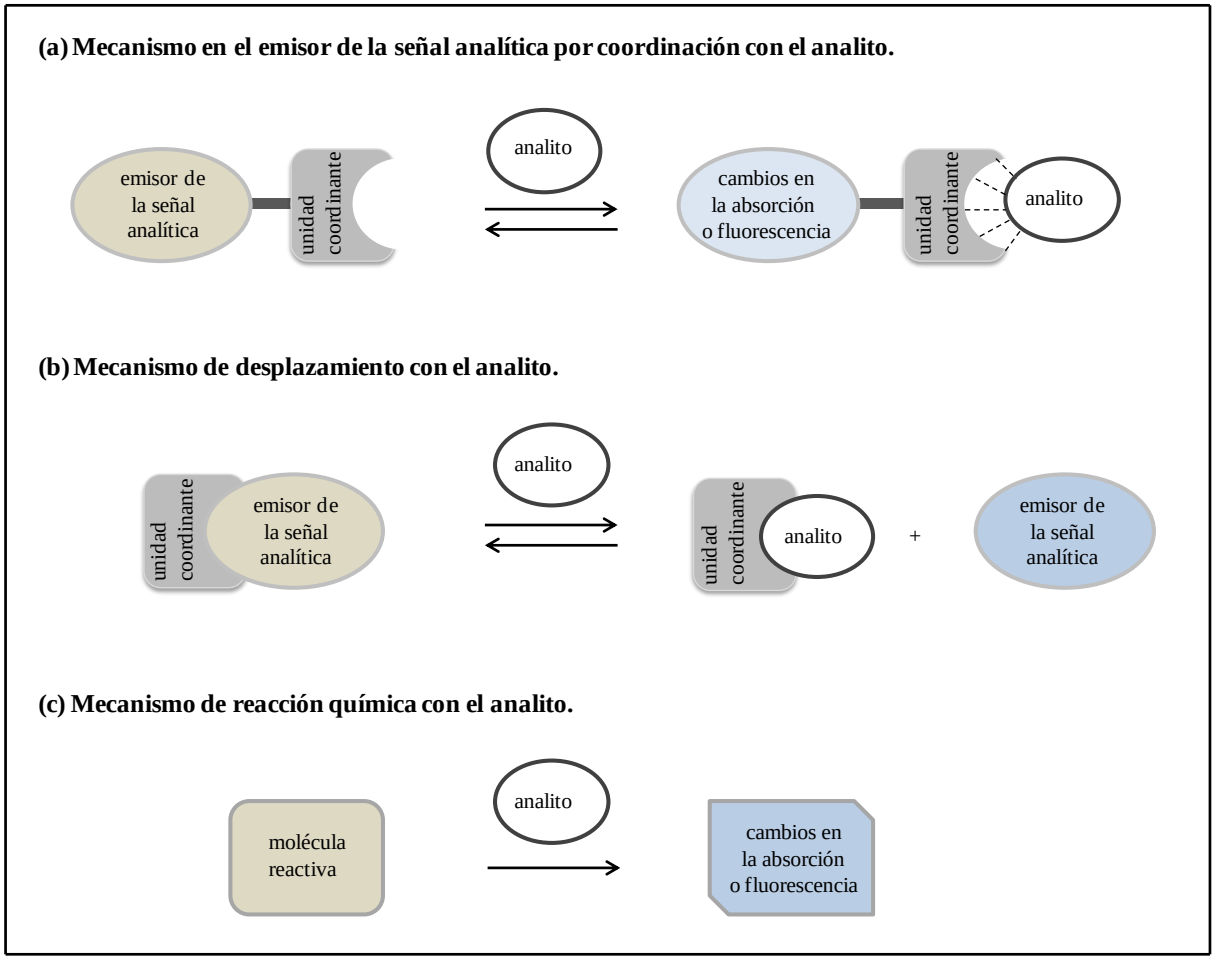

Figura 7. Esquema de actuación de los sensores cromogénicos y fluorogénicos en presencia de un analito.

En las últimas décadas se han desarrollado numerosos sensores fluorogénicos, cromogénicos y electroquímicos mediante la aplicación de los mecanismos descritos anteriormente.

Por otro lado, algunos investigadores han publicado trabajos basados en la inclusión de más de una unidad indicadora en la estructura de ciertos sensores[65,66,67,68]. También se han desarrollado sensores

[65] A. P. de Silva, D. B. Fox, T. S. Moody, S. M. Weir, "The development of molecular fluorescent switches" Trends Biotechnol. 19 (2001) 29-34.
[66] A. P. de Silva, H. Q. N. Gunaratne, C. P. McCoy, "Molecular photoionic and logic gates with bright fluorescence and "off-on" digital action" J. Am. Chem. Soc. 119 (1997) 7891-7892.
[67] F. Sancenón, A. Benito, F. J. Hernández, J. M. Lloris, R. Martínez-Máñez, T. Pardo, J. Soto, "Difuctionalised chemosensors containing electroactive and fluorescent signalling subunits" Eur. J. Inorg. Chem. 2002 (2002) 866-875.
[68] F. Zapata, A. Caballero, A. Espinosa, A. Tárraga, P. Molina, "Cation coordination Induced modulation of the anion sensing properties of a ferrocene-imidazophenanthroline dyad: multichannel recognition from phosphate-related to chloride anions" J. Org. Chem., 73 (2008) 4034–4044.

funcionalizados con solo una subunidad indicadora capaz de dar dos o más señales medibles, por ejemplo variaciones simultaneas de color y de intensidad de fluorescencia[69,70,71].

Se denomina fluoróforo a aquella molécula que tiene la capacidad de emitir luz por fluorescencia, tras un proceso de absorción. En un sensor fluorogénico, el fluoróforo estará unido a una unidad receptora o coordinante. La unidad coordinante es la responsable de la selectividad y eficiencia de coordinación con un analito determinado. Esta selectividad y eficiencia depende de la naturaleza de la unidad coordinante, las características químicas del analito y el disolvente en el que se lleva a cabo la interacción. La interacción del analito con la unidad coordinante va a afectar a los procesos fotoluminiscentes de la unidad de señalización ocasionando variaciones que van a permitir su detección, como la aparición o desaparición de fluorescencia, el desplazamiento del máximo de una banda de emisión y/o cambios en la intensidad de fluorescencia.

La detección y cuantificación de la acidez y/o basicidad en diferentes medios, como vapores o los sistemas acuosos, y en las industrias químicas y farmacéuticas, es de vital importancia para lograr un control ambiental. Si bien la presencia de protones (H^+) o iones hidroxilo (OH^-) en medios acuosos se determina empleando técnicas convencionales disponibles en cualquier laboratorio (como el papel indicador de pH o métodos pontenciométricos que emplean membranas sensibles al pH como los electrodos de membrana de vidrio), surge la necesidad de desarrollar métodos alternativos que satisfagan esta demanda. Los sensores químicos ópticos han adquirido gran popularidad en la detección de pH[72,73,74], tanto en el intervalo de trabajo habitual como en condiciones extremas.

También la detección de metales[75] en el medioambiente tiene mucha importancia, y en particular los más contaminantes como el mercurio. El mercurio es un metal pesado conocido por su alta toxicidad que supone un problema a nivel mundial. La mayoría de las emisiones de mercurio (Hg(0) y Hg (II)) al medioambiente son antropogénicas, como por ejemplo, la descarga de refinerías y fábricas, así como

[69] A. P. de Silva, H. Q. N. Gunaratne, M. Lynch, "Luminescence and charge transfer. Part 4. "On-off" fluorescent PET (photoinduced electron transfer) sensors with pyridine receptors: 1,3-diaryl-5-pyridyl-4,5-dihydropyrazoles" J. Chem. Soc., Perkin Trans. 2 (1995) 685-690.
[70] M. Zhu, M. Yuan, X. Liu, J. Xu, J. Lv, C. Huang, H. Liu, Y. Li, S. Wang, D. Zhu, "Visible Near-Infrared chemosensor for mercury ion" Org. Lett., 10 (2008) 1481-1484.
[71] M. Schmittel, H. W. Lin, Angew. Chem. Int. Ed. Engl., 46 (2007) 893-896.
[72] W. Niu, L. Fan, M. Nan, Z. Li, D. Lu, M. S. Wong, S. Shuang, C. Dong, "Ratiometric emission fluorescent pH probe for imaging of living cells in extreme acidity" Anal. Chem. 87 (2015) 2788-2793.
[73] J. L. Tan, T. T. Yang, Y. Liu, X. Zhang, S. J. Cheng, H. Zou, H. He, "Sensitive detection of strong acidic condition by a novel rhodamine-based fluorescent pH chemosensor" Luminiscence 31 (2016) 865-870.
[74] J. L. Tan, X. Zhang, F. Zhang, T. T. Yang, Y. Liu, Z. B. Li, H. Zuo, "A novel "off-on" colororimetric and fluorescent rhodamine based pH chemosensor for extreme acidity" Spectrochimia Acta Part A: Molecular and Biomolecular Spectroscopy 140 (2015) 489-494.
[75] M. Trigo-López, A. Muñoz, S. Ibeas, F. Serna, F. C. García, J. M. García, "Colorimetric detection and determination of Fe(III), Co(II), Cu(II) and Sn(II) in aqueous media by acrylic polymers with pendant terpyridine motifs" Sens. Actuators B Chem. 226 (2016) 118-126.

la escorrentía de vertederos y campos de cultivo. Entre las fuentes no antropogénicas se encuentran las emisiones volcánicas y los incendios forestales.

Los vapores de mercurio emitidos se difunden fácilmente en la atmósfera, y se oxidan a Hg (II). La deposición atmosférica del Hg (II) conduce a su acumulación en la vegetación, en el suelo y en los sistemas acuosos, siendo la contaminación de las aguas la mayor fuente de exposición para los humanos. Las bacterias que residen en las branquias e intestinos de los peces convierten parte del Hg (II) incorporado al agua en metilmercurio ($CH_3Hg(I)$). El metilmercurio se absorbe rápidamente pero se elimina con mucha dificultad por lo que acaba entrando en la cadena alimenticia humana, a través de la ingesta de peces como tiburón, caballa, atún, pez espada o ballena[76].

Además, la bioacumulación de mercurio también tiene lugar en las plantas, lo que supone otra vía de entrada en la cadena alimenticia[77]. El mercurio bioacumulado vuelve a entrar en los suelos y aguas a través de la lluvia o la putrefacción de las plantas.

La absorción de mercurio tiene consecuencias graves para la salud humana. La bioacumulación en el cerebro y los riñones causa serios problemas y puede conducir a enfermedades neurológicas, trastornos cognitivos y de movimiento, pérdida de visión y muerte.

Aunque se ha restringido el uso industrial de mercurio, se siguen encontrando altas concentraciones en algunos ecosistemas. Es por ello que existe una demanda cada vez mayor para la detección eficiente, económica y rápida de mercurio en sistemas acuosos, alimentos, aire y suelo. En consecuencia, el desarrollo de sensores cromogénicos y fluorogénicos para la detección y cuantificación del catión Hg (II) ha ganado terreno en los últimos años, como así lo demuestran los numerosos trabajos publicados en la bibliografía especializada. Algunos de estos trabajos describen sensores basados en derivados de rodamina[78,79,80], otros contienen tiourea en su estructura[81,82], compuestos heterocíclicos que contienen

[76] N. E. Selin, "Global Biogeochemical Cycling of Mercury: A review." Annu. Rev. Environ. Resour. 34 (2009) 43-64.
[77] R. P. Mason, F. M. M. Morel, H. F. Hemond, "The role of microorganisms in elemental mercury formation in natural waters" Water Air Soil Pollut. 80 (1995) 775-787.
[78] K. Bera, A. K. Das, M. Nag, S. Basak, "Development of a Rhodamine−Rhodanine-Based Fluorescent Mercury Sensor and Its Use to Monitor Real-Time Uptake and Distribution of Inorganic Mercury in Live Zebrafish Larvae". Anal. Chem. 86 (2014) 2740–2746.
[79] M. Wang, J. Wen, Z. Qin, H. Wang, "A new coumarin-rhodamine FRET system as an efficient ratiometric fluorescent probe for Hg^{2+} in aqueous solution and living cells" Dyes Pigm. 120 (2015) 208–212.
[80] W. Lin, X. Cao, Y. Ding, L. Yuan, Q. Yu, "A reversible fluorescent Hg2+ chemosensor based on a receptor composed of a thiol atom and an alkene moiety for living cell fluorescence imaging" Org. Biomol. Chem. 8 (2010) 3618–3620.
[81] F. Otón, A. Espinosa, A. Tárraga, I. Ratera, K. Wurst, J. Veciana, P. Molina, "Mononuclear Ferrocenophane Structural motifs with two thiourea arms acting as a dual binding site for anions and cations" Inorg. Chem. 48 (2009) 1566-1576.
[82] F. Lv, Y. Chen, T. Tang, Y. Chen, D. Xu, "A New Reactive 1,8-Naphthalimide Derivative for Highly Selective and Sensitive Detection of Hg^{2+}" J. Fluoresc. 27 (2017) 1285–1292.

nitrógeno, grupos azo o con bases de Schiff[83,84]; amina o tioéter[85,86]; moléculas que contienen cumarina[87,88,89] o sensores conteniendo macrociclos[90,91].

En la presente Tesis (Capítulo 3), se ha preparado y estudiado un nuevo sensor sólido polimérico reversible en sistemas acuosos para la detección de mercurio.

1.7 1,8-naftalimidas. Transferencia electrónica fotoinducida (PET) y transferencia de carga intramolecular (ICT).

Los derivados de la 1,8-naftalimida sustituidos en la posición 4 han sido reconocidos por sus excelentes propiedades fotofísicas, sus altos rendimientos cuánticos de fluorescencia y buenos desplazamientos de Stokes, lo que sumado a la relativa simplicidad de obtener derivados, ha hecho que tengan numerosas aplicaciones en una variedad de áreas diferentes. Así pues, han adquirido interés como sensores de cationes metálicos[92,93,94,95], aniones[96,97,98] y protones[99,100], agentes

[83] R. Arabahmadi, M. Orojloob, S. Amani, "Azo Schiff bases as colorimetric and fluorescent sensors for recognition of F^-, Cd^{2+} and Hg^{2+} ions" Anal. Methods, 6 (2014) 7384-7393.
[84] A. R. Chowdhury, P. Ghosh, B. G. Roy, S. K. Mukhopadhyay, P. Mitra, P. Banerjee, "A simple and dual responsive efficient new Schiff base chemoreceptor for selective sensing of F^- and Hg^{2+}: application to bioimaging in living cells and mimicking of molecular logic gates " RSC Adv. 5 (2015) 62017–62023.
[85] K. C. Song, J. S. Kim, S. M. Park, K. C. Chung, S. Ahn, S. K. Chang, "Fluorogenic Hg2+-selective chemodosimeter derived from 8-hydroxyquinoline" Org. Lett., 8 (2006) 3413-3416.
[86] G. Dhaka, J. Singh, N. Kaur "Benzothiazole based chemosensors having appended amino group(s): Selective binding of Hg^{2+} ions by three related receptors" 462 (2017) 152-157.
[87] M. G. Choi, Y. H. Kim, J. E. Namgoong, S. K. Chang, "Hg^{2+}-selective chromogenic and fluorogenic chemodosimeter based on thiocoumarins" Chem. Commun. (2009) 3560–3562.
[88] H. J. Kim, J. E. Park, M. G. Choi, S Ahn, S. K. Chang, "Selective chromogenic and fluorogenic signalling of Hg2+ ions using a fluorescein-coumarin conjugate" Dyes Pigm. 84 (2010) 54-58.
[89] C. Wu, J. Wang, J Shen, C. Bi, H. Zhou, "Coumarin-based Hg2+ fluorescent probe: Synthesis and turn-on fluorescence detection in neat aqueous solution" Sens. Actuators, B 243 (2017) 678-683.
[90] A. Jana, J. S. Kim, H. S. Jung, P. K. Bharadwaj, "A cryptand based chemodosimetric probe for naked-eye detection of mercury(II) ion in aqueous medium and its application in live cell imaging" Chem. Commun. (2009) 4417–4419.
[91] J. V. Ros-Lis, R. Casasus, M. Comes, C. Coll, M. D. Marcos, R. Martínez-Máñez, F. Sancenón, J. Soto, P. Amoros, "A Mesoporous 3D Hybrid Material with Dual Functionality for Hg^{2+} Detection and Adsorption" Chem. Eur. J. 14 (2008) 8267-8278.
[92] D. Staneva, D. Makki, T. Sobahi, P. Bosch, R. Abdel-Rahman, A. Asiri, I. Grabchev, "Synthesis and spectral characterization of a new blue fluorescent tripod for detecting metal cations and protons" J. Lumin., 162 (2015) 149-154.
[93] S. M. Dimov, N. I. Georgiev, A. M. Asiri, V. B. Bojinov, "Synthesis and Sensor Activity of a PET-based 1, 8-naphthalimide Probe for Zn2+ and pH Determination" J Fluoresc, 24 (2014) 1621-1628.
[94] X. Zhang, W. Shi, X. Chen, Z. Xie, "Isocyano-functionalized, 1,8-naphthalimide-based chromophore as efficient ratiometric fluorescence probe for Hg^{2+} in aqueous medium." Sens. Actuators B 255 (2018) 3074-3084.
[95] N. Marinova, N. Georgiev, V. Bojinov, "Facile synthesis, sensor activity and logic behaviour of 4-aryloxy substituted 1,8-naphthalimide" J Photochem Photobiol A Chem 254 (2013) 54–56.
[96] E. B. Veale, T. Gunnlaugsson, "Bidirectional Photoinduced Electron-Transfer Quenching Is Observed in 4-animo-1,8-naphthalimide-Based Fluorescent Anion Sensors" J. Org. Chem. 73 (2008) 8073-8076.

anticancerígenos[101,102], marcadores fluorescentes en biología[103,98], abrillantadores fluorescentes[104], en células solares[105,106] y en medicina[107].

Si estos sensores basados en 1,8-naftalimida se diseñan de manera que el fluoróforo y el receptor están unidos a través de un espaciador, el mecanismo de interacción con analitos se producirá a través de un proceso de transferencia electrónica fotoinducida (PET)[108], que puede dar lugar a un proceso de encendido "turn-on" o apagado "turn-off" de la fluorescencia.

El proceso "turn-on"[109] se observa en receptores con pares de electrones no enlazantes (N ó O). Como se puede observar en la Figura 8, cuando se excita el fluoróforo, promociona un electrón desde el orbital molecular ocupado de más alta energía (HOMO) al orbital molecular no ocupado de más baja energía (LUMO). El par de electrones de no enlace, que se encuentra en un nivel energético intermedio entre los orbitales HOMO y LUMO del fluoróforo, transfiere un electrón al orbital HOMO del fluoróforo, lo que conduce a la desactivación de la fluorescencia. El fluoróforo excitado transfiere el electrón del LUMO al orbital de energía intermedia, restaurándose el estado fundamental. Tras la

[97] E. B. Veale, G. M. Tocci, F. M. Pfeffer, P. E. Kruger, T. Gunnlaugsson, "Demonstration of bidirectional photoinduced electron transfer (PET) sensing in 4-amino-1,8-naphthalimide based thiourea anion sensors" Org. Biomol. Chem. 7 (2009) 3447-3454.
[98] H. H. Lin, Y. C. Chan, J. W. Chen, C. C. Chang, "Aggregation-induced emission enhancement characteristics of naphthalimide derivatives and their applications in cell imaging" J. Mater. Chem. 21 (2011) 3170-3177.
[99] A. Schulz, J. Wotschadlo, T. Heinze, G. J. Mohr, "Fluorescent nanoparticles for ratiometric pH-monitoring in the neutral range" J. Mater. Chem. 20 (2010) 1475-1482.
[100] A. M. Asiri, A. Qusti, K. Alamry, V. Bojinov, "Design and synthesis of pH-selective fluorescence sensing PAMAM light-harvesting dendrons based on 1,8-naphthalimides" Sens. Actuators B: Chem. 190 (2014) 185–198.
[101] S. Banerjee, E. B. Veale, C. M. Phelan, S. A. Murphy, G. M. Tocci, L. J. Gillespie, D. O. Frimannsson, J. M. Kelly, T. Gunnlaugsson, "Recent advances in the development of 1,8-naphthalimide based DNA targeting binders, anticancer and fluorescent cellular imaging agents" Chem. Soc. Rev. 42 (2013) 1601-1618.
[102] L. González-Bulnes, J. Gallego, "Indirect Effects Modulating the Interaction between DNA and a Cytotoxic Bisnaphthalimide Reveal a Two-Step Binding Process" J. Am. Chem. Soc. 131 (2009) 7781-7791.
[103] J. Zhou, C. Fang, T. Chang, X. Liu, D. Shangguan, "A pH sensitive ratiometric fluorophore and its application for monitoring the intracellular and extracellular pHs simultaneously" J. Mater. Chem. B 1 (2013) 661-667.
[104] V. Bojinov, I. Grabchev, "A new method for synthesis of 4-allyloxy-1,8-naphthalimide derivatives for use as fluorescent brighteners" Dyes Pigments 51 (2001) 57-61.
[105] A. S. A. Almalki, A. Alhadhrami, A. M. A. Adam, I. Grabchev, M. Almeataq, J. Y. Al-Humaidi, T. Sharshar, M. S. Refat, "Preparation of elastic polymer slices have the semiconductors properties for use in solar cells as a source of new and renewable energy" journal of Photochemistry and Photobiology A: Chemistry 15 (2018) 76-85.
[106] Y. J. Lin, J. W. Chen, P. T. Hsiao, Y. L. Tung, C. C. Chang, C. M. Chen, "Efficiency improvement of dye-sensitized solar cells by in situ fluorescence resonance energy transfer" J. Mater. Chem. A 5 (2017) 9081-9089.
[107] H. H. Gong, D. Addla, J. S. Lv, C. H. Zhou, "Heterocyclic Naphthalimides as New Skeleton Structure of Compounds with Increasingly Expanding Relational Medicinal Applications" Curr. Top. Med. Chem. 16 (2016) 3303–64.
[108] P. Panchenko, O. Fedorova, Y. Fedorov, "Fluorescent and colorimetric chemosensors for cations besed on 1,8-naphthalimide derivatives: design principles and optical signaling mechanisms" Russ. Chem. Rev. 83 (2014) 155-182.
[109] L. J. Fan, Y. Zhang, C. B. Murphy, S. E. Angell, M. F. L. Parker, B. R. Flynn, W. E. Joner, Jr., "Fluorescent conjugated polymer molecular wire chemosensors for transition metal ion recognition and signaling" Coord. Chem. Rev. 253 (2009) 410-422.

coordinación con el analito, el orbital intermedio entre el HOMO y LUMO del fluoróforo baja en energía de manera que la transferencia electrónica ya no es posible y se produce un aumento en la intensidad de fluorescencia.

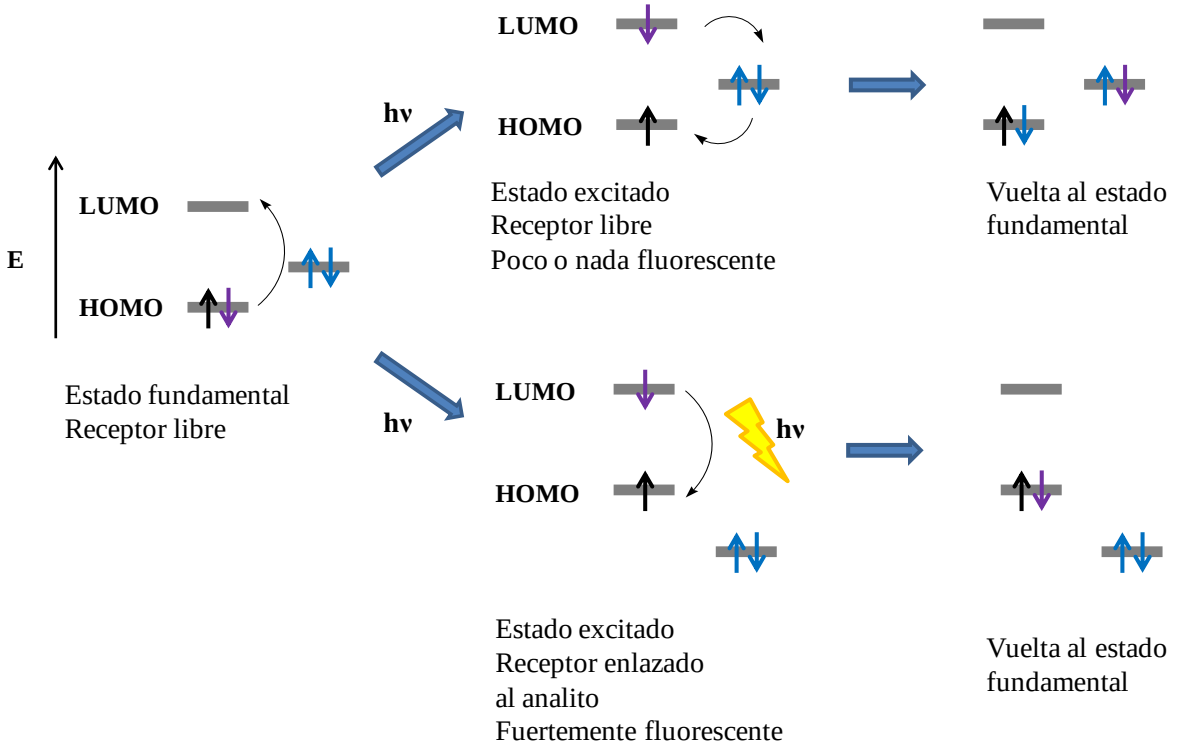

Figura 8. Esquema del proceso "turn-on" PET.

El proceso "turn-off"[109] tiene lugar cuando el nivel energético del LUMO del analito se encuentra entre el HOMO y el LUMO del receptor. Por lo tanto, tras la interacción entre el receptor y el analito, se proporciona un camino no radiativo para disipar la energía de excitación, dando lugar al apagado o quencheo de fluorescencia, como se representa en la Figura 9.

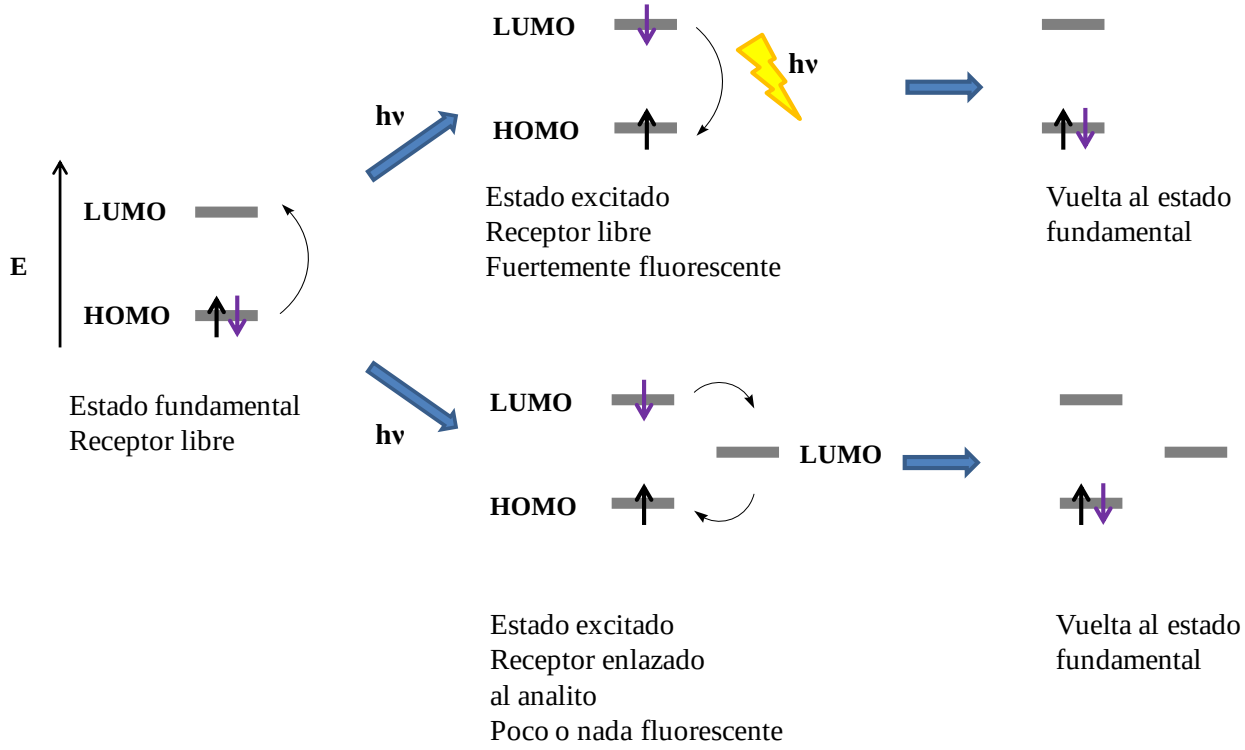

Figura 9. Esquema del proceso "turn-off" PET.

Si el sensor posee un grupo electrodonador conjugado con un grupo electroaceptor[108], experimentará una transferencia de carga intramolecular, desde el donador al aceptor. Cuando un analito interacciona con el grupo donador de electrones reducirá el carácter electrodonador de éste, lo que desestabiliza el momento dipolar en el estado excitado, produciéndose un desplazamiento hipsocrómico de la banda de absorción y, en el caso de las 1,8-naftalimidas un apagado de su fluorescencia ("turn-off"). Dicho mecanismo se ilustra en la figura 10(a). Por el contrario, cuando un analito interacciona con el grupo electroaceptor, incrementará el carácter aceptor de electrones de éste, estabilizando el estado excitado y produciéndose un desplazamiento batocrómico (Fig. 10(b)).

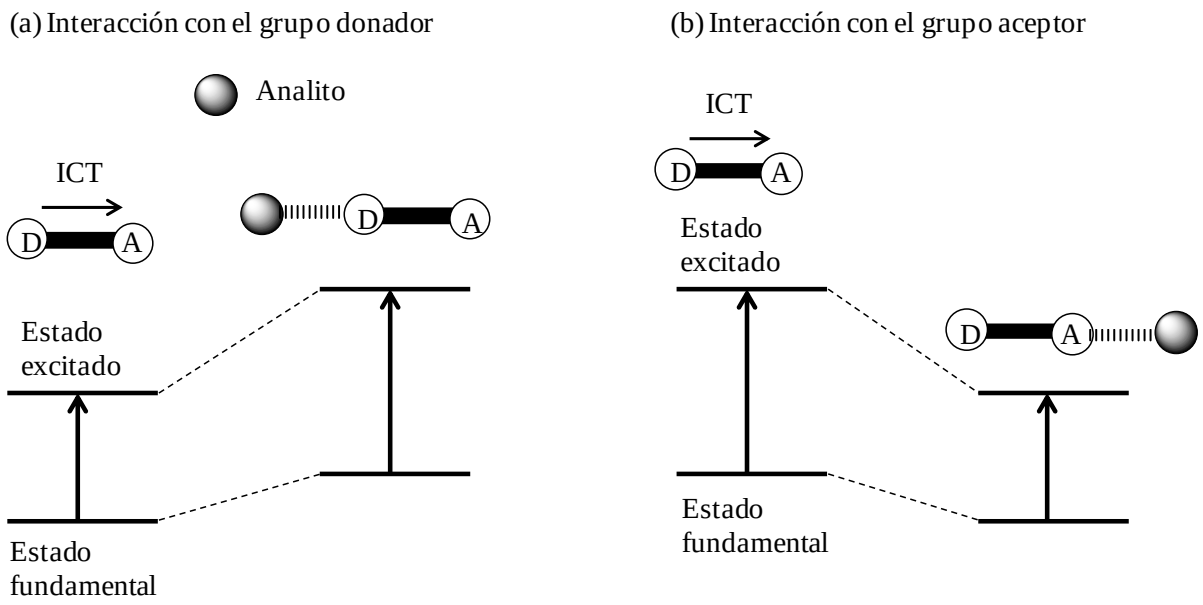

Figura 10. Mecanismo de transferencia de carga intramolecular (ICT). El analito puede interactuar con el grupo donador (a) o con el aceptor (b).

En este Trabajo se ha sintetizado una serie de moléculas derivadas de la 1,8-naftalimida, que actúan como sensores fluorogénicos a través del mecanismo PET y a través la inhibición de la transferencia de carga intramolecular, ICT "turn-off", como es el caso del derivado dimetil amino en posición 4 de la 1,8 naftalimida.

En la figura 11(a) se muestra el proceso PET "turn-on" de encendido fluorescente que presentan en medio ácido las 1,8-naftalimidas sustituidas en la posición 4 con piperacinas. En la figura 11(b) se muestra el proceso "turn-off" de la ICT en el derivado sin espaciador, 4-dimetilamino (donador) 1,8-naftalimida (aceptor) en presencia de protones en el medio.

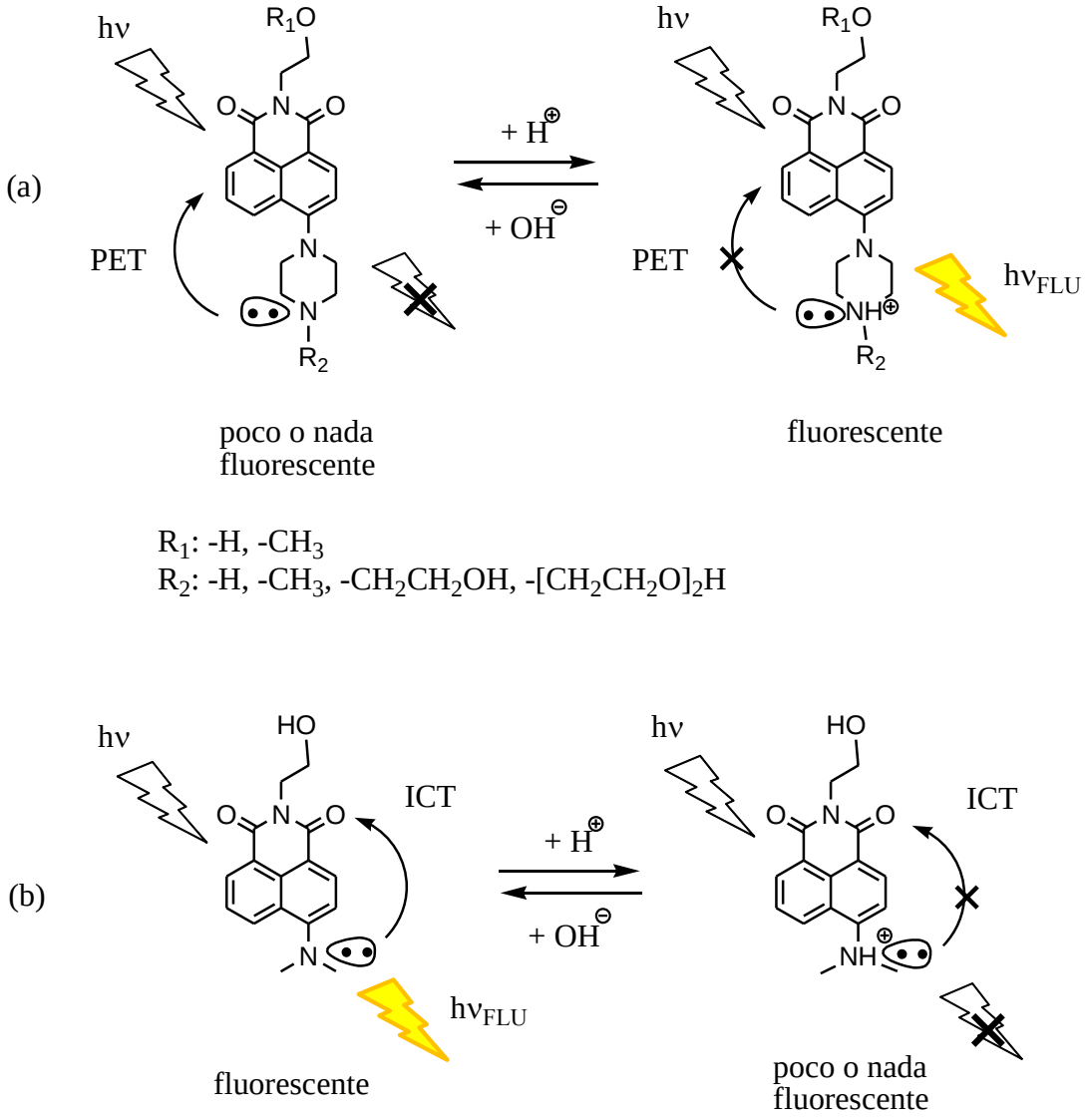

Figura 11. Estructura química de los derivados de la 1,8-naftalimida que actúan a través del mecanismo PET "turn-on" (a) e ICT "turn-off".

En el caso de los derivados de la 1,8-naftalimida, el anillo naftaleno con sustituyente electrodonador actúa como subunidad de señalización o fluoróforo, y el N (que tiene un par electrónico disponible) en la posición 4 del anillo actúa como unidad coordinante que cambia su emisión.

1.8 Polímeros como sensores químicos fluorogénicos y cromogénicos.

Después del desarrollo de una molécula sensor fluorogénica y/o cromogénica para la detección del analito de interés, surge la necesidad de incorporarla a un soporte sólido para que sus aplicaciones prácticas sean óptimas[55].

Este soporte debe reunir una serie de condiciones:

- Permitir la difusión del analito a través del mismo o tener una superficie sensible al analito.
- Buenas propiedades físicas, químicas, térmicas y mecánicas.
- Transparencia.
- Fácil procesado.
- Bajo coste.

Los polímeros soporte de moléculas sensores pueden prepararse o transformarse en filmes[110], o recubrimientos[111], por lo que ambos tipos de sustratos poliméricos han sido ampliamente utilizados.

Paralelamente a la producción de sistemas sensores de base polimérica, se han desarrollado otros sistemas en los que se emplean materiales soporte tales como partículas de sílice[112], superficies de vidrio[113] y oro[114].

En función de la estructura polimérica de los sensores químicos descritos en la literatura[115], los sistemas sensores poliméricos se pueden clasificar en:

- Polímeros lineales no conjugados[116,117]
- Polímeros lineales conjugados[118]

[110] S. Vallejos, A. Muñoz, F. C. García, R. Colleoni, R. Biesuz, G. Alberti, J. M. García, "Colorimetric detection, quantification and extraction of Fe(III) in water by acrylic polymers with pendant Kojic acid motifs" Sens. Actuators B Chem. 233 (2016) 120-126.
[111] J. P. Anzenbacher, Y. Liuand, M. E. Kozelkova, "Hydrophilic polymer matrices in opical array sensing" Curr. Opin. Chem. Biol. 14 (2010) 1-12.
[112] Q. Meng, X. Zhang, C. He, G. He, P. Zhou, C. Duan, "Multifuctional mesoporous silica material used for detection and adsorption of Cu^{2+} in aqueous solution and biological applications in vitro and in vivo" Adv, Funct. Mater. 20 (2010) 1903-1909.
[113] P. Qin, C. Han, D. Huang, R. Tang, F. Gan, C. Niu, "A wide range fluorescent sensor for 2,4,6-trinitrophenol prepared from covalent immobilization of allyltetraiodofluorescein on activated glass surface" Sensor Letters 12 (1) (2014) 172-176.
[114] S. Sun, X. Ning, G. Zhang, Y. C. Wang, C. Peng, J. Zheng, "Dimerization of organic dyes on luminescent gold nanoparticles for ratiometric pH sensing" Angew Chem. Int. Ed. Engl. 55(7) (2016) 2421-2424.
[115] H. N. Kim, Z. Guo, W. Zhu, J. Yoon, H. Tian, "Recent progress on polymer-based fluorescent and colorimetric chemosensors" Chem. Soc. Rev. 40 (2011) 79-93.
[116] Z. Guo, W. Zhu, H. Tian, "Hydrophilic copolymer bearing dicyanomethylene-4H-pyran moiety as fluorescent film sensor for $Cu^{2+}$and pyrophosphate anion" Macromolecules 43 (2) (2010) 739-744.
[117] S. Ghosh, C. K. Dey, "Epoxy-bases polymer bearing activated azo dye (methyl orange) units: novel colorimetric indicator for amines" Supramol. Chem. 21 (2009) 591-596.

- Polímeros dendríticos[119]
- Polímeros impresos molecularmente (MIPs)[120]
- Redes poliméricas tridimensionales

Los métodos más comunes de inmovilización de las moléculas sensores en matrices poliméricas son la dispersión y la unión covalente. La dispersión de la molécula a través de la matriz es el método más común y sencillo. Sin embargo, este método da lugar a materiales no homogéneos y proporciona problemas de estabilidad debido a la lixiviación de la molécula, reduciendo la vida útil y la reproducibilidad del material sensor. A pesar de ello, este método se utiliza para la preparación de filmes delgados sensibles o microesferas[121,122]. Para la mejora de la estabilidad de estos materiales, la alternativa es la unión covalente al polímero de la molécula sensor, siendo esta unión posible después de la polimerización si el polímero contiene grupos funcionales reactivos, o por copolimerización directa de la molécula sensor si ésta posee grupos polimerizables.

Existen en la bibliografía trabajos dedicados al desarrollo de sensores sólidos para la detección de cationes mercurio (II) en medios acuosos[123,124,125,126,127,128]. Sin embargo, son bastante escasos en la literatura los ejemplos de sensores para la detección cromogénica de pH[129,130].

[118] Y. Chen, K. Y. Pu, Q. L. Fan, X. Y. Qi, Y. Q. Huang, X. M. Lu, W. Huang, "Water-soluble anionic conjugated polymers for metal ion sensing: Effect of interchain aggregation" J. Polym. Sci. Part A: Polym. Chem. 47 (2009) 5057-5067.
[119] J. S. Kim, S. Y. Lee, J. Yoon, J. Vicens, "Hyperbranched calixarenes: synthesis and applications as fluorescent probes" Chem. Commun. 0 (2009) 4791-4802.
[120] W. Zhang, W. Liu, P. Li, H. Xiao, H. Wang, B. Tang, "A fluorescence nanosensor for glycoproteins with activity based on the molecularly imprinted spatial structure of the target and boronate affinity" Angew Chem., Int. Ed. 53 (2014) 12489-12493.
[121] Y. Amao, "Probes and polymers for optical sensing of oxygen" Microchim. Acta 143 (2003) 1-12.
[122] K. J. Albert, S. D. Gill, "Automatic decoding of sensor types within randomly ordered, high-density optical sensor arrays" Anal. Bioanal. Chem. 373 (2002) 792-802.
[123] H. El Kaoutit, P. Estévez, S. Ibeas, F. C. García, F. Serna, F. B. Benabdelouahab, J. M. García, "Chromogenic and fluorogenic detection of cations in aqueous media by means of an acrylic polymer chemosensor with pendant Rhodamine-based dyes" Dyes Pigment 96 (2013) 414-423.
[124] J. L. Pablos, S. Ibeas, A. Muñoz, F. Serna, F. C. García, J. M. García, "Solid polymer and metallogel networks based on a fluorene derivative as fluorescent and colourimetric chemosensors for Hg(II)" React. Funct. Polym. 79 (2014) 14-23.
[125] S. Hussain, S. De, P. K. Iyer, "Thiazole-containing conjugated polymer as a visual and fluorometric sensor for iodine and mercury" ACS Appl. Mater. Interfaces 5 (2013) 2234-2240.
[126] S. A. Shahamirifard, M. Ghaedi, "Design and construction of a new optical solid-state mercury(II) sensor based on PVC membrane sensitized with colloidal carbon dots" New J. Chem. 41 (2017) 11533-11545.
[127] E. Ermakova, J. Michalak, M. Meyer, V. Arslanov, A. Tsivadze, R. Guilard, A. Bessmertnykh-Lemeune, "Colorimetric Hg^{2+} sensing in water: from molecules toward low-cost solid devices" Org. Lett. 15 (2013) 662-665.
[128] L. Q. Xu, K-G. Neoh, E-T. Kang, G. D. Fu, "Rhodamine derivative-modified filter papers for colorimetric and fluorescent detection of Hg^{2+} in aqueous media" J. Mater. Chem. A 1 (2013) 2526-2532.
[129] M. Trigo-López, J. L. Pablos, A. Muñoz, S. Ibeas, F. Serna, F. C. García, J. M. García, "Aromatic polyamides and acrylic polymers as solid sensory materials and smart coated fibres for high acidity colorimetric sensing" Polym. Chem. 6 (2015) 3110-3120.

En este Trabajo, se ha llevado a cabo la modificación superficial de filmes de copolímeros de etileno-acrilato de butilo (EBA)[131] mediante reacciones en fase heterogénea empleando radiación microondas. La modificación consiste en tres pasos: hidrólisis parcial de los ésteres butílicos a carboxilatos, protonación a ácido carboxílico y conversión de los grupos ácido a cloruro de ácido. Los copolímeros así modificados superficialmente se han funcionalizado por esterificación con 4-dimetilamino-N-(2-hidroxietil)-1,8-naftalimida. Posteriormente se han tratado con plasma de oxígeno para mejorar las propiedades hidrofílicas de la superficie de los filmes y mejorar el tiempo de respuesta en la detección en sistemas acuosos.

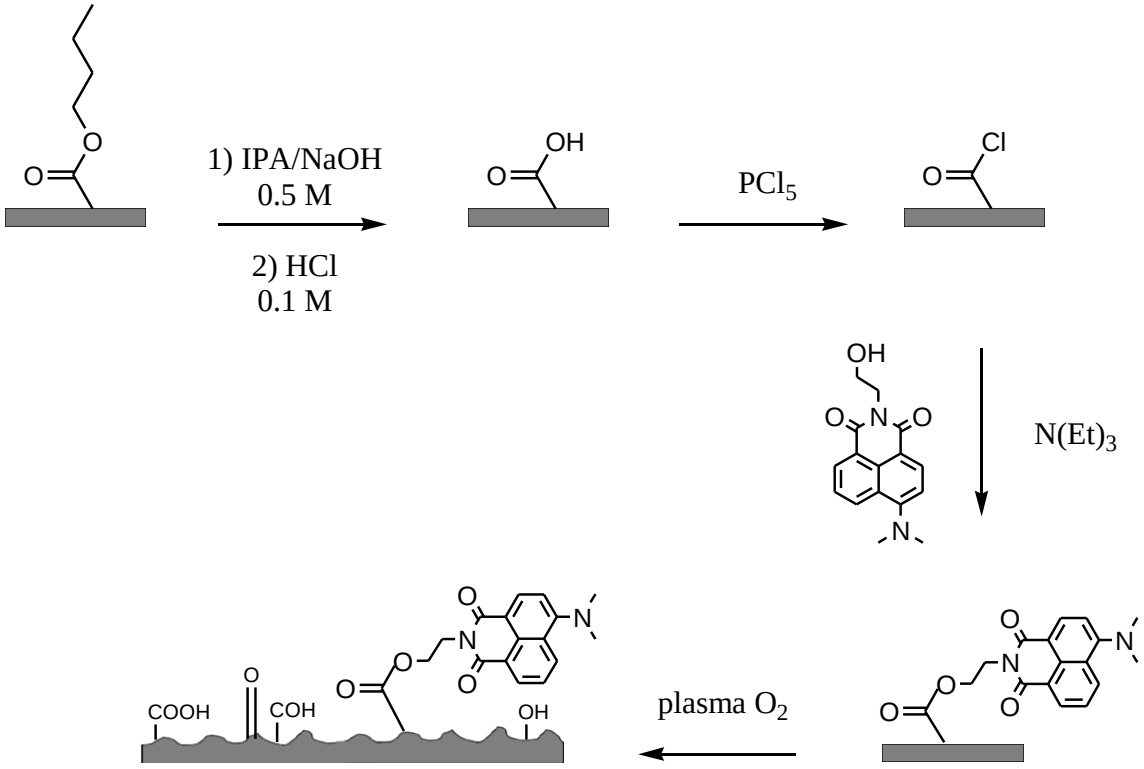

Figura 12. Secuencia de reacciones para la modificación superficial de EBA y posterior tratamiento con plasma.

[130] J. L. Pablos, P. Estévez, A. Muñoz, S. Ibeas, F. Serna, F. C. García, J. M. García, "Polymer chemosensors as solid films and coated fibres for extreme acidity colorimetric sensing" J. Mater. Chem. A 3 (2015) 2833-2843.
[131] S. Fernández-Alonso, T. Corrales, J. L. Pablos, F. Catalina, "Surface modification of poly(ethylene-butyl acrylate) copolymers by microwave methodology and functionalization with 4-dimethylamino-N-(2-hydroxyethyl)-1,8-naphthalimide for acidity sensing" React. Funct. Polym. 107 (2016) 78-86.

Por otra parte, se prepararon membranas poliméricas fotoentrecruzadas, con comportamiento de hidrogel con grado de hinchamiento controlado en medios acuosos. Para ello, la estructura del hidrogel se obtuvo a partir de una composición de monómeros diseñada para tener el equilibrio correcto de carácter hidrofóbico e hidrofílico con el fin de tener buenas propiedades mecánicas, lo que hace que los materiales sean manejables y que el hinchamiento en agua sea el adecuado (30% p/p) para mantener una estabilidad dimensional del material. El carácter hidrófilo del polímero, puede controlarse no solo por la naturaleza y/o proporción de los monómeros, sino también por el contenido del agente entrecruzante. La absorción de agua permite la difusión de productos químicos solvatados en la membrana, donde la detección se logra a través de la interacción de las moléculas sensores con el analito.

En esta Tesis, las membranas se han sintetizado por copolimerización de N-vinil-2-pirrolidona (VP), acrilato de butilo (BA), dimetacrilato de etilenglicol (EGDMA) y cloruro de metacriloilo (MACl) empleando Irgacure 2959 como fotoiniciador y en presencia de Argon.

En una segunda etapa, las membranas se funcionalizaron a través del cloruro de ácido presente en la estructura mediante esterificación con las moléculas sensores derivadas de 1,8-naftalimidas y portadoras de un sustituyente hidroxilo para llevar a cabo la reacción de Schotten-Bauman[132,133]. En la siguiente figura se muestra el esquema de síntesis de la membrana y su funcionalización con dos de las estructuras sintetizadas en esta Tesis.

[132] S. Fernández-Alonso, T. Corrales, J. L. Pablos, F. Catalina, "Solid fluorescence sensors obtained by functionalization of photocrosslinked water-swollen acrylic membranes with 4-piperazine naphthalimide derivatives" Polymer 124 (2017) 139-150.

[133] S. Fernández-Alonso, T. Corrales, J. L. Pablos, F. Catalina, "A Switchable fluorescence solid sensor for Hg^{2+} detection in aqueous media based in a photocrosslinked membrane functionalized with (benzimidazolyl)methyl-piperazine derivative of 1,8-naphthalimide" Sens. Actuators B Chem. 270 (2018) 256-262.

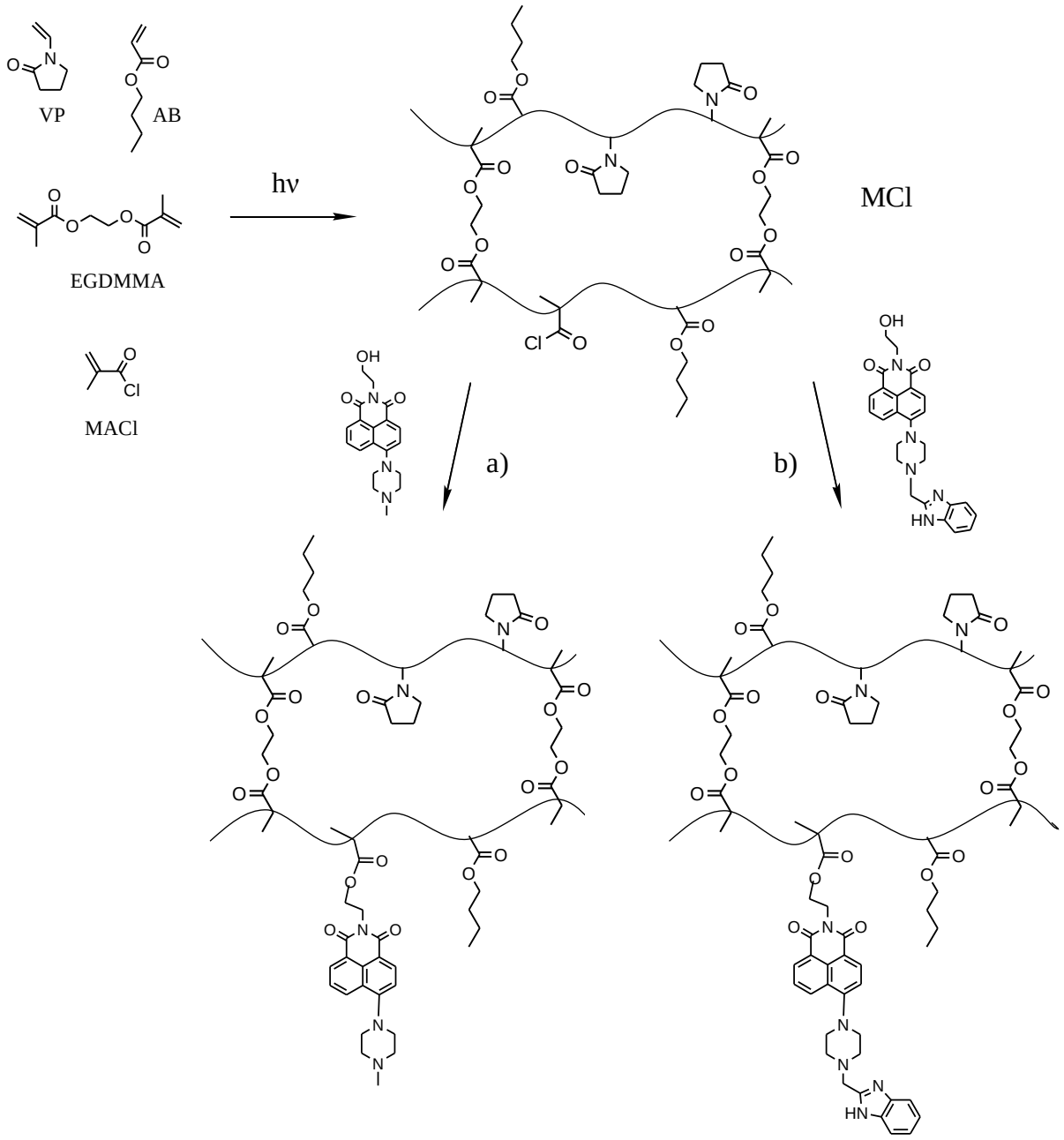

Figura 13. Síntesis de membrana fotoentrecruzada (M-Cl) y posterior funcionalización con derivados de 1,8-naftalimida: a) N-(2-hidroxietil)-4-(4-metilpiperacina-1-il)-1,8-naftalimida y b) N-(2-hidroxietil)-4-(4-(1H-benzo[d]imidazol-2-il)metil)piperacina-1-il)-1,8-naftalimida.

En los siguientes capítulos se detallan los resultados obtenidos incluyendo las tres publicaciones a que han dado lugar estos trabajos.

CAPÍTULO 2

Surface modification of poly (ethylene-butyl acrylate) copolymers by microwave methodology and functionalization with 4-dimethylamino-n-(2-hydroxyethyl)-1,8-naphthalimide for acidity sensing.

2 SURFACE MODIFICATION OF POLY (ETHYLENE-BUTYL ACRYLATE) COPOLYMERS BY MICROWAVE METHODOLOGY AND FUNCTIONALIZATION WITH 4-DIMETHYLAMINO-N-(2-HYDROXYETHYL)-1,8-NAPHTHALIMIDE FOR ACIDITY SENSING

2.1 Abstract

A new procedure was developed for functionalization in the solid phase by using microwave irradiation. Heterogeneous chemical modification of poly(ethylene-butyl acrylate) copolymer (EBA), hydrolysis, chlorination, and Schotten–Baumann reactions were monitored by attenuated total reflection Fourier transform infrared (ATR-FTIR) spectroscopy. EBA was superficially functionalized by a previously synthesized fluorescent dye, 4-dimethylamino-N-(2-hydroxyethyl)-1,8-naphtalimide, and the depth profile of the functionalized polymer was determined by confocal Raman spectroscopy. The new functionalized materials were also evaluated as an acidic pH sensor by determining the change in the spectroscopic properties of absorption and fluorescence with pH of the solution and vapor phases. To improve the wettability of the EBA surface, oxygen plasma treatment was used and the response time of the solid sensor was analyzed.

2.2 Introduction

An effective approach to develop an applicable solid sensor is to modify the surface of the material that already has excellent bulk properties. A grafted surface can be produced primarily either by graft polymerization of monomers or a covalent coupling reaction of existing polymer molecules onto the substrate polymer surface. Many chemical and physical methods[1], such as plasma, e-beam, and sputtering have been used to modify the structure of polymer surfaces and in particular polyethylenes[2]. Most of these techniques are based on the use of high-energy sources that can ultimately damage the polymer surfaces either chemically or physically. Moreover, these methods are usually not versatile enough to allow the design of structurally and chemically modified surfaces through the control of the distribution of chemical functionalities throughout the surface. In an earlier work, we described the microwave-assisted chemical modification of poly(ethylene-butyl acrylate) copolymers[3] (EBA) in solution to bind coumarin derivatives through the acrylic comonomer. In this study, organic functionalities were introduced onto EBA as the polymer substrate in a controlled manner by performing a sequence of chemical reactions on the surface. In the heterogeneous phase, hydrolysis, chlorination and Schotten–Baumann reactions were used to graft a naphthalimide derivative to the surface of EBA. The sequence of reactions carried out is shown in figure 1.

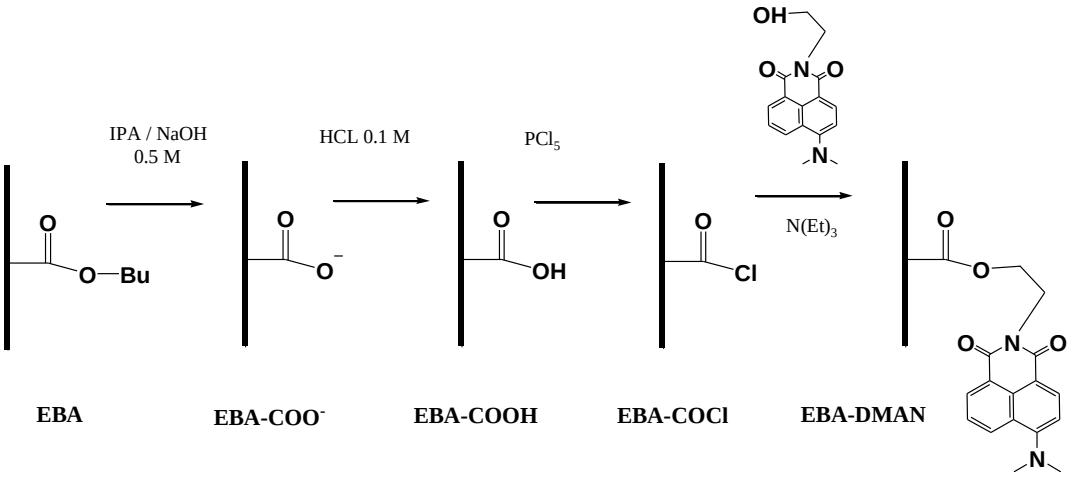

Fig.1. Heterogeneous reaction sequence for surface modification of EBA using microwave methodology.

The introduction of specific functional groups to polymer surfaces by well-defined, classical organic chemical reactions usually involves ionic or polar reactions rather than free radical reactions. Therefore, the polymer surfaces suitable for this type of modification must have sites that are vulnerable to electrophilic or nucleophilic attack.

The modification of the EBA surface opens the possibility to chemically bond numerous organic structures having a terminal group capable of reacting with the functional groups present on the substrate polymer surface. Recently, polymers containing photosensitive functional groups have gained significant attention[4,5,6]. A number of publications have appeared concerning 1,8-naphthalimide derivatives as a special class of environmentally sensitive fluorophores. Their strong fluorescence and good photostability have promoted their applications in a number of areas such as, coloration of polymers[7,8] as laser active media[9], fluorescence markers in biology[10], anticancer agents[11], light-emitting diodes[12], photoinduced electron transfer sensors[13,14], fluorescence switchers[15], electroluminescent materials[16,17], liquid crystal displays[18], ion probes[19] and pH sensors[20].

Hence, in this study, we synthesized a hydroxyl derivative, 4-dimethylamino-N-(2- hydroxyethyl)-1,8-naphtalimide (DMAN) to react with the superficial chlorine acids of the modified EBA to functionalize the polyolefin material with a sensor probe (EBA-DMAN), as shown in Fig. 1. The surface functionalization was studied by attenuated total reflection Fourier transform infrared (ATR-FTIR) spectroscopy and confocal Raman spectroscopy (CRS)[21] to determine the depth profile of the functionalized polymer.

Furthermore, the new functionalized materials were evaluated as an acidic pH sensor by determining the change in the spectroscopic properties of absorption and fluorescence with pH. To improve the wettability of the surface, EBA-DMAN films were treated with oxygen plasma[22]. The plasma-treated materials (EBA-pl-DMAN) exhibited a lower response time for environmental changes of pH in solution and vapors because of surface oxidation.

2.3 Experimental

2.3.1 Materials and reagents and film preparation

Poly(ethylene-co-butyl acrylate) copolymer (EBA) with 7 % (w/w) of butyl acrylate (0.924 $g \cdot ml^{-1}$ of density) was supplied by Repsol company (Madrid, Spain). EBA films of 100 μm of thickness and 50 x 50 mm dimension were prepared by compression molding in automatic Press ATLAS T8 plates with a maximum pressure of 2 tons and of 190 ºC of temperature. The thickness of the films was controlled by specific-size spacer rings.

The following chemicals and solvents were purchased and used as received unless otherwise indicated: 4-bromo-1,8-naphthalic anhydride (Aldrich, 95%). 2-propanol (Scharlau, 99.5%), sodium hydroxide (Panreac, 98-100%), hydrochloric acid (VWR Chemicals, 37%), ultrapure MilliQ water (Millipore), diiodomethane (Aldrich, ≥99.5%), dichloromethane (Aldrich, ≥99.9%), phosphorus

pentachloride (Aldrich, ≥98%), triethylamine (Aldrich, ≥99%), 2-aminoethanol (Aldrich, 99%), ethanol (VWR Chemicals, 99.95%), dimethylformamide (Scharlau, 99.8%), ethyl acetate (Aldrich, ≥99.5%), hexane (Carlo Erba Reagents, 99%), hexadeuterated dimethylsulfoxide (DMSO-d_6, Euriso-top, 99.8%), potassium carbonate (Panreac, 99%), and coumarin 6 (Aldrich, 98%).

2.3.2 Spectroscopic characterization

ATR-FTIR was used to characterize polymer films of EBA before and after MW reactions. ATR-FTIR spectra were obtained using a PERKIN ELMER BX-FTIR Spectrometer coupled with a MIRacle^{TM}ATR accessory from PIKE Technologies, and interferograms were obtained from 32 scans. The degree of hydrolysis and modifications of the EBA films were determined using ATR-FTIR and accessories with the same value of pressure.

Confocal Raman Spectroscopy (CRS). A Renishaw inVia Raman microscope, working in a confocal mode and connected to an Olympus BH2 microscope was used for measuring the Raman spectra. The beam from the 785 line of a He-Ne laser (laser power 320 mW at 100%) was focused by 100 x magnifying length objective (numerical aperture (NA) value of 0.85) in the confocal mode and a charge-coupled device (CCD) camera as detector. Raman light was dispersed by a diffraction grating with 1200 lines/mm using a Raman holographic notch filter. The depth-profile of the sample was obtained by focussing the microscope stepwise at fixed 1 μm intervals within the polymer film and recording 10 accumulative spectra at each step (accumulation time 3 min. per spectrum). The depth resolution of the confocal arrangement in air was previously checked using a sample of silica as a reference material.

Ultraviolet (UV) spectroscopy was used for the quantitative determination of DMAN moieties anchored to EBA in a PERKIN ELMER Lambda 35 spectrometer. DMAN surface loading was determined by measuring the absorbance at the peak maximum of absorption band. This was translated into quantitative DMAN content per unit area by rearrangement of the Beer-Lambert law. Each material was assessed in quintuplicate.

Fluorescence spectra were recorded using a Perkin Elmer LS 55 fluorescence spectrometer. Fluorescence emission spectra of the probe were recorded in the range of 490–700 nm using the maximum of the longest-wavelength absorption band as excitation wavelength. All the spectra were corrected using the response curve of the photomultiplier. The fluorescence quantum yields (ϕ_F) were measured relatively to coumarin 6 (ϕ_F =0.78 in ethanol)[23].

^{1}H- and ^{13}C-nuclear magnetic resonance (NMR) spectra were recorded on *Varian-Mercury* 400 MHz and a Bruker 300 MHz NMR spectrometers using hexadeuterated dimethyl sulfoxide (DMSO-d_6) as the solvent. Chemical shifts were reported in parts per million (ppm). ^{1}H-NMR and ^{13}C-NMR chemical shifts were referenced to DMSO-d_6 (39.52 ppm) as standard.

Mass Spectra (*MS)* were recorded on a HP 5973-MSD spectrometer.

2.3.3 pH measurements and spectroscopic detection of acid in solution and vapors

The pH was measured at room temperature (23 ºC) by using a Mettler Toledo SevenGo Duo Pro meter with an InLab Expert Pro ISM-ID67 electrode that was previously calibrated with standard buffers. The sensing measurements of the solutions of DMAN and surface-modified films of EBA-DMAN were performed using HCl solution in the water:ethanol (4:1) mixture as solvent.

Acid titration by ultraviolet–visible (UV–Vis) and fluorescence spectrometry in aqueous solution and vapors was performed as follows. The titration of the solution with DMAN (water:ethanol 4:1, 10^{-4} M) was carried out by adding dilute HCl to increase the acidity from pH 8 to pH 0.5. After each addition, the solutions were allowed to equilibrate for 10 min, the pH was measured, and UV–Vis and fluorescence spectra were recorded.

In the case of functionalized materials (EBA-DMAN and EBA-pl-DMAN), the films were cut into strips of dimension 1x4 cm and dipped into 100 ml of water (Millipore-Q) using a homemade support that is slotted into the cell holder of the spectrophotometers. To study the effect of increasing the acidity of the medium beyond the pH scale, vials containing 50 ml of HCl at pH 7 to −1.1 (12 M HCl, 37%) were prepared. Strips of the film were immersed in these vials, starting from the vial with the lowest acid concentration, and the UV–Vis and fluorescence spectra were recorded for each pH after a conditioning time of 2 h. The fluorescence detection of acidic vapors was performed by adding 100 µl of HCl (12 M HCl 37%) over a cotton fragment to avoid direct contact and placing it at the bottom of a sealed spectrophotometric cuvette, where the functionalized EBA film is disposed.

2.3.4 Microwave equipment

The microwave equipment used in this study was an Anton Paar Monowave™ 300 microwave synthesis reactor equipped with an infrared sensor (IR pyrometer). All reactions were performed in pressure-resistant 30-ml test tubes sealed with silicon septum with a magnetic stirring bar. The

progress of the reactions was observed by an integrated CCD camera, which directly focuses on the reaction vial.

2.3.5 Plasma treatment and characterization by contact angle measurements and atomic force microscopy

The films were plasma-treated using an RF-Expanded Plasma Cleaner PDC-002 coupled with a PlasmaFlo PDC-FMG gas mixer obtained from Harrick Plasma and a Varian SH-110 vacuum pump. Samples were placed inside the Pyrex chamber (6″ diameter × 6.52″ length), and both sides of all films were treated with high RF power (30 W to the RF coil) for 30 min with oxygen plasma. Gas flow rates and chamber pressure can be altered by manual pressure and flow regulators, and stabilized pressure was fixed at 250 mTorr (0.33 mbar).

Changes in the wettability of plasma-treated polymer surfaces were observed after the determination of water contact angle (CA) by the sessile drop method. CA measurements were performed at 25 °C using a KSV instruments LTD CAM 200 Tensiometer and MilliQ water as wetting solvent. Surface energy was determined using two liquids (water and methylene iodide) for the measurements. On the basis of Owens–Wendt's method[24], the surface energy (γ) and its dispersive (γ^d) and polar (γ^p) parts were calculated using the CAM 200 software.

Surface morphology and roughness of the EBA films modified with DMAN before and after oxygen plasma treatment were examined by the Atomic Force Microscopy (AFM) using a Nanoscope IV system (Digital Instruments) working in tapping mode with a triangular microfabricated cantilever having a length of 115-135 mm, 1- to 10-Ohm-cm phosphorous (n)-doped Si pyramidal tip, and a nominal spring constant of 20-80 Nm^{-1}. The mean roughness value (Ra) represents the arithmetic average of the deviations from the center plane of the sample, which was determined using standard Digital Instruments software.

2.3.6 Surface modification of EBA films by hydrolysis (EBA-COOH) and acid chlorination (EBA-COCl)

EBA (7% of BA) film was cut into strips (1 x 4 cm) and hydrolyzed in the solid state by a modified procedure of the method reported previously[3] to conduct the heterogeneous reaction into a microwave reactor. The EBA film was placed in a 30-ml microwave test tube, and the test tube was then filled with a solution of 0.5 M NaOH in isopropanol. The temperature of the solution was fixed at 65 °C under stirring at 600 rpm for 6 h. After completion of the heterogeneous reaction at room temperature,

the EBA-COO^- film was separated from the médium and neutralized in a microwave-assisted second step by adding 30 ml of aqueous HCl solution (0.1 M) to the polymer and maintaining the mixture at 50 °C for 1 h. The resulting hydrolyzed EBA-COOH film was then washed repeatedly with distilled water and dried under vacuum overnight.

The surface modification of EBA to EBA-COO^- and EBA-COOH was confirmed and evaluated by ATR-FTIR spectroscopy (Fig. 3).

The EBA-COOH film and phosphorus pentachloride (50 mg, 0.24 mmol) were placed in a 30-ml microwave reactor containing 20 ml of CH_2Cl_2 anhydrous solution. Acid chlorination was carried out under microwave irradiation at 55 °C under magnetic stirring at 600 rpm. After 90 min, the EBA-COCl film was washed with dichloromethane and dried under vacuum overnight. The reaction between superficial acid groups and EBA-COCl was quantitative and confirmed by ATR-FTIR spectroscopy (Fig. 3).

2.3.7 Functionalization of EBA-COCl with DMAN

Superficially chlorinated EBA film, EBA-COCl, and 25 mg of DMAN were placed in a vial containing 20 ml of CH_2Cl_2 and 500 μL of triethylamine (TEA) under microwave at 55 ºC for 15 h under magnetic stirring at 600 rpm. The vial was then rapidly cooled down with compressed air to room temperature, and the modified film EBA-DMAN was washed repeatedly with dichloromethane and dried under vacuum overnight. The reaction was confirmed by ATR-FTIR and UV/vis spectroscopy (Fig. 3).

2.3.8 Synthesis of N-(2-hydroxyethyl)- 4-dimethylamino-1,8-naphthalimide

N-(2-hydroxyethyl)-4-bromo-1,8-naphthalimide (compound 1) and N-(2-hydroxyethyl)-4-dimethylamino-1,8-naphthalimide (compound 2) were synthesized following the procedure (Fig. 2) described in refs.[25,26] and using a novel reaction[27] for dimethylamination of compound 1.

In a pressure-resistant microwave test tube, a mixture of 4-bromo-1,8-naphthalic anhydride (1.4 g, 0.005 mol) and ethanol amine (0.4 g, 0.005 mol) in ethanol (15 ml) was heated at 85 ºC and stirred at 600 rpm for 2 h. The resulting mixture was cooled at 5 °C. The solid product obtained was filtered and washed with 30 ml of cold ethanol thrice and then identified as N-hydroxyethyl-4-bromo-1,8-naphthalimide (compound 1) after drying. Yield 90% (1.4 g). M.p.: 206 ± 2 ºC. ^{1}H-NMR (δ_H ppm) (300 MHz, DMSO-d_6, Me_4Si): δ 8.42 (dd, *J* = 13.9, 7.9 Hz, 2H), 8.20 (d, *J* = 7.9 Hz, 1H), 8.10 (d, *J* =

7.8 Hz, 1H), 7.89 (t, *J* = 7.9 Hz, 1H), 4.81 (s, 1H), 4.10 (t, *J* = 6.4 Hz, 2H), 3.61 (t, *J* = 5.9 Hz, 2H). ^{13}C-NMR (δ_C ppm) (100.6 MHz, DMSO-d_6, Me_4Si): δ 162.90, 162.85, 132.41, 131.42, 131.24, 130.80, 129.61, 128.98, 128.67, 128.14, 122.70, 121.92, 57.71, 41.95. FT-IR (wavenumbers, cm^{-1}): ν_{OH} 3386 cm^{-1}; ν_{C-H} 3066 cm^{-1} aromatic stretch vibration $\nu_{C=O}$ 1692, 1658 cm^{-1}; $\nu_{N-C=O}$ 1611 cm^{-1}; ν_{C-C} 1585, 1568 cm^{-1} aromatic ring chain vibrations. Elemental analysis, theoretical value % C 52.52; % H 3.15; % N 4.38; exp.: % C 52.42; % H 3.25; % N 4.25; EI-MS m/z: 321.0 (M^+).

In a pressure-resistant microwave test tube, 1 g of compound 1 (0.003 mol), 4.35 ml of triethylamine (0.03 mol), and 10 ml of DMF:water (1:1) solution were added. The mixture was heated at 120 °C and stirred at 600 rpm for 12 h. After completion of the reaction, the vial was cooled with water to room temperature. The mixture was extracted with ethyl acetate (4 x 50 ml), and the organic layer was dried over K_2CO_3. The solvent was evaporated under reduced pressure, which was purified by silica gel column chromatography using ethyl acetate:hexane (2:1) as eluent to obtain an orange solid product identified as N-(2-hydroxyethyl)-4-dimethylamino-1,8-naphthalimide. Yield: 84 %, M.P. = 135 ± 2 ºC ^{1}H-NMR (δ_H ppm) (400 MHz, DMSO-d_6, Me_4Si): δ 8.51 (dd, *J* = 8.5, 1.1 Hz, 1H), 8.45 (dd, *J* = 7.3, 1.1 Hz, 1H), 8.34 (d, *J* = 8.3 Hz, 1H), 7.75 (dd, *J* = 8.5, 7.3 Hz, 1H), 7.21 (d, *J* = 8.3 Hz, 1H), 4.81 (t, *J* = 6.0 Hz, 1H), 4.13 (t, *J* = 6.6 Hz, 2H), 3.59 (q, *J* = 6.5 Hz, 2H), 3.08 (s, 6H). ^{13}C-NMR (δ_C ppm) (100.6 MHz, DMSO-d_6, Me_4Si): δ 163.69, 163.03, 156.41, 132.12, 131.32, 130.41, 129.56, 124.90, 124.16, 122.37, 113.43, 112.91, 57.87, 44.35, 41.51. FT-IR (wavenumbers, cm^{-1}): ν_{OH} 3474 cm^{-1}; $\nu_{C=O}$ 1680 cm^{-1} and 1628 cm^{-1}, ν_{C-C} 1575 cm^{-1} aromatic ring chain vibrations. Elemental analysis, theoretical value % C 67.59; % H 5.67; % N 9.85; exp.: % C 67.09; % H 5.88; % N 9.88. EI-MS m/z: 285.0 (M^+).

2.4 Result and discussion

2.4.1 Synthesis of the N-(2-hydroxyethyl)- 4-dimethylamino-1,8-naphthalimide

The synthesis route to obtain N-(2-hydroxyethyl)-4-dimethylamino-1,8-naphthalimide is presented in Fig. 2. In the first step, the condensation of 4-bromo-1,8-naphthalic anhydride with 2-hydroxyethylamine under microwave irradiation in ethanol at 85 ºC afforded compound 1 in high yield at a shorter reaction time than conventional conditions. It has been observed[28] that for various amines, imidation of naphthalimides under reflux required 4-16 h. Our results show that the microwave method reduced the reaction time and improved the yields from 72–85% (under conventional conditions) to 96%.

In the second reaction step (Fig. 2), an interesting observation was made while we were optimizing the reaction conditions for the nucleophilic substitution reaction of compound 1 with 2-

methoxyethylamine. When the reaction was carried out in DMF, surprisingly, dimethylamination product (DMAN, compound 2) was also produced. In the absence of the primary amine, DMAN was obtained in very good yield. This reaction has been described[27,29] as a convenient method for the introduction of a dimethylamino group in aromatic compounds through chlorinated derivatives of heterocycles or aromatics using bases as KOH or K_2CO_3, and although the reaction mostly proceeds slowly, it results in good yields.

In our experimental conditions, dimethylamination resulted in the formation of compound 2 in good yield. On the contrary, when no base was added, the reaction did not proceed. Also, the presence of water seemed to be crucial for the amination, and this fact could be attributed to a better solvation of the base. The reaction and the plausible mechanisms for the amination are illustrated in Fig. 2.

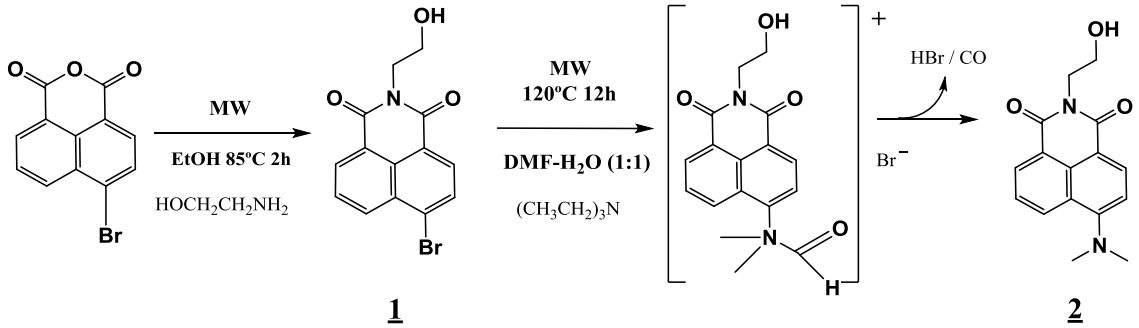

Fig.2. Reaction pathway and mechanism for the synthesis of N-(2-hydroxyethyl)-4-dimethylamino-1,8-naphthalimide (DMAN, compound 2).

The reaction starts with a base-assisted cleavage of DMF to form the required dimethylamine[30,31], which acts as the nucleophile for the formation of the required product. DMF is an easy substitute for dimethylamine, and the reaction occurs in a shorter period of time and produces high yields with microwave irradiation. The best conditions were noted under microwave irradiation for 12 h at 850 W and a ceiling temperature of 120 °C of a mixture of compound 1 together with 10 equiv. of triethylamine in DMF:water (1:1) yielding compound 2 in 90%.

2.4.2 Microwave assisted surface hydrolysis, acid chlorination and functionalization of EBA with naphthalimide groups

The functionalization of EBA (7 % content of BA) was carried out following the sequence of reactions shown in figure 1. The different modifications of EBA, hydrolysis of butyl ester, acid chlorination, and esterification with 4-dimethylamino-N-(2-hydroxyethyl)-naphthalimide (DMAN) were accomplished successfully in solution under microwave irradiation. All the modified EBA films were isolated and characterized by ATR-FTIR spectroscopy (Figure 3).

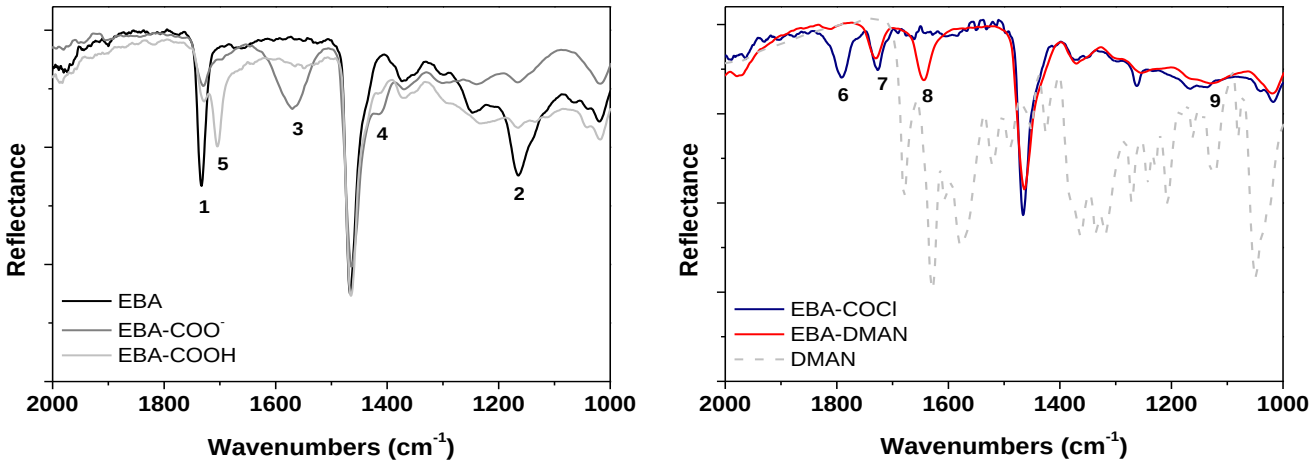

Fig.3. ATR-FTIR spectra in the region between 2000 and 1000 cm^{-1} of EBA (7% of BA content) and the surface modified EBA materials: (1) 1735 cm^{-1} $\nu_{(C=O)}$ butyl ester (EBA), (2) 1165 cm^{-1} $\nu_{(C-O)}$ aliphatic ester (EBA), (3) 1568 cm^{-1} and (4) 1413 cm^{-1} are assigned to $\nu_{as(COO-)}$ and $\nu_{s(COO-)}$ of carboxylate anion respectively (EBA-COO^-), (5) 1703 cm^{-1} $\nu_{(C=O)}$ carboxylic acid (EBA-COOH), (6) 1793 cm^{-1} $\nu_{(C=O)}$ acyl chloride (EBA-COCl), (7) 1730 $\nu_{(C=O)}$ naphthalimide (EBA-DMAN), (8) 1644 cm^{-1} $\nu_{(C=C)}$ naphthalimide aromatic ring (EBA-DMAN) and (9) 1167 cm^{-1} $\nu_{(C-O)}$ aliphatic ester (EBA-DMAN).

Figure 3 shows the characteristics of vibrational bands of the species formed after each functionalization step as described above in the synthesis section. As shown in Fig. 3, butyl ester on the surface was hydrolyzed by microwave irradiation under heterogeneous conditions, and the degree of hydrolysis was determined by ATR-FTIR as described earlier[3] and by using the butyl ester and carboxylate bands. The obtained curves are plotted in Fig. 4.

The spectra at different hydrolysis reaction times show the growth of bands because of the increase in carboxylate content, introduced to the surface of the polyolefin film. This confirms the hydrolysis of the surface with treatment time. Thus, the carboxylate content can be used to follow the modification of EBA surface by ATR-FTIR.

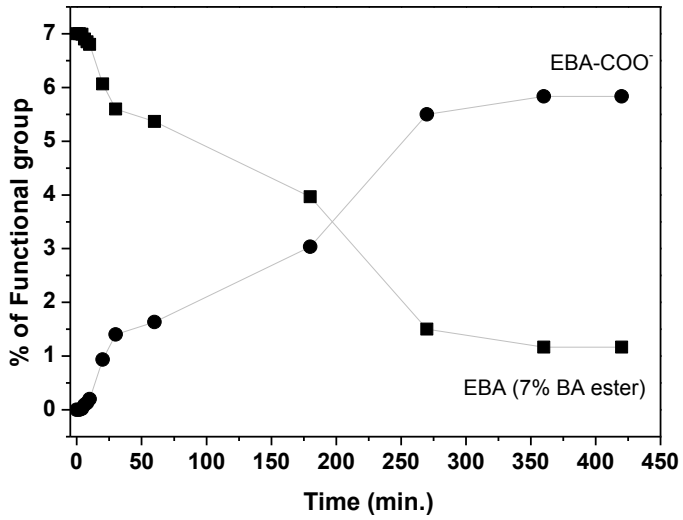

Fig. 4. Relationship between the percentages of surface hydrolysis degree of butyl ester (■) and carboxylate formation (●) with reaction time in EBA films (7 % content in BA), determined from the ATR-FTR spectra.

After reacting sodium hydroxide solution (0.5 M) in isopropanol for 6 h at 65 °C, the conversion of butyl ester to carboxylate (Fig. 4) reaches a value of 83.3% (5.83% of butyl ester content). In our experimental condition, 1.17% of butyl ester remained in the EBA composition after hydrolysis in the superficial thickness of the film analyzed by ATR-FTIR. As found in the hydrolysis reactions carried out in bulk with EBA[3] and ethylene vinyl acetate (EVA) copolymers[32], a plateau was reached in the hydrolysis conversion when the reaction times are longer than 6 h.

The determination of the acid content by ATR-FTIR suggested the carboxylic acid band at 1703 cm^{-1} is attributed to the overlapping of the carbonyl butyl ester band at 1735 cm^{-1}. The asymmetric stretch band of the carboxylate group at 1568 cm^{-1} could therefore be more convenient to follow the hydrolysis conversion.

After protonation of the carboxylate groups in a microwave-assisted second step (HCl aq. solution 0.1 M, 50 ºC, 1 h.), the acid groups present in EBA-COOH were converted to acid chloride under microwave heating. After 1.5 h of reaction with phosphorus pentachloride, the transformation was quantitative, as shown by the band at 1793 cm^{-1} which corresponds to $\nu_{(C=O)}$ acyl chloride (EBA-COCl) and the disappearance of the acid band at 1703 cm^{-1} (Fig. 3).

Finally, functionalization was carried out by reacting EBA-COCl with the previously obtained N-(2-hydroxyethyl)-4-dimethylamino-1,8-naphthalimide derivative. The degree of functionalization

increased with reaction time (3 h: 45%, 5h: 60%, 7 h: 70% and 10 h: 83%). After reacting for 15 h at 55 °C, no acyl halide band in the functionalized EBA-DMAN film could be detected at 1793 cm^{-1}, suggesting that the reaction was quantitative and the content of naphthalimide on the surface remained constant after several washes with dichloromethane.

The amount of naphthalimide superficially bonded to the EBA was determined spectrophotometrically through measurement of absorbance at the peak maximum of the absorption band and using the absorption coefficient of N-(2-hydroxyethyl)-4-dimethylamino-1,8-naphthalimide in water-ethanol (4:1 w/w). (ε_{445} = 1.02 x 10^4 $mol^{-1}\cdot l\cdot cm^{-1}$). Analysis of EBA-DMAN by UV spectroscopy provided a measure of the surface content of DMAN per unit area of polymer, and a concentration value of 2.4 ± 0.20 μg cm^{-2} was calculated for the EBA-DMAN film hydrolyzed after 6 h. For the materials with a lower initial degree of hydrolysis, a good correlation was observed between increasing the extent of acid chlorination on EBA and increased DMAN bonded to the EBA.

2.4.3 Depth profiling of the functionalization by Confocal Raman Spectroscopy (CRS)

Chemical functionalization of EBA-DMAN polymer films was studied using Raman microscopy. Both physical and chemical surface modification reactions generally result in the formation of a concentration gradient of the modifying groups through the film, and we used CRS to characterize the depth profile[33] of DMAN anchored to the EBA-DMAN films.

To obtain the depth profile of the films, a Raman microscope was focused stepwise (1 μm) from near the surface down to the center of each film, and the 1000 to 1800 cm^{-1} region of the spectrum was recorded at each step. In addition to the typical EBA polymer peaks, new characteristic bands emerged for graphitic material EBA-DMAN.

The degree of modification as a function of depth was obtained from the relative intensity of the naphthalimide bands and $\nu_{(C-C)}$ aromatic ring vibrations at 1585 cm^{-1} with respect to the $\nu_{(C-C)}$ aliphatic chain vibrations of the EBA at 1296 cm^{-1}. Hence, signals [I (1585 cm^{-1})/I (1296 cm^{-1})] leads to the relative depth profile which is depicted in Figure 5.

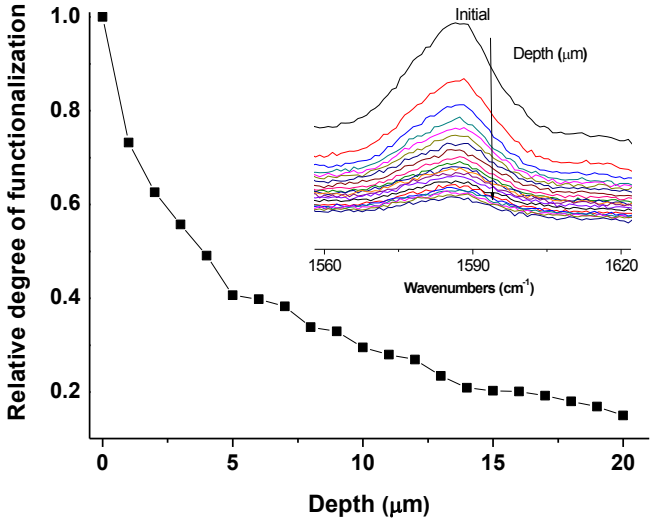

Fig. 5. Relative depth profile of functionalization calculated from the evolution of the Raman band $\nu_{(C-C)}$ aromatic ring vibrations of naphthalimide at 1585 cm^{-1} (inset) versus depth. Spectra of a functionalized EBA-DMAN film (100 μm) were recorded using confocal Raman spectroscopy and normalized with respect to the intensity of the $\nu_{(C-C)}$ band at 1296 cm^{-1} of the aliphatic chain vibrations of the EBA.

The shape of the curve shown in Fig 5 confirms that the EBA has not only been modified at the surface, but a gradient of DMAN was also formed across the first 20 μm of film thickness until the naphthalimide Raman bands are negligible. Relative degrees of hydrolysis of the EBA and the subsequent functionalization are a function of the depth without any interface between the pure EBA layers and functionalized layers. This behavior has been described by other authors using this technique to modify polyvinyl chloride (PVC)[34] and in the nitration of polystyrene[35] without any swelling of the polystyrene film. In our reaction conditions of hydrolysis (6 h at 65 °C using 0.5M NaOH in isopropanol), the polyolefin film did not swell, and hence, the extent of hydrolysis (83.3% of butyl ester content of EBA) is confined to the first 20 μm from the surface down to the film center as the DMAN depth profile.

CRS is a useful technique to measure the functionalization of polymer surface through the depth profile using Raman absorption band characteristics of the anchored functionalities.

2.4.4 Influence of pH on the absorption and fluorescence properties of DMAN and EBA-DMAN

Light excitation of DMAN elicits an electron donor-acceptor interaction between the unbound electron pair of the nitrogen atom at C-4 position toward the electron-accepting *peri*-carboximide groups[36,37]. This intramolecular electron charge transfer (ICT) results in a long-wavelength broad absorption band with absorption maximum at 445 and 402 nm for DMAN (Fig. 6A) and EBA-DMAN (Fig. 6B), respectively. Upon acidification, the maximum intensity of the band decreases from pH approximately 3 to 0 (Fig. 6C). When the aromatic amine of the naphthalimide derivative is protonated at low pH values, the electron-withdrawing effect leads to fluorescence quenching (Fig. 6D). This effect can also be observed for the DMAN bonded to the surface of EBA (Fig. 6B). The effect of pH on the absorbance and fluorescence of DMAN and EBA-DMAN is illustrated in Fig. 6.

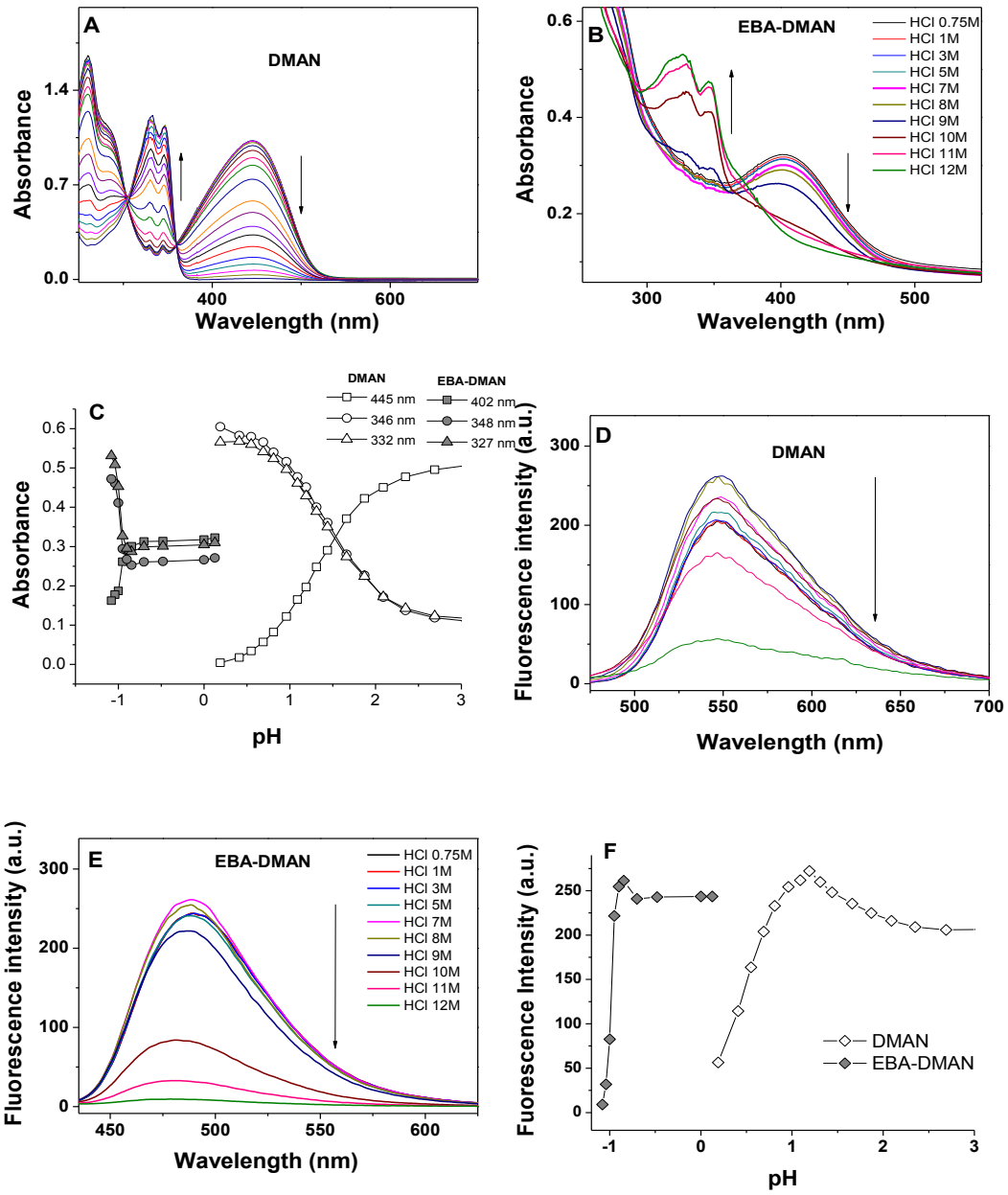

Fig. 6. Spectroscopic characteristics as a function of pH of acid media: Absorption of DMAN (A) and EBA-DMAN (B) and fluorescence of DMAN (D) and EBA-DMAN (E). Comparison of the absorption (C) and fluorescence (F) changes with pH for DMAN and EBA-DMAN.

For EBA-DMAN, the decrease in absorbance and the corresponding quenching of fluorescence due to the amine protonation occurs at lower pH values than that obtained for DMAN (Fig. 6C and 6F). This fact could be due to the hydrophobic character of the EBA surface. Hence, EBA-DMAN films were used to evaluate the molarity of HCl aqueous solutions in the interval of 1-12 M with the change in absorbance (Fig. 6B) and fluorescence (Fig. 6E) characteristics as a function of pH[38]. Table 1 summarizes some spectroscopic parameters obtained from the spectra.

Table 1: Parameters for N-(2-hydroxyethyl)-4-dimethylamino-1,8-naphthalimide (DMAN) in solution and bonded to the polymer film (EBA-DMAN) determined according to pH dependence by UV-Vis absorption and fluorescence spectroscopy[a]

Parameter	DMAN	EBA-DMAN
$\lambda_{ABS\text{-}acid}$	332, 346 nm	327, 348 nm
Log ε_{acid} [b]	4.08 (332 nm)/4.05 (346 nm)	-
$\lambda_{Isobestic}$	305, 360 nm	370 nm
$\lambda_{ABS\text{-}base}$	445 nm	402 nm
Log ε_{base} [b]	4.01 (445 nm)	-
pK_a [c]	1.41	-0.88
$\lambda_{FLU\text{-}acid}$	548 nm	480 nm
$\lambda_{FLU\text{-}base}$	550 nm	488 nm
$\phi_{FLU\text{-}(solvent)}$ [f]	0.032 (Water-Ethanol,4:1, v/v) 0.035 (Ethanol) 0.85 (Hexane)	Water-Ethanol (4:1, v/v) < < Ethanol <<< Hexane
$\Delta\nu$ [g]	4290.1	4425.7

[a] Measured at 10^{-4} M in water-ethanol (4:1, v/v). The subscripts "acid" and "base" refer to the limiting value of a given parameter when the acid or base condition is increased respectively. Fluorescence emission spectra were obtained by excitation at λ_{MAX}.
[b] ε, molar absorptivity in $M^{-1}cm^{-1}$.
[c] Obtained[37] by analyzing the pH dependence of the absorbance (A) at a given wavelength according to the equation $\log[(A_{acid} - A)/(A - A_{base})] = pH - pK_a$.
[f] Relatively to coumarin 6 (ϕ_F =0.78 in ethanol).
[g] Stokes shift (ν_{FLU}-ν_{ABS}) in frequency (cm^{-1}).

When the DMAN chromophore is bonded to the EBA through the 2-hydroxyethyl group, the absorption and fluorescence maxima exhibit a marked hypsochromic shift of 40-60 nm without a decrease in intensity and maintaining the Stokes shift (Table 1). The fluorescence quantum yield of DMAN is low in polar and base-neutral media, but is drastically increased to 0.85 in hexane. These results are in agreement with those obtained by other authors[37] for *N-methyl-4-dimethylamino-1,8-naphthalimide*. The corresponding fluorescence quantum yields of EBA-DMAN were not determined because of difference between the functionalized film and the fluorescence standard used in solution, but the relative fluorescence intensities of EBA-DMAN were in the same intensity order: water:ethanol (4:1, v/v) << ethanol <<< hexane.

The pK_a of EBA-DMAN has a negative value (-0.88) and is lower than that of DMAN (1.41), as the dimethylamine protonation of EBA-DMAN occurs at lower pH than that observed for DMAN (Fig. 6).

The EBA-DMAN material acts as an extreme acidity sensor by its absorbance and fluorescence characteristics. The sensor activity of EBA-DMAN was effective under several acid-water wash cycles (until 4-5 cycles), but with a prolonged response time (~2 h). Also, reversibility was observed with lower recovery of the fluorescence after the fourth cycle. One possibility to decrease the response time to acid media is to increase the hydrophilicity of the EBA surface though oxygen plasma

treatment. In the next section, we report the results obtained from EBA-DMAN before and after plasma treatment as a sensor of acidity.

2.4.5 Plasma treatment of EBA-DMAN films and characterization

To enhance the hydrophilic characteristic of the functionalized EBA, the EBA-DMAN films were exposed to oxygen plasma for 30 min. Plasma treatment causes cleavage of macromolecular chains, generation of free radicals and oxygen-containing functionalities, and subsequent rearrangement of modified chains[39]. Plasma treatment can induce several surface changes[40], with serious impacts on consequent applications such as alterations in biocompatibility and antibacterial properties[41].

These processes have a significant effect on surface wettability. The content of DMAN bonded to the polymer remained constant after the treatment, but important changes were observed in the water CA. The obtained results are summarized in Table 2.

Table 2. Contact angle (CA) and total (γ), polar (γ^p), and disperse (γ^d) surface energy data for EBA (7% of BA content) and the surface-modified EBA materials.

	Static CA (°)		Surface Energy ($mN.m^{-1}$) [a]		
	Water	Diiodomethane	γ	γ^p	γ^d
EBA	106.5	55.0	29.38	0.38	29.00
EBA-COOH	85.9	66.6	29.51	4.99	24.53
EBA-DMAN	92.6	60.8	30.91	2.33	28.58
EBA-pl-DMAN	41.0	51.5	62.39	28.44	33.95

[a] Calculated using Owens-Wendt´s method[24]

The plasma-treated film EBA-pl-DMAN exhibited a hydrophilic characteristic because of the presence of oxidative species on the surface[42]. The value of the water CA of EBA (7% BA), 106.5º, changed to 92.6º for EBA-DMAN, and after 30 min of treatment with oxygen plasma (EBA-pl-DMAN), this value decreased to 41º. The measured CAs were then used to calculate the polar, disperse, and total surface energies of the modified EBA films. The change in the total surface energy (γ) and its polar (γ^p) and dispersive (γ^d) components of the modified EBA films was calculated by the Owens-Wendt´s method. The variation in the values of total, polar and disperse solid surface energies (Table 2) of EBA-DMAN before and after oxygen plasma treatment EBA-pl-DMAN, shows that the total surface

energy of EBA-DMAN increases from 30.91 $mN.m^{-1}$ for untreated film to 62.39 $mN.m^{-1}$ for oxygen plasma-treated film EBA-pl-DMAN. Compared with the untreated film, plasma-treated films have higher total surface energy, particularly for the polar component.

The change in EBA-DMAN surface structure and the topography after oxygen plasma modification were imaged and measured by AFM. The AFM images of the untreated and oxygen plasma-treated films are presented in Fig. 7.

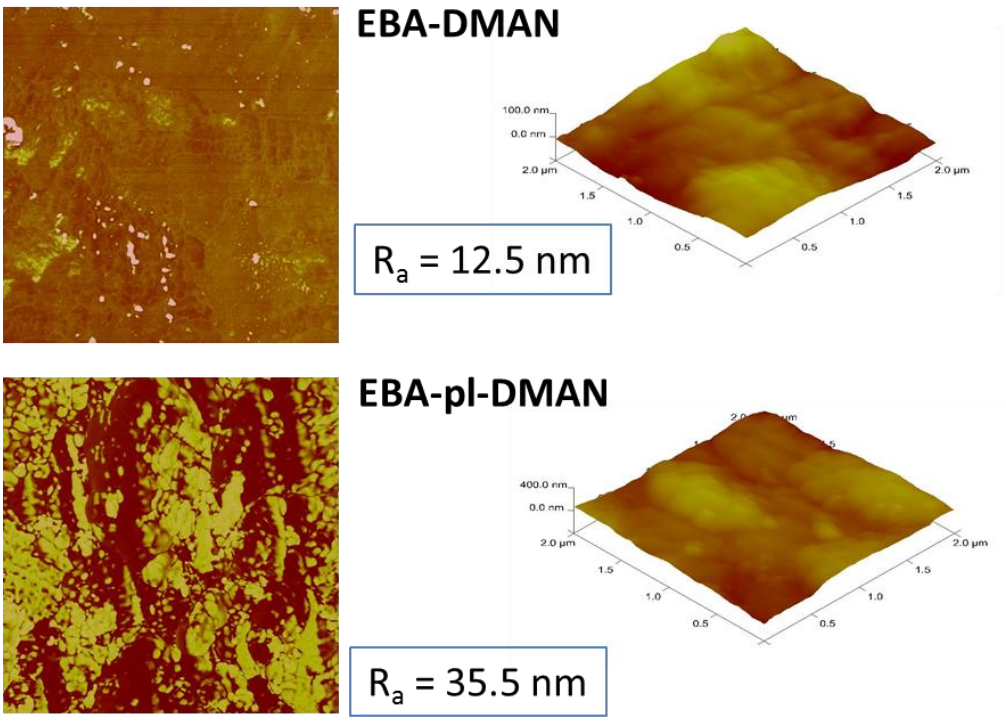

Fig. 7. AFM images and surface roughness (R_a) of the modified polymer films: EBA-DMAN and oxygen plasma treated EBA-pl-DMAN.

The average roughness (R_a) of untreated films was 12.5 nm, and their surface pattern was relatively smooth. After 30 min of oxygen plasma treatment, the treated EBA-pl-DMAN exhibited high density of height features distributed on the surface (Fig. 7). As expected, the average roughness was increased to 35.5 nm. The mean surface roughness of EBA-pl-DMAN was increased by approximately three times, confirming that the change in morphology is the result of the ion bombardment and ablation of the polymer surface layer.

2.4.6 Plasma treatment of EBA-DMAN films and response time to acid media

The changes in fluorescence emission with HCl (37%, 12M) as a function of time are shown in Figure 8A and 8B for EBA-DMAN and EBA-pl-DMAN, respectively.

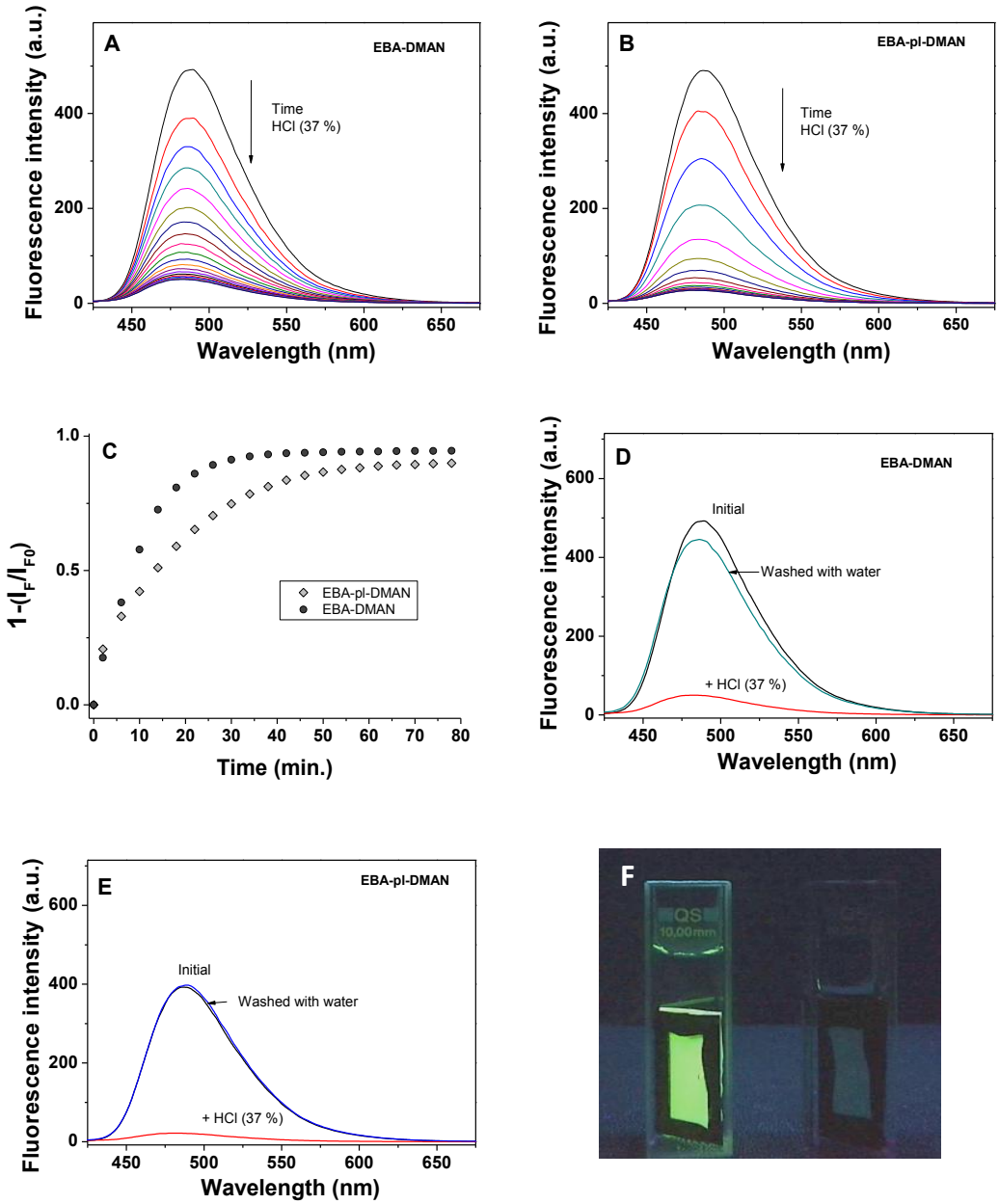

Fig. 8. Fluorescence decay with time for EBA-DMAN (A) and oxygen plasma-treated EBA-pl-DMAN (B) films using HCl (37% w/w, 12 M) aqueous solution. Response time comparison between both materials (C) and reversibility of dimethylamine protonation of the functionalized surfaces of EBA-DMAN (D) and EBA-pl-DMAN (E) after washing with distilled water and (F) fluorescence cells with EBA-pl-DMAN film, initial and after 30 min.

The oxygen plasma treatment substantially decreased the response time of the DMAN fluorescence in strong acid medium (HCl, 12M) from 80 minutes for EBA-DMAN to 30 min for EBA-pl-DMAN (Fig. 8C), together with a larger decay of fluorescence in the plasma-treated film. The increase in hydrophilicity imparted by the oxidative plasma on the film surface facilitates the penetration of the proton into the coordination sphere of the DMAN functional groups anchored to the first 20 μm of the film. The remaining nonprotonated DMAN chromophore after acid treatment was higher for the EBA-DMAN film, as the residual fluorescence intensity is stronger than that observed for the EBA-pl-DMAN film. This fact confirms a deeper penetration of protons into the plasma treatment material. Also, the reversibility of the dimethylamine protonation after washing with water was compared for both materials. Again, the extent of deprotonation is lower for EBA-DMAN (Fig. 8D), as the fluorescence intensity of EBA-pl-DMAN (Fig. 8E) was totally recovered after washing with distilled water. Thus, oxygen plasma treatment improved the sensitivity of the functionalized EBA surface to the acid medium.

The response time of functionalized films to the extremely acid environment was also studied in the vapor phase, it was observed that the spectroscopic characteristics of DMAN bonded to the polymer were sensitive to the acid vapor medium. It was necessary to maintain the film for approximately 1 h to observe the effective change in absorption and fluorescence properties. The results are shown in Fig. 9.

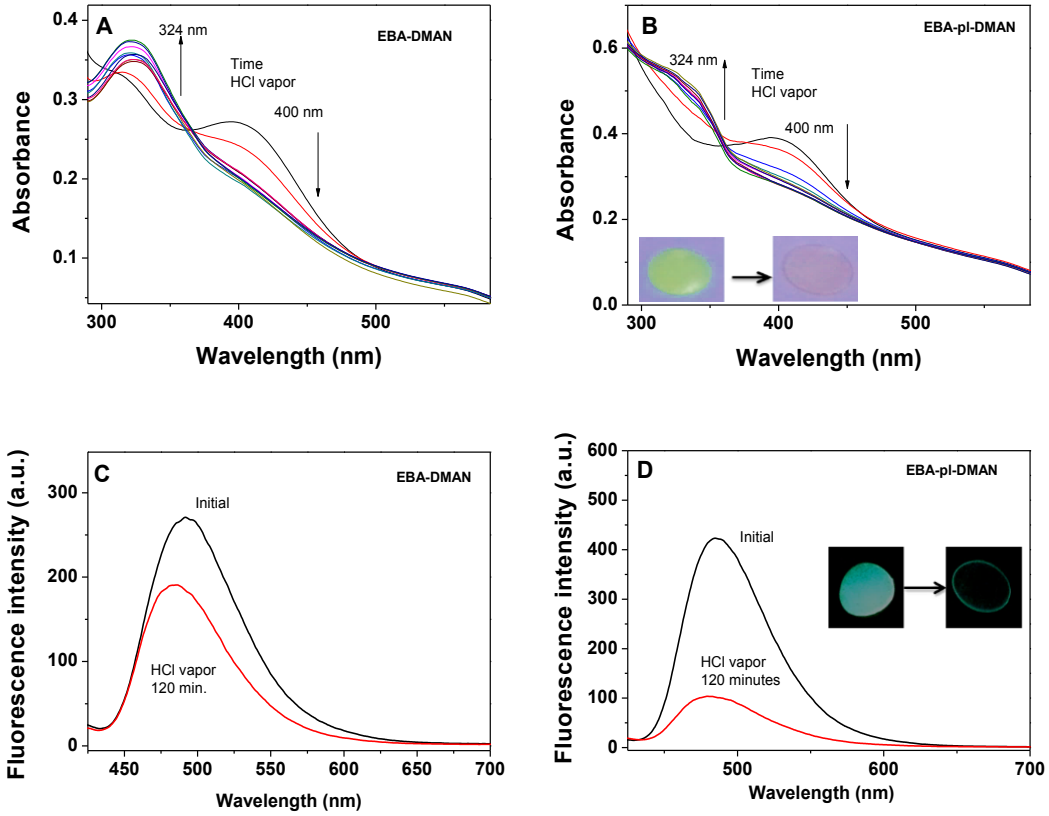

Fig. 9. Absorption changes with HCl vapors as a function of time (0-120 min) for functionalized films of EBA-DMAN (A) and EBA-pl-DMAN (B). Light-blue fluorescence (488 nm) decreases after 120 min. of vapors treatment for EBA-DMAN (C) and EBA-pl-DMAN (D).

Both functionalized materials are sensitive to HCl vapors through their ICT absorption bands at the longest wavelength (Fig. 9A and 9B). The plasma-treated EBA-pl-DMAN film exhibits better behavior in fluorescence decay after 120 min of vapor treatment (Fig. 9D) than the untreated EBA-DMAN film (Fig. 9C). The vapor penetration into the surface materials was improved by the surface oxidation induced by the plasma.

The hydrophilicity of the EBA surface clearly improved the sensor activity of the DMAN chromophore bonded to the surface.

In this study, we have described a useful procedure to modify and functionalize the polyolefin copolymer EBA, thereby opening the possibility of anchoring numerous interesting structures containing functionalities capable of reaction with acid chlorine groups introduced by microwave irradiation. The functionalized surface films of EBA-DMAN act as strong acid sensors in both

solution and vapor phases. The post-functionalization treatment with oxygen plasma decreased the response time to the acid media and increased the penetration of protons into the material. This functionalization with dimethylamine naphthalimide derivatives such as those used in this study or other fluorescence probes could result in a variety of film sensors of significant interest in environmental applications.

2.5 Conclusions

In conclusion, we have demonstrated that microwave irradiation allows rapid and efficient attachment of hydroxyl naphthalimide functionalities to superficially acid-chlorinated ethylene-butyl acrylate copolymers (EBA-COCl). The previous modifications of EBA (7% of BA) films (hydrolysis and acid chlorination) occur efficiently in a heterogeneous phase under our experimental conditions.

CRS was a useful technique to measure the functionalization of the polymer surface through the depth profile, and the results demonstrated that the heterogeneous modification was confined to the first 20 μm from the surface down to the film center.

The surface-modified films with N-(2-hydroxyethyl)-4-dimethylamino-1,8-naphthalimide (EBA-DMAN) at a concentration of 2,4 ± 0.20 μg cm^{-2} determined by UV-spectroscopy exhibited properties as a reversible acidity sensor (until 4-5 cycles). The decrease in absorbance (ICT absorption band) and the corresponding quenching of fluorescence because of the amine protonation of EBA-DMAN film occurs at lower pH values than that obtained for DMAN, and the solid sensor was used to evaluate the molarity of HCl solutions in the interval of 1-12 M.

Oxygen plasma treatment of the functionalized films increased appreciably the hydrophilic characteristic of the surface (EBA-pl-DMAN), and the DMAN content bonded to the polymer remained constant after the treatment. The plasma treatment decreased the response time of the DMAN fluorescence to a strong acid medium (from 80 minutes for EBA-DMAN to 30 min for EBA-pl-DMAN in HCl, 12M) and thus improved reversibility.

DMAN films bonded to the polymer were sensitive to the acid vapor medium, and the films treated with plasma (EBA-pl-DMAN) exhibited a better behavior in fluorescence decay, confirming that vapor penetration into the surface materials was improved by the surface oxidation induced by the plasma.

This new procedure using microwave reactions in a heterogeneous phase opens up the possibility to attach numerous interesting structures to polyolefin surfaces for application in materials of significant value such as environmental solid sensors.

2.6 References

[1] L.S. Penn, H. Wang, "Chemical modification of polymer surfaces: a review" Polym. Advan. Technol. 5 (1994) 809-817.

[2] S.M. Desai, R.P. Singh, "Long-Term Properties of Polyolefins" Adv. Polym. Sci. 169 (2004) 231.

[3] L. López-Vilanova, I. Martinez, T. Corrales, F. Catalina. "Photoreversible crosslinking of poly-(ethylene-butyl-acrylate) copolymers functionalized with coumarin chromophores using microwave methodology" React. Funct. Polym. 85 (2014) 28-35.

[4] V. Gaud, F. Rougé, Y. Gnanou, "Synthesis and properties of new photosensitive triazene and o-nitrobenzene methacrylates" React. Funct. Polym. 72 (2012) 521-532.

[5] M. Kondo, K. Goto, Y. Dozono, N. Kawatsuki, "Molecular reorientation behavior of photocrosslinkable liquid-crystalline polymer films containing phenylamide side chains" React. Funct. Polym. 73 (2013) 1567-1572.

[6] F. Gicogna, S. Coiai, C. Pinzino, F. Ciardelli, E. Passaglia, "Fluorescent polyolefins by free radical post-reactor modification with functional nitroxides" React. Funct. Polym. 72 (2012) 695-702.

[7] I. Grabchev, R. Betcheva, "Copolymerization and photostabilization of methylmethacrylate with 1,8-naphthalimide fluorescent brighteners" J. Photochem. Photobiol. A. 142 (2001) 73-78.

[8] K. Wang, W. Huang, P. Xia, C. Gao, D. Yan, "Fluorescent polymer made from chemical modification of poly(styrene-co-maleic anhydride" React. Funct. Polym. 52 (2002) 143-148.

[9] E. Martin, R. Weigand, A. Pardo, "Solvent dependence of the inhibition of intramolecular charge-transfer in N-substituted 1,8-naphthalimide derivatives as dye lasers" J. Lumin. 68 (1996) 157-164.

[10] W. Stewart, "Synthesis of 3,6-disulfonated 4-aminonaphthalimides" J. Am. Chem. Soc. 103 (1981) 7615-7620.

[11] S. Banerjee, E.B. Veale, C.M. Phelan, S.A. Murphy, G.M. Tocci, L.J. Gillespie, D.O. Frimannsson, J.M. Kelly, T. Gunnlaugsson, "Recent advances in the development of 1,8-naphthalimide based DNA targeting binders, anticancer and fluorescent cellular imaging agents" Chem. Soc. Rev. 42 (2013) 1601-1618.

[12] W. Zhu, C. Hu, K. Chen, H. Tian, "Luminescent properties of copolymeric dyad compounds containing 1,8-naphthalimide and 1,3,4-oxadiazole" Synth. Met. 96 (1998) 151-154.

[13] H. Tian, J. Gan, K. Chen, J. He, Q. Song, X. Hou, "Positive and negative fluorescent imaging by naphthalimide polymers" J. Mater. Chem. 12 (2002) 1262-1267.

[14] I. Grabchev, J.M. Chovelon, "Synthesis and functional properties of green fluorescent poly(methylmethacrylate) for use in liquid crystal systems" Polym. Adv. Technol. 14 (2003) 601-608.

[15] L. Jia, Y. Zhang, X. Guo, X. Qian, "A novel chromatism switcher with double receptors selectively for Ag^+ in neutral aqueous solution: 4,5-diaminoalkeneamino-N-alkyl-1,8-naphthalimides" Tetrahedron Lett. 45 (2004) 3969-3973.

[16] W. Zhu, M. Hu, R. Yao, H. Tian, "A novel family of twisted molecular luminescent materials containing carbazole unit for single-layer organic electroluminescent devices" J. Photochem. Photobiol. A. 154 (2003) 169-177.

[17] I. Grabchev, I. Moneva, V. Bojinov, S. Guittonneau,"Synthesis and properties of fluorescent 1,8-naphthalimides dyes for application in liquid crystal displays" J. Mater. Chem. 10 (2000) 1291-1296.

[18] I. Grabchev, J.M. Chovelon, X. Qian, "A copolymer of 4-N,N-dimethylaminoethylene-N-allyl-1,8-naphthalimide with methylmethacrylate as a selective fluorescent chemosensor in homogeneous systems for metal cations" J. Photochem. Photobiol. A. 158 (2003) 37-43.

[19] F. Cosnard, V. Wintgens, "A new fluoroionophore derived from 4-amino-N-methyl-1,8-naphthalimide" Tetrahedron Lett. 39 (1998) 2751-2754.

[20] P.L. Shuai Zheng, T.E.R. Mark Lynch, T.S. Moody, H.Q.N. Gunaratne, A.P. de Silva, "Structural effects on the pH-dependent fluorescence of naphthalenic derivatives and consequences for sensing/switching" Photochem. Photobiol. Sci. 11 (2012) 1675-1681.

[21] S. Hajatdoost, M. Olsthoorn, J. Yarwood, "Depth profiling study of effect of annealing temperature on polymer/polymer interfaces in laminates using Confocal Raman Microspectroscopy" Appl. Spectrosc., 51 (1997) 1784-1790.

[22] P. Slepicka, Z. Malá, S. Rimpelova, N.S. Kasalkova, V. Svorcik, "Plasma treatment of the surface of poly(hydroxybutyrate) foil and non-woven fabric and assessment of the biological properties" React. Funct. Polym. 95 (2015) 71-79.

[23] G. Reynolds K. Drexhage, "New coumarin dyes with rigidized structure for flashlamp-pumped dye lasers" Opt. Commun. 13 (1975) 222-225.

[24] G.K. Owens, R.C. Wendt, "Estimation of the surface free energy of polymers" J. Appl. Polym. Sci. 13 (1969) 1741-1747.

[25] H. Tian, J. Gan, K. Chen, J. He, Q.L. Song, X.Y. Hou, "Positive and negative fluorescent imaging induced by naphthalimide polymers" J. Mater. Chem. 12 (2002) 1262-1267.
[26] Y.Q. Tian, B.R. Shumway, C. Youngbull, A.K.Y. Jen, R.H. Johnson, D.R. Meldrum, "Dually fluorescent sensing of pH and dissolved oxygen using a membrane made from polymerizable sensing monomers" Sens. Actuators B Chem. 147 (2010) 714-722.
[27] Y.H. Cho, J.C. Park, "A very convenient dymethylamination of activated aromatic halides using N,N-dimethylformamide and ethanolamines" Tetrahedron Lett. 38 (1997) 8331-8334.
[28] S. Rouhani, K. Ghraranjig, M.H. Nezhad, "Facile synthesis of 4-nitro-N-substituted-1,8-naphthalimide derivatives using ultrasound in aqueous media" Green Chem. Lett. Rev. 7 (2014) 174-178.
[29] A. Agarwal, P.M.S. Chauhan, "Convenient dimethylamino amination in heterocycles and aromatics with dimethylformanide" Synth. Commun. 34 (2004) 2925-2930.
[30] Y. Wan, M. Alterman, M. Larhed, A. Hallberg, "Dimethylformamide as a carbon monoxide source in fast palladium-catalyzed aminocarbonylations of aryl bromides" J. Org. Chem. 67 (2002) 6232.
[31] A. Sharma, V.P. Mehta, E. Van der Eycken, "A convenient microwave-assisted desulfitative dimethylamination of the 2(1H)-pyrazinone scaffold using N,N-dimethylformamide" Tetrahedron 64 (2008) 2605-2610.
[32] M. Tang, J. Hou, L. Lei, X. Liu, S. Guo, Z.Wamg, K. Chen, "Preparation, characterization and properties of partially hydrolyzed ethylene vinyl acetate copolymer films for controlled drug release" Int. J. Pharm. 400 (2010) 66-73.
[33] S. Hajatdoost, J. Yarwood, "Depth profiling of poly(methyl methacrylate), poly(vinyl alcohol) laminates by Confocal Raman Microspectroscopy" J. Appl. Spectrosc. 50 (1996) 558-564.
[34] J. Sacristán, C. Mijangos, H. Reinecke, J. Spelle, J. Yarwood, "Selective surface modification of PVC films as revealed by Confocal Raman Microspectroscopy" Macromolecular 33 (2000) 6134-6139.
[35] J. Sacristán, H. Reinecke, C. Mijangos, S. Spell, J. Yarwood, "Surface modification of polystyrene films. Depth profiling and mapping by Raman Microscopy" Macromol. Chem. Phys. 203 (2002) 678-685.
[36] M.S. Alexiou, V. Tychopoulos, S. Ghorbanian, J.H.P. Tyman, R.G. Brown, P.I. Brittain, "The UV-Visible absorption and fluorescence of some substituted 1,8-naphthalimides and naphthalic anhydrides" J. Chem. Soc. Perkin Trans. 2 (1990) 837-842.
[37] P.A. Panchencko, O.A. Fedorova, Y.V. Fedorov, "Fluorescent and colorimetric chemosensors for cations based on 1,8-naphthalimide derivatives: design principles and optical signaling mechanisms" Russ. Chem. Rev. 82 (2014) 155-182.
[38] K.A. Connors, Binding Constants: The Measurement of Complex Stability, Wiley, New York, 1987.
[39] N. Slepičková Kasálková, P. Slepička, Z. Kolská, P. Sajdl, L. Bačáková, S. Rimpelová, V. Švorčík, "Cell adhesion and proliferation on polyethylene grafted with Au nanoparticles" Nucl. Instrum. Meth. B 272 (2012) 391-395.
[40] P. Slepička, S. Trostová, N. Slepičková Kasálková, Z. Kolská, P. Sajdl, V. Švorčík, "Surface modification of biopolymers by argon plasma and thermal treatment" Plasma Process. Polym. 9 (2012) 197-206.
[41] P. Slepička, N. Kasálková-Slepičková, J. Siegel, Z. Kolská, L. Bačáková, V. Švorčík, "Nano-structured and functionalized surfaces for cytocompatibility improvement and bactericidal action" Biotech. Adv. 33 (2015) 1120-1129.
[42] Y. Zheng, J. Miao, F. Zhang, C. Cai, A. Koh, T. Simmons, S. A. Mousa, R. J. Linhardt, "Surface modification of a polyethylene film for anticoagulant and antimicrobial catheter" React. Funct. Polym. 100 (2016) 142-150.

CAPÍTULO 3

Fluorescence sensors obtained by functionalization of photocrosslinked water-swollen acrylic membranes with 4-piperazine naphthalimide derivatives.

3 FLUORESCENCE SENSORS OBTAINED BY FUNCTIONALIZATION OF PHOTOCROSSLINKED WATER-SWOLLEN ACRYLIC MEMBRANES WITH 4-PIPERAZINE NAPHTHALIMIDE DERIVATIVES.

3.1 Abstract

A photocrosslinked membrane (M-Cl) based on vinyl-pyrrolidone/butyl acrylate containing ethylene glycol dimethacrylate as a crosslinking agent and methacryloyl chloride as reactive monomer has been prepared for further functionalization. A series of hydroxy substituted piperazine naphthalimide compounds have been synthetized as pH sensitive Off-On fluorescence probes using two methods: microwave and reflux. Three of the derivatives were selected to be anchored to the M-Cl membrane through the acid chloride groups by the Schotten-Baumann reaction. All the obtained water-swollen membranes were characterized using different techniques. Photo-induced electron transfer (PET) and its pH-dependent optical changes were investigated and various photochemical parameters were determined by using pH-dependent absorption and fluorescence spectroscopies. In the pH range of 9.0-4.0, these solid sensors undergo PET process from the piperazine to the naphthalimide moiety leading to a fluorescence quenching. However, in the pH range of 4.0–1.0, the PET is inhibited to give a fluorescence enhancement. The sensitivity of the functionalized membranes to pH changes depended on the size and position of the naphthalimide substituents.

3.2 Introduction

Polymeric membranes have been widely utilized as a support material for various types of sensors and also used in systems where the environmental information is gathered by the measurement of photons. The most commonly used method is fluorescence emission. Its applications include optical chemical[1,2] and biological[3] sensors. Hydrophilic polymer matrices are widely used for immobilization of optical indicators due to their advantages such as fast response time, low cost, flexibility and their capability for deposition into various types of substrates.

In recent years, the developments of fluorescence pH sensors have attracted considerable attention because of their potential application in environmental analytics, medical diagnostics and process control[4,5]. Compared to small organic compounds, polymer based optical sensors display several important advantages as they can be non-invasive or minimally invasive, disposable, easily miniaturized and simple to process as a membrane, coating or solid layer on adequate surfaces[6,7]. The most widely used technique amongst optical sensors is the measurement of fluorescence intensity. Among the large number of fluorescent structures that have been developed, 1,8-naphthalimide derivatives have numerous applications in a variety of different areas. They have gained increasing interest as fluorescent probes for pH[8,9], metal cations[10,11,12,13] and anions[14] because they have been recognized for excellent photophysical properties with excellent stability, visible excitation and emission exhibiting high fluorescence quantum yields and large Stokes' shift that minimize the effects of the background fluorescence.

Polymerizable naphthalimide derivatives have been copolymerized with different co-monomers such as methyl methacrylate[15] and styrene[16,17], 2-hydroxyethyl methacrylate[18] and acrylamide[19,20]. In particular alkylpiperazinyl derivatives of naphthalimides have been studied and their behavior as proton “off–on” switch sensors has been demonstrated as very sensitive[21,22] and interesting for applications[23] in complex media.

In an earlier work, we modified the surface of a film based on a copolymer of ethylene butyl acrylate with a naphthalimide derivative as an acidity sensor [24]. Even though the functionalized film was effective as an acid sensor, the hydrophobicity of the polyolefin surface modified with 4-dimethylamino-1,8-naphthalimide (water contact angle value of 92.6º) increased the time of its response to acid media.

Vinyl-pyrrolidone (VP) based materials exhibit highly interesting properties due to its unique combination of physical and chemical properties (biocompatibility, nontoxicity, chemical stability, good solubility in water and many organic solvents, affinity to both hydrophobic and hydrophilic complex substances). Also, VP copolymers with acrylic monomers such as butyl acrylate (BA) have important applications[25,26].

In this work we have prepared a photocrosslinked membrane based in vinyl-pyrrolidone/butyl acrylate and added ethylene glycol dimethacrylate as the crosslinking agent and methacryloyl chloride as the reactive monomer for further functionalization. Through the acid chloride groups, three derivatives of naphthalimide were anchored to obtain solid fluorescence sensors. The membrane preparation and the functionalization with naphthalimides are shown in Fig. 1.

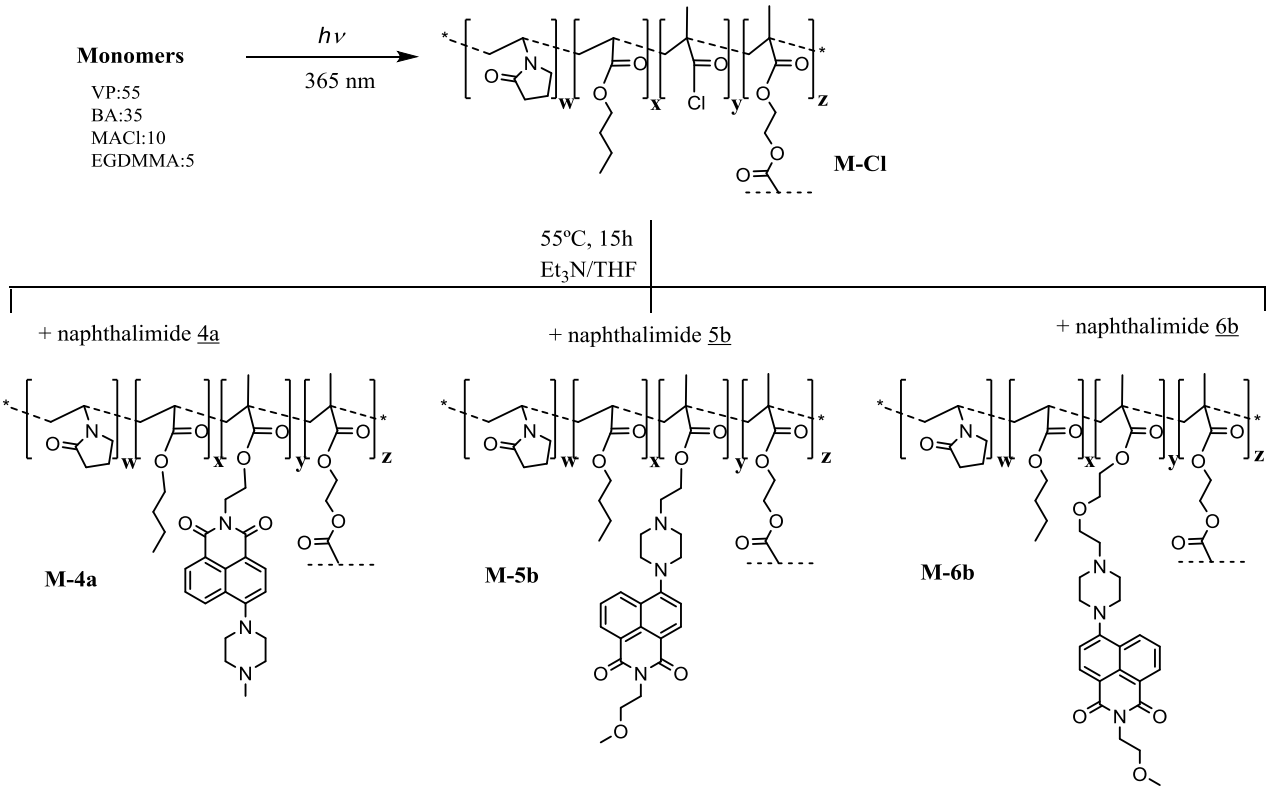

Fig.1. Synthesis of the photocrosslinked acrylic membrane containing acid chloride groups (M-Cl) and functionalization with the selected naphthalimide structures.

The naphthalimides linked to the membrane containing acid chloride (M-Cl) were selected from a series of naphthalimide derivatives previously synthetized in this work using two methods: microwave and reflux. The structures of the series (Fig. 2) are hydroxyl derivatives of piperazine 1,8-naphthalimides which have been reported to have excellent fluorescence properties[21,22]. The membranes were characterized and the spectroscopic characteristics of the naphthalimide derivatives and the membranes were studied in function of pH and of different solvent polarities using UV-vis and fluorescence spectroscopies.

3.3 Experimental

3.3.1 Materials and reagents

All materials and solvents were commercially available and used as received, unless otherwise indicated. The materials included: sodium hydroxide (Panreac, 98-100.5%), hydrochloric acid (VWR Chemicals, 37%), ultrapure MilliQ water (Millipore), triethylamine (Aldrich, ≥99%), 4-bromo-1,8-naphthalic anhydride (Aldrich, 95%), potassium carbonate (Panreac, 99%), 2-aminoethanol (Aldrich, 99%), 2-methoxyethylamine (Aldrich, 99%), piperazine (Aldrich, 99%), 1-methylpiperazine (Aldrich, 99%), 1-(2-hydroxyethyl)piperazine (Aldrich, 98%), 1-[2-(2-hydroxyethoxy)ethyl]piperazine (Aldrich, 95%) ethanol (VWR Chemicals, 99.95%), dimethylformamide (Scharlau, 99.8%), Irgacure 2959 photoinitiator (BASF), ethyl acetate (Aldrich, ≥99.5%), hexane (Carlo Erba Reagents, 99%), 2-propanol (Scharlau, 99.5%), dichloromethane (Aldrich, ≥99.9%), toluene (Merck, ≥99.9%), diethyl ether (Carlo Ebra, >99.8%), 1,4-dioxan (Panreac, 99%), tetrahydrofuran (Aldrich, 99.9%), chloroform (Scharlau, 99%), acetone (Scharlau, 99.5%), acetonitrile (Aldrich, ≥99.5%), 1-butanol (Panreac, 99.5%), methanol (Aldrich, ≥99.8%), coumarin 6 (Aldrich, 98%), dimethylsulfoxide D6 (Euriso-top, 99.8% D), chloroform-d (Aldrich, 99.8% D), diiodomethane (Aldrich, 99%).

Monomers, 1-vinyl-2-pyrrolidone (Aldrich, ≥97%), butyl acrylate (Aldrich, ≥99%) and ethylene glycol dimethacrylate (Aldrich, 98%) and methacryloyl chloride (Aldrich, ≥97%) were distilled under vacuum to remove the inhibitor before use.

3.3.2 Spectroscopic characterization and thermal analysis

Attenuated Total Reflectance / FT-Infrared Spectroscopy (ATR-FTIR) was used to characterize naphthalimide derivatives and membranes. ATR-FTIR spectra were obtained using a PERKIN ELMER BX-FTIR Spectrometer coupled with a MIRacle^{TM}ATR accessory, from PIKE Technologies and interferograms were obtained from 32 scans.

UV spectroscopy was employed for the quantitative determination of each hydroxyl-piperazine-naphthalimide derivative anchored to acrylic membranes in a *PERKIN ELMER Lambda 35* spectrometer. The naphthalimide content was determined through measurement of absorbance at the peak maximum of the absorption band. Assessment was made in quintuplicate for each material.

Fluorescence spectra were recorded using a Perkin Elmer LS 55 Fluorescence Spectrometer. Fluorescence emission spectra of the probe were recorded in the range 490–700 nm using as the excitation wavelength the maximum of the longest wavelength absorption band. All the spectra were

corrected using the response curve of the photomultiplier. The fluorescence quantum yields (ϕ_F) were measured relatively to Coumarin 6 (ϕ_F =0.78 in ethanol)[27].

Nuclear magnetic resonance, ^{1}H- and ^{13}C- NMR spectra were recorded on a *Varian-Mercury* 400 MHz and a Bruker 300 MHz Nuclear Magnetic Resonance Spectrometers using hexadeuterated dimethyl sulfoxide (DMSO-d_6) and chloroform-d ($CDCl_{3)}$ as the solvent. Chemical shifts were reported in parts per million (ppm). ^{1}H-NMR and ^{13}C-NMR chemical shifts were referenced to DMSO-d_6 (2.5 and 39.52 ppm respectively) or $CDCl_3$ (7.25 and 77.0 ppm respectively) as standard.

Mass Spectra (*MS)* were recorded on a HP 5973-MSD spectrometer.

Differential Scanning Calorimetry (DSC) was performed on a METTLER DSC-823e instrument (30–180 ºC) previously calibrated with an indium standard (Tm= 429 K, ΔHm= 25.75 Jg^{-1}). Samples (10 mg) were tightly sealed onto the DSC pans and heating or cooling at 10 ºC·min^{-1} rates under nitrogen. DSC was used to measure the glass transition temperature of the acrylic membranes and the melting points of the naphthalimide derivatives. The glass transition temperature of the membranes (T_g) were determined in a second scan after erasing the previous thermal history of the material in a first scan. Rate of 10 ºC /min under nitrogen flow (30 psi).

Thermogravimetric Analysis (TGA) was carried out in a TGA Q-500 TA Instruments coupled to a Pfeiffer Vacuum ThermoStar^{TM} mass spectrometer. The weight loss was measured as a function of temperature, and the evolved gas masses were directly monitored. The heating rate for the dynamic conditions was 10 ºC·min^{-1}, and the nitrogen flow was maintained constant at 60 ml·min^{-1}. The onset degradation temperature (T_{Onset}) was defined as the initial temperature of degradation, corresponding to the intersection of the tangent drawn at the decomposition step with the horizontal zero-line of the TG curve.

Elemental analysis (EA) was carried out on a Carlo Erba EA1108 elemental analyzer (% of C, H, N).

3.3.3 Swelling Ratio and water contact angle measurements

Swelling degree (SD) in water and THF of the crosslinked membranes were measured by immersing dried and weighed sample films (W_d) into deionized water or THF at 30 ºC for 24 h. The superficial solvent was removed and the samples were immediately weighed (W_s). The SD were calculated as follows: SD *(%)* = $((W_s - W_d)/W_d)\times 100$, where W_s and W_d are the weight of the swollen and dry sample, respectively.

Contact angle (CA) measurements were performed at 25 °C using a KSV instruments LTD CAM200 Tensiometer and MilliQ water as wetting solvent. Surface energy was determined using two liquids (water and methylene iodide) for the measurements. On the basis of Owens–Wendt's method[28], the surface energy (γ) and its dispersive (γ^d) and polar (γ^p) parts were calculated using the CAM 200 software.

3.3.4 Microwave and UV irradiation equipments

The microwave equipment used in this work was an *Anton Paar Monowave™ 300* microwave synthesis reactor provided with an infrared sensor (IR pyrometer). All reactions were performed in pressure-resistant 30-mL test tubes sealed with silicon septum and using a magnetic stirring bar.

The photopolymerization reactions were carried out in a Biolink™ BLX-365 type Bio-link apparatus (Vilbert Lourmat™).

3.3.5 Membrane preparation by photopolymerization (M-Cl) and functionalization with HO-piperazine-naphthalimide derivatives

The reaction scheme for the photopolymerization reaction and the membrane functionalization with naphthalimide is shown in Figure 1.

A crosslinked membrane (M-Cl) was obtained by the bulk photopolymerization of a mixture of monomers: N-vinylpyrrolidone (VP), butyl acrylate (BA), ethylene glycol dimethacrylate (EGDMMA) as the crosslinking agent and methacryloyl chloride (MACl) as the reactive monomer. The monomer molar ratio of the feed mixture was VP:55/BA:35/MACl:10/EGDMMA:5 and the photoinitiator (Irgacure 2959) was added to the mixture at 1% (w/w). The homogenous mixture was transferred to an ampoule, degassed by argon bubbling for 15 min and injected into a previously degassed silanized glass mould. The two glass pieces were separated by a Teflon spacer of 180 µm thick to define the reaction chamber. After 40 minutes of irradiation at 365 nm (dose 20 J cm^{-2}), the transparent crosslinked membrane (180 µm of thickness) was demoulded and conditioned (12h) at room temperature under argon atmosphere. The crosslinked membranes were then washed several times with ethanol and dried under vacuum at 40 °C to remove the un-reacted monomers. The presence of acid chloride was confirmed by ATR-FTIR (wavenumbers,cm^{-1}), $\nu_{C=O}$ acyl chloride 1795 cm^{-1}; ν_{C-Cl} 898 cm^{-1} together with the characteristic co-monomers bands of VP $\nu_{C=O}$ lactam, amide-I 1675 cm^{-1} and BA, $\nu_{C=O}$ ester 1725 cm^{-1}; ν_{C-O} (O-CH_2-) ester 1161 cm^{-1}. The quantitative

determination of chlorine in the membrane (2.8%) was carried out by TGA-MS (Table 1 and Fig. 3B and C).

In a second step, the M-Cl film was cut into strips (1 × 4 cm) and functionalized in the solid state with the naphthalimide derivatives synthetized in this work (Fig 2). The procedure was as follows: the M-Cl membrane was placed in an ace round-bottom pressure flask with 20 mL of THF. 10 mg of hydroxy-piperazine naphthalimide derivative (4a, 5b or 6b) and 500 µL of triethylamine were added under argon atmosphere. The mixture was heated at 55 °C for 15h. After this reaction time, the corresponding modified membranes M-4a, M-5b and M-6b were washed with cold ethanol and with water thrice in order to remove the unreacted acid chloride groups and the unreacted naphthalimide. The hydrolysis reaction of unreacted acid chloride groups was confirmed by ATR-FTIR and by TGA-MS as the characteristic peak of acid chloride was not present (Fig. 3C). After drying, the transparent functionalized membranes exhibited an intense yellow–green fluorescence and the content of naphthalimide was quantitatively determined by UV–Vis spectroscopy (Table 1). The characteristic peaks of naphthalimide structures in the membranes were not clearly observed in the ATR-FTIR spectra due to their low intensity and their overlap with the broad absorptions of the membrane functional groups.

3.3.6 Synthesis of the naphthalimide derivatives

Compound 2a was synthesized following the procedure (Fig. 2) described in the bibliography. All the naphthalimide derivatives were synthetized using microwave (MW) and reflux (RF) methods with the same experimental conditions but differing in reaction times and yields. The RF reactions times were larger (15 h for all the reactions) and RF yields were lower than those obtained under MW irradiation. The synthesis path-ways, naphthalimide structures and reaction data are shown in Fig.2.

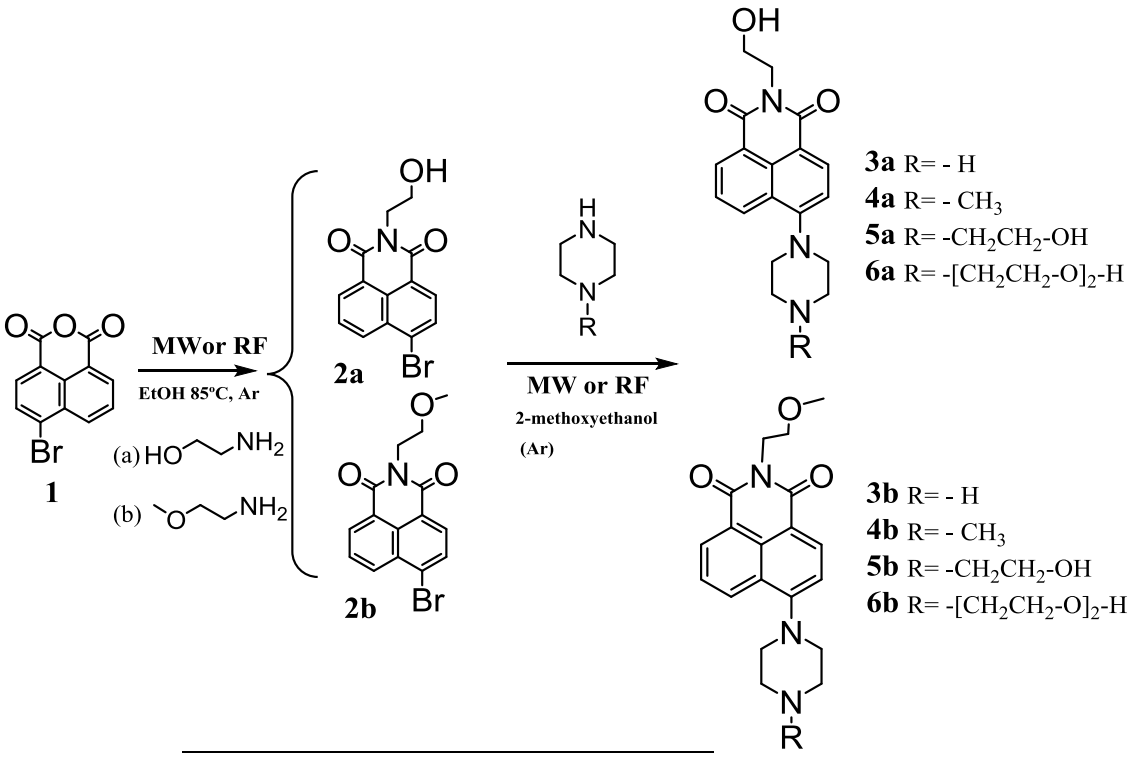

Structure	MW method		Reflux method	
	t (h.)	**Y** (%)	**t** (h.)	**Y** (%)
2a	2	90	15	76
2b	2	93	15	80
3a	1	84	15	64
4a	1	85	15	67
5a	1	88	15	68
6a	1	85	24	70
3b	1	84	15	69
4b	1	83	15	73
5b	1	84	15	71
6b	1	85	24	69

Fig.2. Synthesis of the naphthalimide derivatives and their corresponding reaction times and yields for microwave (MW) and reflux (RF) methods.

To synthesize the desired piperazinyl derivative of naphthalimide, two bromide derivatives of naphthalimide containing 2-hydroxyethyl (Compound 2a) and 2-methoxyethyl (Compound 2b) groups were synthesized following the procedure described in the bibliography[29,30]. In a second step, the bromide atom was substituted by piperazinyl groups (Fig. 2) following a modified method similar to that reported by Tian et al.[19].

3.3.6.1 Synthesis of N-(2-hydroxyethyl)-4-bromo-1,8-naphthalimide (2a)

In a pressure-resistant microwave test tube, a mixture of 4-bromo-1,8-naphthalic anhydride (compound 1) (1.4 g, 5 mmol) and ethanol amine (0.4 g, 5 mmol) in ethanol (15 ml) was heated under argon at 85 ºC and stirred at 600 rpm for 2h. The resulting mixture was cooled at 5 °C. The solid separated was filtered and washed with cold ethanol (3 x 30 ml) and after dried was identified as N-hydroxyethyl-4-bromo-1,8-naphthalimide (compound 2a). Yield 90% (1.4 g). M.p.: 206 ± 2 ºC. ^{1}H-NMR (δ_H ppm) (300 MHz, DMSO-d_6, Me_4Si): δ 8.42 (dd, *J* = 13.9, 7.9 Hz, 2H), 8.20 (d, *J* = 7.9 Hz, 1H), 8.10 (d, *J* = 7.8 Hz, 1H), 7.89 (t, *J* = 7.9 Hz, 1H), 4.81 (s, 1H), 4.10 (t, *J* = 6.4 Hz, 2H), 3.61 (t, *J* = 5.9 Hz, 2H). ^{13}C-NMR (δ_C ppm) (100.6 MHz, DMSO-d_6, Me_4Si): δ 162.90, 162.85, 132.41, 131.42, 131.24, 130.80, 129.61, 128.98, 128.67, 128.14, 122.70, 121.92, 57.71, 41.95. FT-IR (wavenumbers, cm^{-1}): ν_{OH} 3386 cm^{-1}; ν_{C-H} 3066 cm^{-1} aromatic stretch vibration $\nu_{C=O}$ 1692, 1658 cm^{-1}; $\nu_{N-C=O}$ 1611 cm^{-1}; ν_{C-C} 1585, 1568 cm^{-1} aromatic ring chain vibrations. EA: theoretical values: %C 52.52; %H 3.15; %N 4.38; experimental values: %C 52.42; %H 3.25; %N 4.25. EI-MS m/z calculated for $C_{14}H_{10}BrNO_3$ $(M+H)^+$ 321.0; found 321.0.

3.3.6.2 Synthesis of N-(2-methoxyethyl)-4-bromo-1,8-naphthalimide (2b)

Compound 2b was synthetized following the same procedure described for compound 2a from but using 2-Methoxyethylamine (0.38 g, 5 mmol) as a reactive amine. Yield 93% (1.55 g). M.p.: 163.57 ± 2 ºC. ^{1}H-NMR (δ_H ppm) (300 MHz, $CDCl_3$, Me_4Si): δ 8.62 (d, *J* = 7.3 Hz, 1H), 8.52 (d, *J* = 8.4 Hz, 1H), 8.38 (d, *J* = 7.9 Hz, 1H), 8.00 (d, *J* = 7.9 Hz, 1H), 7.85 – 7.77 (m, 1H), 4.42 (t, *J* = 5.8 Hz, 2H), 3.72 (t, *J* = 5.8 Hz, 2H), 3.37 (s, 3H). ^{13}C-NMR (δ_C ppm) (100.6 MHz, $CDCl_3$, Me_4Si): δ 163.80, 163.78, 133.38, 132.26, 131.43, 131.18, 130.68, 130.40, 129.12, 128.16, 123.09, 122.23, 69.68, 58.92, 39.50. FT-IR (wavenumbers, cm^{-1}): ν_{C-H} 3065 cm^{-1} aromatic stretch vibration; ν_{O-CH3} 2824,2832 cm^{-1}; $\nu_{C=O}$ 1698, 1655 cm^{-1}; $\nu_{N-C=O}$ 1613 cm^{-1}; ν_{C-C} 1589, 1570 cm^{-1} aromatic ring chain vibrations. EA: theoretical values: %C 53.91; %H 3.62; % N 4.19; experimental values % C 53.82; % H 3.65; % N 4.22. EI-MS m/z calculated for $C_{15}H_{12}BrNO_3$ $(M+H)^+$ 335.0; found 335.0.

Synthesis of compounds 2a and 2b were also carried out in an ace round-bottom pressure flask and conventional heating during 15 h yielded 75 and 80 % respectively.

3.3.6.3 Synthesis of N-(2-hydroxyethyl)-4-(piperazine-1-yl)-1,8-naphthalimide (3a)

In a pressure-resistant microwave test tube, compound 2a (0.20 g, 0.625 mmol) and piperazine (0.16 g, 1.875 mmol) were mixed in 2-methoxyethanol (5 mL) and heated at 130 ºC in argon atmosphere under constant stirring (600 rpm) for 1 h. The mixture was poured into cooled ice/water at 5 °C and the residue was filtered and washed with hot ethanol (30 mL). The solution was filtered and the solvent removed under reduced pressure in order to obtain the yellow solid compound. M.p.: 219.23 ± 2 ºC. MW-yield: 84%. RF method for compound 3a yielded a 64% after 15 h of reaction time. ^{1}H NMR (300 MHz, DMSO-d_6) δ 8.48 – 8.41 (m, 2H), 8.38 (d, *J* = 8.1 Hz, 1H), 7.79 (t, *J* = 7.8 Hz, 1H), 7.30 (d, *J* = 8.2 Hz, 1H), 4.78 (s, 1H), 4.13 (t, *J* = 6.4 Hz, 2H), 3.60 (s, 2H), 3.13 (s, 4H), 3.00 (s, 4H). ^{13}C NMR (75 MHz, DMSO) δ 163.65, 163.11, 156.20, 132.14, 130.48, 129.15, 125.78, 125.22, 122.59, 115.33, 114.79, 57.86, 54.10, 45.67, 41.60. FT-IR (wavenumbers, cm^{-1}): ν_{NH} 3248 cm^{-1}; $\nu_{C\text{-}H}$ 3066 cm^{-1} aromatic stretch vibration; $\nu_{C=O}$ 1685, 1642 cm^{-1}; $\nu_{N\text{-}C=O}$ 1613 cm^{-1}; $\nu_{C\text{-}C}$ 1586, 1571 cm^{-1} aromatic ring chain vibrations; ν_{NH} 1514 cm^{-1} flexion. EA: theoretical values: %C 66.45; %H 5.89; %N 12.91; experimental values: %C 66.55; %H 5.93; %N 12.96. EI-MS m/z calculated for $C_{18}H_{19}N_3O_3$: $(M+H)^+$ 326.1, found. 326.0 (M^+).

3.3.6.4 Synthesis of N-(2-hydroxyethyl)-4-(4-methylpiperazine-1-yl)-1,8-naphthalimide (4a)

The synthesis of compound 4a was similar to the preparation procedure of the compound 3a but using 1-methylpiperazine (208 µL, 1.875 mmol) as a reactive amine. The MW yield was 85% after 1 h and RF yield 67% after 15h. Compound 4a was purified by silica gel column chromatography using dichloromethane:methanol (20:1) as an eluent to obtain a yellow solid. M.p.: 188.43 ± 2 ºC. Yield: 85%. ^{1}H NMR (300 MHz, DMSO-d_6) δ 8.43 (dd, *J* = 11.9, 8.1 Hz, 2H), 8.37 (d, *J* = 8.2 Hz, 1H), 7.79 (t, *J* = 7.8 Hz, 1H), 7.31 (d, *J* = 8.1 Hz, 1H), 4.81 (t, *J* = 5.7 Hz, 1H), 4.12 (t, *J* = 6.4 Hz, 2H), 3.59 (d, *J* = 6.2 Hz, 2H), 3.22 (s, 4H), 2.63 (s, 4H), 2.30 (s, 3H).^{13}C NMR (75 MHz, DMSO) δ 163.61, 163.07, 155.51, 132.04, 130.48, 130.31, 129.08, 125.87, 125.20, 122.59, 115.56, 114.93, 57.85, 54.63, 52.50, 45.74, 41.60. FT-IR (wavenumbers, cm^{-1}): ν_{OH} 3435 cm^{-1}; $\nu_{C\text{-}H}$ 3060 cm^{-1} aromatic stretch vibration; $\nu_{C=O}$ 1692, 1635 cm^{-1}; $\nu_{N\text{-}C=O}$ 1612 cm^{-1}; $\nu_{C\text{-}C}$ 1585 cm^{-1} aromatic ring chain vibrations. Elemental analysis, theoretical value %C 67.24; %H 6.24; %N 12.38; calculate %C 67.15; %H 6.15; %N 12.29. EI-MS m/z calculated for $C_{19}H_{21}N_3O_3$: $(M+H)^+$ 340.2, found. 340.3 (M^+).

3.3.6.5 Synthesis of N-(2-hydroxyethyl)-4-(4-(2-hydroxyethyl)-piperazine-1-yl)-1,8-naphthalimide (5a)

The synthesis of compound 5a was similar to the preparation procedure of the compound 3a but using 1-(2-Hydroxyethyl)piperazine (230 µL, 1.875 mmol) as a reactive amine. Compound 5a was purified by silica gel column chromatography using dichloromethane:methanol (20:1) as an eluent to obtain an yellow solid. M.p.: 178.36 ± 2 ºC. The MW yield was 88% after 1 h and RF yield 68% after 15h. ^{1}H NMR (300 MHz, DMSO-d_6) δ 8.49 – 8.41 (m, 2H), 8.39 (d, *J* = 8.1 Hz, 1H), 7.84 – 7.76 (m, 1H), 7.33 (d, *J* = 8.1 Hz, 1H), 4.81 (t, *J* = 5.9 Hz, 1H), 4.49 (t, *J* = 5.3 Hz, 1H), 4.13 (t, *J* = 6.5 Hz, 2H), 3.65 – 3.51 (m, 6H), 3.23 (s, 4H), 2.74 (s, 4H). ^{13}C NMR (75 MHz, DMSO) δ 163.94, 163.41, 155.88, 132.38, 130.82, 130.67, 129.42, 126.19, 125.51, 122.92, 115.85, 115.17, 60.57, 58.95, 58.19, 53.50, 53.00, 41.94. FT-IR (wavenumbers, cm^{-1}): ν_{OH} 3260, 3146 cm^{-1}; ν_{C-H} 3052 cm^{-1} aromatic stretch vibration; $\nu_{C=O}$ 1695, 1644 cm^{-1}; $\nu_{N-C=O}$ 1613 cm^{-1}; ν_{C-C} 1589, 1576 cm^{-1} aromatic ring chain vibrations. EA: theoretical values %C 65.03; %H 6.28; %N 11.37; experimental values: %C 65.00; %H 6.25; %N 11.31. EI-MS m/z calculated for $C_{20}H_{23}N_3O_4$: $(M+H)^+$ 370.17, found 370.2 (M^+).

3.3.6.6 Synthesis of N-(2-hydroxyethyl)-4-(4-[2-(2-hydroxyethoxy)ethyl]-piperazine-1-yl)-1,8-naphthalimide (6a)

The synthesis of compound 6a was similar to the preparation procedure of the compound 3a but using 1-[2-(2-hydroxyethoxy)ethyl]piperazine (308 µL, 1.875 mmol) as a reactive amine. After completion of the reaction, the solvent was evaporated under reduced pressure and the crude product was then diluted in 50 ml of water. The precipitated product was then filtered off. The aqueous part was extracted with dichloromethane (3 x 30 mL) and the organic layer was dried over K_2CO_3. The solvent was evaporated under reduced pressure to obtain a yellow solid. M.p.: 170.20± 2 ºC. For compound 6a the MW yield was 85% after 1 h and RF yield 70% after 24h. ^{1}H NMR (300 MHz, DMSO-d_6) δ 8.47 – 8.39 (m, 2H), 8.37 (d, *J* = 8.1 Hz, 1H), 7.79 (t, *J* = 7.9 Hz, 1H), 7.31 (d, *J* = 8.2 Hz, 1H), 4.79 (t, *J* = 5.8 Hz, 1H), 4.63 (t, *J* = 5.0 Hz, 1H), 4.13 (t, *J* = 6.5 Hz, 2H), 3.62 – 3.54 (m, 4H), 3.54 – 3.48 (m, 2H), 3.45 (d, *J* = 4.6 Hz, 2H), 3.22 (s, 4H), 2.75 (s, 4H), 2.65 – 2.58 (m, 2H).^{13}C NMR (75 MHz, DMSO) δ 163.63, 163.09, 155.52, 132.07, 130.51, 130.35, 129.08, 125.88, 125.18, 122.58, 115.53, 114.88, 72.29, 68.31, 60.32, 57.88, 57.28, 53.15, 52.64, 41.62. FT-IR (wavenumbers, cm^{-1}): ν_{OH} 3374 cm^{-1}; ν_{C-H} 3066 cm^{-1} aromatic stretch vibration; $\nu_{C=O}$ 1690, 1650 cm^{-1}; $\nu_{N-C=O}$ 1616 cm^{-1}; ν_{C-C} 1588 cm^{-1} aromatic ring chain vibrations. EA: theoretical values %C 63.91; %H 6.58; %N 10.16; experimental values: %C 63.97; %H 6.62; %N 9.60. EI-MS m/z calculated for $C_{22}H_{27}N_3O_5$: $(M+H)^+$ 414.20, found 414.2 (M^+).

3.3.6.7 Synthesis of N-(2-methoxyethyl)-4-(piperazine-1-yl)-1,8-naphthalimide (3b)

Compound 2b (0.20 g, 0.598 mmol) and piperazine (0.155 g, 1.794 mmol) were mixed in 2-methoxyethanol (5 mL) and heated under MW radiation at 130 ºC in an argon atmosphere under constant stirring (600 rpm) for 1 h. After completion of the reaction, the solvent was evaporated under reduced pressure and the crude was washed with water and filtered to obtain the compound as a yellow solid. M.p.: 145.60 ± 2ºC. The MW yield was 84% after 1 h and by conventional heating, RF yield 69% after 15h. ^{1}H NMR (300 MHz, DMSO-d_6) δ 8.48 – 8.41 (m, 2H), 8.40 (s, 1H), 7.83 – 7.75 (m, 1H), 7.30 (d, *J* = 8.1 Hz, 1H), 4.23 (t, *J* = 6.1 Hz, 2H), 3.57 (t, *J* = 6.1 Hz, 2H), 3.26 (s, 3H), 3.15 (s, 4H), 3.00 (s, 4H). ^{13}C NMR (75 MHz, DMSO) δ 163.50, 162.94, 156.29, 132.25, 130.58, 129.09, 125.75, 125.17, 122.33, 115.00, 114.77, 68.67, 57.94, 54.08, 45.66, 38.33. FT-IR (wavenumbers, cm^{-1}): ν_{NH} 3248 cm^{-1}; ν_{C-H} 3069 cm^{-1} aromatic stretch vibration; ν_{O-CH3} 2828, 2808 cm^{-1} $\nu_{C=O}$ 1690, 1650 cm^{-1}; $\nu_{N-C=O}$ 1613 cm^{-1}; ν_{C-C} 1588, 1572 cm^{-1} aromatic ring chain vibrations; ν_{NH} 1514 cm^{-1} flexion. EA: theoretical values %C 67.24; %H 6.24; %N 12.38; experimental values: %C 67.20; %H 6.18; %N 12.31. EI-MS m/z calculated for $C_{19}H_{21}N_3O_3$: $(M+H)^+$ 340.1, found. 340.0 (M^+).

3.3.6.8 Synthesis of N-(2-methoxyethyl)-4-(4-methylpiperazine-1-yl)-1,8-naphthalimide (4b)

Compound 4b was synthetized by mixing compound 2b (0.2 g, 0.598 mmol), 1-methylpiperazine (200 µL, 1.7964 mmol) in 5 mL of 2-methoxyethanol and following the same procedure as for compound 3b. M.p.: 139.44 ± 2 ºC. The MW yield was 83% after 1 h and by conventional heating, RF yield 73% after 15h. ^{1}H NMR (300 MHz, DMSO-d_6) δ 8.42 (dd, *J* = 12.3, 8.0 Hz, 2H), 8.36 (d, *J* = 8.1 Hz, 1H), 7.83 – 7.73 (m, 1H), 7.31 (d, *J* = 8.2 Hz, 1H), 4.22 (t, *J* = 6.1 Hz, 2H), 3.57 (t, *J* = 6.1 Hz, 2H), 3.25 (s, 3H), 3.22 (s, 4H), 2.63 (s, 4H), 2.30 (s, 3H). ^{13}C NMR (75 MHz, DMSO) δ 163.51, 162.97, 155.66, 132.21, 130.64, 130.51, 129.08, 125.93, 125.21, 122.40, 115.29, 114.99, 68.67, 57.94, 52.49, 45.73, 38.36. FT-IR (wavenumbers, cm^{-1}): ν_{C-H} 3067 cm^{-1} aromatic stretch vibration; $\nu_{C=O}$ 1695, 1650 cm^{-1}; $\nu_{N-C=O}$ 1613 cm^{-1}; ν_{C-C} 1586, 1574 cm^{-1} aromatic ring chain vibrations. EA: theoretical values %C 67.97; %H 6.56; %N 11.89; experimental values %C 67.87; %H 6.56; %N 11.80. EI-MS m/z calculated for $C_{20}H_{23}N_3O_3$: $(M+H)^+$ 354.17, found 354.2 (M^+).

3.3.6.9 Synthesis of N-(2-methoxyethyl)-4-(4-(2-hydroxyethyl)-piperazine-1-yl)-1,8-naphthalimide (5b)

The synthesis of compound 5b was similar the preparation procedure of the compound 3b but using 1-(2-Hydroxyethyl)piperazine (220 µL, 1.796 mmol) as a reactive amine. Compound 5b was purified by silica gel column chromatography using dichloromethane:methanol (20:1) as an eluent to obtain an

yellow solid. M.p.: 124.17 ± 2 ºC. Yield: 84%.^{1}H NMR (300 MHz, Chloroform-*d*) δ 8.57 (d, *J* = 7.2 Hz, 1H), 8.50 (d, *J* = 8.0 Hz, 1H), 8.39 (d, *J* = 8.4 Hz, 1H), 7.67 (t, *J* = 7.8 Hz, 1H), 7.20 (d, *J* = 8.0 Hz, 1H), 4.41 (t, *J* = 5.6 Hz, 2H), 3.71 (t, *J* = 5.3 Hz, 4H), 3.36 (s, 3H), 3.30 (s, 4H), 2.84 (s, 4H), 2.75 – 2.65 (m, 2H). ^{13}C NMR (75 MHz, $CDCl_3$) δ 164.94, 164.45, 156.25, 133.07, 131.63, 130.66, 130.32, 126.53, 126.05, 123.55, 117.09, 115.33, 70.09, 59.83, 59.18, 58.31, 53.48, 53.41, 39.49. FT-IR (wavenumbers, cm^{-1}): ν_{OH} 3140 cm^{-1}; ν_{C-H} 3052 cm^{-1} aromatic stretch vibration; $\nu_{C=O}$ 1696, 1645 cm^{-1}; $\nu_{N-C=O}$ 1613 cm^{-1}; ν_{C-C} 1589, 1576 cm^{-1} aromatic ring chain vibrations. Elemental analysis, theoretical value %C 65.78; %H 6.57; %N 10.96; calculate %C 65.87; %H 6.68; %N 11.04. EI-MS: m/z calculated for $C_{21}H_{25}N_3O_4$ $(M+H)^+$ 384.18; found 384.2 (M^+).

3.3.6.10 Synthesis of N-(2-methoxyethyl)-4-(4-[2-(2-Hydroxyethoxy)ethyl]-piperazine-1-yl)-1,8-naphthalimide (6b)

Compound 2b (0.2 g, 0.5988 mmol), 2-[2-(1-Piperazinyl)ethoxy]ethanol (295µL, 1.7964 mmol) was mixed in 5 mL of 2-methoxyethanol and heated at 130 °C in argon atmosphere. The mixture was stirred at 600 rpm for 1 h. After completion of the reaction, the solvent was evaporated under reduced pressure and the crude product was then diluted in 50 ml of water. The precipitated product was then filtered off. The aqueous part was extracted with dichloromethane (3 x 30 mL) and the organic layer was dried over K_2CO_3. The solvent was evaporated under reduced pressure to obtain a yellow solid. M.p.: 219.73 ± 2 ºC. The MW yield was 85% after 1 h and by conventional heating, RF yield 69 % after 24 h. ^{1}H NMR (300 MHz, DMSO-d_6) δ 8.43 (dd, *J* = 11.0, 8.0 Hz, 2H), 8.37 (d, *J* = 8.1 Hz, 1H), 7.82 – 7.75 (m, 1H), 7.31 (d, *J* = 8.2 Hz, 1H), 4.64 (s, 1H), 4.22 (t, *J* = 6.1 Hz, 2H), 3.58 (q, *J* = 6.0 Hz, 4H), 3.53 – 3.48 (m, 2H), 3.45 (d, *J* = 4.7 Hz, 2H), 3.25 (s, 3H), 3.22 (s, 4H), 2.75 (s, 4H), 2.62 (t, *J* = 5.8 Hz, 2H).^{13}C NMR (75 MHz, DMSO) δ 163.54, 162.99, 155.68, 132.24, 130.67, 130.55, 129.08, 125.94, 125.20, 122.39, 115.27, 114.94, 72.28, 68.70, 68.31, 60.30, 57.97, 57.26, 53.13, 52.64, 38.39. FT-IR (wavenumbers, cm^{-1}): ν_{O-H} 3356 cm^{-1}; ν_{C-H} 3065 cm^{-1} aromatic stretch vibration; $\nu_{C=O}$ 1687, 1648 cm^{-1}; $\nu_{N-C=O}$ 1613 cm^{-1}; ν_{C-C} 1585 cm^{-1} aromatic ring chain vibrations. EA: theoretical value %C 64.62; %H 6.84; %N 9.83; experimental values %C 64.60; %H 6.93; %N 9.76. EI-MS: m/z calculated for $C_{23}H_{29}N_3O_5$ $(M+H)^+$ 428.2; found 428.3 (M^+).

3.3.7 pH measurements

Measurements of pH were obtained with a Mettler Toledo SevenGo Duo Pro meter with an InLab Expert Pro ISM-ID67 electrode at room temperature (23 ºC) and previously calibrated with standard buffers. The sensing measurements determined from the solutions of naphthalimide derivatives and

functionalized membranes were performed using HCl and NaOH solutions for pH variation in the mixture water:ethanol (4:1) as solvent.

The acid titration by UV/Vis and fluorescence in aqueous solution was performed as follows. The titration in solution with naphthalimide derivatives (water:ethanol 4:1, naphthalimide concentration 10^{-4} M and pH=12.0 fixed by addition of NaOH solution) was carried out by increasing the acidity from pH 12.0 to pH 2.0 by adding aliquots of the diluted hydrochloric acid. After each addition, the pH was measured after the solutions were allowed to equilibrate for 10 min and the UV/Vis and fluorescence spectra were recorded.

In the case of functionalized crosslinked membranes, films were cut into strips of 1x4 cm and fixed in a homemade support that can also be slotted into the cell holder of the spectrophotometers. To study the effect of the pH in the spectroscopic properties of the membranes, film strips were immersed in previously prepared vials (50 mL) containing solutions from pH 12.0 to pH 2.0. The UV/Vis and fluorescence spectra for each pH were taken after 20 min. of conditioning time.

3.4 Results and discussion

3.4.1 Synthesis of naphthalimide derivatives

The synthesis route3,4 to obtain N-hydroxy alkyl piperazine naphthalimides is presented in Fig. 2. In the first step, the condensation of 4-bromo-1,8-naphthalic anhydride with 2-hydroxyethylamine (series a) or 2-methoxyethylamine (series b) under microwave irradiation in ethanol at 85 °C afforded 2a and 2b respectively in high yield at a shorter reaction time than conventional conditions.

In the second reaction step (Fig. 2), compounds 2a and 2b reacted with 3 equiv. of each piperazine derivative as detailed in the experimental description (section 2.6.) to obtain the piperazine-naphthalimides derivatives shown in Fig. 2. Hence, we have prepared piperazine substituted derivatives with hydrogen and methyl groups[19] as substituents on the amine groups (structures 3 and 4 respectively), but also with bigger substituents (structures 5 and 6) in order to study their PET processes and their protonation in acid media.

The best synthesis conditions were noted under MW irradiation for 1 h at 850W and a ceiling temperature of 130 °C in 2-methoxyethanol. In contrast, the best conditions for the synthesis carried out under reflux by conventional heating required reaction times of 15 h and 24 h for compounds 6a and 6b when 2-[2-(1-Piperazinyl)ethoxy]ethanol was used as reactive amine.

In all the cases, MW irradiation allowed higher yields at shorter reaction times than the conventional RF method. These results are in agreement with those reported in the literature[24,19].

3.4.2 Membrane preparation, functionalization with piperazine naphthalimides sensors and characterization

The membrane prepared containing acid chloride functionalities (M-Cl) as a base material for further functionalization was obtained by bulk photopolymerization of a mixture of monomers combining the hydrophilic character of VP (55%) with the hydrophobic nature of BA (35%) and adding MACl (10%) as the reactive monomer for functionalization. A 5% of EGDMMA as the crosslinking agent of the mixture controlled the crosslinking degree of the final membrane. This produced a reversible water-swollen membrane (Fig. 1). After the bulk photopolymerization, all the experiments reached >98 % of conversion (determined by weight differences), and the resulting crosslinked acrylic membrane contained 2.8% of chlorine in the structure (Fig. 3B).

In a second step, the M-Cl membrane was functionalized with the three naphthalimide derivatives from the series synthetized in this work (Fig. 1) that contained mono hydroxy alkyl piperazine, derivatives 4a, 5b and 6b. This functionalization was accomplished successfully by conventional heating in THF at 55 ºC for 15h under very low stirring speed. This selected reaction temperature is 10°C below the THF boiling point to be sure there isn't any damage of the membrane in the heterogeneous reaction, such as breaks, wrinkles and warps that could decrease the optical quality of the membrane. Under these experimental conditions, the Schotten-Baumann reaction used to graft the naphthalimide derivatives to the M-Cl membrane proceeded very slowly. This allowed a good control in homogeneity of functionalization without physically damaging the membrane. The unreacted acid chloride group disappeared after hydrolysis when the membranes were washed as shown in Fig 3C. The amount of naphthalimide grafted to the membranes (Table 1) was determined from the UV-Vis absorbance using the absorption coefficient of each derivative (Table 3) previously calculated in water-ethanol (4:1, v/v).

Table 1. Content of chlorine and naphthalimide derivative in the membranes and thermal properties determined by DSC and TGA.

Membrane	**Cl Content[(a)]** (%)	**Naphthalimide Content[(b)]** ($mol \cdot L^{-1}$) $x10^3$	**T_g [(c)]** (^oC)	**T_5[(d)]** (°C)	**T_{10} [(d)]** (°C)
M-Cl	2.8	-	46.9	214	337
M-4a	0	2.73	45.3	326	369
M-5b	0	3.27	45.4	337	371
M-6b	0	4.72	45.6	334	372

[a] Determined by TGA peak at 175ºC corresponding to Cl, EI-MS m/z 36 (M^+); [b] Determined from the membrane (180 microns of thickness) by UV spectroscopy; [c] Measured by DSC second heating run at a heating rate of $10^oC \cdot min^{-1}$; [d] Temperatures corresponding to 5% and 10% weight loss.

After 15 hours of reaction time the content of the naphthalimide derivative in the membrane was very low (Table 1) but the concentration is adequate for sensing applications by UV-vis and fluorescence spectroscopies.

The good physical characteristics of the functionalized membranes are similar than those observed by other authors[25] with copolymers of VP/BA. All DSC thermograms of the membranes revealed the presence of a single glass transition temperature for all the membranes confirming copolymer miscibility. The characteristic T_g values for the membranes are shown in Table 1 and the DSC thermograms (second scan) obtained for M-Cl and M-5b samples are plotted in Fig. 3A. The observed step for M-Cl appeared at a similar temperature (46.9 ºC) than the corresponding steps for the functionalized membranes (Table 1) due to the low content of C-Cl dipoles present in the M-Cl membrane.

The thermal stability of the membranes was evaluated using TGA and Table 1 shows the thermal data, in terms of characteristic weight loss (T_5 and T_{10} respectively).

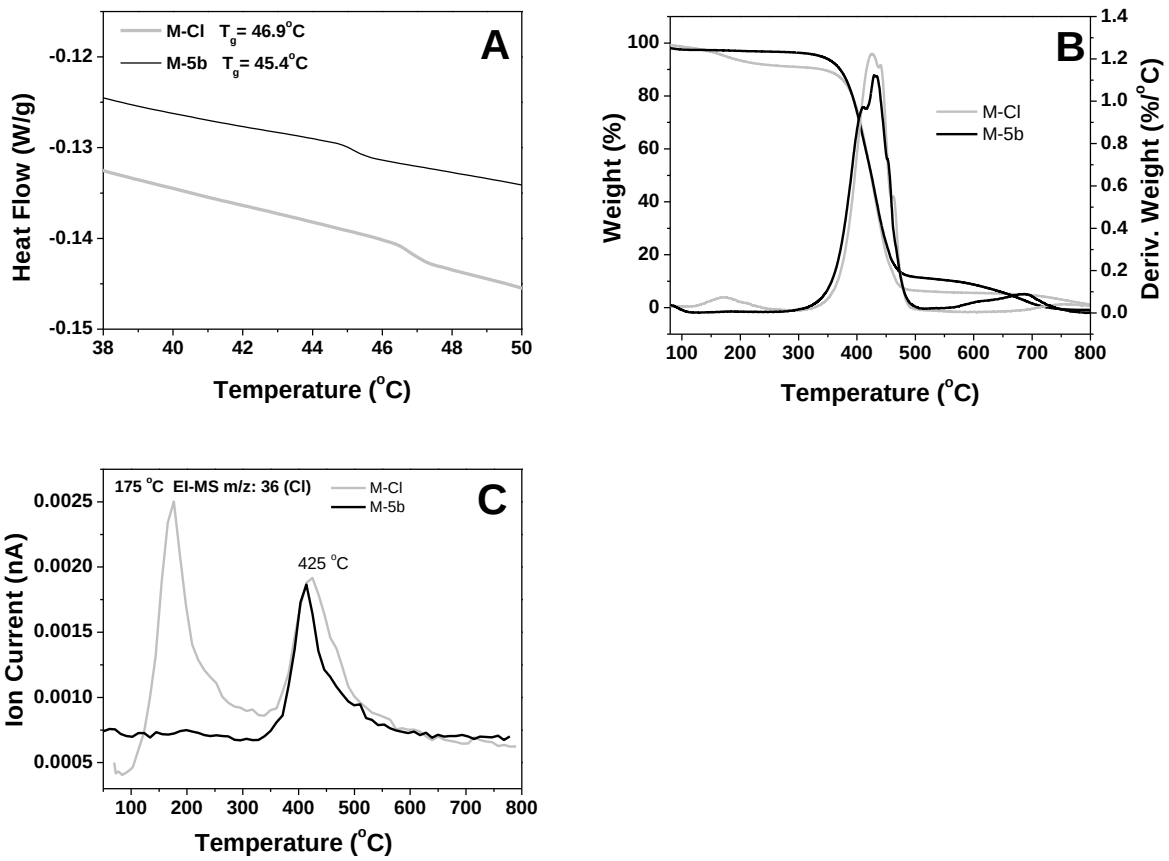

Fig.3. DSC thermograms (A), TGA and DTGA curves (B) and evolved gas analysis by MS detector (C) of the M-Cl crosslinked membrane and M-5b membrane functionalized with naphthalimide derivative 5b.

Figure 3B shows the TGA thermograms obtained for the M-Cl and M-5b membranes and their corresponding first derivative curves. The M-Cl membrane exhibits a weight loss of 2.8% that was identified by MS analysis of evolved gas at 175 ºC as chlorine (EI-MS m/z: 36 (Cl)), as it is shown in fig. 3C. After functionalization, the chlorine weight was not observed confirming the total hydrolysis of unreacted acid chloride. For all functionalized membranes two peaks were observed, as it is shown for M-5b in Fig. 3B. The highest weight loss rate that was observed at 410 °C corresponds to the degradation of acrylic components of the membrane and the second one observed at 431 °C has been attributed[7] to the lactam subgroup degradation.

The swelling properties of the membranes were examined by measuring the swelling (%) after immersion in water and THF and are detailed in Table 2.

Table 2. Swelling degree (SD) in water and THF, advancing contact angle (CA) and total (γ), polar (γ^p), and disperse (γ^d) surface energy data for the crosslinked membranes.

Membrane	SD (%)[a]		Static CA (°)		Surface Energy ($mN.m^{-1}$)[b]		
	Water	THF	Water	Diiodomethane	γ	γ^p	γ^d
M-Cl	29.8	45.4	59.9	41.6	51.64	13.48	38.16
M-4a	29.9	61.2	69.6	42	45.43	9.25	36.18
M-5b	30.4	62.0	71.7	38.6	45.75	6.56	39.19
M-6b	29.9	63.5	71	46.1	46.22	6.88	39.34

[a]±0.3; [b] Calculated using Owens-Wendt´s method

The SD in water (approx. 30 %) and in THF (approx. 60 %) confirms the hydrophilic character of the membranes and the adequate swelling for solid sensors in water and organic media. Also, the hydrophilicity of the membrane surfaces was characterized by static contact angle determination. The measured CAs were then used to calculate the polar, disperse, and total surface energies of the membranes. The change in the total surface energy (γ) and its polar (γ^p) and dispersive (γ^d) components of the M-Cl and functionalized membranes with naphthalimides (M-4a, M-5b and M-6b) was calculated by the Owens–Wendt's method[28] (Table 2). The variation in the values of the total, polar, and disperse solid surface energies before (M-Cl) and after functionalization (M-4a, M-5b and M-6b), shows that the total surface energy of the functionalized membranes decreases from 51.64 $mN \cdot m^{-1}$ for M-Cl to 45-46 $mN \cdot m^{-1}$ for the membranes containing naphthalimide moieties and, particularly for the polar component.

The functionalized membranes with piperazine-naphthalimide groups were easily handled materials and exhibited convenient properties for solid sensor applications, such as swelling in water, thermal stability, flexibility, optical transparency and dimensional stability to be reused. The obtained three-dimensional cross-linked hydrophilic polymer networks are capable of swelling or de-swelling reversibly in water and retaining a controlled and reproducible volume of liquid in the swollen state. This behaviour, as will be seen in the next section, allowed controllable responses to external environmental changes of pH.

3.4.3 Effect of pH on the absorption and fluorescence properties of piperazine naphthalimides derivatives and membranes

Piperazine substituted naphthalimides such as the structures synthetized in this work (Fig. 2) exhibit interesting fluorescence properties, hence 4-amino-1,8-naphthalimide fluorophore can be quenched by the PET process that occurs from the alkylated amine donor to the 4-amino-1,8-naphthalimide

fluorophore through the piperazinyl ring. The fluorescence of the 4-amino-1,8-naphthalimide fluorophore is quenched. The PET path can be switched off either by the protonation or quaternization of the amine and the fluorescence of the naphthalimide fluorophore is then recovered as is shown for the derivative 4a anchored to the membranes in figure 4.

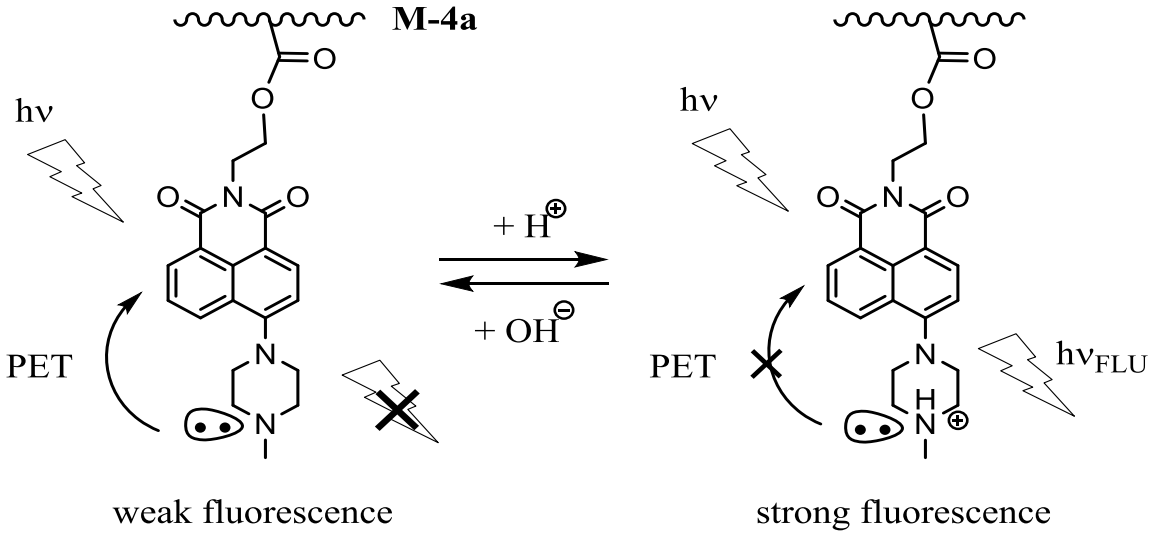

Fig.4. Fluorescence response of piperazine-naphthalimide structure to pH though PET mechanism.

The effect of pH variation on the absorbance and fluorescence properties of these derivatives is illustrated in figure 5 for the naphthalimide derivative 4a in solution and the corresponding membrane M-4a under the same conditions.

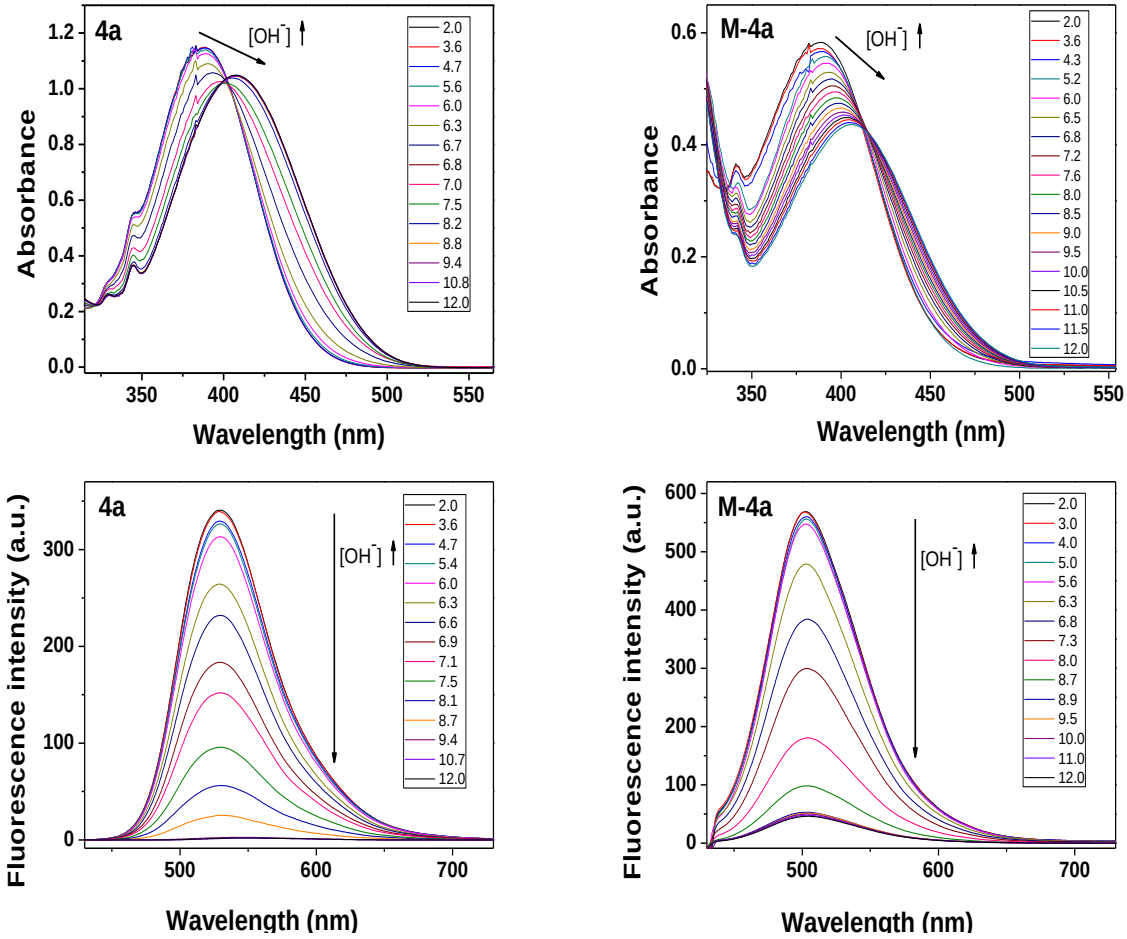

Fig. 5. Spectroscopic characteristics as a function of pH (2.0-12.0) of absorption and fluorescence of naphthalimide derivative 4a and M-4a membrane.

All the absorption spectra of the naphthalimide derivatives and membranes exhibit (as solution or as 180 µm-membrane) similar band shapes in the absorption range of 350-500 nm. As it is shown in figure 5, for the compound 4a and membrane M-4a, their absorption peaks were red-shifted from 388 to 408 nm with a clear isosbestic point at 402 nm when pH values were changed from 2.0 to 12.0 in water:ethanol (4:1) by adjusting pH values with NaOH and HCl aqueous solutions. As expected, the fluorescence intensities originating from 4a and M-4a fluorophores were varied upon different pH values (Figure 5), resulting in a strong enhancement in acid media due to the protonation of the piperazine and its subsequent PET blocking effect (Fig. 4). In the case of compound 4a the factor of enhancement (FE) was about 25 times in fluorescence intensity when adjusting the pH from 12.0 to 2.0 (Table 3). Moreover, the wavelength emission maxima were red-shifted by around 20 nm (Table 3) by changing the pH values from 2.0 to 12.0 for all the naphthalimide derivatives in solution except for naphthalimide 3b and 4b that do not have hydroxyl substituents in their structures and the red-shift

for them was about 2-3 nm. For the naphthalimide fluorophores bonded to the membranes though the hydroxyl groups, the bathochromic shift of the fluorescence maxima with pH was also 2-3 nm.

All the spectral data measured as a function of pH values for the naphthalimide derivatives and the three functionalized membranes are summarized in Table 3.

Table 3. Various parameters for piperazine-1,8-naphthalimide derivatives (a and b structures) in solution[(a)] and bonded to the polymer membrane (M) determined according to pH dependence by UV–Vis absorption and fluorescence spectroscopy.

Parameter	3a	4a	5a	6a	3b	4b	5b	6b	M-4a	M-5b	M-6b
$\lambda_{ABS\text{-}acid}$	389	388	388	388	389	389	389	388	388	388	390
$Log\ \varepsilon_{acid}$ (b)	4.07	4.06	4.05	4.06	4.06	4.06	4.056	4.06	-	-	-
$\lambda_{Isobestic}$	403	402	402	402	404	402	402	402	403	402	402
$\lambda_{ABS\text{-}base}$	413	408	408	408	410	409	409	409	407	408	408
$Log\ \varepsilon_{base}$ (b)	4.04	4.02	4.01	4.02	4.01	4.02	4.02	4.02	-	-	-
pK_a (c)	8.24	7.37	6.99	6.65	8.62	7.30	6.82	6.71	7.62	7.25	6.40
$\lambda_{FLU\text{-}acid}$	533	529	530	530	531	529	530	529	502	503	503
$\phi_{FLU\text{-}acid}$ (d)	0.097	0.330	0.184	0.238	0.084	0.274	0.170	0.197	-	-	-
$\phi_{FLU\ pH=7}$ (d)	0.093	0.304	0.101	0.099	0.079	0.249	0.095	0.091	-	-	-
$\phi_{FLU\ ethanol}$ (d)	0.017	0.025	0.022	0.026	0.026	0.020	0.017	0.024	water:ethanol (4:1, v/v)<		
$\phi_{FLU\ hexane}$ (d)	0.203	0.389	0.285	0.293	0.213	0.365	0.270	0.275	< Ethanol <<< hexane		
$\lambda_{FLU\text{-}base}$	543	548	550	550	532	532	554	545	505	506	504
$\phi_{FLU\text{-}base}$ (d)	0.010	0.013	0.010	0.009	0.005	0.010	0.009	0.007	-	-	-
pK_a^* (c)	7.1	6.93	6.95	6.4	7.15	7.11	7.04	6.48	7.15	6.71	6.5
$\Delta\nu$ (e)	6329	6258	6070	6061	6293	6123	6070	5998	5515	5618	5539
FE (f)	8.5	25.3	19.1	22.0	18.1	17.9	22.0	27.1	12.3	8.0	9.5

(a) Measured at 10^{-4} M in water-ethanol (4:1, v/v) unless specifically stated otherwise. The subscripts "acid" and "base" refer to the limiting value of a given parameter when the acid or base condition is increased until pH=2.0 or pH=12.0 respectively. Fluorescence emission spectra were obtained by excitation at $\lambda_{Isobestic}$; (b) ε, molar absorptivity in $M^{-1}cm^{-1}$; (c) Obtained [24] by analyzing the pH dependence of the absorbance (A) or emission intensity (I) at a given wavelength according to the equation $log[(A_{acid} - A)/(A - A_{base})] = pH - pK_a$ or $log[(I_{FLU\text{-}acid} - I)/(I - I_{FLU\text{-}base})] = pH - pK_a^*$ (d) Relatively to coumarin 6 (ϕ_F=0.78 in ethanol), uncertainty = 0.001 or 10%, whichever is the larger; (e) Stokes shift ($\nu_{FLU} - \nu_{ABS}$) in frequency (cm^{-1}); (f) Acid- induced fluorescence enhancement factor $FE = A_{FLU\text{-}acid}/A_{FLU\text{-}.base}$

The quantum yields of fluorescence in acid media (Table 3) for the hydroxy alkyl substituted piperazine naphthalimides derivatives ($\phi_{FLU\text{-}acid}$ =0.33-0.084) are lower than that of the non-hydroxylated derivative N-butyl-4-N′-methylpiperazino-1,8-naphthalimide ($\phi_{FLU\text{-}acid}$=0.55)[22]. Also, the quantum yields of fluorescence in basic media (Table 3) are higher ($\phi_{FLU\text{-}base}$ = 0.005-0.010) than that measured for N-butyl-4-N′-methylpiperazino-1,8-naphthalimide ($\phi_{FLU\text{-}base}$ = 0.001)[22]. The quantum yield of fluorescence for the membranes couldn't be calculated due to the difference in geometry between the fluorescence standard in solution and the membranes. The factor of fluorescence enhancement for the membranes in acid media was calculated (Table 3) by comparing the increase of intensities from basic to acid media and the enhancement was around 8-12 times. This enhancement in

acid media (FE = 8-12.3) is higher than that obtained by other authors[23], where an enhancement of 4.7 was reported with a membrane obtained by copolymerization of *N*-allyl-4-(4´-methyl-piperazinyl)-1,8-naphthalimide with 2-hydroxyethyl methacrylate and acrylamide.

The presence of hydroxyl groups in the naphthalimide derivatives studied here and the ester functionality as a linking group of the naphthalimides in the membranes reduced the factor of enhancement of fluorescence in acid media with respect to that for other similar structures having only N-alkyl substituents[21,22]. Even though FE values obtained with the membranes confirm their interesting proton "off–on" switch behaviour as an optical pH solid sensor.

The pK_a values of naphthalimide derivatives and the functionalized membranes were calculated[31] from the curves of absorption changes in the presence of increasing acidity (from pH= 12.0 to 2.0) and the obtained values are compiled in Table 3.

The smaller substituents on the amine groups (structures 3 with hydrogen or 4 with methyl as substituents) enabled a higher pK_a as they are more easily protonated than the bigger substituents (structures 5 and 6). The pK_a values obtained for the functionalized membranes are close to those values measured for the corresponding piperazine derivatives (Table 3) confirming a similar sensitivity to acid media. The pK_a of the functionalized membranes is close to the pH of 7.0 which makes it adequate for sensors in biological and environmental applications[19].

The fluorescence response of the piperazine derivatives and the functionalized membranes at different pH was compared and the results are plotted in figure 6.

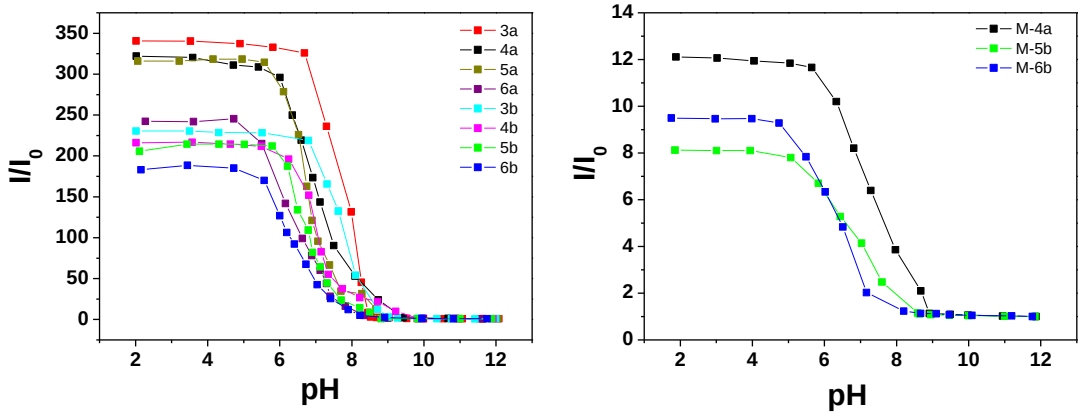

Fig.6. Comparison of the fluorescence intensity changes (I/I_o) with pH (2.0-12.0) for the piperazine-naphthalimide derivatives in solution (A) and for functionalized membranes (B). (I_0 and I are the fluorescence intensities of initial (pH=12.0) and that after acidification respectively).

All the synthesized naphthalimides (Fig. 6A) exhibited a sensitive fluorescence change towards pH but with different intervals and slopes of changes depending of the size of the amino substituents. For the functionalized membranes (Fig. 6B) the fluorescence intensity increased as the pH values decreased from 9.0 to 5.0 for M-4a and from 8.5 to 4.0 for the membranes obtained by linking the naphthalimides to the substituent of the piperazine structure, M-5b and M-6b. In the acidic pH range, especially for pH lower than 4.0, the fluorescence intensity attained its maximum and kept unchanged as well as in the basic pH range up to 9.0 where the fluorescence intensity reached its minimum. The pK_a* values (Table 3) for the excited state do not differ strongly from the corresponding pK_a for the ground state except for the structures 3a and 3b where the substituent of the piperazine is a hydrogen. For the rest of the structures and membranes the position of the inflection points in the fluorometric titration is similar to those obtained from the absorbance changes with pH.

The fluorescence quantum yields of the naphthalimides derivatives studied here are relatively low in polar solvents (water, ethanol) in comparison to those values obtained in non-polar solvents such us hexane (Table 3). This fact is probably due to the photo-induced electron transfer from the piperazine to the fluorophore and the fact that in polar solvents the orbit energy of HOMO becomes lower facilitating the PET process. The polarity effect on the photophysical properties of the naphthalimide derivatives was studied by measuring their absorption and fluorescence spectra in solvents of increasing solvent polarity parameter $E_T(30)$. All the naphthalimide derivatives exhibited similar solvathochromic UV-Vis and emission spectra. As an illustrative example in figure 7, the values of absorption and emission maxima are plotted for different solvents.

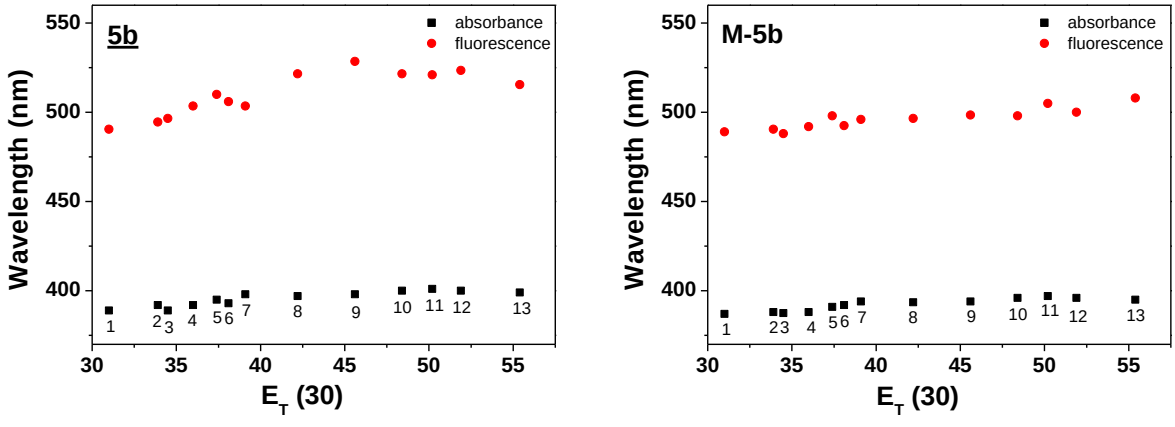

Fig. 7. Dependence of absorbance and Fluorescence emission wavelengths maxima of naphthalimide derivative 5b and the membrane M-5b on the empirical solvent polarity parameter, $E_T(30)$. Solvents: 1. Hexane, 2. Toluene, 3. Diethyl ether, 4. Dioxane, 5. THF, 6. Ethyl acetate, 7. Chloroform, 8. Acetone, 9. Acetonitrile, 10. 2-propanol, 11. Butanol, 12. Ethanol, 13. Methanol.

The maximum wavelengths of the absorption and fluorescence emissions are slightly red shifted with increasing solvent polarity except for the H-bonding solvents in the case of naphthalimide 5b. This is due to the presence of hydroxyl groups in the structure that provoke specific solute-solvent interaction. In general, the absorption maxima are less sensitive to the influence of solvent polarity than the fluorescence maximum. In the membranes, as shown in Fig. 6 for M-5b, the low bathochromic shifts in the fluorescence maximum with an increase of solvent polarity are consistent with small differences between the dipole moments of the ground and excited states.

3.4.4 Response time to pH of the functionalized membranes

The reversibility of the pH induced fluorescence signal was evaluated by determining the absorbance and fluorescence of the membranes by alterning their immersion in solutions of pH 2.0 and pH 12.0. Several cycles of successfull enhancement/quenching of fluorescence were carried out with each membrane without loss of fluorescent emission. The protonation of the aliphatic amine group involved seems quite reversible and no noticeable hysteresis effect was observed in the solid sensors.

The pH response of the membranes is dependent upon the proton permeability into the photocrosslinked material. Hence, the response time of the absorption and fluorescence spectra of the functionalized membranes was studied and the obtained results are plotted in Fig. 8.

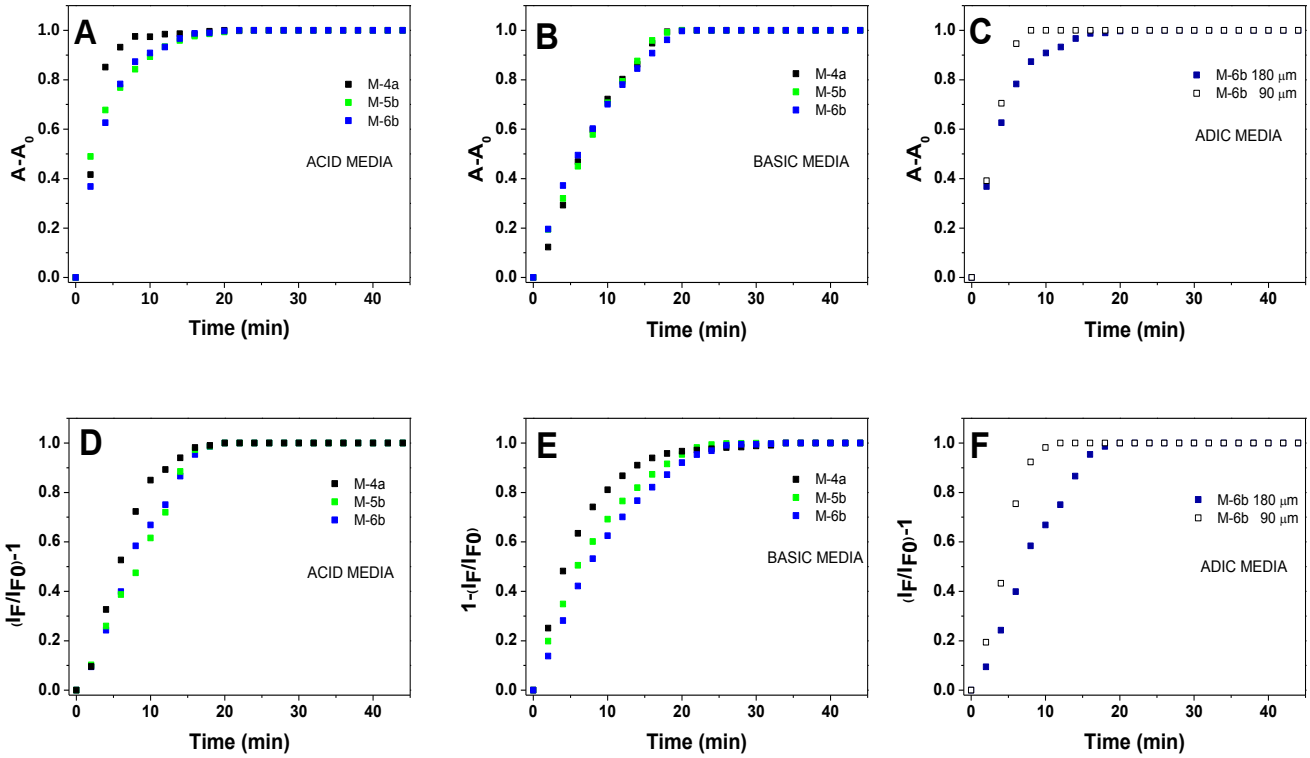

Fig. 8. Time response to pH of the functionalized membranes: Absorbance (A) and fluorescence (D) to acid media (pH=2.0), absorbance (B) and fluorescence (E) to basic media (pH=12.0) and effect of the membrane thickness in time response to acid media in absorbance (C) and fluorescence (F).

The pH response of the membranes is dependent upon the proton permeability into the crosslinked matrix and the three membranes exhibited a high sensitivity to pH in water. The absorbance and fluorescence of the membranes to acidic media (Fig. 8A and 8D respectively) reached the equilibrium in less than 15 min. The sensitivity to the basic medium of the membranes (Fig. 8B and 8E) is lower than that observed in acid media showing a slow response of around 20 min. Hence, the protonation process of the aliphatic piperazine group involved seems to be slower than the deprotonation process.

The time response of the membrane M-4a is shorter that those of the membrane b type. In the membrane M-4a the naphthalimide sensing functionality is linked to the polymer matrix through the imide group and the piperazine group is far from the polymer main chain. Hence, the interaction of the amino group of the piperazine with a proton is much easier than those of M-5b and M-6b where the piperazine is closer to the polymer main chain that can impair the mobility and hence the interactions of the sensing moiety.

The sensitivity of the solid sensor is directly related to the thickness of the pH sensitive membrane. To see the influence of the membrane thickness in the time response to the pH of the sensor, we prepared a membrane under the same experimental conditions but with 90 microns of thickness that was also an easily handled material and with good physical properties. As expected, the time response of this M-6b 90 µm-membrane (Fig. 8C and 8F) was notably shorter than that of the corresponding M-6b 180 µm-membrane.

In this study, we have described a useful procedure to obtain a water-swollen photocrosslinked membrane containing acid chloride groups capable of reacting with sensing molecules containing adequate functionalities, such as hydroxyl groups. The functionalization of M-Cl membrane was carried out using three derivatives of piperazine naphthalimide selected from a series of compounds that had been previously synthetized and spectrophotometrically characterized as a function of pH variations. The dependence of the pH sensitivity was related to the size and structure of the piperazine-naphthalimide substituents linked to the membrane. The solid sensors functionalized with naphthalimides acted as an acid sensor with interesting ranges of sensitivity to pH changes, from 9.0 to 4.0, which are adequate for medical and environmental sensing applications.

3.5 Conclusions

In summary, we have developed a procedure to obtain, using a photopolymerization reaction, water-swollen membranes capable of functionalization with naphthalimide fluorescence sensors and with a pH response.

The obtained results in the synthesis of the series of substituted piperazine naphthalimide derivatives carried out in this work suggested that microwave-assisted syntheses led to higher yields within very short reaction times in comparison to the conventional methods.

The new solid sensors exhibited controlled swelling in water (30%) and sensitive fluorescence changes towards pH between 9.0 and 4.0, and showed a very strong fluorescence at pH < 5.0.

The time response of the functionalized membranes to pH is dependent on the thickness of the membrane, the size of the substituents and the naphthalimide position of linkage to the membrane. The pH induced fluorescence signal of the solid sensors is reversible and several cycles of enhancement/quenching of fluorescence were successfully carried out without a noticeable hysteresis effect.

The present functionalized membranes could be applied as “Off-On” pH-fluorescence sensor in medical and environmental applications with satisfactory results.

3.6 References

[1] C. McDonagh, C.S. Burke, B.D. MacCraith, Optical chemical sensors, Chem. Rev. 108 (2008) 400–422.
[2] H.H. Qazi, A.B.B. Mohammad, M. Akram, Recent progress in optical chemical sensors, Sensors 12 (2012) 16522–16556.
[3] S.M. Borisov, O.S. Wolfbeis, Optical biosensors, Chem. Rev. 108 (2008) 423–461.
[4] A.S. Jeevarajan, S. Vani, T.D. Taylor, M.M. Anderson, Continuous pH monitoring in a perfused bioreactor system using an optical pH sensor, Biotechnol. Bioeng. 78 (2002) 467–472.
[5] I. Grabchev, P. Bosch, M. McKenna, A. Nedelcheva, Synthesis and spectral properties of new green fluorescent poly(propyleneimine) dendrimers modified with 1,8-naphthalimide as sensors for metal cations, Polymer 48 (2007) 6755-6762.
[6] H.N. Kim, Z. Guo, W. Zhu, J. Yoon, H. Tian, Recent progress on polymer-based fluorescent and colorimetric chemosensors, Chem. Soc. Rev. 40 (2011) 79–93.
[7] D. Staneva, I. Grabchev, P. Bosch, Fluorescent Hydrogel–Textile Composite Material Synthesized by Photopolymerization, Int. J. Polym. Mater. Polym. Biomater. 64 (2015) 838–847.
[8] J. Xie, Y.H. Chen, W. Yang, D.M. Xu, K.D. Zhang, Water soluble 1,8-naphthalimide fluorescent pH probes and their application to bioimagings, J. Photochem. Photobiol. A:Chem. 223 (2011) 11–118.
[9] J. Qi, D. Liu, X. Liu, S. Guan, F. Shi, H. Chang, H. He, G. Yang, Fluorescent pH Sensors for Broad-Range pH Measurement Based on a Single Fluorophore, Anal. Chem. 87 (2015) 5897−5904.
[10] S. Lee, J.H. Lee, T. Pradhan, C.S. Lim, B.R. Cho, S. Bhuniya, S. Kim, J.S. Kim, Fluorescent turn-on Zn^{2+} sensing in aqueous and cellular media, Sens. Actuators B 160 (2011) 1489–1493.
[11] C. Hou, A.M. Urbanec, H. Cao, A rapid Hg^{2+} sensor based on aza-15-crown-5 ether functionalized 1,8-naphthalimideTetrahedron Lett. 52 (2011) 4903–4905.
[12] L.P. Duan, Y.F. Xu, X.H. Qian, Highly sensitive and selective Pd^{2+} sensor of naphthalimide derivative based on complexation with alkynes and thio-heterocycle, Chem. Commun. (2008) 6339–6341.
[13] Y. Wang, H-Q. Chang, W-N. Wu, X-J. Mao, X-L. Zhao, Y. Yang, Z-Q. Xu, Z-H. Xu, L. Jia, A highly sensitive and selective colorimetric and off–on fluorescent chemosensor for Cu^{2+} based on rhodamine 6G hydrazide bearing thiosemicarbazide moiety, J. Photochem. Photobiol. A:Chem. 335 (2017) 10-15.
[14] Y. Li, L. Cao, H. Tian, Fluoride Ion-Triggered Dual Fluorescence Switch Based on Naphthalimides Winged Zinc Porphyrin, J. Org. Chem. 71 (2006) 8279–8282.
[15] J. Jiamg, B. Leng, X. Xiao, P. Zhao, H. Tian, Off-On-Off" fluorescent proton switch synthesized by RAFT polymerization, Polymer 50 (2009) 5681-5684.
[16] I. Grabchev, X. Qian, Y. Xiao, R. Zhang, Novel heterogeneous PET fluorescent sensors selective for transition metal ions or protons: polymers regularly labelled with naphthalimide, New J. Chem. 26 (2002) 920–925.
[17] I. Grabchev, J-M. Chovelon, New blue fluorescent sensors for metal cations, and protons based on 1,8-naphthalimide, Dyes Pigments 77 (2008) 1-6.
[18] L. Shen, X. Lu, H. Tian, W. Zhu, A Long Wavelength Fluorescent Hydrophilic Copolymer Based on Naphthalenediimide as pH Sensor with Broad Linear Response Range, Macromolecules 44 (2011) 5612–5618.
[19] Y. Tian, F. Su, W. Weber, V. Nandakumar, B.R. Shumway, Y. Jin, X. Zhou, M.R. Holl, R.H. Johnson, D.R. Meldrum, A series of naphthalimide derivatives as intra and extracellular pH sensors, Biomaterials 31 (2010) 7411-7422.
[20] J. Jiang, X. Xiao, P. Zhao, H. Tian, Colorimetric Naked-Eye Recognizable Anion Sensors Synthesized via RAFT Polymerization, J. Polym. Sci., Part A: Polym. Chem. 48 (2010) 1551-1556.
[21] J. Gan, K. Chen, C-P. Chang, H. Tian, Luminescent properties and photo-induced electron transfer of naphthalimides with piperazine substituent, Dyes Pigments 57 (2003) 21–28.
[22] S. Zheng, P.L.M. Lynch, T.E. Rice, T.S. Moody, H.Q.N. Gunaratne, A.P. De Silva, Structural effects on the pH-dependent fluorescence of naphthalenic derivatives and consequences for sensing/switching, Photochem. Photobiol. Sci. 11 (2012) 1675-1681.
[23] Ch-G. Niu, G-M. Zeng, L-X. Chen, G-L. Shen, R-Q. Yu, Proton "off-on" behaviour of methylpiperazinyl derivative of naphthalimide: a pH sensor based on fluorescence enhancement, Analyst 129 (2004) 20–24.
[24] S. Fernández-Alonso, T. Corrales, J.L. Pablos, F. Catalina, Surface modification of poly(ethylene-butyl acrylate) copolymers by microwave methodology and functionalization with 4-dimethylamino-N-(2-hydroxyethyl)-1,8-naphthalimide for acidity sensing, React. Funct. Polym. 107 (2016) 78-86.
[25] B. Redondo-Foj, M. Carsí, P. Ortiz-Serna, M.J. Sanchis, S. Vallejos, F. García, J.M. García, Effect of the Dipole−Dipole Interactions in the Molecular Dynamics of Poly(vinylpyrrolidone)-Based Copolymers, Macromolecules 47 (2014) 5334-5346.
[26] V. Bühler, Polyvinylpyrrolidone Excipients for Pharmaceuticals:Povidone, Crospovidone and Copovidone, Springer, Berlin, 2005.

[27] G.A. Reynolds, K.H. Drexhage, New coumarin dyes with rigidized structure for flashlamp-pumped dye lasers, Opt. Commun. 13 (1975) 222-225.
[28] D.K. Owens, R.C. Wendt, Estimation of the Surface Free Energy of Polymers, J. Appl. Polym. Sci. 13 (1969) 1741-1747.
[29] H. Tian, J. Gan, K. Chen, J. He, Q.L. Song, X.Y. Hou, Positive and negative fluorescent imaging induced by naphthalimide polymers, J. Mater. Chem. 12 (2002) 1262-1267.
[30] Y. Tian, B.R. Shumway, A.C. Youngbull, Y. Li, A.K.-Y. Jen, R.H. Johnson, D.R. Meldrum, Dually fluorescent sensing of pH and dissolved oxygen using a membrane made from polymerizable sensing monomers, Sens. Actuators B Chem. 147 (2010) 714-722.
[31] J. Reijenga, A.van Hoof, A. van Loon, B. Teunissen, Review: Development of Methods for the Determination of pKa Values, Anal. Chem. Insights 8 (2013) 53–71.

CAPÍTULO 4

A Switchable fluorescence solid sensor for Hg^{2+} detection in aqueous media based on a photocrosslinked membrane functionalized with (benzimidazolyl)methyl-piperazine derivative of 1,8-naphthalimide.

4 A SWITCHABLE FLUORESCENCE SOLID SENSOR FOR HG^{2+} DETECTION IN AQUEOUS MEDIA BASED ON A PHOTOCROSSLINKED MEMBRANE FUNCTIONALIZED WITH (BENZIMIDAZOLYL)METHYL-PIPERAZINE DERIVATIVE OF 1,8-NAPHTHALIMIDE

4.1 Abstract

A Selective fluorescence solid sensor for Hg^{2+} detection in aqueous solution (M-MBZN) has been developed by grafting N-(2-hydroxyethyl)-4-(4-(1H-benzo[d]imidazol-2-yl)methyl) piperazine-1-yl)-1,8-naphthalimide (MBZN) to a photo-crosslinked M-Cl membrane reaction through the acid chloride groups. The resulting fluorescence sensor undergoes fluorescence enhancement upon binding mercuric ions which provokes a photo-induced electron transfer (PET) inhibition process from the piperazine to the naphthalimide moiety. Various photochemical parameters were determined by using pH-dependent absorption and fluorescence spectroscopies as well as the selective detection of Hg^{2+}. The sensing membrane possesses a switchable "turn-on" fluorescence response to Hg^{2+} in pure water; it is easy to use and reusable and shows high selectivity and sensitivity.

4.2 Introduction

The selective and sensitive detection of low concentrations of Mercury (II) in aqueous media is essential because it is a highly toxic and dangerous heavy metal with a lethal effect on the environment and living organisms[1,2]. Thus, a convenient, rapid, highly sensitive and *in-situ* detection of Hg^{2+} is highly desirable.

There are several classical mercury quantitative analytical methods for water samples including colorimetry [3], inductively coupled plasma mass spectrometry (ICP-MS) [4], atomic fluorescence spectroscopy (AFS) [5], atomic absorption spectroscopy [6], X-ray absorption spectroscopy [7,8] and electrochemical techniques[9]. Even though these techniques are sensitive, selective, and accurate for Hg^{2+} detection, most of them are time-consuming, require sophisticated instruments and are inappropriate for on-line or field monitoring.

Relative to the mentioned methods, the fluorescence technique has the advantages of higher sensitivity, simplicity and lower cost for the monitoring of metal ions. Chemical sensing of Hg^{2+} with all types of fluorescent probes, via Hg^{2+}-induced changes in fluorescence, has attracted much attention and has become a very active field of research[10]. Fluorescent probes for Hg^{2+} described in the literature are mainly based on the effective quenching of a fluorescence "turn-off" by Hg^{2+} ions[11,12,13], even though the quenching of the fluorescence signal is not as sensitive as a fluorescence enhancement signal. Therefore, much attention had been paid recently to the development of Hg^{2+} "off-on" fluorescent probes[14,15,16,17].

Derivatives of 1,8-naphthalimide have numerous applications in a variety of different areas as fluorescent probes because they have been recognized for excellent photophysical properties with excellent stability, visible excitation and emission exhibiting high fluorescence quantum yields and large Stokes' shift that minimize the effects of the background fluorescence. Among most of the reported naphthalimide derivatives as fluorescent probes for Hg^{2+}, the recognition group was linked to the 4-position of the naphthalene ring[14,17,18,19]. In this study we designed a sensor MBZN (Fig. 1) by incorporating a (benzimidazolyl)methyl-piperazine substituent in the position 4 of N-(2-hydroxyethyl)-1,8-naphthalimide, in which this benzimidazol structure linked to an piperazine by a methylene spacer is responsible for the specific recognition of Hg^{2+} ions by forming a stable complex structure of the Hg-MBZN that resulted in strong fluorescence in the presence of Hg^{2+}.

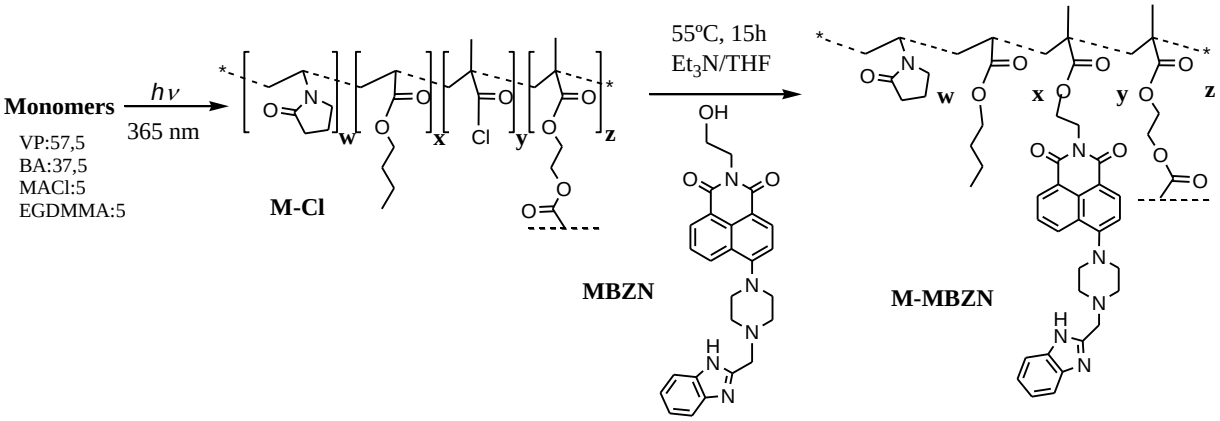

Fig.1. Synthesis of the photo-crosslinked membrane containing acid chloride groups (M-Cl) and functionalization with N-(2-hydroxyethyl)-4-(4-(1H-benzo[d]imidazol-2-yl)methyl)piperazine-1-yl)-1,8-naphthalimide (M-MBZN).

The use of polymeric solid supports containing organic structures capable of acting as sensors against the presence of metals[20,21,22] in the medium are very useful in the applied point of view and, in particular, *on-site* detection of Hg^{2+} ions. However, only very few sensors for Hg^{2+} based on covalently bonded probes onto the support matrixes have been reported[18,23,24,25,26]. In a recent publication[27] we prepared a photo-crosslinked membrane containing acid chloride groups (M-Cl) capable of functionalization with hydroxy derivatives of naphthalimides in a second step. In this work, we designed a novel functionalized membrane (Fig. 1) with the proposed naphthalimide graphed to the structure M-MBZN for one-step fluorescence assay to detect Hg^{2+} ions in environmental water samples.

4.3 Experimental

4.3.1 Materials and reagents

All materials and solvents were commercially available and used as received, unless otherwise indicated. The materials included: sodium hydroxide (Panreac, 98-100.5%), hydrochloric acid (VWR Chemicals, 37%), ultrapure MilliQ water (Millipore), 4-bromo-1,8-naphthalic anhydride (Aldrich, 95%), 2-aminoethanol (Aldrich, 99%), 2-(chloromethyl)benzimidazole (Aldrich, 98%), piperazine (Aldrich, 98%), Irgacure 2959 photoinitiator (BASF), triethylamine (Aldrich, ≥99%), coumarin-6 (Aldrich, 98%) and dimethylsulfoxide-D6 (Euriso-top, 99.8%-D). All metal salts and solvents

employed in this work were purchased from Aldrich. Also, monomers, 1-vinyl-2-pyrrolidone, butyl acrylate and ethylene glycol dimethacrylate and methacryloyl chloride were supplied by Aldrich and distilled under vacuum prior to use.

4.3.2 Spectroscopic characterization and thermal analysis

Attenuated Total Reflectance / FT-Infrared Spectroscopy (ATR-FTIR) were obtained using a PERKIN ELMER BX-FTIR Spectrometer coupled with a MIRacle^{TM}ATR accessory, from PIKE Technologies.

UV spectroscopy was carried out in a *PERKIN ELMER Lambda 35* spectrometer. The assessment of naphthalimide content was made in quintuplicate for each material.

Fluorescence spectroscopy was measured on a Perkin Elmer LS-55 Fluorescence Spectrometer. Fluorescence emission spectra of the probe were recorded by excitation at the isosbestic wavelength of 405 nm (Table 1). All the spectra were corrected using the response curve of the photomultiplier. The fluorescence quantum yields (ϕ_F) were measured relatively to Coumarin 6 (ϕ_F =0.78 in ethanol)[28].

In the case of the crosslinked M-MBZN membrane, films were cut into strips of 1×4 cm and fixed in a homemade support that can also be slotted into the cell holder of the spectrophotometers. Film strips were immersed in previously prepared vials containing solutions of fixed concentrations of Hg^{2+} or other metal ions (Na^+, K^+, Mg^{2+}, Ca^{2+}, Mn^{2+}, Fe^{3+}, Co^{2+}, Ni^{2+}, Zn^{2+}, Al^{2+}, Pb^{2+}, Ag^+, Cu^{2+}). The UV/Vis and fluorescence spectra for each Hg^{2+} concentration were taken after 20 min. of conditioning time in order to obtain a stable fluorescence signal.

Nuclear magnetic resonance, ^{1}H- and ^{13}C- NMR spectra were recorded on a *Varian-Mercury* 400 MHz and a Bruker 300 MHz Nuclear Magnetic Resonance Spectrometers using DMSO-d_6 as the solvent. ^{1}H-NMR and ^{13}C-NMR chemical shifts were referenced to DMSO-d_6 (2.5 and 39.52 ppm, respectively) as standard.

Mass Spectra (MS) were recorded under electron impact (EI) condition on a HP 5973-MSD spectrometer.

Thermogravimetric Analysis (TGA) was carried out in a TGA Q-500 TA Instruments coupled to a Pfeiffer Vacuum ThermoStar^{TM} mass spectrometer.

Elemental analysis (EA) was carried out on a Carlo Erba EA1108 elemental analyzer (% of C, H, N).

4.3.3 Swelling Ratio and pH measurements

Swelling degree (SD) in water and THF of the crosslinked membranes were measured by immersing dried and weighed sample films (W_d) into deionized water or THF at 30 ºC for 24 h. The SD were calculated as follows: SD *(%) = ((W_s −W_d)/W_d)*×100, where W_s and W_d are the weight of the swollen and dry sample, respectively.

The pH of the solutions were measured with a Mettler Toledo SevenGo Duo Pro meter coupled with an InLab Expert Pro ISM-ID67 electrode at room temperature (23 ºC) and previously calibrated with standard buffers.

4.3.4 Microwave and UV irradiation equipment

The microwave equipment used in this work was an *Anton Paar Monowave™ 300* microwave synthesis reactor provided with an infrared sensor (IR pyrometer). All reactions were performed in pressure-resistant 30-mL test tubes sealed with silicon septum and using a magnetic stirring bar.

The photopolymerization reactions were carried out in a Biolink™ BLX-365 type Bio-link apparatus (Vilbert Lourmat™).

4.3.5 Synthesis

The synthesis procedure for the fluorescence probe N-(2-hydroxyethyl)-4-(4-(1H-benzo[d]imidazol-2-yl)methyl)piperazine-1-yl)-1,8-naphthalimide (MBZN) is shown in Fig. 2.

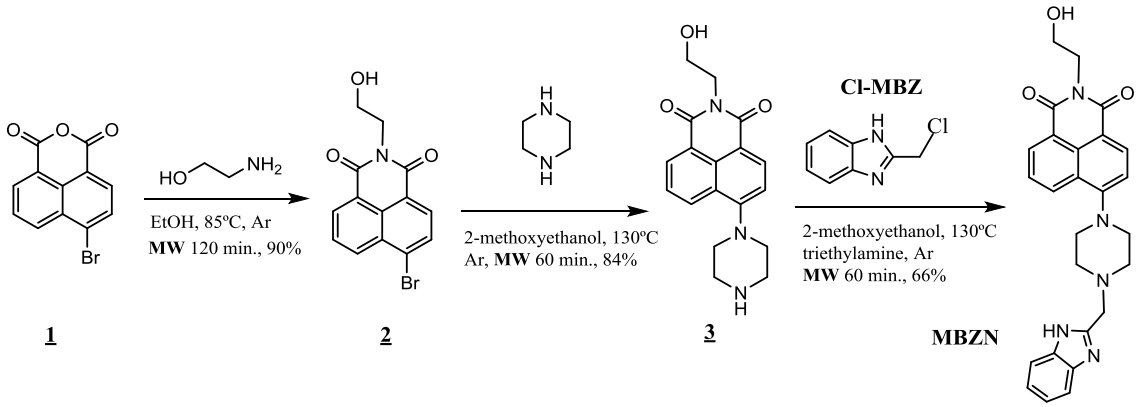

Fig.2. Reaction pathway for the microwave (MW) synthesis of N-(2-hydroxyethyl)-4-(4-(1H-benzo[d]imidazol-2-yl)methyl) piperazine-1-yl)-1,8-naphthalimide (**MBZN**).

Synthesis of N-(2-hydroxyethyl)-4-(4-(1H-benzo[d]imidazol-2-yl)methyl) piperazine-1-yl)-1,8-naphthalimide (MBZN)

Compound 2 and 3 were synthesized from 4-bromo-1,8-naphthalic anhydride (compound 1) following the procedures (Fig. 2) described previously in the bibliography[27,29]. MBZN was synthetized in a pressure-resistant microwave test tube where compound 3 (0.20 g, 0.624 mmol), 2-(chloromethyl)benzimidazole (0.104 g, 0.624 mmol) and triethylamine (88 µL, 0.624 mmol) were mixed in 2-methoxyethanol (10 mL) and heated at 130 ºC in argon atmosphere under stirring (600 rpm) for 1 h. The mixture was poured into diethyl ether and the unreacted precipitated product was filtered. The solvent was evaporated under reduced pressure, and 200 mL of water was added. The mixture was stirred 15 minutes and the residue filtered and identified as the desired product. Yield: 66 %. M.p.: 152.60 ± 2 ºC. ^{1}H NMR (400 MHz, DMSO-d_6) δ 12.37 (s, 1H), 8.44 (d, *J* = 7.3 Hz, 1H), 8.41 (d, *J* = 8.5 Hz, 1H), 8.37 (d, *J* = 8.1 Hz, 1H), 7.78 (t, *J* = 7.9 Hz, 1H), 7.58 (d, *J* = 7.4 Hz, 1H), 7.47 (d, *J* = 7.4 Hz, 1H), 7.32 (d, *J* = 8.2 Hz, 1H), 7.15 (t, *J* = 7.7 Hz, 2H), 4.79 (s, 1H), 4.13 (t, *J* = 6.5 Hz, 2H), 3.89 (s, 2H), 3.67 – 3.56 (m, 2H), 3.27 (s, 4H), 2.82 (s, 4H). ^{13}C NMR (101 MHz, DMSO) δ: 163.65, 163.12, 155.48, 151.47, 143.07, 134.39, 132.07, 130.54, 130.39, 129.13, 125.98, 125.24, 122.65, 121.82, 121.00, 118.54, 115.70, 114.95, 111.20, 57.85, 55.57, 52.74, 52.57, 41.62. FT-IR (wavenumbers, cm^{-1}): ν_{NH},ν_{OH} 3255 cm^{-1}; ν_{C-H} 2949, 2823 cm^{-1} aromatic stretch vibration; $\nu_{C=O}$ 1691, 1644 cm^{-1}; $\nu_{N-C=O}$ 1614 cm^{-1}; ν_{C-C} 1586 cm^{-1} aromatic ring chain vibrations; ν_{NH} 1514 cm^{-1} flexion. EA: theoretical values: %C 68.56; %H 5.53; %N 15.37; experimental values: %C 68.36; %H 5.59; %N 15.29. EI-MS *m/z* calculated for $C_{26}H_{25}N_5O_3$: (M + H$^+$) 456.2; found 456.2 (M$^+$).

4.3.6 Membrane preparation by photopolymerization (M-Cl) and functionalization with N-(2-hydroxyethyl)-4-(4-(1H-benzo[d]imidazol-2-yl)methyl)piperazine-1-yl)-1,8-naphthalimide (M-MBZN)

As shown in Fig. 1, a crosslinked membrane (M-Cl) was obtained in a first step by the bulk photopolymerization of a mixture of monomers: N-vinylpyrrolidone (VP), butyl acrylate (BA), ethylene glycol dimethacrylate (EGDMMA) as the crosslinking agent and methacryloyl chloride (MACl) as the reactive monomer following the procedure described in a recent publication[27]. In this work, the monomer molar ratio of the feed mixture was VP:57.5/BA:37.5/ MACl:5/EGDMMA:5 and the photoinitiator (Irgacure 2959) was added to the mixture at 1% (w/w). After 40 minutes of irradiation at 365 nm (dose 20 J cm^{-2}), the transparent crosslinked membrane was demoulded, conditioned (12 h) at room temperature under argon atmosphere, washed several times with ethanol and dried under vacuum at 40 °C to remove the un-reacted monomers. The presence of acid chloride was confirmed by ATR-FTIR (wavenumbers, cm^{-1}), $\nu_{C=O}$ acyl chloride 1795 cm^{-1}; ν_{C-Cl} 898 cm^{-1}

together with the characteristic co-monomers bands of VP $\nu_{C=O}$ lactam, amide-I 1675 cm^{-1} and BA, $\nu_{C=O}$ ester 1725 cm^{-1}; ν_{C-O} (O-CH_2-) ester 1161 cm^{-1}. The quantitative determination of chlorine in the M-Cl membrane was carried out by TGA-MS. A content of 1.4 % was determined by MS analysis of evolved gas at 175 ºC as chlorine (EI-MS m/ z: 36 (Cl)), as it is shown in Fig. S1, (Supporting Information).

In a second step[27], the M-Cl film was cut into strips (1 × 4 cm) and functionalized in heterogeneous phase with MBZN (Fig 1). The M-Cl membrane was placed in an ace round-bottom pressure flask with 20 mL of THF. 10 mg of MBZN were added under argon atmosphere. The mixture was heated at 55 °C for 15h. After this reaction time, the corresponding modified membrane (M-MBZN) was washed with cold ethanol and with water thrice in order to remove the unreacted acid chloride groups and the unreacted naphthalimide. The hydrolysis reaction of unreacted acid chloride groups was confirmed by ATR-FTIR and by TGA-MS by the disappearance of the characteristic peaks of acid chloride (Fig. S1). The content of naphthalimide was quantitatively determined by UV–Vis spectroscopy.

4.4 Results and discussion

4.4.1 Synthesis of MBZN, preparation of M-MBZN membrane and characterization

The synthetic route to obtain *N-(2-hydroxyethyl)-4-(4-(1H-benzo[d]imidazol-2-yl)methyl)piperazine-1-yl)-1,8-naphthalimide (M-MBZN)* is shown in Fig. 2. Compounds 2 and 3 were formed in 90 % and 64 % yields in 2 and 1 hours, respectively, using literature procedures[18,27,29] modified to carry out the reactions under microwave radiation from the 4-bromo-1,8-naphthalic anhydride (1). Compound 3 was then reacted under MW with 2-(chloromethyl)benzimidazole in basic medium in the presence of triethylamine at 130 ºC as described before (see Experimental section 2.5). After 60 min. of reaction time under MW, MBZN as a yellow precipitate was obtained in 66 % yield. An acrylic membrane containing acid chloride functionalities (M-Cl) was obtained by photopolymerization as described previously[27] by thorough mixing of the hydrophilic monomer VP (57.5%) with the hydrophobic nature of BA (37.5%) and adding MACl (5 %) as the reactive monomer for functionalization. After the bulk photopolymerization (conversion >98%), a reversible water-swollen crosslinked acrylic membrane was produced (Fig. 1) with a 1.4 % of chlorine content in the structure as expected by the composition feed and confirmed by TGA-MS (Fig. S1, Supplementary data). Finally, the M-Cl membrane was successfully functionalized[27] with the naphthalimide derivative MBZN (Fig. 1) by conventional heating in THF at 55 ºC for 15 hours. The amount of naphthalimide bonded to the M-MBZN membrane was determined spectrophotometrically (1.6×10^{-4} M) at the peak maximum of the

absorption band (407 nm) and using the absorption coefficient of MBZN in water:ethanol (4:1 w/w) ($\varepsilon_{407} = 9.55\times10^3$ $mol^{-1}l$ cm^{-1}) previously calculated (Table 1).

The thermal stability of the M-Cl and M-MBZN membranes were evaluated using TGA and Table S1 (Supplementary data) shows characteristic weight loss temperatures (T_5 and T_{10}, respectively). For both membranes two peaks were observed (Fig. S1). The highest weight loss rate that was observed at 411 ºC corresponds to the degradation of acrylic components of the membrane and the second one observed at 438 ºC has been attributed[30] to the lactam subgroup degradation.

Also, the degree of swelling in water of both membranes (Table S1) was approx. SD=31% confirming the hydrophilic character of the membranes and the adequate swelling for solid sensors in water. The SD value of the M-MBZN in THF (61.5 %) is higher than that of the M-Cl membrane (47.1%) indicating the strong influence of the naphthalimide derivative in the SD in organic solvents, even at this low naphthalimide content in the membrane.

The cross-linked hydrophilic membrane M-MBZN obtained in this work was capable of swelling or de-swelling reversibly in water and retaining a controlled and reproducible volume of liquid in the swollen state. This behaviour, as will be seen in the next section, allowed controllable responses to external concentrations of Hg^{2+} cations.

4.4.2 Spectroscopic characteristics of MBZN and M-MBZN. Effect of pH.

Table 1 presents the spectral characteristics of MBZN and the corresponding functionalized membrane M-MBZN in water-ethanol (4:1, v/v) such as, absorption (λ_{ABS}) and fluorescence (λ_{FLU}) maxima in acid (pH=2.0) and neutral media (pH=7.0), the corresponding absorption coefficient (logε), Stokes shift ($\Delta\nu$), and quantum yields of fluorescence (ϕ_{FLU}).

Table 1: Parameters determined by UV-VIS absorption and fluorescence spectroscopies[a] related to titration of Hg^{2+} cations and pH-dependence for MBZN naphthalimide in solution and M-MBZN membrane sensor[b].

Parameter	MBZN	M-MBZN
$\lambda_{ABS\text{-}neutral}$ [c]	407 nm	407 nm
Log $\varepsilon_{neutral}$ [d]	3.98	-
$\lambda_{ABS\text{-}acid}$ [c]	390 nm	390 nm
Log ε_{acid} [d]	4.0	-
$\lambda_{Isobestic}$	405 nm	405 nm
$\lambda_{FLU\text{-}neutral}$ [e]	535 nm	512 nm
$\lambda_{FLU\text{-}acid}$	530 nm	510 nm
pK_a [f]	5.3	5.3
$\phi_{FLU\text{-}neutral}$ [g]	0.01	-
$\phi_{FLU\text{-}acid}$	0.18	-
$\phi_{FLU\ ethanol}$	0.03	water:ethanol (4:1,v/v)<
$\phi_{FLU\ hexane}$	0.20	< Ethanol << hexane
pK_a^* [e]	5.0	4.8
$\Delta\nu$ [h]	6000	5160
Hg^{2+}: Working range of pH	-	5.5-8.0
Hg^{2+}: LOD- Detect. limit (M)[i]	7.3×10^{-8}	2.5×10^{-6}
Hg^{2+}: FE [j]	6	3
Hg^{2+}: response time (membrane thickness µm) [k]	-	10 min (40 µm); 18 min (80 µm); 25 min (180 µm)

[a] Measured at 10^{-5} M in water-ethanol (4:1, v/v) unless specifically stated otherwise; [b] membrane thickness 80 µm and content of MBZN:1.6×10^{-4} M; [c] The subscripts "acid" and "neutral" refer to the limiting value of a given parameter in strong acid (pH=2.0) or neutral (pH=7.0) media, respectively; [d] ε, molar absorptivity in $M^{-1}\cdot cm^{-1}$; [e] Fluorescence emission spectra were obtained by excitation at $\lambda_{Isobestic}$ = 405 nm; [f] Obtained[31] by analyzing the pH dependence of the absorbance (A) or emission intensity (I) at a given wavelength according to the equation $\log[(A_{acid} - A)/(A - A_{base})] = pH - pK_a$ or $\log[(I_{FLU\text{-}acid} - I)/(I - I_{FLU\text{-}base})] = pH - pK_a^*$; [g] relatively to Coumarin 6 (ϕ_F =0.78 in ethanol); [h] Stokes shift (ν_{FLU}-ν_{ABS}) in frequency (cm^{-1}); [i] LOD= 3SD/s, where SD is the standard deviation of 10 measurements of the blank sample and s is the slope of the calibration curve in the region of low analyte content; [j] Hg^{2+}-induced fluorescence enhancement of naphthalimide, factor FE = $A_{FLU\text{-}Hg\ (max.)}$ / $A_{FLU\ absence\ Hg}$; [k] Data from Fig.6B.

The spectral characteristic of MBZN and M-MBZN displayed similar pH-dependence in all the studied media as can be seen from the values listed in Table 1. The low fluorescence emission of MBZN and M-MBZN in all the studied solvents can be attributed to an efficient PET process (Fig. 3) that takes place between the photoexcited 1,8-naphthalimide and the lone-pair electrons of the nitrogen of the piperazine substituent.

The pK_a values of MBZN and the functionalized membrane M-MBZN were calculated[31] from the curves of absorption changes (Fig.S2) in the presence of increasing pH from 2.0 to 12.0. The protonation of the benzimidazole structure of MBZN (pK_a=5.3) takes place at a lower pH than the 2-

methyl benzimidazole structure[32], pK_a=6.1, allowing the use of this structure as a sensor for Hg^{2+} cations in neutral of basic water media as we will see in the next section.

4.4.3 Sensitivity of MBZN and M-MBZN in Hg^{2+}sensing

Figure 3 shows the absorption and fluorescence spectra of the MBZN (water:ethanol 4:1,v/v) (A and C) and M-MBZN (B and D) in buffered water (pH= 7.0) upon addition of different concentrations of Hg^{2+}. With the increase of Hg^{2+} concentration, the relative fluorescence intensities were drastically enhanced caused by Hg^{2+} interaction and the formation of a MBZN-Hg complex, which constituted the basis for the determination of Hg^{2+} concentrations with the MBZN-sensor.

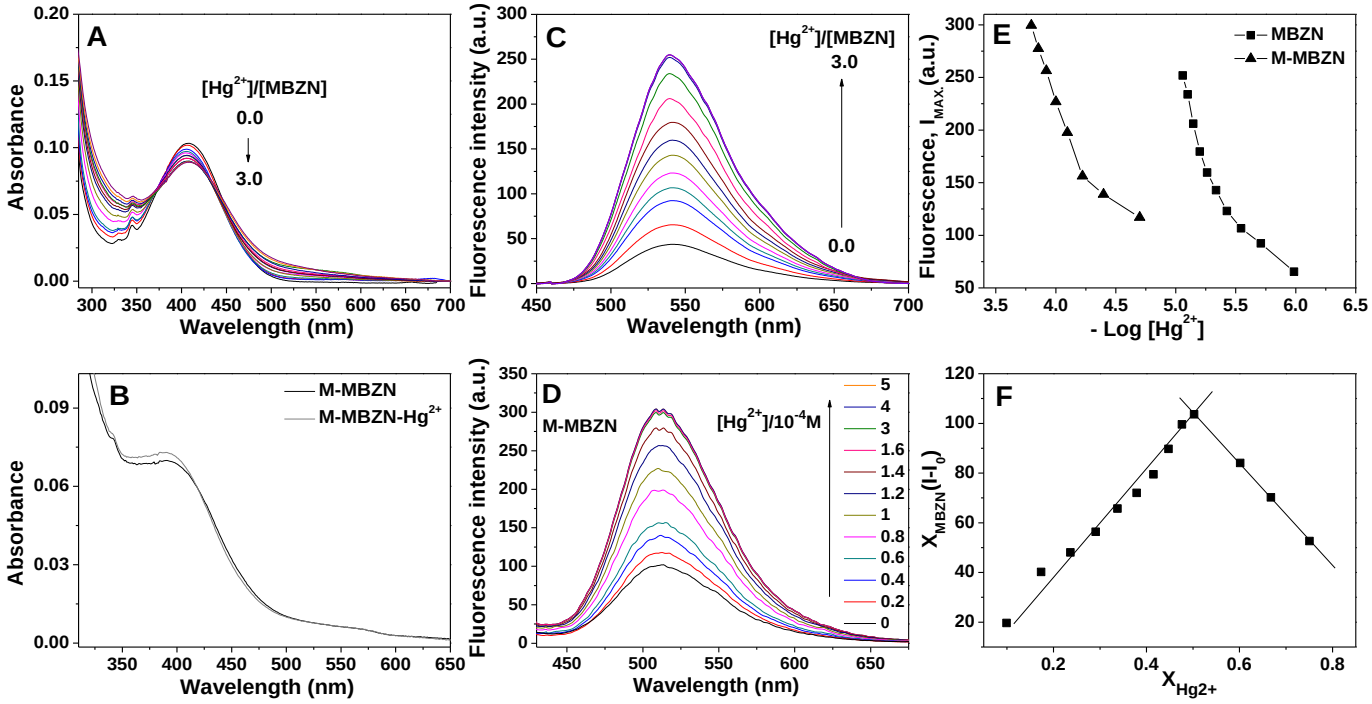

Fig.3. Absorption and fluorescence spectra of MBZN (A,C) at a concentration of 10^{-5} M in water:ethanol 4:1 (v/v) and M-MBZN (B,D) containing 1.6×10^{-4}M of bonded naphthalimide in buffered water (pH= 7.0) in the presence of increasing concentrations of Hg^{2+} 0-3 equiv. (E) Fluorescence emission intensity change with –log[Hg^{2+}]. (F) Job´s plot showing the stoichiometry of MBZN-Hg complex in buffered water.

The comparative increase of fluorescence for MBZN and the membrane M-MBZN is shown in Fig. 3E. The binding stoichiometry 1:1 for the MBZN-Hg complex was confirmed by the Job´s plot shown

in Fig.3F in which the maximum fluorescence signal was observed at the Hg^{2+} mole fraction value of 0.5.

The association constants K_a of the MBZN-Hg and M-MBZN-Hg complexes were then calculated to be 9657 M^{-1} and 3627 M^{-1}, respectively, by the ratio intercept/slope (Fig.S3) of the corresponding linear relationship by Benesi–Hildebrand[33] equation Eq. (1).

$$\frac{1}{F-F_0} = \frac{1}{K_a(F_{max}-F_0)[Hg^{2+}]} + \frac{1}{F_{max}-F_0} \qquad (1)$$

where F_{max}, F, and F_0 are fluorescence intensities of MBZN or M-MBZN in the presence of Hg^{2+} at saturation, any intermediate Hg^{2+} concentration, and free sensor, respectively.

The limit of detection (LOD) was calculated by the following equation: LOD=3×SD/*s*, where SD is the standard deviation of 10 measurements of the blank and *s* is the slope of plot of fluorescence intensity as a function of the Hg^{2+} concentrations in the region of low analyte content. The calculated values of LOD are shown in Table 1, 7.3×10^{-8}M and 2.5×10^{-6}M for MBZN and M-MBZN, respectively. Compared with the previously reported values of Hg^{2+}-fluorescence sensors, the LOD of M-MBZN membrane presented here is lower or in the same range[18,14].

4.4.4 Binding mode MBZN with Hg^{2+} ion, reversibility and pH stability of the MBZN-Hg complex

NMR studies provided direct evidence of MBZN-Hg interactions. As shown in Fig. 4, ^{1}H-NMR spectra show the displacement of the (benzimidazolyl)methyl-piperazine protons Fig.4(a) in the presence of Hg^{2+}, Fig. 4(b): the protons of the methylene bridge from 3.89 (2H-10) ppm to 4.45 (1H-10) and 3.96 (1H-10) and the protons of the piperazine from 2.82 (4H-9) to 3.07 (4H-9). Also, the Hg^{2+} complexation induced an increase of the electron density of the benzimidazolyl group resulting a downfield shift of the aromatic H-11, H-12 and H-13 protons. The NH peak of the benzimidazole ring also was displaced from 12.37 ppm to 14.21 in the complex.

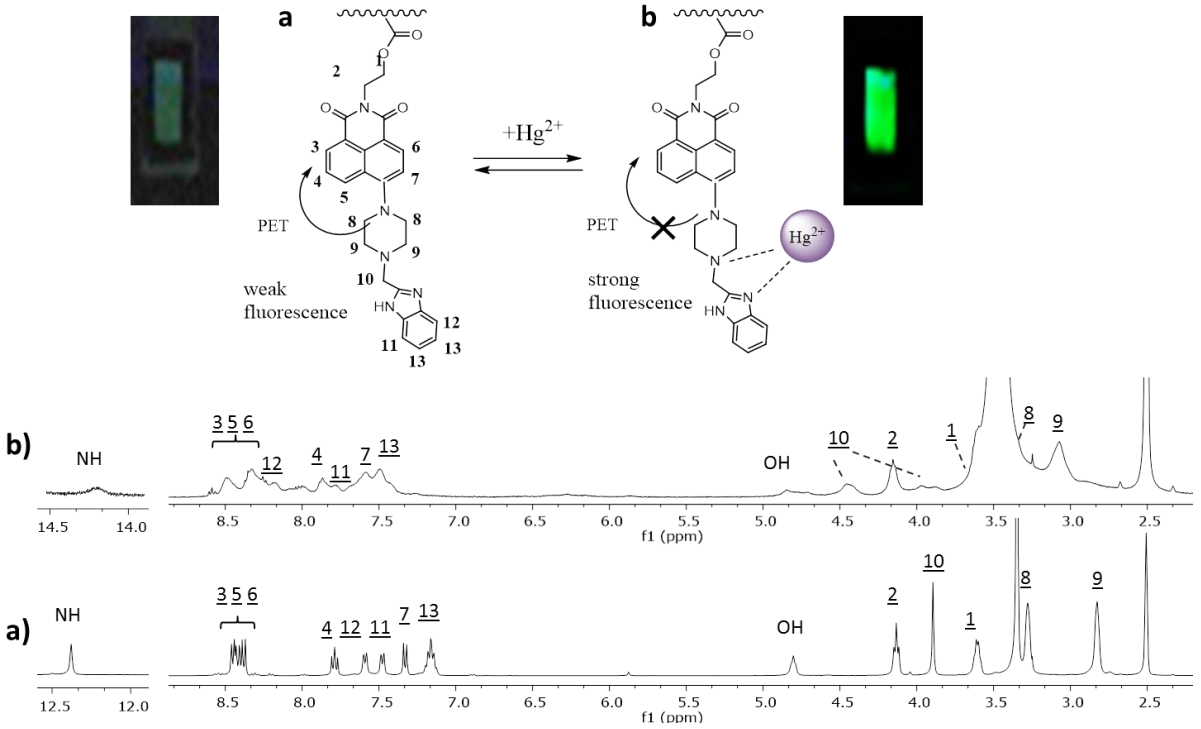

Fig.4. Proposed reversible binding mode with Hg^{2+} together with partial ^{1}H-NMR of MBZN in DMSO at 25ºC: (a) in the absence and (b) after addition of 1 equiv. of Hg^{2+}.

The reversibility of the Hg^{2+} induced fluorescence signal of the M-MBZN membrane was evaluated by alternating its immersion in solutions of blank buffered solution (pH=7.0) until the fluorescence intensity of the membrane reached again the original low value prior to the next measurement and water buffered Hg^{2+} solution. Previously to each cycle the membrane should be washed with HCl solution (pH=1.0) since the reversibility is probably caused by the protonation of the piperazine of the MBZN structure resulting in the release of the Hg^{2+} at higher acidity. Ten successive cycles were carried out as it is shown in Fig. 5A for the membrane sensor.

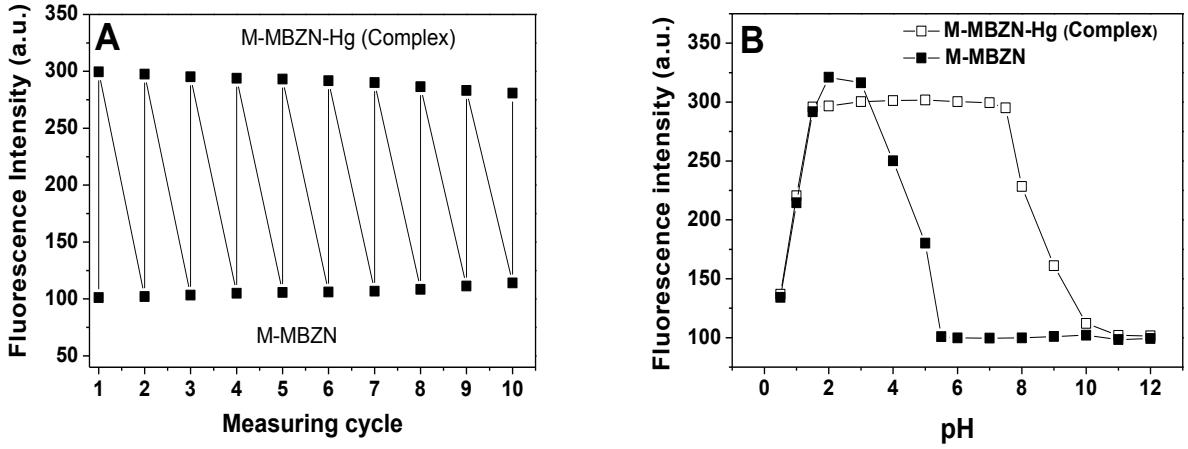

Fig.5. (A) Reversibility for the M-MBZN membrane sensor. (B) pH-effect on the fluorescence intensity of M-MBZN and M-MBZN-Hg complex in water.

As shown in Fig. 5(B), the MBZN-Hg^{2+} complex produced in the membrane sensor exhibits stability of the fluorescence emission in the range of pH 2.0–7.5. The decrease in fluorescence emission upon pH values higher than 7.5 might be attributed to the formation of $Hg(OH)_2$[34] and the rapid decrease at pH values lower than 2.0, due to the destruction of the Hg^{2+} complex by the protonation of the piperazine. These results show that the M-MBZN membrane is a fully reversible sensor for the detection of Hg^{2+} in water which is adequate for real environmental applications and biological samples[35].

4.4.5 Selectivity of M-MBZN membrane sensor to Hg^{2+} with various cations and time response to detection

To investigate the selectivity of the sensor towards Hg^{2+} ions, the fluorescence of M-MBZN (with a bonded content of MBZN of 1.6×10^{-4}M) and 1 equiv. of other metal ions were studied (Fig. 6A). The competition experiments show no significant variation in the fluorescence emission at 512 nm confirming the excellent selectivity of the membrane sensor.

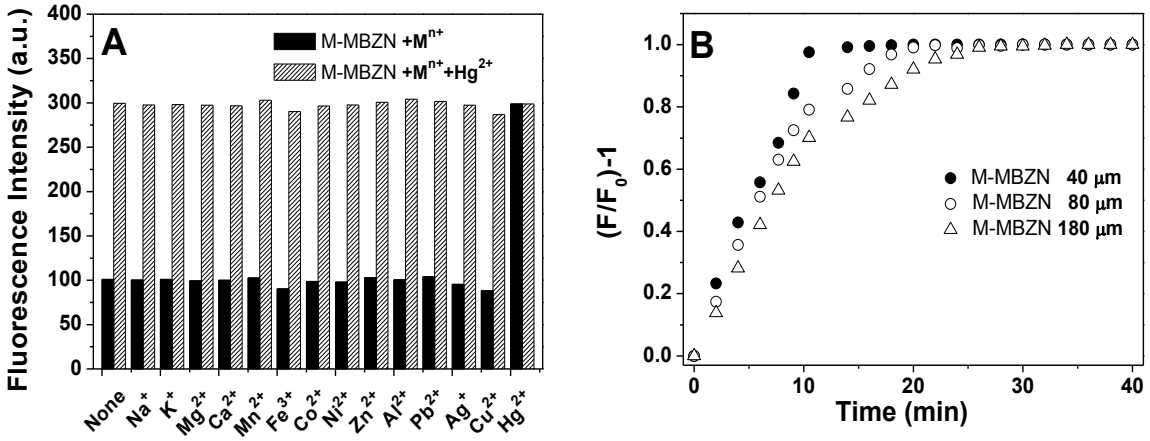

Fig.6. Metal ion selectivity of the M-MBZN membrane (A) containing 1.6×10^{-4}M of bonded MBZN. (B) Time response for the fluorescence emission to Hg^{2+} for M-MBZN membranes of different thickness. F_0 and F are the fluorescence intensities in the absence of Hg^{2+} and that after the addition of 1 equiv. of Hg^{2+}, respectively.

Fluorescence analysis indicated that the recognition interaction between MBZN and Hg^{2+} was accomplished immediately by simply shaking for a few seconds. In contrast, the M-MBZN membrane sensor exhibits a time response which is dependent upon the metal ion permeability into the photo-crosslinked material and their thickness. To see the influence of the membrane thickness in the time response to the Hg^{2+} of the M-MBZN membrane sensor (Fig.6B), we prepared another two membranes under the same experimental conditions but with 40 and 180 μm of thickness.

4.5 Conclusions

The novel water-swollen photo-crosslinked membrane sensor M-MBZN with pendant highly Hg^{2+}-selective "turn-on" 1,8-naphthalimide-type probe MBZN was developed and based on a specific Hg^{2+}-interaction with the (benzimidazolyl)methyl-piperazine substituent in the 4-position. The membrane sensor exhibited a 3fold increase in fluorescence intensity towards Hg^{2+} ions over other metal ions in pure water solution over a wide pH range. Also, M-MBZN shows a reversible behaviour which is an important feature for many applications. The new solid sensor reported here meets the requirements of fluorescence detection of Hg^{2+} ions and offers great potential for the further fabrication of an economical *on-site* tool for the detection of Hg^{2+} in aqueous environments.

4.6 References

[1] D.W. Boening. Ecological effects, transport, and fate of mercury: a general review, Chemosphere 40 (2000) 1335–1351.

[2] X. Niu, Y. Ding, C. Chen, H. Zhao, M.A. Lan, A novel electrochemical biosensor for Hg^{2+} determination based on Hg^{2+}-induced DNA hybridization, Sens. Actuators B:Chem. 158 (2011) 383–387.

[3] Z. Yan, M-F. Yuen, L. Hu, P. Sun, Ch-S. Lee, Advances for the colorimetric detection of Hg^{2+} in aqueous solution, RSC Adv. 4 (2014) 48373-48388.

[4] H. Louie, C. Wong, Y.J. Huang, S. Fredrickson, A study of techniques for the preservation of mercury and other trace elements in water for analysis by inductively coupled plasma mass spectrometry (ICP-MS). Anal. Methods 4 (2012) 522–529.

[5] Y.W. Chen, J. Tong, A. D'Ulivo, N. Belzile, Determination of mercury by continuous flow cold vapor atomic fluorescence spectrometry using micromolar concentration of sodium tetrahydroborate as reductant solution, Analyst 127 (2002) 1541–1546.

[6] L. B. Escudero, R. A. Olsina, R.G. Wuilloud, Polymer-supported ionic liquid solid phase extraction for trace inorganic and organic mercury determination in water samples by flow injection-cold vapor atomic absorption spectrometry, Talanta 116 (2013) 133–140.

[7] G. N. George, S.P. Singh, G.J. Myers, G.E. Watson, I.J. Pickering, The chemical forms of mercury in human hair: a study using X-ray absorption spectroscopy, J. Biol. Inorg. Chem. 15 (2010) 709–715.

[8] A. Bernaus, X. Gaona, J.M. Esbrí, P. Higueras, G. Falkenberg, M. Valiente, Microprobe techniques for speciation analysis and geochemical characterization of mine environments: the mercury district of Almadén in Spain, Environ Sci. Technol. 40 (2006) 4090–4095.

[9] R.S. N'Dri, M. Coulibaly, A.N. Yao, D. Bamba, E.G. Zoro, An electrochemical method for the determination of trace mercury(II) by formation of complexes with Indigo Carmine food dye and its analytical application, Int. J. Electrochem. Sci. 11 (2016) 5342–5350.

[10] M. Saleem, M. Rafiq, M. Hanif, Organic material based fluorescent sensor for Hg^{2+}: a brief review on recent development, J. Fluoresc. 27 (2017) 31–58.

[11] F. Yan, Y. Zou, M. Wang, Highly photoluminescent carbon dots-based fluorescent chemosensors for sensitive and selective detection of mercury ions and application of imaging in living cells. Sens. Actuators B 192 (2014) 488–495

[12] H. Tan, Y. Zhang, Y. Chen, Detection of mercury ions (Hg^{2+}) in urine using a terbium chelate fluorescent probe. Sens. Actuators B:Chem. 156 (2011) 120–125.

[13] O. García-Beltrán, N. Mena, T.A. Berríos, E.A. Castro, B.K. Cassels, M.T. Núñez, M.E. Aliaga, A selective fluorescent probe for the detection of mercury (II) in aqueous media and its applications in living cells, Tetrahedron Lett. 53 (2012) 6598–6601.

[14] Z. Zhang, S. Lu, C. Sha, D. Xu, A single thiourea-appended 1,8-naphthalimide chemosensor for three heavy metal ions: Fe^{3+}, Pb^{2+}, and Hg^{2+}, Sens. Actuators B:Chem. 208 (2015) 258–266.

[15] M. Tian, L. Liu, Y. Li, R. Hu, T. Liu, H. Liu, S. Wang, Y. Li, An unusual off-on fluorescence sensor for detecting mercury ions in aqueous media and living cells, Chem. Commun. 50 (2014) 2055–2057.

[16] L. Tanga, S. Dinga, X. Zhang, K. Zhonga, S. Houa, Y. Biana, A 2-(2´-hydroxyphenyl)quinazolin-4(3H)-one derived fluorescence 'turn on' probe for recognition of Hg^{2+} in water solution and its live cell imaging, J. Photochem. Photobiol. A:Chem. 340 (2017) 15–20

[17] F. Lv, Y. Chen, T. Tang, Y. Chen, D. Xu, A new reactive 1,8-naphthalimide derivative for highly selective and sensitive setection of Hg^{2+}, J. Fluoresc. 27 (2017) 1285–1292.

[18] X-F. Wu, Q-J. Ma, X-J. Wei, Y-M. Hou, X. Zhu, A selective fluorescent sensor for Hg^{2+} based on covalently immobilized naphthalimide derivative, Sens. Actuators B:Chem. 183 (2013) 565– 573.

[19] Y. Li, Z. Qing, Y. Yu, T. Liu, R. Jiang, Y. Li, Synthesis and Self-Assembly of Dihydroxyperylene Bisimides for the Tuning of Photophysical Properties, Chem. Asian J.7 (2012) 1934 – 1939.

[20] I. Grabchev, J.-M. Chovelon, New blue fluorescent sensors for metal cations, and protons based on 1,8-naphthalimide, Dyes Pig. 77 (2008) 1-6.

[21] I. Grabchev, S. Yordanova, P. Bosch, E. Vasileva-Tonkova, R. Kukeva, S. Stoyanov, R. Stoyanova, Structural characterization of 1,8-naphthalimides and *in vitro* microbiological activity of their Cu(II) and Zn(II) complexes, J. Mol. Struct. 1130 (2017) 974-983.

[22] M.S. Makki, D. Staneva, T.R. Sobahi, P. Bosch, R.M. Abdel-Rahman, I. Grabchev, Design and synthesis of a new fluorescent tripod for chemosensor applications, Tetrahedron, 70 (2014) 9366-9372.

[23] M. Zhu, C. Zhou, Y. Zhao, Y. Li, H. Liu, Y. Li, Synthesis of a Fluorescent Polymer Bearing Covalently Linked Thienylene Moieties and Rhodamine for Efficient Sensing, Macromol. Rapid Commun. 30 (2009) 1339–1344.

[24] Y. Li, T. Liu, H. Liu, M-Z. Tian, Y. Li, Self-Assembly of Intramolecular Charge-Transfer Compounds into Functional Molecular Systems, Acc. Chem. Res. 47 (2014) 1186−1198.
[25] O. Güney, F. Cebeci, Molecularly imprinted fluorescent polymers as chemosensors for the detection of mercury Ions in aqueous media, J. Appl. Polym. Sci. 117 (2010) 2373–2379.
[26] X.R. Guo, B. Li, L.M. Zhang, Y.H. Wang, Selective fluorescent chemosensor for detecting Hg(II) in water based on pyrene functionalized core–shell structured mesoporous silica, J. Luminesc. 132 (2012) 1729–1734.
[27] S. Fernández-Alonso, T. Corrales, J.L. Pablos, F. Catalina, Solid fluorescence sensors obtained by functionalization of photocrosslinked water-swollen acrylic membranes with 4-piperazine naphthalimide derivatives, Polymer 124 (2017) 139-150.
[28] G.A. Reynolds, K.H. Drexhage, New coumarin dyes with rigidized structure for flashlamp-pumped dye lasers, Opt. Commun. 13 (1975) 222-225.
[29] Y.Q. Tian, B.R. Shumway, C. Youngbull, A.K.Y. Jen, R.H. Johnson, D.R. Meldrum, Dually fluorescent sensing of pH and dissolved oxygen using a membrane made from polymerizable sensing monomers, Sens. Actuators B:Chem. 147 (2010) 714-722.
[30] B. Redondo-Foj, M. Carsí, P. Ortiz-Serna, M.J. Sanchis, S. Vallejos, F. García, J.M. García, Effect of the Dipole-Dipole interactions in the molecular dynamics of poly(vinylpyrrolidone)-based copolymers, Macromolecules 47 (2014) 5334-5346.
[31] J. Reijenga, A.van Hoof, A. van Loon, B. Teunissen, Review: Development of methods for the determination of pK_a Values, Anal. Chem. Insights 8 (2013) 53–71.
[32] T.C. Bruice, G.L. Schmir, Imidazole catalysis. II. The reaction of substituted imidazoles with phenyl acetates in aqueous solution. J. Am. Chem. Soc. 80 (1958) 148-155.
[33] H. A. Benesi, J. H. Hildebrand, A spectrophotometric investigation of the interaction of iodine with aromatic hydrocarbons, J. Am. Chem. Soc. 71 (1949) 2703–2707.
[34] Z.X. Han, X.B. Zhang, Z. Li, G.J. Mao, Z. Jin, G.L. Shen, R.Q. Yu, X.Y. Wu, A highly sensitive quinoline-containing rhodamine-B thiohydrazide based fluorescent probe for Hg2+ in aqueous solution and living cells, Anal. Lett. 43 (2010) 2751–2761.
[35] J. Luo, S.S. Jiang, S.H. Qin, H.Q. Wu, Y. Wang, J.Q. Jiang, X.X. Liu, Highly sensitive and selective turn-on fluorescent chemosensor for Hg^{2+} in pure water based on a rhodamine containing water-soluble copolymer. Sens. Actuators B:Chem. 160 (2011) 1191–1197.

Supporting Information

A Switchable fluorescence solid sensor for Hg^{2+} detection in aqueous media based on a photocrosslinked membrane functionalized with (benzimidazolyl)methyl-piperazine derivative of 1,8-naphthalimide.

S. Fernández-Alonso, T. Corrales, J.L. Pablos, F. Catalina[*].

Departamento de Química Macromolecular Aplicada, Instituto de Ciencia y Tecnología de Polímeros (CSIC), C/ Juan de la Cierva, 3, 28006-Madrid, Spain.

E-mail: fcatalina@ictp.csic.es

List of contents:

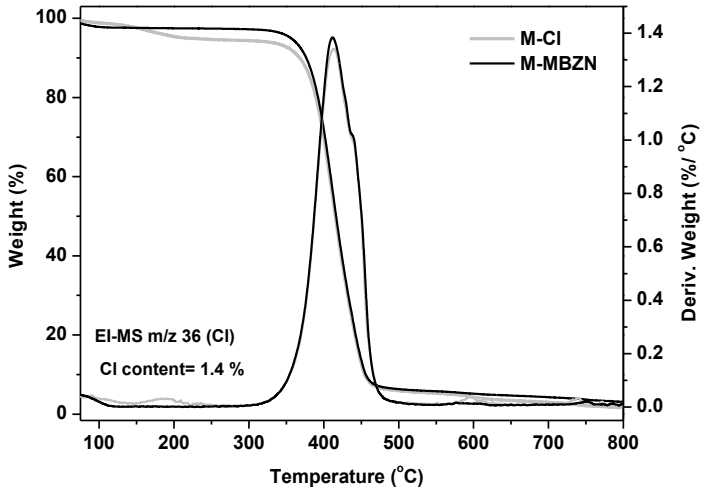

Fig. S1. TGA-MS and DTGA curves of the M-Cl crosslinked membrane and M-MBZN functionalized membrane with the naphthalimide sensor.

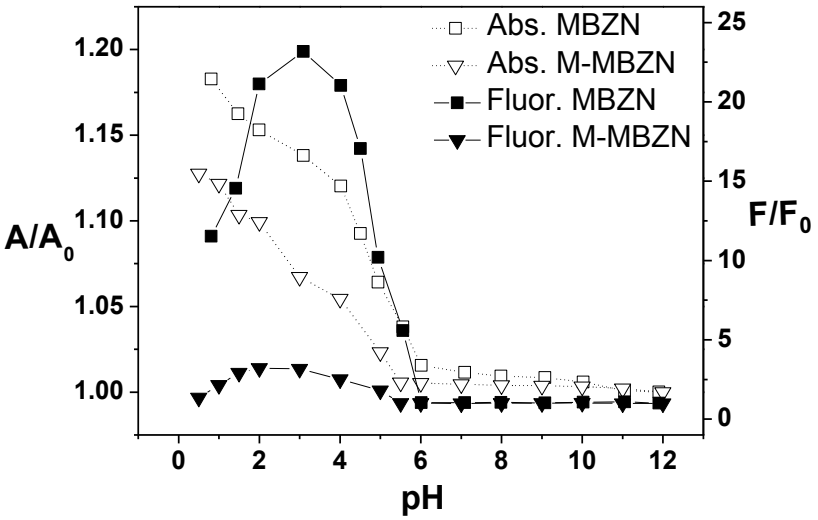

Fig. S2. Plot of the Absorbance (A/A_0) and Fluorescence (F/F_0) relative intensities (subscript 0 indicates initial intensity at pH=12) of the MBZN (10^{-5} M) and M-MBZN ([MBZN] bonded to the membrane 1.6×10^{-4} M) sensors in water:ethanol 4:1 (v/v) as a function of pH variation.

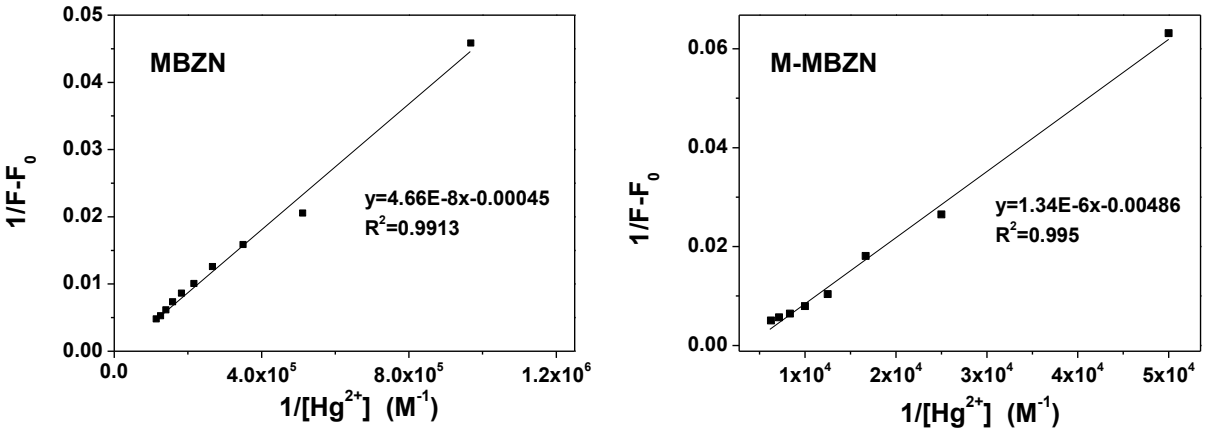

Fig. S3. Benesi-Hildebrand plot of MBZN (A) and M-MBZN (B) using 1:1 stoichiometry for association between MBZN and Hg^{2+}.

Table S1. Membrane characterization: Swelling degree (SD) in water and THF, content of chlorine and naphthalimide derivative in the membranes and thermal properties determined by TGA.

Membrane	SD (%)[a]		Cl (%)[b]	[MBZN][c] $(mol \cdot L^{-1}) \times 10^4$	T_5[d] (°C)	T_{10}[d] (°C)
	Water	THF				
M-Cl	31.6	47.1	1.4	-	217	368
M-MBZN	31.1	61.5	0	1.6	356	376

[a] ±0.3; [b] Determined by TGA peak at 175ºC corresponding to Cl, EI-MS m/z36 (M^+) ;[c] Naphthalimide content determined in M-MBZN membrane (80 µm of thickness) by UV spectroscopy; [e] Temperatures corresponding to 5% and 10% weight loss.

CAPÍTULO 5

Conclusiones.

Las conclusiones extraídas de estos Trabajos publicados y que constituyen la presente Tesis, se pueden resumir en los siguientes puntos:

- Se ha llevado a cabo eficazmente la modificación superficial de filmes de copolímeros de etileno-acrilato de butilo (EBA con 7% de AB) y su posterior funcionalización con una molécula fluorescente, 4-dimetilamino-N-(2-hidroxietil)-1,8-naftalimida (DMAN), mediante reacciones en fase heterogénea empleando radiación microondas. Mediante el perfil de profundidad obtenido por espectroscopía Raman-Confocal (CRS) se ha comprobado que la funcionalización del filme se produce en un espesor superficial de 20 μm.

- Los filmes funcionalizados (EBA-DMAN) mostraron eficientes propiedades como sensores de acidez reversibles (hasta 4-5 ciclos). La disminución en la banda de absorción de transferencia de carga intramolecular (ICT) y la disminución en la banda de fluorescencia debido a la protonación de la amina en el sensor polimérico tiene lugar a pKa -0.88, siendo menor que el valor obtenido para la molécula libre (DMAN), 1.41.

- El tratamiento de los filmes con plasma de oxígeno (EBA-pl-DMAN) produce un aumento de la hidrofilia del material de EBA modificado superficialmente disminuyendo notablemente el tiempo de respuesta a la detección de protones en el medio (de 80 min para EBA-DMAN a 30 min para EBA-pl-DMAN en HCl, 12 M). La reversibilidad y el contenido de DMAN anclado a la superficie permaneció inalterado tras el tratamiento con plasma.

- Los filmes funcionalizados (EBA-DMAN) y los filmes funcionalizados tratados con plasma (EBA-pl-DMAN) mostraron sensibilidad frente vapores ácidos, siendo también la sensibilidad mayor para el caso de los materiales funcionalizados tratados con plasma.

- Este nuevo método desarrollado en esta Tesis que utiliza reacciones de microondas en fase heterogénea abre la posibilidad de unir numerosas estructuras a las superficies de poliolefinas para su aplicación como sensores sólidos de interés medioambiental o biológico.

- Mediante una combinación optimizada de monómeros se ha conseguido la obtención de membranas fotoentrecruzadas de buenas propiedades mecánicas y que presenta un grado de hinchamiento controlado en agua (30%). Además estas membranas contienen funciones cloruro de ácido que permiten su posterior funcionalización con diversas moléculas de interés aplicado como sensores de pH y de cationes mercurio (II).

- Las moléculas sensores derivadas de 1,8-naftalimida y portadoras de un sustituyente hidroxilo, han sido sintetizadas empleando radiación microondas obteniéndose mejores rendimientos y a

tiempos de reacción más cortos, en comparación con la metodología de calentamiento convencional.

- Las nuevas membranas funcionalizadas con naftalimidas portadoras de grupos piperacina mostraron eficientes propiedades como sensores reversibles de pH en el intervalo comprendido entre 9.0 y 4.0. El tiempo de respuesta de los materiales depende de su espesor, del tamaño de los sustituyentes y de la posición de unión de la naftalimida a la membrana.

- Las nuevas membranas sensores funcionalizadas con la naftalimida portadora del grupo (bencimidazolil)metilpiperacina fueron desarrolladas en base a la interacción específica de este grupo con los cationes Hg (II).

- La intensidad de fluorescencia de estas membranas funcionalizadas aumenta (3 veces) al interaccionar con iones Hg(II) en disolucion acuosa. El "encendido" de la fluorescencia en un amplio intervalo de pH es selectivo con el mercurio incluso en presencia de otros iones metálicos. Además estos sensores son reutilizables.

ANEXO

Publicaciones completas.

Reactive and Functional Polymers 107 (2016) 78–86

Contents lists available at ScienceDirect

Reactive and Functional Polymers

journal homepage: www.elsevier.com/locate/react

Surface modification of poly(ethylene-butyl acrylate) copolymers by microwave methodology and functionalization with 4-dimethylamino-*N*-(2-hydroxyethyl)-1,8-naphthalimide for acidity sensing

S. Fernández-Alonso, T. Corrales, J.L. Pablos, F. Catalina *

Departamento de Química Macromolecular Aplicada, Instituto de Ciencia y Tecnología de Polímeros (CSIC), C/Juan de la Cierva, 3, 28006 Madrid, Spain

ARTICLE INFO

Article history:
Received 28 June 2016
Received in revised form 25 August 2016
Accepted 28 August 2016
Available online 30 August 2016

Keywords:
Surface functionalization
Microwave
Ethylene-butyl acrylate copolymers
Naphthalimide sensor
Plasma treatment

ABSTRACT

A new procedure was developed for functionalization in the solid phase by using microwave irradiation. Heterogeneous chemical modification of poly(ethylene-butyl acrylate) copolymer (EBA), hydrolysis, chlorination, and Schotten–Baumann reactions were monitored by attenuated total reflection Fourier transform infrared (ATR-FTIR) spectroscopy. EBA was superficially functionalized by a previously synthesized fluorescent dye, 4-dimethylamino-*N*-(2-hydroxyethyl)-1,8-naphthalimide, and the depth profile of the functionalized polymer was determined by confocal Raman spectroscopy. The new functionalized materials were also evaluated as an acidic pH sensor by determining the change in the spectroscopic properties of absorption and fluorescence with pH of the solution and vapor phases. To improve the wettability of the EBA surface, oxygen plasma treatment was used and the response time of the solid sensor was analyzed.

1. Introduction

An effective approach to develop an applicable solid sensor is to modify the surface of the material that already has excellent bulk properties. A grafted surface can be produced primarily by either graft polymerization of monomers or a covalent coupling reaction of existing polymer molecules onto the substrate polymer surface. Many chemical and physical methods [1] such as plasma, e-beam, and sputtering have been used to modify the structure of polymer surfaces and in particular polyethylenes [2]. Most of these techniques are based on the use of high-energy sources that can ultimately damage the polymer surfaces either chemically or physically. Moreover, these methods are usually not versatile enough to allow the design of structurally and chemically modified surfaces through the control of the distribution of chemical functionalities throughout the surface. In an earlier work, we described the microwave-assisted chemical modification of poly(ethylene-butyl acrylate) copolymers [3] (EBA) in solution to bind coumarin derivatives through the acrylic comonomer. In this study, organic functionalities were introduced onto EBA as the polymer substrate in a controlled manner by performing a sequence of chemical reactions on the surface. In the heterogeneous phase, hydrolysis, chlorination, and Schotten–Baumann reactions were used to graft a naphthalimide derivative to the surface of EBA. The sequence of reactions carried out is shown in Fig. 1.

The introduction of specific functional groups to polymer surfaces by well-defined, classical organic chemical reactions usually involves ionic or polar reactions rather than free radical reactions. Therefore, the polymer surfaces suitable for this type of modification must have sites that are vulnerable to electrophilic or nucleophilic attack.

The modification of the EBA surface opens the possibility to chemically bond numerous organic structures having a terminal group capable of reacting with the functional groups present on the substrate polymer surface. Recently, polymers containing photosensitive functional groups have gained significant attention [4,5,6]. A number of publications have appeared concerning 1,8-naphthalimide derivatives as a special class of environmentally sensitive fluorophores. Their strong fluorescence and good photostability have promoted their applications in a number of areas such as coloration of polymers [7,8], as laser active media [9], fluorescence markers in biology [10], anticancer agents [11], light-emitting diodes [12], photoinduced electron transfer sensors [13,14], fluorescence switchers [15], electroluminescent materials [16,17], liquid crystal displays [18], ion probes [19], and pH sensors [20].

Hence, in this study, we synthesized a hydroxyl derivative, 4-dimethylamino-*N*-(2-hydroxyethyl)-1,8-naphthalimide (DMAN) to react with the superficial chlorine acids of the modified EBA to functionalize the polyolefin material with a sensor probe (EBA-DMAN), as shown in Fig. 1. The surface functionalization was studied by attenuated total reflection Fourier transform infrared (ATR-FTIR)

* Corresponding author.
E-mail address: fcatalina@ictp.csic.es (F. Catalina).

http://dx.doi.org/10.1016/j.reactfunctpolym.2016.08.009
1381-5148/

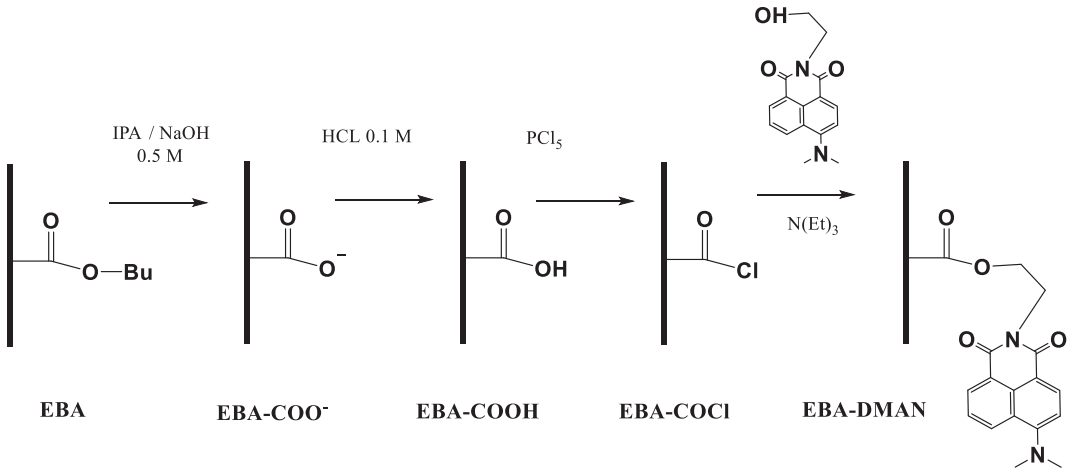

Fig. 1. Heterogeneous reaction sequence for surface modification of EBA using microwave methodology.

spectroscopy and confocal Raman spectroscopy (CRS) [21] to determine the depth profile of the functionalized polymer.

Furthermore, the new functionalized materials were evaluated as an acidic pH sensor by determining the change in the spectroscopic properties of absorption and fluorescence with pH. To improve the wettability of the surface, EBA-DMAN films were treated with oxygen plasma [22]. The plasma-treated materials (EBA-pl-DMAN) exhibited a lower response time for environmental changes of pH in solution and vapors because of surface oxidation.

2. Experimental

2.1. Materials, reagents, and film preparation

Poly(ethylene-*co*-butyl acrylate) copolymer (EBA) with 7% (w/w) of butyl acrylate (0.924 g ml^{-1} of density) was supplied by Repsol company (Madrid, Spain). EBA films of 100 μm thickness and 50 × 50 mm dimension were prepared by compression molding in automatic Press ATLAS T8 plates with a maximum pressure of 2 tons and temperature of 190 °C. The thickness of the films was controlled by specific-size spacer rings.

The following chemicals and solvents were purchased and used as received unless otherwise indicated: 4-bromo-1,8-naphthalic anhydride (Aldrich, 95%), 2-propanol (Scharlau, 99.5%), sodium hydroxide (Panreac, 98–100%), hydrochloric acid (VWR Chemicals, 37%), ultrapure MilliQ water (Millipore), diiodomethane (Aldrich, ≥99.5%), dichloromethane (Aldrich, ≥99.9%), phosphorus pentachloride (Aldrich, ≥98%), triethylamine (Aldrich, ≥99%), 2-aminoethanol (Aldrich, 99%), ethanol (VWR Chemicals, 99.95%), dimethylformamide (DMF, Scharlau, 99.8%), ethyl acetate (Aldrich, ≥99.5%), hexane (Carlo Erba Reagents, 99%), hexadeuterated dimethylsulfoxide (DMSO-d_6, Euriso-top, 99.8%), potassium carbonate (Panreac, 99%), and coumarin 6 (Aldrich, 98%).

2.2. Spectroscopic characterization

ATR-FTIR was used to characterize the polymer films of EBA before and after MW reactions. ATR-FTIR spectra were obtained using a PerkinElmer BX-FTIR spectrometer coupled with a MIRacle™ ATR accessory from PIKE Technologies, and interferograms were obtained from 32 scans. The degree of hydrolysis and modifications of the EBA films were determined using ATR-FTIR and accessories with the same value of pressure.

Confocal Raman Spectroscopy (CRS). A Renishaw inVia Raman microscope, working in a confocal mode and connected to an Olympus BH2 microscope was used for measuring the Raman spectra. The beam from the 785 line of a He–Ne laser (laser power 320 mW at 100%) was focused by 100× magnifying length objective (numerical aperture (NA) value of 0.85) in the confocal mode and a charge-coupled device (CCD) camera as detector. Raman light was dispersed by a diffraction grating with 1200 lines/mm using a Raman holographic notch filter.

The depth profile of the sample was obtained by focusing the microscope stepwise at fixed 1-μm intervals within the polymer film and recording 10 accumulative spectra at each step (accumulation time, 3 min per spectrum). The depth resolution of the confocal arrangement in air was previously checked using a sample of silica as a reference material.

Ultraviolet (UV) spectroscopy was used for the quantitative determination of DMAN moieties anchored to EBA in a PerkinElmer Lambda 35 spectrometer. DMAN surface loading was determined by measuring the absorbance at the peak maximum of absorption band. This was translated into quantitative DMAN content per unit area by rearrangement of the Beer–Lambert law. Each material was assessed in quintuplicate.

Fluorescence spectra were recorded using a PerkinElmer LS 55 fluorescence spectrometer. Fluorescence emission spectra of the probe were recorded in the range of 490–700 nm using the maximum of the longest-wavelength absorption band as excitation wavelength. All the spectra were corrected using the response curve of the photomultiplier. The fluorescence quantum yields (ϕ_F) were measured relatively to coumarin 6 ($\phi_F = 0.78$ in ethanol) [23].

^{1}H- and ^{13}C-nuclear magnetic resonance (NMR) spectra were recorded on *Varian-Mercury* 400 MHz and Bruker 300 MHz NMR spectrometers using hexadeuterated dimethyl sulfoxide (DMSO-d_6) as the solvent. Chemical shifts were reported in parts per million (ppm). ^{1}H NMR and ^{13}C NMR chemical shifts were referenced to DMSO-d_6 (39.52 ppm) as standard.

Mass spectra (MS) were recorded on a HP 5973-MSD spectrometer.

2.3. pH measurements and spectroscopic detection of acid in solution and vapors

The pH was measured at room temperature (23 °C) by using a Mettler Toledo SevenGo Duo pro meter with an InLab Expert Pro ISM-ID67 electrode that was previously calibrated with standard buffers. The sensing measurements of the solutions of DMAN and surface-modified films of EBA-DMAN were performed using HCl solution in the water:ethanol (4:1) mixture as solvent.

Acid titration by ultraviolet–visible (UV–Vis) and fluorescence spectrometry in aqueous solution and vapors was performed as follows. The titration of the solution with DMAN (water:ethanol 4:1, 10^{-4} M) was carried out by adding dilute HCl to increase the acidity from pH 8 to pH 0.5. After each addition, the solutions were allowed to equilibrate for 10 min, the pH was measured, and UV–Vis and fluorescence spectra were recorded.

In the case of functionalized materials (EBA-DMAN and EBA-pl-DMAN), the films were cut into strips of dimension 1 × 4 cm and dipped into 100 ml of water (Millipore-Q) using a homemade support that is slotted into the cell holder of the spectrophotometers. To study the effect of increasing the acidity of the medium beyond the pH scale, vials containing 50 ml of HCl at pH 7 to −1.1 (12 M HCl, 37%) were prepared. Strips of the film were immersed in these vials, starting from the vial with the lowest acid concentration, and the UV–Vis and fluorescence spectra were recorded for each pH after a conditioning time of 2 h. The fluorescence detection of acidic vapors was performed by adding 100 μl of HCl (12 M HCl 37%) over a cotton fragment to avoid direct contact and placing it at the bottom of a sealed spectrophotometric cuvette, where the functionalized EBA film is disposed.

2.4. Microwave equipment

The microwave equipment used in this study was an Anton Paar Monowave™ 300 microwave synthesis reactor equipped with an infrared sensor (IR pyrometer). All reactions were performed in pressure-resistant 30-ml test tubes sealed with silicon septum with a magnetic stirring bar. The progress of the reactions was observed by an integrated CCD camera, which directly focuses on the reaction vial.

2.5. Plasma treatment and characterization by contact angle measurements and atomic force microscopy

The films were plasma-treated using an RF-Expanded Plasma Cleaner PDC-002 coupled with a PlasmaFlo PDC-FMG gas mixer obtained from Harrick Plasma and a Varian SH-110 vacuum pump. Samples were placed inside the Pyrex chamber (6″ diameter × 6.52″ length), and both sides of all films were treated with high RF power (30 W to the RF coil) for 30 min with oxygen plasma. Gas flow rates and chamber pressure can be altered by manual pressure and flow regulators, and stabilized pressure was fixed at 250 mTorr (0.33 mbar).

Changes in the wettability of plasma-treated polymer surfaces were observed after the determination of water contact angle (CA) by the sessile drop method. CA measurements were performed at 25 °C using a KSV instruments LTD CAM 200 Tensiometer and MilliQ water as wetting solvent. Surface energy was determined using two liquids (water and methylene iodide) for the measurements. On the basis of Owens–Wendt's method [24], the surface energy (γ) and its dispersive (γ^d) and polar (γ^p) parts were calculated using the CAM 200 software.

Surface morphology and roughness of the EBA films modified with DMAN before and after oxygen plasma treatment were examined by atomic force microscopy (AFM) using a Nanoscope IV system (Digital Instruments) working in tapping mode with a triangular microfabricated cantilever having a length of 115–135 mm, 1- to 10-Ohm-cm phosphorous (*n*)-doped Si pyramidal tip, and a nominal spring constant of 20–80 N m^{-1}. The mean roughness value (Ra) represents the arithmetic average of the deviations from the center plane of the sample, which was determined using standard Digital Instruments software.

2.6. Surface modification of EBA films by hydrolysis (EBA-COOH) and acid chlorination (EBA-COCl)

EBA (7% of BA) film was cut into strips (1 × 4 cm) and hydrolyzed in the solid state by a modified procedure of the method reported previously [3] to conduct the heterogeneous reaction in a microwave reactor. The EBA film was placed in a 30-ml microwave test tube, and the test tube was then filled with a solution of 0.5 M NaOH in isopropanol. The temperature of the solution was fixed at 65 °C under stirring at 600 rpm for 6 h. After completion of the heterogeneous reaction at room temperature, the EBA-COO^- film was separated from the medium and neutralized in a microwave-assisted second step by adding 30 ml of aqueous HCl solution (0.1 M) to the polymer and maintaining the mixture at 50 °C for 1 h. The resulting hydrolyzed EBA-COOH film was then washed repeatedly with distilled water and dried under vacuum overnight. The surface modification of EBA to EBA-COO^- and EBA-COOH was confirmed and evaluated by ATR-FTIR spectroscopy (Fig. 3).

The EBA-COOH film and phosphorus pentachloride (50 mg, 0.24 mmol) were placed in a 30-ml microwave reactor containing 20 ml of CH_2Cl_2 anhydrous solution. Acid chlorination was carried out under microwave irradiation at 55 °C under magnetic stirring at 600 rpm. After 90 min, the EBA-COCl film was washed with dichloromethane and dried under vacuum overnight. The reaction between superficial acid groups and EBA-COCl was quantitative and confirmed by ATR-FTIR spectroscopy (Fig. 3).

2.7. Functionalization of EBA-COCl with DMAN

Superficially chlorinated EBA film, EBA-COCl, and 25 mg of DMAN were placed in a vial containing 20 ml of CH_2Cl_2 and 500 μl of triethylamine (TEA) under microwave at 55 °C for 15 h under magnetic stirring at 600 rpm. The vial was then rapidly cooled down with compressed air to room temperature, and the modified EBA-DMAN film was washed repeatedly with dichloromethane and dried under vacuum overnight. The reaction was confirmed by ATR-FTIR and UV–Vis spectroscopy (Fig. 3).

2.8. Synthesis of N-(2-hydroxyethyl)-4-dimethylamino-1,8-naphthalimide

N-(2-hydroxyethyl)-4-bromo-1,8-naphthalimide (compound 1) and *N*-(2-hydroxyethyl)-4-dimethylamino-1,8-naphthalimide (compound 2) were synthesized following the procedure (Fig. 2) described in refs. [25,26] and using a novel reaction [27] for dimethylamination of compound 1.

In a pressure-resistant microwave test tube, a mixture of 4-bromo-1,8-naphthalic anhydride (1.4 g, 0.005 mol) and ethanol amine (0.4 g, 0.005 mol) in ethanol (15 ml) was heated at 85 °C and stirred at 600 rpm for 2 h. The resulting mixture was cooled at 5 °C. The solid product obtained was filtered and washed with 30 ml of cold ethanol thrice and then identified as *N*-hydroxyethyl-4-bromo-1,8-naphthalimide (compound 1) after drying. Yield 90% (1.4 g). M.p.: 206 ± 2°. ^{1}H NMR (δ_H ppm) (300 MHz, DMSO-d_6, Me_4Si): δ 8.42 (dd, J = 13.9, 7.9 Hz, 2H), 8.20 (d, J = 7.9 Hz, 1H), 8.10 (d, J = 7.8 Hz, 1H), 7.89 (t, J = 7.9 Hz, 1H), 4.81 (s, 1H), 4.10 (t, J = 6.4 Hz, 2H), 3.61 (t, J = 5.9 Hz, 2H). ^{13}C NMR (δ_C ppm) (100.6 MHz, DMSO-d_6, Me_4Si): δ 162.90, 162.85, 132.41, 131.42, 131.24, 130.80, 129.61, 128.98, 128.67, 128.14, 122.70, 121.92, 57.71, 41.95. FTIR (wavenumbers, cm^{-1}): ν_{OH}3386 cm^{-1}; ν_{C-H}3066 cm^{-1} aromatic stretch vibration; $\nu_{C=O}$ 1692, 1658 cm^{-1}; $\nu_{N-C=O}$ 1611 cm^{-1}; ν_{C-C} 1585, 1568 cm^{-1} aromatic ring chain vibrations. Elemental analysis, theoretical values: %C 52.52; %H 3.15; %N 4.38; experimental values: %C 52.42; %H 3.25; %N 4.25; EI–MS *m/z*: 321.0 (M^+).

In a pressure-resistant microwave test tube, 1 g of compound 1 (0.003 mol), 4.35 ml of triethylamine (0.03 mol), and 10 ml of DMF:water (1:1) solution were added. The mixture was heated at 120 °C and stirred at 600 rpm for 12 h. After completion of the reaction, the vial was cooled with water to room temperature. The mixture was extracted with ethyl acetate (4 × 50 ml), and the organic layer was dried over K_2CO_3. The solvent was evaporated under reduced pressure, which was purified by silica gel column chromatography using ethyl acetate:hexane (2:1) as eluent to obtain an orange solid product, which is identified as *N*-(2-hydroxyethyl)-4-dimethylamino-1,8-

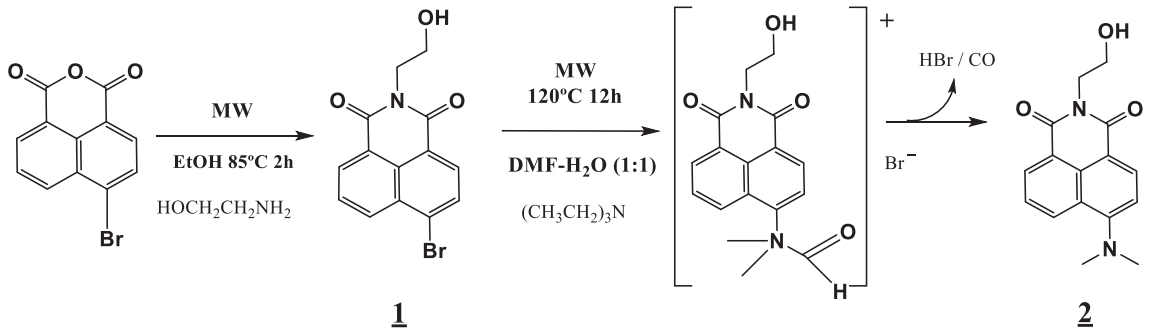

Fig. 2. Reaction pathway and mechanism for the synthesis of *N*-(2-hydroxyethyl)-4-dimethylamino-1,8-naphthalimide (DMAN, compound 2).

naphthalimide. Yield: 84%, M.p. = 135 ± 2 °C. ^{1}H NMR (δ_H ppm) (400 MHz, DMSO-d_6, Me_4Si): δ 8.51 (dd, J = 8.5, 1.1 Hz, 1H), 8.45 (dd, J = 7.3, 1.1 Hz, 1H), 8.34 (d, J = 8.3 Hz, 1H), 7.75 (dd, J = 8.5, 7.3 Hz, 1H), 7.21 (d, J = 8.3 Hz, 1H), 4.81 (t, J = 6.0 Hz, 1H), 4.13 (t, J = 6.6 Hz, 2H), 3.59 (q, J = 6.5 Hz, 2H), 3.08 (s, 6H). ^{13}C NMR (δ_C ppm) (100.6 MHz, DMSO-d_6, Me_4Si): δ 163.69, 163.03, 156.41, 132.12, 131.32, 130.41, 129.56, 124.90, 124.16, 122.37, 113.43, 112.91, 57.87, 44.35, 41.51. FTIR (wavenumbers, cm^{-1}): ν_{OH} 3474 cm^{-1}; $\nu_{C=O}$ 1680 cm^{-1} and 1628 cm^{-1}, ν_{C-C} 1575 cm^{-1} aromatic ring chain vibrations. Elemental analysis, theoretical value: %C 67.59; %H 5.67; %N 9.85; experimental values: %C 67.09; %H 5.88; %N 9.88. EI-MS m/z: 285.0 (M^+).

3. Result and discussion

3.1. Synthesis of N-(2-hydroxyethyl)-4-dimethylamino-1,8-naphthalimide

The synthesis route to obtain *N*-(2-hydroxyethyl)-4-dimethylamino-1,8-naphthalimide is presented in Fig. 2. In the first step, the condensation of 4-bromo-1,8-naphthalic anhydride with 2-hydroxyethylamine under microwave irradiation in ethanol at 85 °C afforded compound 1 in high yield at a shorter reaction time than conventional conditions. It has been observed [28] that for various amines, imidation of naphthalimides under reflux required 4–16 h. Our results show that the microwave method reduced the reaction time and improved the yield from 72–85% (under conventional conditions) to 96%.

In the second reaction step (Fig. 2), an interesting observation was made while we were optimizing the reaction conditions for the nucleophilic substitution reaction of compound 1 with 2-methoxyethylamine. When the reaction was carried out in DMF, surprisingly, dimethylamination product (DMAN, compound 2) was also produced. In the absence of the primary amine, DMAN was obtained in very good yield. This reaction has been described [27,29] as a convenient method for the introduction of a dimethylamino group in aromatic compounds through chlorinated derivatives of heterocycles or aromatics using bases such as KOH or K_2CO_3, and although the reaction mostly proceeds slowly, it results in good yields.

In our experimental conditions, dimethylamination resulted in the formation of compound 2 in good yield. On the contrary, when no base was added, the reaction did not proceed. Also, the presence of water seemed to be crucial for the amination, and this fact could be attributed to a better solvation of the base. The reaction and the plausible mechanisms for the amination are illustrated in Fig. 2.

The reaction starts with a base-assisted cleavage of DMF to form the required dimethylamine [30,31], which acts as the nucleophile for the formation of the required product. DMF is an easy substitute for dimethylamine, and the reaction occurs in a shorter period of time and produces high yields with microwave irradiation. The best conditions were noted under microwave irradiation for 12 h at 850 W and a ceiling temperature of 120 °C of a mixture of compound 1 together with 10 equiv. of triethylamine in DMF:water (1:1) yielding compound 2 in 90%.

3.2. Microwave-assisted surface hydrolysis, acid chlorination, and functionalization of EBA with naphthalimide groups

The functionalization of EBA (7% content of BA) was carried out following the sequence of reactions shown in Fig. 1. The different modifications of EBA, hydrolysis of butyl ester, acid chlorination, and esterification with DMAN were accomplished successfully in solution under microwave irradiation. All the modified EBA films were isolated and characterized by ATR-FTIR spectroscopy (Fig. 3).

Fig. 3 shows the characteristics of vibrational bands of the species formed after each functionalization step as described above in the synthesis section. As shown in Fig. 3, butyl ester on the surface was hydrolyzed by microwave irradiation under heterogeneous conditions, and the degree of hydrolysis was determined by ATR-FTIR as described earlier [3] and by using the butyl ester and carboxylate bands. The obtained curves are plotted in Fig. 4.

The spectra at different hydrolysis reaction times show the growth of bands because of the increase in carboxylate content, introduced to the surface of the polyolefin film. This confirms the hydrolysis of the surface with treatment time. Thus, the carboxylate content can be used to follow the modification of EBA surface by ATR-FTIR.

After reacting sodium hydroxide solution (0.5 M) in isopropanol for 6 h at 65 °C, the conversion of butyl ester to carboxylate (Fig. 4) reaches a value of 83.3% (5.83% of butyl ester content). In our experimental condition, 1.17% of butyl ester remained in the EBA composition after hydrolysis in the superficial thickness of the film analyzed by ATR-FTIR. As found in the hydrolysis reactions carried out in bulk with EBA [3] and ethylene vinyl acetate (EVA) copolymers [32], a plateau was reached in the hydrolysis conversion when the reaction times are longer than 6 h.

The determination of the acid content by ATR-FTIR suggested the carboxylic acid band at 1703 cm^{-1} is attributed to the overlapping of the carbonyl butyl ester band at 1735 cm^{-1}. The asymmetric stretch band of the carboxylate group at 1580 cm^{-1} could therefore be more convenient to follow the hydrolysis conversion.

After protonation of the carboxylate groups in a microwave-assisted second step (HCl aq. solution 0.1 M, 50 °C, 1 h), the acid groups present in EBA-COOH were converted to acid chloride under microwave heating. After 1.5 h of reaction with phosphorus pentachloride, the transformation was quantitative, as shown by the band at 1793 cm^{-1}, which corresponds to $\nu_{(C=O)}$ acyl chloride (EBA-COCl) and the disappearance of the acid band at 1703 cm^{-1} (Fig. 3).

Finally, functionalization was carried out by reacting EBA-COCl with the previously obtained *N*-(2-hydroxyethyl)-4-dimethylamino-1,8-naphthalimide derivative. The degree of functionalization increased with reaction time (3 h: 45%; 5 h: 60%; 7 h: 70%; and 10 h: 83%). After reacting for 15 h at 55 °C, no acyl halide band in the functionalized EBA-DMAN film could be detected at 1793 cm^{-1}, suggesting that the

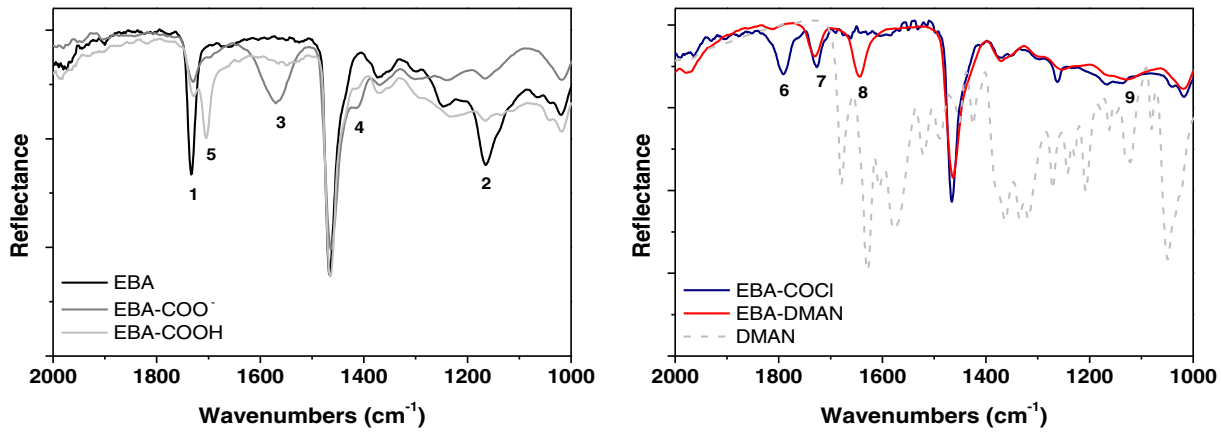

Fig. 3. ATR-FTIR spectra in the region between 2000 and 1000 cm^{-1} of EBA (7% of BA content) and the surface-modified EBA materials: (1) 1735 cm^{-1} $\nu_{(C=O)}$ butyl ester (EBA), (2) 1165 cm^{-1} $\nu_{(C-O)}$ aliphatic ester (EBA), (3) 1568 cm^{-1} and (4) 1413 cm^{-1} are assigned to $\nu_{as(COO-)}$ and $\nu_{s(COO-)}$ of carboxylate anion, respectively, (EBA-COO^-), (5) 1703 cm^{-1} $\nu_{(C=O)}$ carboxylic acid (EBA-COOH), (6) 1793 cm^{-1} $\nu_{(C=O)}$ acyl chloride (EBA-COCl), (7) 1730 cm^{-1} $\nu_{(C=O)}$ naphthalimide (EBA-DMAN), (8) 1644 cm^{-1} $\nu_{(C=C)}$ naphthalimide aromatic ring (EBA-DMAN), and (9) 1167 cm^{-1} $\nu_{(C-O)}$ aliphatic ester (EBA-DMAN).

reaction was quantitative and the content of naphthalimide on the surface remained constant after several washes with dichloromethane.

The amount of naphthalimide superficially bonded to the EBA was determined spectrophotometrically through the measurement of absorbance at the peak maximum of the absorption band and using the absorption coefficient of *N*-(2-hydroxyethyl)-4-dimethylamino-1,8,-naphthalimide in water:ethanol (4:1 w/w) ($\varepsilon_{445} = 1.02 \times 10^4$ mol^{-1} l cm^{-1}). Analysis of EBA-DMAN by UV spectroscopy provided a measure of the surface content of DMAN per unit area of polymer, and a concentration value of 2.4 ± 0.20 μg cm^{-2} was calculated for the EBA-DMAN film hydrolyzed after 6 h. For the materials with a lower initial degree of hydrolysis, a good correlation was observed between increasing the extent of acid chlorination on EBA and increased content of DMAN bonded to the EBA.

3.3. Depth profiling of the functionalization by CRS

Chemical functionalization of EBA-DMAN polymer films was studied using Raman microscopy. Both physical and chemical surface modification reactions generally result in the formation of a concentration gradient of the modifying groups through the film, and we used CRS to characterize the depth profile [33] of DMAN anchored to the EBA-DMAN films.

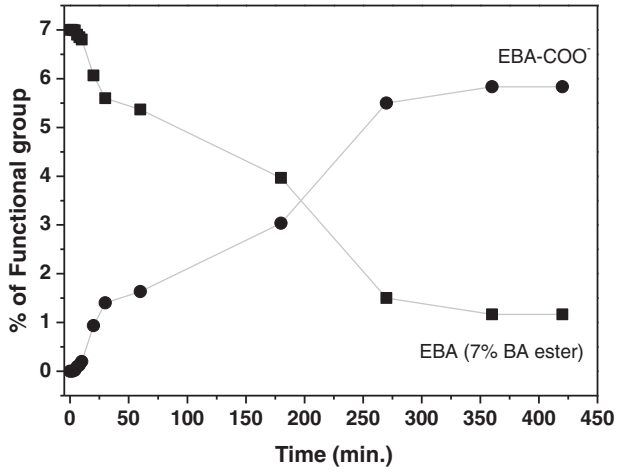

Fig. 4. Relationship between the percentages of surface hydrolysis degree of butyl ester (▪) and carboxylate formation (•) and reaction time in EBA films (7% content in BA) determined from the ATR-FTR spectra.

To obtain the depth profile of the films, a Raman microscope was focused stepwise (1 μm) from near the surface down to the center of each film, and the 1000- to 1800-cm^{-1} region of the spectrum was recorded at each step. In addition to the typical EBA polymer peaks, new characteristic bands emerged for graphitic material EBA-DMAN.

The degree of modification as a function of depth was obtained from the relative intensity of the naphthalimide bands and $\nu_{(C-C)}$ aromatic ring vibrations at 1585 cm^{-1} with respect to the $\nu_{(C-C)}$ aliphatic chain vibrations of the EBA at 1296 cm^{-1}. Hence, signals [I (1585 cm^{-1})/I (1296 cm^{-1})] lead to the relative depth profile, which is depicted in Fig. 5.

The shape of the curve shown in Fig. 5 confirms that the EBA has not only been modified at the surface, but a gradient of DMAN was also formed across the first 20 μm of film thickness until the naphthalimide Raman bands are negligible. Relative degrees of hydrolysis of the EBA and the subsequent functionalization are a function of the depth without any interface between the pure EBA layers and functionalized layers. This behavior has been described by other authors using this technique to modify polyvinyl chloride (PVC) [34] and in the nitration of polystyrene [35] without any swelling of the polystyrene film. In our reaction conditions of hydrolysis (6 h at 65 °C using 0.5 M NaOH in isopropanol),

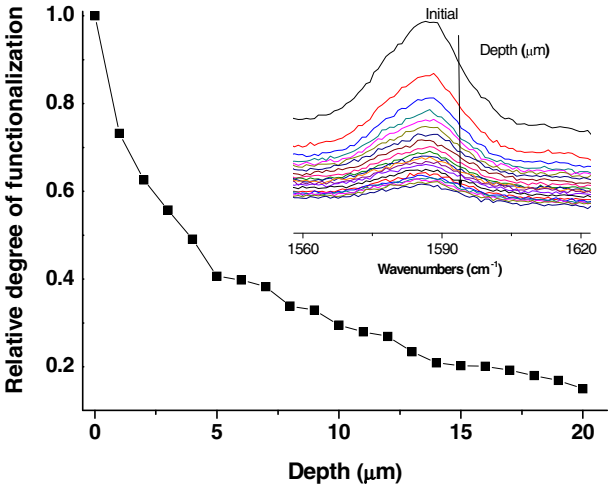

Fig. 5. Relative depth profile of functionalization calculated from the evolution of the Raman band $\nu_{(C-C)}$ aromatic ring vibrations of naphthalimide at 1585 cm^{-1} (inset) versus depth. Spectra of a functionalized EBA-DMAN film (100 μm) were recorded using confocal Raman spectroscopy and normalized with respect to the intensity of the $\nu_{(C-C)}$ band at 1296 cm^{-1} of the aliphatic chain vibrations of the EBA.

the polyolefin film did not swell, and hence, the extent of hydrolysis (83.3% of butyl ester content of EBA) is confined to the first 20 μm from the surface down to the film center as the DMAN depth profile.

CRS is a useful technique to measure the functionalization of polymer surface through the depth profile using Raman absorption band characteristics of the anchored functionalities.

3.4. Effect of pH on the absorption and fluorescence properties of DMAN and EBA-DMAN

Light excitation of DMAN elicits an electron donor–acceptor interaction between the unbound electron pair of the nitrogen atom at C-4 position toward the electron-accepting *peri*-carboximide groups [36,37]. This intramolecular electron charge transfer (ICT) results in a long-wavelength broad absorption band with absorption maxima at 445 and 402 nm for DMAN (Fig. 6A) and EBA-DMAN (Fig. 6B), respectively. Upon acidification, the maximum intensity of the band decreases from pH approximately 3 to 0 (Fig. 6C). When the aromatic amine of the naphthalimide derivative is protonated at low pH values, the electron-withdrawing effect leads to fluorescence quenching (Fig. 6D). This effect can also be observed for the DMAN bonded to the surface of EBA (Fig. 6B). The effect of pH on the absorbance and fluorescence of DMAN and EBA-DMAN is illustrated in Fig. 6.

For EBA-DMAN, the decrease in absorbance and the corresponding quenching of fluorescence due to the amine protonation occurs at lower pH values than that obtained for DMAN (Fig. 6C and F). This fact could be due to the hydrophobic characteristic of the EBA surface. Hence, EBA-DMAN films were used to evaluate the molarity of HCl aqueous solutions in the interval of 1–12 M with the change in absorbance (Fig. 6B) and fluorescence (Fig. 6E) characteristics as a function of pH [38]. Table 1 summarizes some spectroscopic parameters obtained from the spectra.

When the DMAN chromophore is bonded to the EBA through the 2-hydroxyethyl group, the absorption and fluorescence maxima exhibit a marked hypsochromic shift of 40–60 nm without a decrease in intensity and maintaining the Stokes shift (Table 1). The fluorescence quantum yield of DMAN is low in polar and base–neutral media, but is drastically increased to 0.85 in hexane. These results are in agreement with those obtained by other authors [37] for *N-methyl-4-dimethylamino-1,8-naphthalimide*. The corresponding fluorescence quantum yields of EBA-DMAN were not determined because of difference between the functionalized film and the fluorescence standard used in solution, but the relative fluorescence intensities of EBA-DMAN were in the same intensity order: water:ethanol (4:1, v/v) << ethanol ⋘ hexane.

Table 1
Parameters for *N*-(2-hydroxyethyl)-4-dimethylamino-1,8-naphthalimide (DMAN) in solution and bonded to the polymer film (EBA-DMAN) determined according to pH dependence by UV–Vis absorption and fluorescence spectroscopy[a].

Parameter	DMAN	EBA-DMAN
$\lambda_{ABS\text{-}acid}$	332, 346 nm	327, 348 nm
Log ε_{acid}[b]	4.08 (332 nm)/4.05 (346 nm)	–
$\lambda_{Isobestic}$	305, 360 nm	370 nm
$\lambda_{ABS\text{-}base}$	445 nm	402 nm
Log ε_{base}[b]	4.01 (445 nm)	–
pK_a[c]	1.41	−0.88
$\lambda_{FLU\text{-}acid}$	548 nm	480 nm
$\lambda_{FLU\text{-}base}$	550 nm	488 nm
$\phi_{FLU\text{-}(solvent)}$[f]	0.032 (water:ethanol, 4:1, v/v)	water:ethanol
	0.035 (ethanol)	(4:1, v/v) << ethanol ⋘ hexane
	0.85 (hexane)	
$\Delta\nu$[g]	4290.1	4425.7

[a] Measured at 10^{-4} M in water:ethanol (4:1, v/v). The subscripts "acid" and "base" refer to the limiting value of a given parameter when the acid or base condition is increased, respectively. Fluorescence emission spectra were obtained by excitation at λ_{MAX}.
[b] ε, molar absorptivity in $M^{-1}\,cm^{-1}$.
[c] Obtained [37] by analyzing the pH dependence of the absorbance (A) at a given wavelength according to the equation $\log[(A_{acid} - A)/(A - A_{base})] = pH - pK_a$.
[f] Relatively to coumarin 6 ($\phi_F = 0.78$ in ethanol).
[g] Stokes shift (ν_{FLU}-ν_{ABS}) in frequency (cm^{-1}).

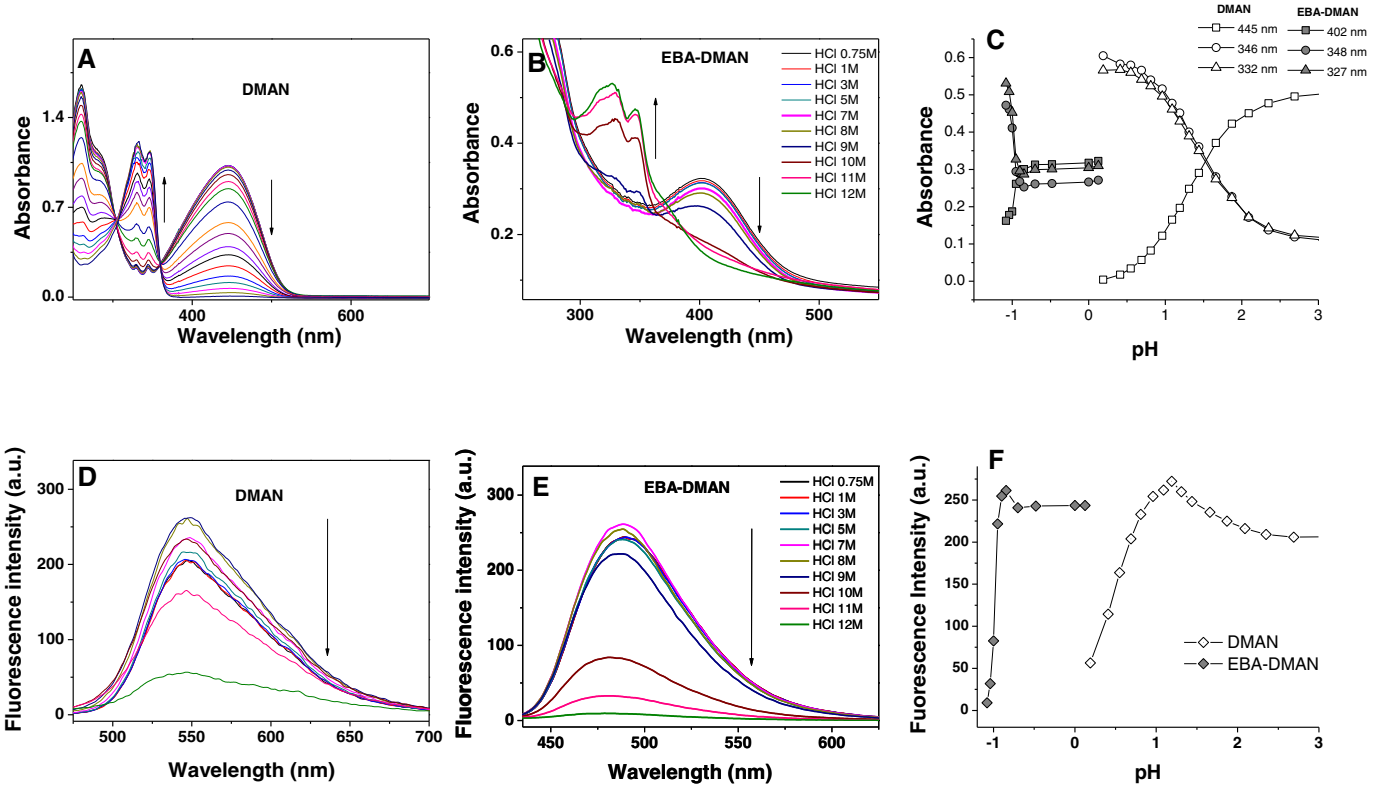

Fig. 6. Spectroscopic characteristics as a function of pH of acid media: Absorption of DMAN (A) and EBA-DMAN (B) and fluorescence of DMAN (D) and EBA-DMAN (E). Comparison of the absorption (C) and fluorescence (F) changes with pH for DMAN and EBA-DMAN.

The pK_a of EBA-DMAN has a negative value (−0.88) and is lower than that of DMAN (1.41), as the dimethylamine protonation of EBA-DMAN occurs at lower pH than that observed for DMAN (Fig. 6).

The EBA-DMAN material acts as an extreme acidity sensor by its absorbance and fluorescence characteristics. The sensor activity of EBA-DMAN was effective under several acid–water wash cycles (until 4–5 cycles), but with a prolonged response time (~2 h). Also, reversibility was observed with lower recovery of the fluorescence after the fourth cycle. One possibility to decrease the response time to acid media is to increase the hydrophilicity of the EBA surface though oxygen plasma treatment. In the next section, we report the results obtained from EBA-DMAN before and after plasma treatment as a sensor of acidity.

3.5. Plasma treatment of EBA-DMAN films and characterization

To enhance the hydrophilic characteristic of the functionalized EBA, the EBA-DMAN films were exposed to oxygen plasma for 30 min. Plasma treatment causes cleavage of macromolecular chains, generation of free radicals and oxygen-containing functionalities, and subsequent rearrangement of modified chains [39]. Plasma treatment can induce several surface changes [40], with serious impacts on consequent applications such as alterations in biocompatibility and antibacterial properties [41].

These processes have a significant effect on surface wettability. The content of DMAN bonded to the polymer remained constant after the treatment, but important changes were observed in the water CA. The obtained results are summarized in Table 2.

The plasma-treated film EBA-pl-DMAN exhibited a hydrophilic characteristic because of the presence of oxidative species on the surface [42]. The value of the water CA of EBA (7% BA), 106.5°, changed to 92.6° for EBA-DMAN, and after 30 min of treatment with oxygen plasma (EBA-pl-DMAN), this value further decreased to 41°. The measured CAs were then used to calculate the polar, disperse, and total surface energies of the modified EBA films. The change in the total surface energy (γ) and its polar (γ^p) and dispersive (γ^d) components of the modified EBA films was calculated by Owens–Wendt's method. The variation in the values of the total, polar, and disperse solid surface energies (Table 2) of EBA-DMAN before and after oxygen plasma treatment, EBA-pl-DMAN, shows that the total surface energy of EBA-DMAN increases from 30.91 mN m^{-1} for untreated film to 62.39 mN m^{-1} for oxygen plasma-treated film EBA-pl-DMAN. Compared with the untreated film, plasma-treated films have higher total surface energy, particularly for the polar component.

The change in EBA-DMAN surface structure and the topography after oxygen plasma modification were imaged and measured by AFM. The AFM images of the untreated and oxygen plasma-treated films are presented in Fig. 7.

The average roughness (R_a) of untreated films was 12.5 nm, and their surface pattern was relatively smooth. After 30 min of oxygen plasma treatment, the treated EBA-pl-DMAN exhibited high density of height features distributed on the surface (Fig. 7). As expected, the average roughness was increased to 35.5 nm. The mean surface roughness of EBA-pl-DMAN was increased by approximately three times, confirming that the change in morphology is the result of the ion bombardment and ablation of the polymer surface layer.

Table 2
Contact angle (CA) and total (γ), polar (γ^p), and disperse (γ^d) surface energy data for EBA (7% of BA content) and the surface-modified EBA materials.

	Static CA (°)		Surface energy (mN m−1)[a]		
	Water	Diiodomethane	γ	γ^p	γ^d
EBA	106.5	55.0	29.38	0.38	29.00
EBA-COOH	85.9	66.6	29.51	4.99	24.53
EBA-DMAN	92.6	60.8	30.91	2.33	28.58
EBA-pl-DMAN	41.0	51.5	62.39	28.44	33.95

[a] Calculated using Owens–Wendt's method [24].

3.6. Plasma treatment of EBA-DMAN films and response time to acid media

The changes in fluorescence emission with HCl (37%, 12 M) as a function of time are shown in Fig. 8A and B for EBA-DMAN and EBA-pl-DMAN, respectively.

The oxygen plasma treatment substantially decreased the response time of the DMAN fluorescence in strong acid medium (HCl, 12 M) from 80 min for EBA-DMAN to 30 min for EBA-pl-DMAN (Fig. 8C), together with a larger decay of fluorescence in the plasma-treated film. The increase in hydrophilicity imparted by the oxidative plasma on the film surface facilitates the penetration of proton into the coordination sphere of the DMAN functional groups anchored to the first 20 μm of the film. The remaining nonprotonated DMAN chromophore after acid treatment was higher for the EBA-DMAN film, as the residual fluorescence intensity is stronger than that observed for the EBA-pl-DMAN film. This fact confirms a deeper penetration of protons into the plasma treatment material. Also, the reversibility of dimethylamine protonation after washing with water was compared for both materials. Again, the extent of deprotonation is lower for EBA-DMAN (Fig. 8D), as the fluorescence intensity of EBA-pl-DMAN (Fig. 8E) was totally recovered after washing with distilled water. Thus, oxygen plasma treatment improved the sensitivity of the functionalized EBA surface to the acid medium.

The response time of functionalized films to the extremely acidic environment was also studied in the vapor phase, it was observed that the spectroscopic characteristics of DMAN bonded to the polymer were sensitive to the acid vapor medium. It was necessary to maintain the film for approximately 1 h to observe the effective change in absorption and fluorescence properties. The results are shown in Fig. 9.

Both functionalized materials are sensitive to HCl vapors through their ICT absorption bands at the longest wavelength (Fig. 9A and B). The plasma-treated EBA-pl-DMAN film exhibits better behavior in fluorescence decay after 120 min of vapor treatment (Fig. 9D) than the untreated EBA-DMAN film (Fig. 9C). The vapor penetration into the surface materials was improved by the surface oxidation induced by the plasma.

The hydrophilicity of the EBA surface clearly improved the sensor activity of the DMAN chromophore bonded to the surface.

In this study, we have described a useful procedure to modify and functionalize the polyolefin copolymer EBA, thereby opening the possibility of anchoring numerous interesting structures containing functionalities capable of reaction with acid chlorine groups introduced by microwave irradiation. The functionalized surface films of EBA-DMAN act as strong acid sensors in both solution and vapor phases. The post-functionalization treatment with oxygen plasma decreased the response time to the acid media and increased the penetration of protons into the material. This functionalization with dimethylamine naphthalimide derivatives such as those used in this study or other fluorescence probes could result in a variety of film sensors of significant interest in environmental applications.

4. Conclusions

In conclusion, we have demonstrated that microwave irradiation allows rapid and efficient attachment of hydroxyl naphthalimide functionalities to superficially acid-chlorinated ethylene-butyl acrylate copolymers (EBA-COCl). The previous modifications of EBA (7% of BA) films (hydrolysis and acid chlorination) occur efficiently in a heterogeneous phase under our experimental conditions.

CRS was a useful technique to measure the functionalization of the polymer surface through the depth profile, and the results demonstrated that the heterogeneous modification was confined to the first 20 μm from the surface down to the film center.

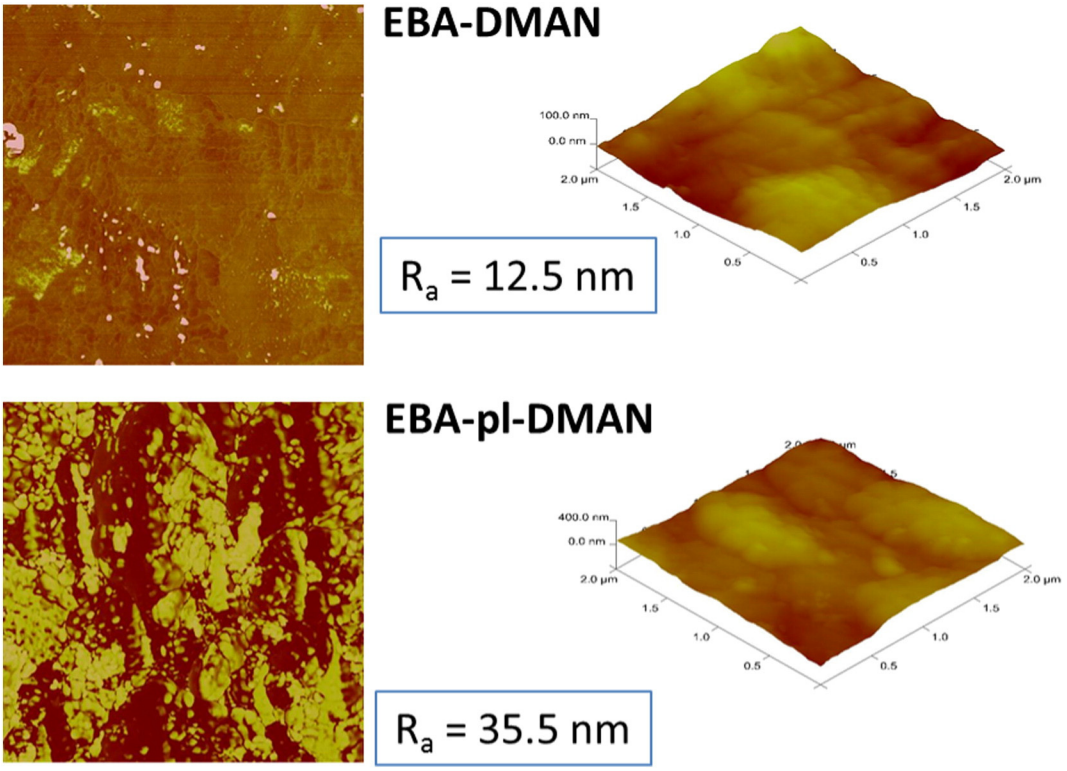

Fig. 7. AFM images and surface roughness (Ra) of the modified polymer films: EBA-DMAN and oxygen plasma-treated EBA-pl-DMAN.

The surface-modified films with *N*-(2-hydroxyethyl)-4-dimethylamino-1,8-naphthalimide (EBA-DMAN) at a concentration of $2.4 \pm 0.20\ \mu g\ cm^{-2}$ determined by UV-spectroscopy exhibited properties as a reversible acidity sensor (until 4–5 cycles). The decrease in absorbance (ICT absorption band) and the corresponding quenching of fluorescence because of the amine protonation of EBA-DMAN films occurs at lower pH values than that obtained for DMAN, and the solid sensor was used to evaluate the molarity of HCl solutions in the interval of 1–12 M.

Oxygen plasma treatment of the functionalized films increased appreciably the hydrophilic characteristic of the surface (EBA-pl-DMAN),

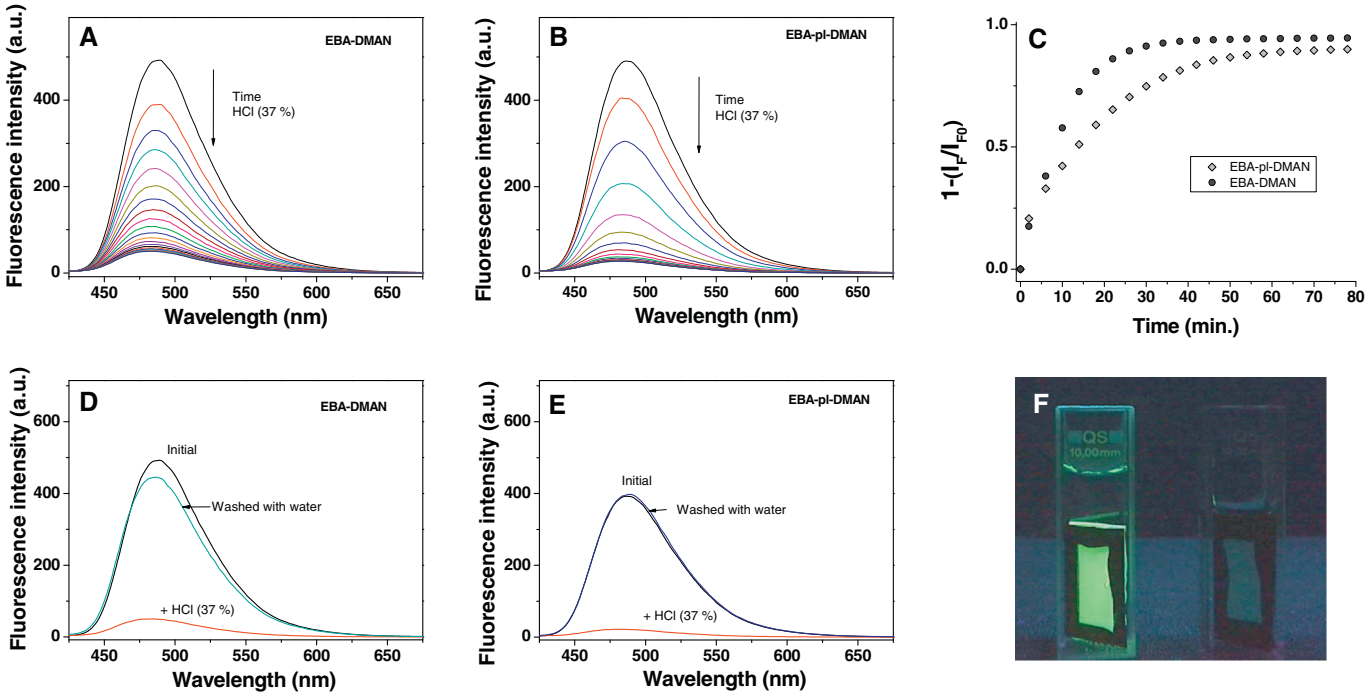

Fig. 8. Fluorescence decay with time for EBA-DMAN (A) and oxygen plasma-treated EBA-pl-DMAN (B) films using HCl (37% w/w, 12 M) aqueous solution. Response time comparison between both materials (C) and reversibility of dimethylamine protonation of the functionalized surfaces of EBA-DMAN (D) and EBA-pl-DMAN (E) after washing with distilled water and (F) fluorescence cells with EBA-pl-DMAN film, initial and after 30 min.

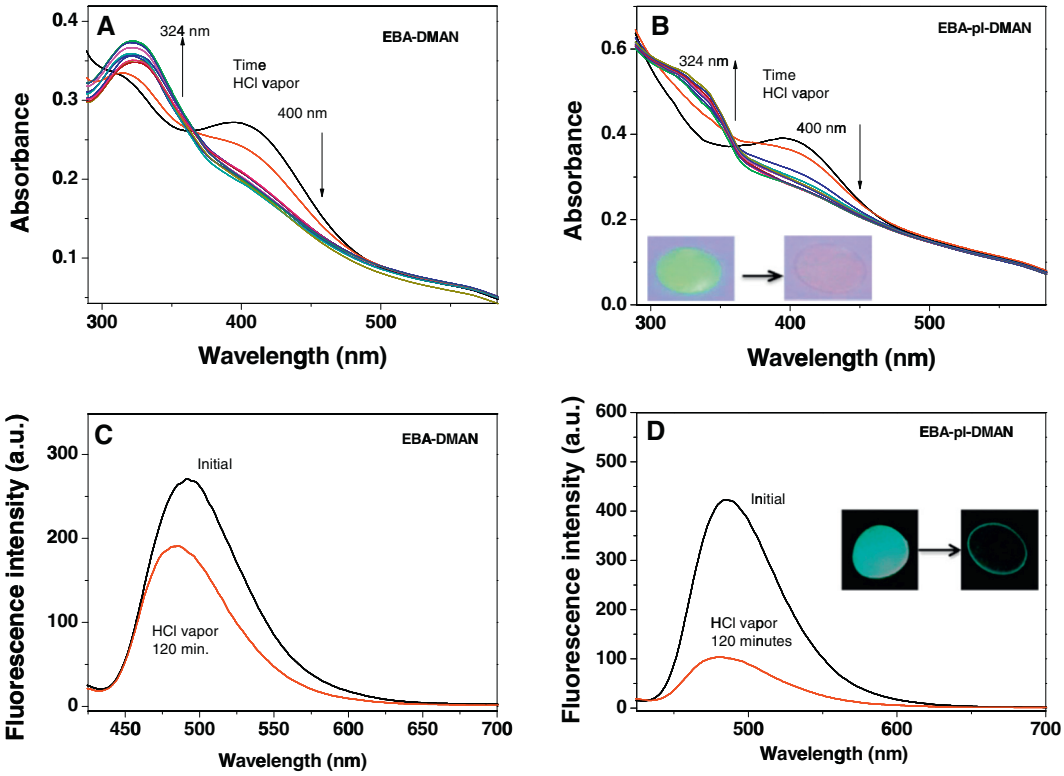

Fig. 9. Absorption changes with HCl vapors as a function of time (0–120 min) for functionalized films of EBA-DMAN (A) and EBA-pl-DMAN (B). Light blue fluorescence (488 nm) decreases after 120 min of vapors treatment for EBA-DMAN (C) and EBA-pl-DMAN (D). (For interpretation of the references to color in this figure legend, the reader is referred to the web version of this article.)

and the DMAN content bonded to the polymer remained constant after the treatment. The plasma treatment decreased the response time of the DMAN fluorescence to a strong acid medium (from 80 min for EBA-DMAN to 30 min for EBA-pl-DMAN in HCl, 12 M) and thus improved reversibility.

DMAN films bonded to the polymer were sensitive to the acid vapor medium, and the films treated with plasma (EBA-pl-DMAN) exhibited a better behavior in fluorescence decay, confirming that vapor penetration into the surface materials was improved by the surface oxidation induced by the plasma.

This new procedure using microwave reactions in a heterogeneous phase opens up the possibility to attach numerous interesting structures to polyolefin surfaces for application in materials of significant value such as environmental solid sensors.

Acknowledgments

This study was supported by MINECO (Project Ref. MAT2012-31709). S. Fernández-Alonso thanks MINECO for a pre-doctoral fellowship linked to the project.

References

[1] L.S. Penn, H. Wang, Polym. Advan. Technol. 5 (1994) 809.
[2] S.M. Desai, R.P. Singh, Adv. Polym. Sci. 169 (2004) 231.
[3] L. López-Vilanova, I. Martinez, T. Corrales, F. Catalina, React. Funct. Polym. 85 (2014) 28.
[4] V. Gaud, F. Rougé, Y. Gnanou, React. Funct. Polym. 72 (2012) 521.
[5] M. Kondo, K. Goto, Y. Dozono, N. Kawatsuki, React. Funct. Polym. 73 (2013) 1567.
[6] F. Gicogna, S. Coiai, C. Pinzino, F. Ciardelli, E. Passaglia, React. Funct. Polym. 72 (2012) 885.
[7] I. Grabchev, R. Betcheva, J. Photochem. Photobiol. A. 73 (2001) 142.
[8] K. Wang, W. Huang, P. Xia, C. Gao, D. Yan, React. Funct. Polym. 52 (2002) 143.
[9] E. Martin, R. Weigand, A. Pardo, J. Lumin. 68 (1996) 157.
[10] W. Stewart, J. Am. Chem. Soc. 103 (1981) 7615.
[11] S. Banerjee, E.B. Veale, C.M. Phelan, S.A. Murphy, G.M. Tocci, L.J. Gillespie, D.O. Frimannsson, J.M. Kelly, T. Gunnlaugsson, Chem. Soc. Rev. 42 (2013) 1601.
[12] W. Zhu, C. Hu, K. Chen, H. Tian, Synth. Met. 96 (1998) 151.
[13] H. Tian, J. Gan, K. Chen, J. He, Q. Song, X. Hou, J. Mater. Chem. 12 (2002) 1262.
[14] I. Grabchev, J.M. Chovelon, Polym. Adv. Technol. 14 (2003) 601.
[15] L. Jia, Y. Zhang, X. Guo, X. Qian, Tetrahedron Lett. 45 (2004) 3969.
[16] W. Zhu, M. Hu, R. Yao, H. Tian, J. Photochem. Photobiol. A. 154 (2003) 169.
[17] I. Grabchev, I. Moneva, V. Bojinov, S. Guittonneau, J. Mater. Chem. 10 (2000) 1291.
[18] I. Grabchev, J.M. Chovelon, X. Qian, J. Photochem. Photobiol. A. 158 (2003) 37.
[19] F. Cosnard, V. Wintgens, Tetrahedron Lett. 39 (1998) 2751.
[20] P.L. Shuai Zheng, T.E.R. Mark Lynch, T.S. Moody, H.Q.N. Gunaratne, A.P. de Silva, Photochem. Photobiol. Sci. 11 (2012) 1675.
[21] S. Hajatdoost, M. Olsthoorn, J. Yarwood, Appl. Spectrosc. 51 (1997) 1784.
[22] P. Slepicka, Z. Malá, S. Rimpelova, N.S. Kasalkova, V. Svorcik, React. Funct. Polym. 95 (2015) 71.
[23] G. Reynolds, K. Drexhage, Opt. Commun. 13 (1979) 222.
[24] G.K. Owens, R.C. Wendt, J. Appl. Polym. Sci. 13 (1969) 1741.
[25] H. Tian, J. Gan, K. Chen, J. He, Q.L. Song, X.Y. Hou, J. Mater. Chem. 12 (2002) 1262.
[26] Y.Q. Tian, B.R. Shumway, C. Youngbull, A.K.Y. Jen, R.H. Johnson, D.R. Meldrum, Sens. Actuators B Chem. 147 (2010) 714.
[27] Y.H. Cho, J.C. Park, Tetrahedron Lett. 38 (1997) 8331.
[28] S. Rouhani, K. Ghraranjig, M.H. Nezhad, Green Chem. Lett. Rev. 7 (2014) 174.
[29] A. Agarwal, P.M.S. Chauhan, Synth. Commun. 34 (2004) 2925.
[30] Y. Wan, M. Alterman, M. Larhed, A. Hallberg, J. Org. Chem. 67 (2002) 6232.
[31] A. Sharma, V.P. Mehta, E. Van der Eycken, Tetrahedron 64 (2008) 2605.
[32] M. Tang, J. Hou, L. Lei, X. Liu, S. Guo, Z. Wamg, K. Chen, Int. J. Pharm. 400 (2010) 66.
[33] S. Hajatdoost, J. Yarwood, J. Appl. Spectrosc. 50 (1996) 558.
[34] J. Sacristán, C. Mijangos, H. Reinecke, J. Spelle, J. Yarwood, Macromolecular 33 (2000) 6140.
[35] J. Sacristán, H. Reinecke, C. Mijangos, S. Spell, J. Yarwood, Macromol. Chem. Phys. 203 (2002) 678.
[36] M.S. Alexiou, V. Tychopoulos, S. Ghorbanian, J.H.P. Tyman, R.G. Brown, P.I. Brittain, J. Chem. Soc. Perkin Trans. 2 (1990) 837.
[37] P.A. Panchencko, O.A. Fedorova, Y.V. Fedorov, Russ. Chem. Rev. 82 (2014) 155.
[38] K.A. Connors, Binding Constants: The Measurement of Complex Stability, Wiley, New York, 1987.
[39] N. Slepičková Kasálková, P. Slepička, Z. Kolská, P. Sajdl, L. Bačáková, S. Rimpelová, V. Švorčík, Nucl. Instrum. Meth. B 272 (2012) 391.
[40] P. Slepička, S. Trostová, N. Slepičková Kasálková, Z. Kolská, P. Sajdl, V. Švorčík, Plasma Process. Polym. 9 (2012) 197.
[41] P. Slepička, N. Kasálková-Slepičková, J. Siegel, Z. Kolská, L. Bačáková, V. Švorčík, Biotech. Adv. 33 (2015) 1120.
[42] Y. Zheng, J. Miao, F. Zhang, C. Cai, A. Koh, T. Simmons, React. Funct. Polym. 100 (2016) 142.

Polymer 124 (2017) 139–150

Contents lists available at ScienceDirect

Polymer

journal homepage: www.elsevier.com/locate/polymer

Solid fluorescence sensors obtained by functionalization of photocrosslinked water-swollen acrylic membranes with 4-piperazine naphthalimide derivatives

S. Fernández-Alonso, T. Corrales, J.L. Pablos, F. Catalina*

Departamento de Química Macromolecular Aplicada, Instituto de Ciencia y Tecnología de Polímeros (CSIC), C /Juan de la Cierva, 3, 28006 Madrid, Spain

ARTICLE INFO

Article history:
Received 20 April 2017
Received in revised form
10 July 2017
Accepted 14 July 2017
Available online 15 July 2017

Keywords:
Photopolymerization
Membrane functionalization
Naphthalimide fluorescence probe

ABSTRACT

A photocrosslinked membrane (M-Cl) based on vinyl-pyrrolidone/butyl acrylate containing ethylene glycol dimethacrylate as a crosslinking agent and methacryloyl chloride as reactive monomer has been prepared for further functionalization. A series of hydroxy substituted piperazine naphthalimide compounds have been synthetized as pH sensitive Off-On fluorescence probes using two methods: microwave and reflux. Three of the derivatives were selected to be anchored to the M-Cl membrane through the acid chloride groups by the Schotten-Baumann reaction. All the obtained water-swollen membranes were characterized using different techniques. Photo-induced electron transfer (PET) and its pH-dependent optical changes were investigated and various photochemical parameters were determined by using pH-dependent absorption and fluorescence spectroscopies. In the pH range of 9.0–4.0, these solid sensors undergo PET process from the piperazine to the naphthalimide moiety leading to a fluorescence quenching. However, in the pH range of 4.0–1.0, the PET is inhibited to give a fluorescence enhancement. The sensitivity of the functionalized membranes to pH changes depended on the size and position of the naphthalimide substituents.

1. Introduction

Polymeric membranes have been widely utilized as a support material for various types of sensors and also used in systems where the environmental information is gathered by the measurement of photons. The most commonly used method is fluorescence emission. Its applications include optical chemical [1,2] and biological [3] sensors. Hydrophilic polymer matrices are widely used for immobilization of optical indicators due to their advantages such as fast response time, low cost, flexibility and their capability for deposition into various types of substrates.

In recent years, the developments of fluorescence pH sensors have attracted considerable attention because of their potential application in environmental analytics, medical diagnostics and process control [4,5]. Compared to small organic compounds, polymer based optical sensors display several important advantages as they can be non-invasive or minimally invasive, disposable, easily miniaturized and simple to process as a membrane, coating or solid layer on adequate surfaces [6,7]. The most widely used technique amongst optical sensors is the measurement of fluorescence intensity. Among the large number of fluorescent structures that have been developed, 1,8-naphthalimide derivatives have numerous applications in a variety of different areas. They have gained increasing interest as fluorescent probes for pH [8,9], metal cations [10–13] and anions [14] because they have been recognized for excellent photophysical properties with excellent stability, visible excitation and emission exhibiting high fluorescence quantum yields and large Stokes' shift that minimize the effects of the background fluorescence.

Polymerizable naphthalimide derivatives have been copolymerized with different co-monomers such as methyl methacrylate [15] and styrene [16,17], 2-hydroxyethyl methacrylate [18] and acrylamide [19,20]. In particular alkylpiperazinyl derivatives of naphthalimides have been studied and their behaviour as proton “off–on” switch sensors has been demonstrated as very sensitive [21,22] and interesting for applications [23] in complex media.

In an earlier work, we modified the surface of a film based on a copolymer of ethylene butyl acrylate with a naphthalimide derivative as an acidity sensor [24]. Even though the functionalized film

* Corresponding author.
E-mail address: fcatalina@ictp.csic.es (F. Catalina).

http://dx.doi.org/10.1016/j.polymer.2017.07.039
0032-3861/

was effective as an acid sensor, the hydrophobicity of the polyolefin surface modified with 4-dimethylamino-1,8-naphthalimide (water contact angle value of 92.6°) increased the time of its response to acid media.

Vinyl-pyrrolidone (VP) based materials exhibit highly interesting properties due to its unique combination of physical and chemical properties (biocompatibility, nontoxicity, chemical stability, good solubility in water and many organic solvents, affinity to both hydrophobic and hydrophilic complex substances). Also, VP copolymers with acrylic monomers such as butyl acrylate (BA) have important applications [25,26].

In this work we have prepared a photocrosslinked membrane based in vinyl-pyrrolidone/butyl acrylate and added ethylene glycol dimethacrylate as the crosslinking agent and methacryloyl chloride as the reactive monomer for further functionalization. Through the acid chloride groups, three derivatives of naphthalimide were anchored to obtain solid fluorescence sensors. The membrane preparation and the functionalization with naphthalimides are shown in Fig. 1.

The naphthalimides linked to the membrane containing acid chloride (M-Cl) were selected from a series of naphthalimide derivatives previously synthetized in this work using two methods: microwave and reflux. The structures of the series (Fig. 2) are hydroxyl derivatives of piperazine 1,8-naphthalimides which have been reported to have excellent fluorescence properties [21,22]. The membranes were characterized and the spectroscopic characteristics of the naphthalimide derivatives and the membranes were studied in function of pH and of different solvent polarities using UV-vis and fluorescence spectroscopies.

2. Experimental

2.1. Materials and reagents

All materials and solvents were commercially available and used as received, unless otherwise indicated. The materials included: sodium hydroxide (Panreac, 98–100.5%), hydrochloric acid (VWR Chemicals, 37%), ultrapure MilliQ water (Millipore), triethylamine (Aldrich, ≥99%), 4-bromo-1,8-naphthalic anhydride (Aldrich, 95%), potassium carbonate (Panreac, 99%), 2-aminoethanol (Aldrich, 99%), 2-methoxyethylamine (Aldrich, 99%), piperazine (Aldrich, 99%), 1-methylpiperazine (Aldrich, 99%), 1-(2-hydroxyethyl)piperazine (Aldrich, 98%), 1-[2-(2-hydroxyethoxy)ethyl]piperazine (Aldrich, 95%) ethanol (VWR Chemicals, 99.95%), dimethylformamide (Scharlau, 99.8%), Irgacure 2959 photoinitiator (BASF), ethyl acetate (Aldrich, ≥99.5%), hexane (Carlo Erba Reagents, 99%), 2-propanol (Scharlau, 99.5%), dichloromethane (Aldrich, ≥99.9%), toluene (Merck, ≥99.9%), diethyl ether (Carlo Ebra, >99.8%), 1,4-dioxan (Panreac, 99%), tetrahydrofuran (Aldrich, 99.9%), chloroform (Scharlau, 99%), acetone (Scharlau, 99.5%), acetonitrile (Aldrich, ≥99.5%), 1-butanol (Panreac, 99.5%), methanol (Aldrich, ≥99.8%), coumarin 6 (Aldrich, 98%), dimethylsulfoxide D6 (Eurisotop, 99.8% D), chloroform-d (Aldrich, 99.8% D), diiodomethane (Aldrich, 99%).

Monomers, 1-vinyl-2-pyrrolidone (Aldrich, ≥97%), butyl acrylate (Aldrich, ≥99%) and ethylene glycol dimethacrylate (Aldrich, 98%) and methacryloyl chloride (Aldrich, ≥97%) were distilled under vacuum to remove the inhibitor before use.

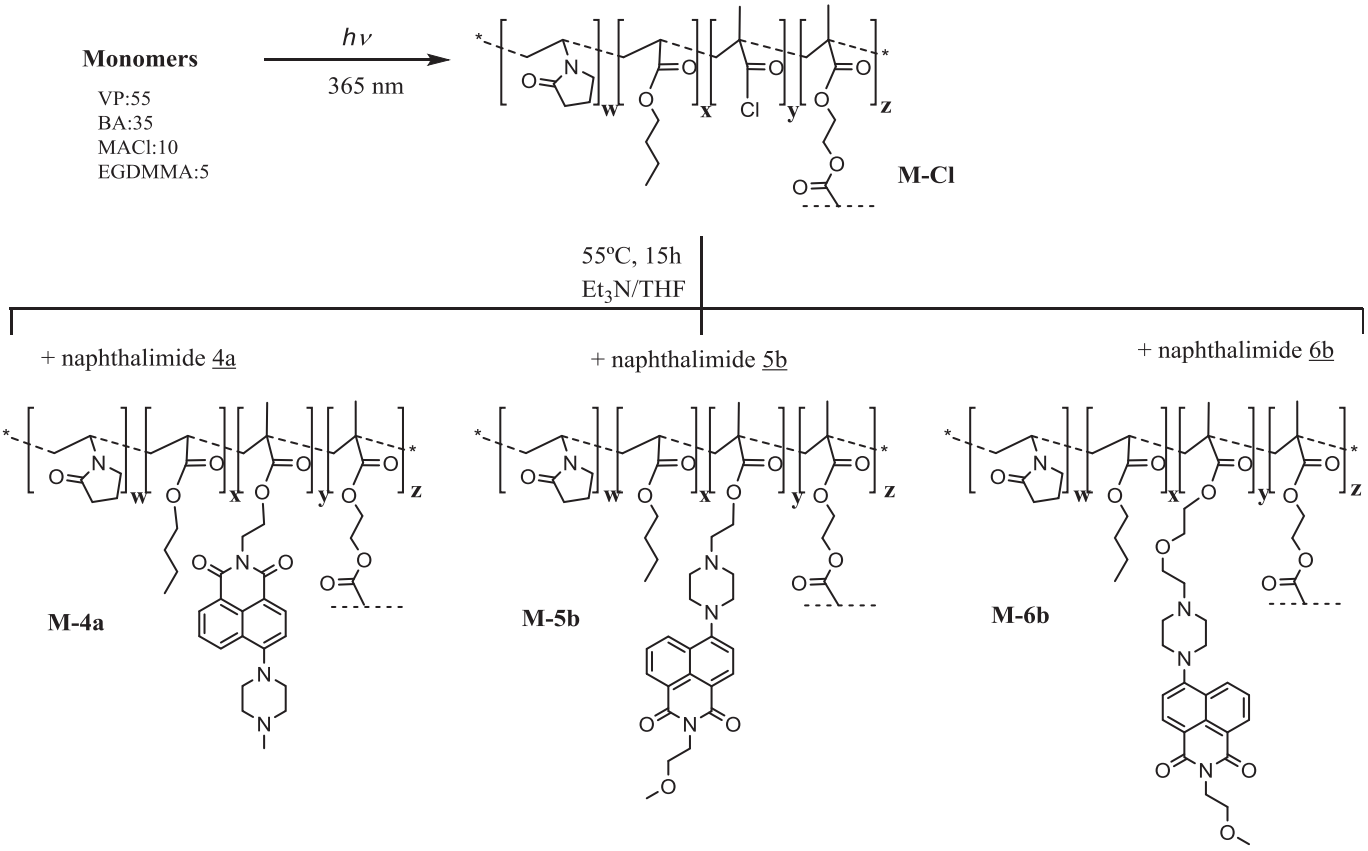

Fig. 1. Synthesis of the photocrosslinked acrylic membrane containing acid chloride groups (M-Cl) and functionalization with the selected naphthalimide structures.

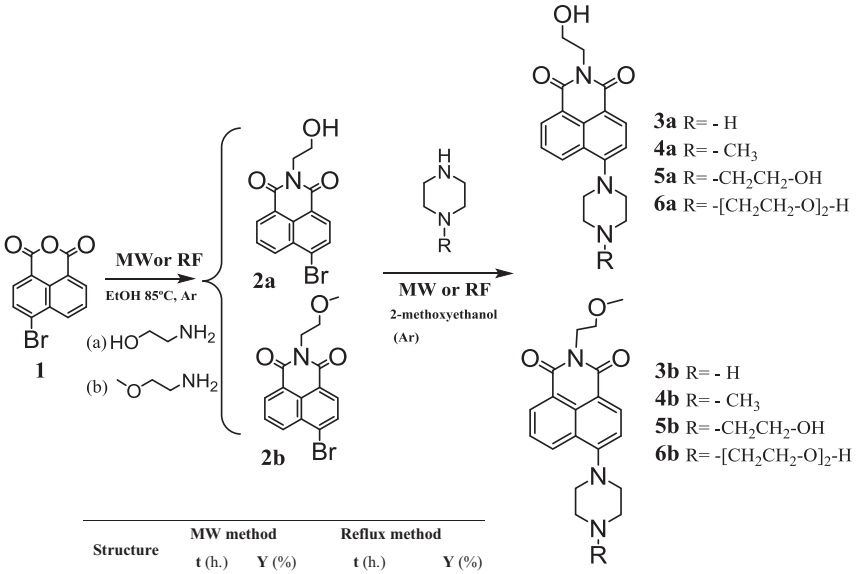

Structure	MW method		Reflux method	
	t (h.)	Y (%)	t (h.)	Y (%)
2a	2	90	15	76
2b	2	93	15	80
3a	1	84	15	64
4a	1	85	15	67
5a	1	88	15	68
6a	1	85	24	70
3b	1	84	15	69
4b	1	83	15	73
5b	1	84	15	71
6b	1	85	24	69

Fig. 2. Synthesis of the naphthalimide derivatives and their corresponding reaction times and yields for microwave (MW) and reflux (RF) methods.

2.2. Spectroscopic characterization and thermal analysis

Attenuated Total Reflectance/FT-Infrared Spectroscopy (ATR-FTIR) was used to characterize naphthalimide derivatives and membranes. ATR-FTIR spectra were obtained using a PERKIN ELMER BX-FTIR Spectrometer coupled with a MIRacle™ATR accessory, from PIKE Technologies and interferograms were obtained from 32 scans.

UV spectroscopy was employed for the quantitative determination of each hydroxyl-piperazine-naphthalimide derivative anchored to acrylic membranes in a *PERKIN ELMER Lambda 35* spectrometer. The naphthalimide content was determined through measurement of absorbance at the peak maximum of the absorption band. Assessment was made in quintuplicate for each material.

Fluorescence spectra were recorded using a Perkin Elmer LS 55 Fluorescence Spectrometer. Fluorescence emission spectra of the probe were recorded in the range 490–700 nm using as the excitation wavelength the maximum of the longest wavelength absorption band. All the spectra were corrected using the response curve of the photomultiplier. The fluorescence quantum yields (ϕ_F) were measured relatively to Coumarin 6 ($\phi_F = 0.78$ in ethanol) [27].

Nuclear magnetic resonance, ^{1}H- and ^{13}C- NMR spectra were recorded on a *Varian-Mercury* 400 MHz and a Bruker 300 MHz Nuclear Magnetic Resonance Spectrometers using hexadeuterated dimethyl sulfoxide (DMSO-d_6) and chloroform-d ($CDCl_3$) as the solvent. Chemical shifts were reported in parts per million (ppm). ^{1}H NMR and ^{13}C NMR chemical shifts were referenced to DMSO-d_6 (2.5 and 39.52 ppm respectively) or $CDCl_3$ (7.25 and 77.0 ppm respectively) as standard.

Mass Spectra (*MS*) were recorded on a HP 5973-MSD spectrometer.

Differential Scanning Calorimetry (DSC) was performed on a METTLER DSC-823e instrument (30–180 °C) previously calibrated with an indium standard (Tm = 429 K, ΔHm = 25.75 Jg^{-1}). Samples (10 mg) were tightly sealed onto the DSC pans and heating or cooling at 10 °C·min^{-1} rates under nitrogen. DSC was used to measure the glass transition temperature of the acrylic membranes and the melting points of the naphthalimide derivatives. The glass transition temperature of the membranes (T_g) were determined in a second scan after erasing the previous thermal history of the material in a first scan. Rate of 10 °C/min under nitrogen flow (30 psi).

Thermogravimetric Analysis (TGA) was carried out in a TGA Q-500 TA Instruments coupled to a Pfeiffer Vacuum ThermoStar™ mass spectrometer. The weight loss was measured as a function of temperature, and the evolved gas masses were directly monitored. The heating rate for the dynamic conditions was 10 °C·min^{-1}, and the nitrogen flow was maintained constant at 60 mL min^{-1}. The onset degradation temperature (T_{Onset}) was defined as the initial temperature of degradation, corresponding to the intersection of the tangent drawn at the decomposition step with the horizontal zero-line of the TG curve.

Elemental analysis (EA) was carried out on a Carlo Erba EA1108 elemental analyzer (% of C, H, N).

2.3. Swelling ratio and water contact angle measurements

Swelling degree (SD) in water and THF of the crosslinked membranes were measured by immersing dried and weighed sample films (W_d) into deionized water or THF at 30 °C for 24 h. The superficial solvent was removed and the samples were immediately weighed (W_s). The SD were calculated as follows: SD

(%) = $((W_s - W_d)/W_d) \times 100$, where W_s and W_d are the weight of the swollen and dry sample, respectively.

Contact angle (CA) measurements were performed at 25 °C using a KSV instruments LTD CAM200 Tensiometer and MilliQ-water as wetting solvent. Surface energy was determined using two liquids (water and methylene iodide) for the measurements. On the basis of Owens–Wendt's method [28], the surface energy (γ) and its dispersive (γ^d) and polar (γ^p) parts were calculated using the CAM 200 software.

2.4. Microwave and UV irradiation equipments

The microwave equipment used in this work was an *Anton Paar Monowave™ 300* microwave synthesis reactor provided with an infrared sensor (IR pyrometer). All reactions were performed in pressure-resistant 30-mL test tubes sealed with silicon septum and using a magnetic stirring bar.

The photopolymerization reactions were carried out in a Bio-link™ BLX-365 type Bio-link apparatus (Vilbert Lourmat™).

2.5. Membrane preparation by photopolymerization (M-Cl) and functionalization with HO-piperazine-naphthalimide derivatives

The reaction scheme for the photopolymerization reaction and the membrane functionalization with naphthalimide is shown in Fig. 1.

A crosslinked membrane (M-Cl) was obtained by the bulk photopolymerization of a mixture of monomers: N-vinyl-pyrrolidone (VP), butyl acrylate (BA), ethylene glycol dimethacrylate (EGDMMA) as the crosslinking agent and methacryloyl chloride (MACl) as the reactive monomer. The monomer molar ratio of the feed mixture was VP:55/BA:35/MACl:10/EGDMMA:5 and the photoinitiator (Irgacure 2959) was added to the mixture at 1% (w/w). The homogenous mixture was transferred to an ampoule, degassed by argon bubbling for 15 min and injected into a previously degassed silanized glass mould. The two glass pieces were separated by a Teflon spacer of 180 μm thick to define the reaction chamber. After 40 min of irradiation at 365 nm (dose 20 J cm^{-2}), the transparent crosslinked membrane (180 μm of thickness) was demoulded and conditioned (12 h) at room temperature under argon atmosphere. The crosslinked membranes were then washed several times with ethanol and dried under vacuum at 40 °C to remove the un-reacted monomers. The presence of acid chloride was confirmed by ATR-FTIR (wavenumbers,cm^{-1}), $\nu_{C=O}$ acyl chloride 1795 cm^{-1}; $\nu_{C\text{-}Cl}$ 898 cm^{-1} together with the characteristic co-monomers bands of VP $\nu_{C=O}$ lactam, amide-I 1675 cm^{-1} and BA, $\nu_{C=O}$ ester 1725 cm^{-1}; $\nu_{C\text{-}O}$ (O-CH_2-) ester 1161 cm^{-1}. The quantitative determination of chlorine in the membrane (2.8%) was carried out by TGA-MS (Table 1 and Fig. 3B and C).

In a second step, the M-Cl film was cut into strips (1 × 4 cm) and functionalized in the solid state with the naphthalimide derivatives synthetized in this work (Fig. 2). The procedure was as follows: the M-Cl membrane was placed in an ace round-bottom pressure flask with 20 mL of THF. 10 mg of hydroxy-piperazine naphthalimide derivative (4a, 5b or 6b) and 500 μL of triethylamine were added under argon atmosphere. The mixture was heated at 55 °C for 15 h. After this reaction time, the corresponding modified membranes M-4a, M-5b and M-6b were washed with cold ethanol and with water thrice in order to remove the unreacted acid chloride groups and the unreacted naphthalimide. The hydrolysis reaction of unreacted acid chloride groups was confirmed by ATR-FTIR and by TGA-MS as the characteristic peak of acid chloride was not present (Fig. 3C). After drying, the transparent functionalized membranes exhibited an intense yellow–green fluorescence and the content of naphthalimide was quantitatively determined by UV–Vis spectroscopy (Table 1). The characteristic peaks of naphthalimide structures in the membranes were not clearly observed in the ATR-FTIR spectra due to their low intensity and their overlap with the broad absorptions of the membrane functional groups.

2.6. Synthesis of the naphthalimide derivatives

Compound 2a was synthesized following the procedure (Fig. 2) described in the bibliography All the naphthalimide derivatives were synthetized using microwave (MW) and reflux (RF) methods with the same experimental conditions but differing in reaction times and yields. The RF reactions times were larger (15 h for all the reactions) and RF yields were lower than those obtained under MW irradiation. The synthesis path-ways, naphthalimide structures and reaction data are shown in Fig. 2.

To synthesize the desired piperazinyl derivative of naphthalimide, two bromide derivatives of naphthalimide containing 2-hydroxyethyl (Compound 2a) and 2-methoxyethyl (Compound 2b) groups were synthesized following the procedure described in the bibliography [29,30]. In a second step, the bromide atom was substituted by piperazinyl groups (Fig. 2) following a modified method similar to that reported by Tian et al. [19].

2.6.1. Synthesis of N-(2-hydroxyethyl)-4-bromo-1,8-naphthalimide (2a)

In a pressure-resistant microwave test tube, a mixture of 4-bromo-1,8-naphthalic anhydride (compound 1) (1.4 g, 5 mmol) and ethanol amine (0.4 g, 5 mmol) in ethanol (15 mL) was heated under argon at 85 °C and stirred at 600 rpm for 2 h. The resulting mixture was cooled at 5 °C. The solid separated was filtered and washed with cold ethanol (3 × 30 mL) and after dried was identified as N-hydroxyethyl-4-bromo-1,8-naphthalimide (compound 2a). Yield 90% (1.4 g). M. p.: 206 ± 2 °C. ^{1}H-NMR (δ_H ppm) (300 MHz, DMSO-d_6, Me_4Si): δ 8.42 (dd, J = 13.9, 7.9 Hz, 2H), 8.20 (d, J = 7.9 Hz, 1H), 8.10 (d, J = 7.8 Hz, 1H), 7.89 (t, J = 7.9 Hz, 1H), 4.81 (s, 1H), 4.10 (t, J = 6.4 Hz, 2H), 3.61 (t, J = 5.9 Hz, 2H). ^{13}C-NMR (δ_C ppm) (100.6 MHz, DMSO-d_6, Me_4Si): δ 162.90, 162.85, 132.41, 131.42, 131.24, 130.80, 129.61, 128.98, 128.67, 128.14, 122.70, 121.92, 57.71, 41.95. FT-IR (wavenumbers, cm^{-1}): ν_{OH} 3386 cm^{-1}; $\nu_{C\text{-}H}$ 3066 cm^{-1}

Table 1
Content of chlorine and naphthalimide derivative in the membranes and thermal properties determined by DSC and TGA.

Membrane	Cl Content[a] (%)	Naphthalimide Content[b] (mol·L^{-1}) x10^3	T_g[c] (°C)	T_5[d] (°C)	T_{10}[d] (°C)
M-Cl	2.8	–	46.9	214	337
M-4a	0	2.73	45.3	326	369
M-5b	0	3.27	45.4	337	371
M-6b	0	4.72	45.6	334	372

[a] Determined by TGA peak at 175 °C corresponding to Cl, EI-MS m/z 36 (M+).
[b] Determined from the membrane (180 μm of thickness) by UV spectroscopy.
[c] Measured by DSC second heating run at a heating rate of 10 °C·min^{-1}.
[d] Temperatures corresponding to 5% and 10% weight loss.

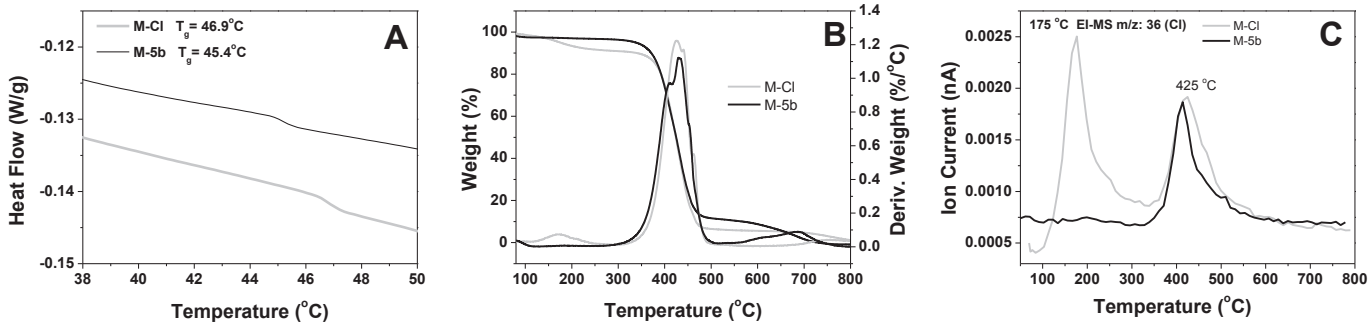

Fig. 3. DSC thermograms (A), TGA and DTGA curves (B) and evolved gas analysis by MS detector (C) of the M-Cl crosslinked membrane and M-5b membrane functionalized with naphthalimide derivative 5b.

aromatic stretch vibration $\nu_{C=O}$ 1692, 1658 cm^{-1}; $\nu_{N\text{-}C=O}$ 1611 cm^{-1}; $\nu_{C\text{-}C}$ 1585, 1568 cm^{-1} aromatic ring chain vibrations. EA: theoretical values: %C 52.52; %H 3.15; %N 4.38; experimental values: %C 52.42; %H 3.25; %N 4.25. EI-MS *m/z* calculated for $C_{14}H_{10}BrNO_3$ $(M + H)^+$ 321.0; found 321.0.

2.6.2. Synthesis of N-(2-methoxyethyl)-4-bromo-1,8-naphthalimide (2b)

Compound 2b was synthetized following the same procedure described for compound 2a from but using 2-Methoxyethylamine (0.38 g, 5 mmol) as a reactive amine. Yield 93% (1.55 g). M. p.: 163.57 ± 2 °C. ^{1}H-NMR (δ_H ppm) (300 MHz, $CDCl_3$, Me_4Si): δ 8.62 (d, J = 7.3 Hz, 1H), 8.52 (d, J = 8.4 Hz, 1H), 8.38 (d, J = 7.9 Hz, 1H), 8.00 (d, J = 7.9 Hz, 1H), 7.85–7.77 (m, 1H), 4.42 (t, J = 5.8 Hz, 2H), 3.72 (t, J = 5.8 Hz, 2H), 3.37 (s, 3H). ^{13}C-NMR (δ_C ppm) (100.6 MHz, $CDCl_3$, Me_4Si): δ 163.80, 163.78, 133.38, 132.26, 131.43, 131.18, 130.68, 130.40, 129.12, 128.16, 123.09, 122.23, 69.68, 58.92, 39.50. FT-IR (wavenumbers, cm^{-1}): $\nu_{C\text{-}H}$ 3065 cm^{-1} aromatic stretch vibration; $\nu_{O\text{-}CH3}$ 2824,2832 cm^{-1}; $\nu_{C=O}$ 1698, 1655 cm^{-1}; $\nu_{N\text{-}C=O}$ 1613 cm^{-1}; $\nu_{C\text{-}C}$ 1589, 1570 cm^{-1} aromatic ring chain vibrations. EA: theoretical values: %C 53.91; %H 3.62; % N 4.19; experimental values % C 53.82; % H 3.65; % N 4.22. EI-MS *m/z* calculated for $C_{15}H_{12}BrNO_3$ $(M + H)^+$ 335.0; found 335.0.

Synthesis of compounds 2a and 2b were also carried out in an ace round-bottom pressure flask and conventional heating during 15 h yielded 75 and 80% respectively.

2.6.3. Synthesis of N-(2-hydroxyethyl)-4-(piperazine-1-yl)-1,8-naphthalimide (3a)

In a pressure-resistant microwave test tube, compound 2a (0.20 g, 0.625 mmol) and piperazine (0.16 g, 1.875 mmol) were mixed in 2-methoxyethanol (5 mL) and heated at 130 °C in argon atmosphere under constant stirring (600 rpm) for 1 h. The mixture was poured into cooled ice/water at 5 °C and the residue was filtered and washed with hot ethanol (30 mL). The solution was filtered and the solvent removed under reduced pressure in order to obtain the yellow solid compound. M. p.: 219.23 ± 2 °C. MW-yield: 84%. RF method for compound 3a yielded a 64% after 15 h of reaction time. ^{1}H NMR (300 MHz, DMSO-d_6) δ 8.48–8.41 (m, 2H), 8.38 (d, J = 8.1 Hz, 1H), 7.79 (t, J = 7.8 Hz, 1H), 7.30 (d, J = 8.2 Hz, 1H), 4.78 (s, 1H), 4.13 (t, J = 6.4 Hz, 2H), 3.60 (s, 2H), 3.13 (s, 4H), 3.00 (s, 4H). ^{13}C NMR (75 MHz, DMSO) δ 163.65, 163.11, 156.20, 132.14, 130.48, 129.15, 125.78, 125.22, 122.59, 115.33, 114.79, 57.86, 54.10, 45.67, 41.60. FT-IR (wavenumbers, cm^{-1}): ν_{NH} 3248 cm^{-1}; $\nu_{C\text{-}H}$ 3066 cm^{-1} aromatic stretch vibration; $\nu_{C=O}$ 1685, 1642 cm^{-1}; $\nu_{N\text{-}C=O}$ 1613 cm^{-1}; $\nu_{C\text{-}C}$ 1586, 1571 cm^{-1} aromatic ring chain vibrations; ν_{NH} 1514 cm^{-1} flexion. EA: theoretical values: %C 66.45; %H 5.89; %N 12.91; experimental values: %C 66.55; %H 5.93; %N 12.96. EI-MS *m/z* calculated for $C_{18}H_{19}N_3O_3$: $(M + H)^+$ 326.1, found. 326.0 (M^+).

2.6.4. Synthesis of N-(2-hydroxyethyl)-4-(4-methylpiperazine-1-yl)-1,8-naphthalimide (4a)

The synthesis of compound 4a was similar to the preparation procedure of the compound 3a but using 1-methylpiperazine (208 μL, 1.875 mmol) as a reactive amine. The MW yield was 85% after 1 h and RF yield 67% after 15 h. Compound 4a was purified by silica gel column chromatography using dichloromethane:methanol (20:1) as an eluent to obtain a yellow solid. M. p.: 188.43 ± 2 °C. Yield: 85%. ^{1}H NMR (300 MHz, DMSO-d_6) δ 8.43 (dd, J = 11.9, 8.1 Hz, 2H), 8.37 (d, J = 8.2 Hz, 1H), 7.79 (t, J = 7.8 Hz, 1H), 7.31 (d, J = 8.1 Hz, 1H), 4.81 (t, J = 5.7 Hz, 1H), 4.12 (t, J = 6.4 Hz, 2H), 3.59 (d, J = 6.2 Hz, 2H), 3.22 (s, 4H), 2.63 (s, 4H), 2.30 (s, 3H). ^{13}C NMR (75 MHz, DMSO) δ 163.61, 163.07, 155.51, 132.04, 130.48, 130.31, 129.08, 125.87, 125.20, 122.59, 115.56, 114.93, 57.85, 54.63, 52.50, 45.74, 41.60. FT-IR (wavenumbers, cm^{-1}): ν_{OH} 3435 cm^{-1}; $\nu_{C\text{-}H}$ 3060 cm^{-1} aromatic stretch vibration; $\nu_{C=O}$ 1692, 1635 cm^{-1}; $\nu_{N\text{-}C=O}$ 1612 cm^{-1}; $\nu_{C\text{-}C}$ 1585 cm^{-1} aromatic ring chain vibrations. Elemental analysis, theoretical value %C 67.24; %H 6.24; %N 12.38; calculate %C 67.15; %H 6.15; %N 12.29. EI-MS *m/z* calculated for $C_{19}H_{21}N_3O_3$: $(M + H)^+$ 340.2, found. 340.3 (M^+).

2.6.5. Synthesis of N-(2-hydroxyethyl)-4-(4-(2-hydroxyethyl)-piperazine-1-yl)-1,8-naphthalimide (5a)

The synthesis of compound 5a was similar to the preparation procedure of the compound 3a but using 1-(2-Hydroxyethyl) piperazine (230 μL, 1.875 mmol) as a reactive amine. Compound 5a was purified by silica gel column chromatography using dichloromethane:methanol (20:1) as an eluent to obtain an yellow solid. M. p.: 178.36 ± 2 °C. The MW yield was 88% after 1 h and RF yield 68% after 15 h. ^{1}H NMR (300 MHz, DMSO-d_6) δ 8.49–8.41 (m, 2H), 8.39 (d, J = 8.1 Hz, 1H), 7.84–7.76 (m, 1H), 7.33 (d, J = 8.1 Hz, 1H), 4.81 (t, J = 5.9 Hz, 1H), 4.49 (t, J = 5.3 Hz, 1H), 4.13 (t, J = 6.5 Hz, 2H), 3.65–3.51 (m, 6H), 3.23 (s, 4H), 2.74 (s, 4H). ^{13}C NMR (75 MHz, DMSO) δ 163.94, 163.41, 155.88, 132.38, 130.82, 130.67, 129.42, 126.19, 125.51, 122.92, 115.85, 115.17, 60.57, 58.95, 58.19, 53.50, 53.00, 41.94. FT-IR (wavenumbers, cm^{-1}): ν_{OH} 3260, 3146 cm^{-1}; $\nu_{C\text{-}H}$ 3052 cm^{-1} aromatic stretch vibration; $\nu_{C=O}$ 1695, 1644 cm^{-1}; $\nu_{N\text{-}C=O}$ 1613 cm^{-1}; $\nu_{C\text{-}C}$ 1589, 1576 cm^{-1} aromatic ring chain vibrations. EA: theoretical values %C 65.03; %H 6.28; %N 11.37; experimental values: %C 65.00; %H 6.25; %N 11.31. EI-MS *m/z* calculated for $C_{20}H_{23}N_3O_4$: $(M + H)^+$ 370.17, found 370.2 (M^+).

2.6.6. Synthesis of N-(2-hydroxyethyl)-4-(4-[2-(2-hydroxyethoxy) ethyl]-piperazine-1-yl)-1,8-naphthalimide (6a)

The synthesis of compound 6a was similar to the preparation

procedure of the compound 3a but using 1-[2-(2-hydroxyethoxy) ethyl]piperazine (308 μL, 1.875 mmol) as a reactive amine. After completion of the reaction, the solvent was evaporated under reduced pressure and the crude product was then diluted in 50 mL of water. The precipitated product was then filtered off. The aqueous part was extracted with dichloromethane (3 × 30 mL) and the organic layer was dried over K_2CO_3. The solvent was evaporated under reduced pressure to obtain a yellow solid. M. p.: 170.20± 2 °C. For compound 6a the MW yield was 85% after 1 h and RF yield 70% after 24 h. ^{1}H NMR (300 MHz, DMSO-d_6) δ 8.47–8.39 (m, 2H), 8.37 (d, J = 8.1 Hz, 1H), 7.79 (t, J = 7.9 Hz, 1H), 7.31 (d, J = 8.2 Hz, 1H), 4.79 (t, J = 5.8 Hz, 1H), 4.63 (t, J = 5.0 Hz, 1H), 4.13 (t, J = 6.5 Hz, 2H), 3.62–3.54 (m, 4H), 3.54–3.48 (m, 2H), 3.45 (d, J = 4.6 Hz, 2H), 3.22 (s, 4H), 2.75 (s, 4H), 2.65–2.58 (m, 2H)· ^{13}C NMR (75 MHz, DMSO) δ 163.63, 163.09, 155.52, 132.07, 130.51, 130.35, 129.08, 125.88, 125.18, 122.58, 115.53, 114.88, 72.29, 68.31, 60.32, 57.88, 57.28, 53.15, 52.64, 41.62. FT-IR (wavenumbers, cm^{-1}): ν_{OH} 3374 cm^{-1}; $\nu_{C\text{-}H}$ 3066 cm^{-1} aromatic stretch vibration; $\nu_{C=O}$ 1690, 1650 cm^{-1}; $\nu_{N\text{-}C=O}$ 1616 cm^{-1}; $\nu_{C\text{-}C}$ 1588 cm^{-1} aromatic ring chain vibrations. EA: theoretical values %C 63.91; %H 6.58; %N 10.16; experimental values: %C 63.97; %H 6.62; %N 9.60. EI-MS m/z calculated for $C_{22}H_{27}N_3O_5$: $(M + H)^+$ 414.20, found 414.2 (M^+).

2.6.7. Synthesis of N-(2-methoxyethyl)-4-(piperazine-1-yl)-1,8-naphthalimide (3b)

Compound 2b (0.20 g, 0.598 mmol) and piperazine (0.155 g, 1.794 mmol) were mixed in 2-methoxyethanol (5 mL) and heated under MW radiation at 130 °C in an argon atmosphere under constant stirring (600 rpm) for 1 h. After completion of the reaction, the solvent was evaporated under reduced pressure and the crude was washed with water and filtered to obtain the compound as a yellow solid. M. p.: 145.60 ± 2° The MW yield was 84% after 1 h and by conventional heating, RF yield 69% after 15 h. ^{1}H NMR (300 MHz, DMSO-d_6) δ 8.48–8.41 (m, 2H), 8.40 (s, 1H), 7.83–7.75 (m, 1H), 7.30 (d, J = 8.1 Hz, 1H), 4.23 (t, J = 6.1 Hz, 2H), 3.57 (t, J = 6.1 Hz, 2H), 3.26 (s, 3H), 3.15 (s, 4H), 3.00 (s, 4H). ^{13}C NMR (75 MHz, DMSO) δ 163.50, 162.94, 156.29, 132.25, 130.58, 129.09, 125.75, 125.17, 122.33, 115.00, 114.77, 68.67, 57.94, 54.08, 45.66, 38.33. FT-IR (wavenumbers, cm^{-1}): ν_{NH} 3248 cm^{-1}; $\nu_{C\text{-}H}$ 3069 cm^{-1} aromatic stretch vibration; $\nu_{O\text{-}CH3}$ 2828, 2808 cm^{-1} $\nu_{C=O}$ 1690, 1650 cm^{-1}; $\nu_{N\text{-}C=O}$ 1613 cm^{-1}; $\nu_{C\text{-}C}$ 1588, 1572 cm^{-1} aromatic ring chain vibrations; ν_{NH} 1514 cm^{-1} flexion. EA: theoretical values %C 67.24; %H 6.24; %N 12.38; experimental values: %C 67.20; %H 6.18; %N 12.31. EI-MS m/z calculated for $C_{19}H_{21}N_3O_3$: $(M + H)^+$ 340.1, found. 340.0 (M^+).

2.6.8. Synthesis of N-(2-methoxyethyl)-4-(4-methylpiperazine-1-yl)-1,8-naphthalimide (4b)

Compound 4b was synthetized by mixing compound 2b (0.2 g, 0.598 mmol), 1-methylpiperazine (200 μL, 1.7964 mmol) in 5 mL of 2-methoxyethanol and following the same procedure as for compound 3b. M. p.: 139.44 ± 2 °C. The MW yield was 83% after 1 h and by conventional heating, RF yield 73% after 15 h. ^{1}H NMR (300 MHz, DMSO-d_6) δ 8.42 (dd, J = 12.3, 8.0 Hz, 2H), 8.36 (d, J = 8.1 Hz, 1H), 7.83–7.73 (m, 1H), 7.31 (d, J = 8.2 Hz, 1H), 4.22 (t, J = 6.1 Hz, 2H), 3.57 (t, J = 6.1 Hz, 2H), 3.25 (s, 3H), 3.22 (s, 4H), 2.63 (s, 4H), 2.30 (s, 3H). ^{13}C NMR (75 MHz, DMSO) δ 163.51, 162.97, 155.66, 132.21, 130.64, 130.51, 129.08, 125.93, 125.21, 122.40, 115.29, 114.99, 68.67, 57.94, 52.49, 45.73, 38.36. FT-IR (wavenumbers, cm^{-1}): $\nu_{C\text{-}H}$ 3067 cm^{-1} aromatic stretch vibration; $\nu_{C=O}$ 1695, 1650 cm^{-1}; $\nu_{N\text{-}C=O}$ 1613 cm^{-1}; $\nu_{C\text{-}C}$ 1586, 1574 cm^{-1} aromatic ring chain vibrations. EA: theoretical values %C 67.97; %H 6.56; %N 11.89; experimental values %C 67.87; %H 6.56; %N 11.80. EI-MS m/z calculated for $C_{20}H_{23}N_3O_3$: $(M + H)^+$ 354.17, found 354.2 (M^+).

2.6.9. Synthesis of N-(2-methoxyethyl)-4-(4-(2-hydroxyethyl)-piperazine-1-yl)-1,8-naphthalimide (5b)

The synthesis of compound 5b was similar the preparation procedure of the compound 3b but using 1-(2-Hydroxyethyl) piperazine (220 μL, 1.796 mmol) as a reactive amine. Compound 5b was purified by silica gel column chromatography using dichloromethane:methanol (20:1) as an eluent to obtain an yellow solid. M. p.: 124.17 ± 2 °C. Yield: 84%.^{1}H NMR (300 MHz, Chloroform-d) δ 8.57 (d, J = 7.2 Hz, 1H), 8.50 (d, J = 8.0 Hz, 1H), 8.39 (d, J = 8.4 Hz, 1H), 7.67 (t, J = 7.8 Hz, 1H), 7.20 (d, J = 8.0 Hz, 1H), 4.41 (t, J = 5.6 Hz, 2H), 3.71 (t, J = 5.3 Hz, 4H), 3.36 (s, 3H), 3.30 (s, 4H), 2.84 (s, 4H), 2.75–2.65 (m, 2H). ^{13}C NMR (75 MHz, $CDCl_3$) δ 164.94, 164.45, 156.25, 133.07, 131.63, 130.66, 130.32, 126.53, 126.05, 123.55, 117.09, 115.33, 70.09, 59.83, 59.18, 58.31, 53.48, 53.41, 39.49. FT-IR (wavenumbers, cm^{-1}): ν_{OH} 3140 cm^{-1}; $\nu_{C\text{-}H}$ 3052 cm^{-1} aromatic stretch vibration; $\nu_{C=O}$ 1696, 1645 cm^{-1}; $\nu_{N\text{-}C=O}$ 1613 cm^{-1}; $\nu_{C\text{-}C}$ 1589, 1576 cm^{-1} aromatic ring chain vibrations. Elemental analysis, theoretical value %C 65.78; %H 6.57; %N 10.96; calculate %C 65.87; % H 6.68; %N 11.04. EI-MS: m/z calculated for $C_{21}H_{25}N_3O_4$ $(M + H)^+$ 384.18; found 384.2 (M^+).

2.6.10. Synthesis of N-(2-methoxyethyl)-4-(4-[2-(2-Hydroxyethoxy)ethyl]-piperazine-1-yl)-1,8-naphthalimide (6b)

Compound 2b (0.2 g, 0.5988 mmol), 2-[2-(1-Piperazinyl)ethoxy] ethanol (295 μL, 1.7964 mmol) was mixed in 5 mL of 2-methoxyethanol and heated at 130 °C in argon atmosphere. The mixture was stirred at 600 rpm for 1 h. After completion of the reaction, the solvent was evaporated under reduced pressure and the crude product was then diluted in 50 mL of water. The precipitated product was then filtered off. The aqueous part was extracted with dichloromethane (3 × 30 mL) and the organic layer was dried over K_2CO_3. The solvent was evaporated under reduced pressure to obtain a yellow solid. M. p.: 219.73 ± 2 °C. The MW yield was 85% after 1 h and by conventional heating, RF yield 69% after 24 h ^{1}H NMR (300 MHz, DMSO-d_6) δ 8.43 (dd, J = 11.0, 8.0 Hz, 2H), 8.37 (d, J = 8.1 Hz, 1H), 7.82–7.75 (m, 1H), 7.31 (d, J = 8.2 Hz, 1H), 4.64 (s, 1H), 4.22 (t, J = 6.1 Hz, 2H), 3.58 (q, J = 6.0 Hz, 4H), 3.53–3.48 (m, 2H), 3.45 (d, J = 4.7 Hz, 2H), 3.25 (s, 3H), 3.22 (s, 4H), 2.75 (s, 4H), 2.62 (t, J = 5.8 Hz, 2H)· ^{13}C NMR (75 MHz, DMSO) δ 163.54, 162.99, 155.68, 132.24, 130.67, 130.55, 129.08, 125.94, 125.20, 122.39, 115.27, 114.94, 72.28, 68.70, 68.31, 60.30, 57.97, 57.26, 53.13, 52.64, 38.39. FT-IR (wavenumbers, cm^{-1}): $\nu_{O\text{-}H}$ 3356 cm^{-1}; $\nu_{C\text{-}H}$ 3065 cm^{-1} aromatic stretch vibration; $\nu_{C=O}$ 1687, 1648 cm^{-1}; $\nu_{N\text{-}C=O}$ 1613 cm^{-1}; $\nu_{C\text{-}C}$ 1585 cm^{-1} aromatic ring chain vibrations. EA: theoretical value %C 64.62; %H 6.84; %N 9.83; experimental values %C 64.60; %H 6.93; %N 9.76. EI-MS: m/z calculated for $C_{23}H_{29}N_3O_5$ $(M + H)^+$ 428.2; found 428.3 (M^+).

2.7. pH measurements

Measurements of pH were obtained with a Mettler Toledo SevenGo Duo Pro meter with an InLab Expert Pro ISM-ID67 electrode at room temperature (23 °C) and previously calibrated with standard buffers. The sensing measurements determined from the solutions of naphthalimide derivatives and functionalized membranes were performed using HCl and NaOH solutions for pH variation in the mixture water:ethanol (4:1) as solvent.

The acid titration by UV/Vis and fluorescence in aqueous solution was performed as follows. The titration in solution with naphthalimide derivatives (water:ethanol 4:1, naphthalimide concentration 10^{-4} M and pH = 12.0 fixed by addition of NaOH solution) was carried out by increasing the acidity from pH 12.0 to pH 2.0 by adding aliquots of the diluted hydrochloric acid. After each addition, the pH was measured after the solutions were allowed to equilibrate for 10 min and the UV/Vis and fluorescence spectra

were recorded.

In the case of functionalized crosslinked membranes, films were cut into strips of 1 × 4 cm and fixed in a homemade support that can also be slotted into the cell holder of the spectrophotometers. To study the effect of the pH in the spectroscopic properties of the membranes, film strips were immersed in previously prepared vials (50 mL) containing solutions from pH 12.0 to pH 2.0. The UV/Vis and fluorescence spectra for each pH were taken after 20 min of conditioning time.

3. Results and discussion

3.1. Synthesis of naphthalimide derivatives

The synthesis route [3,4] to obtain N-hydroxy alkyl piperazine naphthalimides is presented in Fig. 2. In the first step, the condensation of 4-bromo-1,8-naphthalic anhydride with 2-hydroxyethylamine (series a) or 2-methoxyethylamine (series b) under microwave irradiation in ethanol at 85 °C afforded 2a and 2b respectively in high yield at a shorter reaction time than conventional conditions.

In the second reaction step (Fig. 2), compounds 2a and 2b reacted with 3 equiv. of each piperazine derivative as detailed in the experimental description (section 2.6.) to obtain the piperazine-naphthalimides derivatives shown in Fig. 2. Hence, we have prepared piperazine substituted derivatives with hydrogen and methyl groups [19] as substituents on the amine groups (structures 3 and 4 respectively), but also with bigger substituents (structures 5 and 6) in order to study comparatively their PET processes and their protonation in acid media.

The best synthesis conditions were noted under MW irradiation for 1 h at 850W and a ceiling temperature of 130 °C in 2-methoxyethanol. In contrast, the best conditions for the synthesis carried out under reflux by conventional heating required reaction times of 15 h and 24 h for compounds 6a and 6b when 2-[2-(1-Piperazinyl)ethoxy]ethanol was used as reactive amine.

In all the cases, MW irradiation allowed higher yields at shorter reaction times than the conventional RF method. These results are in agreement with those reported in the literature [19,24].

3.2. Membrane preparation, functionalization with piperazine naphthalimides sensors and characterization

The membrane prepared containing acid chloride functionalities (M-Cl) as a base material for further functionalization was obtained by bulk photopolymerization of a mixture of monomers combining the hydrophilic character of VP (55%) with the hydrophobic nature of BA (35%) and adding MACl (10%) as the reactive monomer for functionalization. A 5% of EGDMMA as the crosslinking agent of the mixture controlled the crosslinking degree of the final membrane. This produced a reversible water-swollen membrane (Fig. 1). After the bulk photopolymerization, all the experiments reached >98% of conversion (determined by weight differences), and the resulting crosslinked acrylic membrane contained 2.8% of chlorine in the structure (Fig. 3B).

In a second step, the M-Cl membrane was functionalized with the three naphthalimide derivatives from the series synthetized in this work (Fig. 1) that contained mono hydroxy alkyl piperazine, derivatives 4a, 5b and 6b. This functionalization was accomplished successfully by conventional heating in THF at 55 °C for 15 h under very low stirring speed. This selected reaction temperature is 10 °C below the THF boiling point to be sure there isn't any damage of the membrane in the heterogeneous reaction, such as breaks, wrinkles and warps that could decrease the optical quality of the membrane. Under these experimental conditions, the Schotten-Baumann reaction used to graft the naphthalimide derivatives to the M-Cl membrane proceeded very slowly. This allowed a good control in homogeneity of functionalization without physically damaging the membrane. The unreacted acid chloride group disappeared after hydrolysis when the membranes were washed as shown in Fig. 3C. The amount of naphthalimide grafted to the membranes (Table 1) was determined from the UV-Vis absorbance using the absorption coefficient of each derivative (Table 3) previously calculated in water-ethanol (4:1, v/v).

After 15 h of reaction time the content of the naphthalimide derivative in the membrane was very low (Table 1) but the concentration is adequate for sensing applications by UV-vis and fluorescence spectroscopies.

The good physical characteristics of the functionalized membranes are similar than those observed by other authors [25] with copolymers of VP/BA. All DSC thermograms of the membranes revealed the presence of a single glass transition temperature for all the membranes confirming copolymer miscibility. The characteristic T_g values for the membranes are shown in Table 1 and the DSC thermograms (second scan) obtained for M-Cl and M-5b samples are plotted in Fig. 3A. The observed step for M-Cl appeared at a similar temperature (46.9 °C) than the corresponding steps for the functionalized membranes (Table 1) due to the low content of C-Cl dipoles present in the M-Cl membrane.

The thermal stability of the membranes was evaluated using TGA and Table 1 shows the thermal data, in terms of characteristic weight loss (T_5 and T_{10} respectively).

Fig. 3B shows the TGA thermograms obtained for the M-Cl and M-5b membranes and their corresponding first derivative curves. The M-Cl membrane exhibits a weight loss of 2.8% that was identified by MS analysis of evolved gas at 175 °C as chlorine (EI-MS *m/z*: 36 (Cl)), as it is shown in Fig. 3C. After functionalization, the chlorine weight was not observed confirming the total hydrolysis of unreacted acid chloride. For all functionalized membranes two peaks were observed, as it is shown for M-5b in Fig. 3B. The highest weight loss rate that was observed at 410 °C corresponds to the degradation of acrylic components of the membrane and the second one observed at 431 °C has been attributed [7] to the lactam subgroup degradation.

The swelling properties of the membranes were examined by measuring the swelling (%) after immersion in water and THF and are detailed in Table 2.

The SD in water (approx. 30%) and in THF (approx. 60%) confirms the hydrophilic character of the membranes and the adequate swelling for solid sensors in water and organic media. Also, the hydrophilicity of the membrane surfaces was characterized by static contact angle determination. The measured CAs were then used to calculate the polar, disperse, and total surface energies of the membranes. The change in the total surface energy (γ) and its polar (γ^p) and dispersive (γ^d) components of the M-Cl and functionalized membranes with naphthalimides (M-4a, M-5b and M-

Table 2
Swelling degree (SD) in water and THF, advancing contact angle (CA) and total (γ), polar (γ^p), and disperse (γ^d) surface energy data for the crosslinked membranes.

Membrane	SD (%)[a]		Static CA (°)		Surface Energy (mN.m-1)[b]		
	Water	THF	Water	Diiodomethane	γ	γ^p	γd
M-Cl	29.8	45.4	59.9	41.6	51.64	13.48	38.16
M-4a	29.9	61.2	69.6	42	45.43	9.25	36.18
M-5b	30.4	62.0	71.7	38.6	45.75	6.56	39.19
M-6b	29.9	63.5	71	46.1	46.22	6.88	39.34

[a] ±0.3.
[b] Calculated using Owens-Wendt's method.

Table 3
Various parameters for piperazine-1,8-naphthalimide derivatives (a and b structures) in solution[a] and bonded to the polymer membrane (M) determined according to pH dependence by UV–Vis absorption and fluorescence spectroscopy.

Parameter	3a	4a	5a	6a	3b	4b	5b	6b	M-4a	M-5b	M-6b
$\lambda_{ABS\text{-}acid}$	389	388	388	388	389	389	389	388	388	388	390
Log ε_{acid}[b]	4.07	4.06	4.05	4.06	4.06	4.06	4.056	4.06	–	–	–
$\lambda_{Isobestic}$	403	402	402	402	404	402	402	402	403	402	402
$\lambda_{ABS\text{-}base}$	413	408	408	408	410	409	409	409	407	408	408
Log ε_{base}[b]	4.04	4.02	4.01	4.02	4.01	4.02	4.02	4.02	–	–	–
pK_a[c]	8.24	7.37	6.99	6.65	8.62	7.30	6.82	6.71	7.62	7.25	6.40
$\lambda_{FLU\text{-}acid}$	533	529	530	530	531	529	530	529	502	503	503
$\phi_{FLU\text{-}acid}$[d]	0.097	0.330	0.184	0.238	0.084	0.274	0.170	0.197	–	–	–
$\phi_{FLU\ H=7}$[d]	0.093	0.304	0.101	0.099	0.079	0.249	0.095	0.091	–	–	–
$\phi_{FLU\ ethanol}$[d]	0.017	0.025	0.022	0.026	0.026	0.020	0.017	0.024	water:ethanol (4:1, v/v)		
$\phi_{FLU\ hexane}$[d]	0.203	0.389	0.285	0.293	0.213	0.365	0.270	0.275	<< Ethanol <<< hexane		
$\lambda_{FLU\text{-}base}$	543	548	550	550	532	532	554	545	505	506	504
$\phi_{FLU\text{-}base}$[d]	0.010	0.013	0.010	0.009	0.005	0.010	0.009	0.007	–	–	–
pK_a^*[c]	7.1	6.93	6.95	6.4	7.15	7.11	7.04	6.48	7.15	6.71	6.5
$\Delta\nu$[e]	6329	6258	6070	6061	6293	6123	6070	5998	5515	5618	5539
FE[f]	8.5	25.3	19.1	22.0	18.1	17.9	22.0	27.1	12.3	8.0	9.5

[a] Measured at 10^{-4} M in water-ethanol (4:1, v/v) unless specifically stated otherwise. The subscripts "acid" and "base" refer to the limiting value of a given parameter when the acid or base condition is increased until pH = 2.0 or pH = 12.0 respectively. Fluorescence emission spectra were obtained by excitation at $\lambda_{Isobestic}$.
[b] ε, molar absorptivity in $M^{-1}cm^{-1}$.
[c] Obtained [31] by analyzing the pH dependence of the absorbance (A) or emission intensity (I) at a given wavelength according to the equation log $[(A_{acid} - A)/(A - A_{base})] = pH - pK_a$ or log $[(I_{FLU\text{-}acid}-I)/(I-I_{FLU\text{-}base})] = pH\text{-}pK_a^*$.
[d] Relatively to coumarin 6 ($\phi_F = 0.78$ in ethanol), uncertainty = 0.001 or 10%, whichever is the larger.
[e] Stokes shift (ν_{FLU}-ν_{ABS}) in frequency (cm^{-1}).
[f] Acid-induced fluorescence enhancement factor FE = $A_{FLU\text{-}acid}/A_{FLU\text{-}.base}$.

6b) was calculated by the Owens–Wendt's method [28] (Table 2). The variation in the values of the total, polar, and disperse solid surface energies before (M-Cl) and after functionalization (M-4a, M-5b and M-6b), shows that the total surface energy of the functionalized membranes decreases from 51.64 mN m^{-1} for M-Cl to 45–46 mN m^{-1} for the membranes containing naphthalimide moieties and, particularly for the polar component.

The functionalized membranes with piperazine-naphthalimide groups were easily handled materials and exhibited convenient properties for solid sensor applications, such as swelling in water, thermal stability, flexibility, optical transparency and dimensional stability to be reused. The obtained three-dimensional cross-linked hydrophilic polymer networks are capable of swelling or deswelling reversibly in water and retaining a controlled and reproducible volume of liquid in the swollen state. This behaviour, as will be seen in the next section, allowed controllable responses to external environmental changes of pH.

3.3. Effect of pH on the absorption and fluorescence properties of piperazine naphthalimides derivatives and membranes

Piperazine substituted naphthalimides such as the structures synthetized in this work (Fig. 2) exhibit interesting fluorescence properties, hence 4-amino-1,8-naphthalimide fluorophore can be quenched by the PET process that occurs from the alkylated amine donor to the 4-amino-1,8-naphthalimide fluorophore through the piperazinyl ring. The fluorescence of the 4-amino-1,8-naphthalimide fluorophore is quenched. The PET path can be switched off either by the protonation or quaternization of the amine and the fluorescence of the naphthalimide fluorophore is then recovered as is shown for the derivative 4a anchored to the membranes in Fig. 4.

The effect of pH variation on the absorbance and fluorescence properties of these derivatives is illustrated in Fig. 5 for the naphthalimide derivative 4a in solution and the corresponding membrane M-4a under the same conditions.

All the absorption spectra of the naphthalimide derivatives and membranes exhibit (as solution or as 180 μm-membrane) similar band shapes in the absorption range of 350–500 nm. As it is shown in Fig. 5, for the compound 4a and membrane M-4a, their absorption peaks were red-shifted from 388 to 408 nm with a clear isosbestic point at 402 nm when pH values were changed from 2.0 to 12.0 in water:ethanol (4:1) by adjusting pH values with NaOH and HCl aqueous solutions. As expected, the fluorescence intensities originating from 4a and M-4a fluorophores were varied upon different pH values (Fig. 5), resulting in a strong enhancement in acid media due to the protonation of the piperazine and its subsequent PET blocking effect (Fig. 4). In the case of compound 4a the factor of enhancement (FE) was about 25 times in fluorescence intensity when adjusting the pH from 12.0 to 2.0 (Table 3). Moreover, the wavelength emission maxima were red-shifted by around 20 nm (Table 3) by changing the pH values from 2.0 to 12.0 for all the naphthalimide derivatives in solution except for naphthalimide 3b and 4b that do not have hydroxyl substituents in their structures and the red-shift for them was about 2–3 nm. For the naphthalimide fluorophores bonded to the membranes though the hydroxyl groups, the bathochromic shift of the fluorescence maxima with pH was also 2–3 nm.

All the spectral data measured as a function of pH values for the naphthalimide derivatives and the three functionalized membranes are summarized in Table 3.

The quantum yields of fluorescence in acid media (Table 3) for the hydroxy alkyl substituted piperazine naphthalimides derivatives ($\phi_{FLU\text{-}acid}$ = 0.33–0.084) are lower than that of the non-hydroxylated derivative N-butyl-4-N′-methylpiperazino-1,8-naphthalimide ($\phi_{FLU\text{-}acid}$ = 0.55) [22]. Also, the quantum yields of fluorescence in basic media (Table 3) are higher ($\phi_{FLU\text{-}base}$ = 0.005–0.010) than that measured for N-butyl-4-N′-methylpiperazino-1,8-naphthalimide ($\phi_{FLU\text{-}base}$ = 0.001) [22]. The quantum yield of fluorescence for the membranes couldn't be calculated due to the difference in geometry between the fluorescence standard in solution and the membranes. The factor of fluorescence enhancement for the membranes in acid media was calculated (Table 3) by comparing the increase of intensities from basic to acid media and the enhancement was around 8–12 times. This enhancement in acid media (FE = 8–12.3) is higher than that

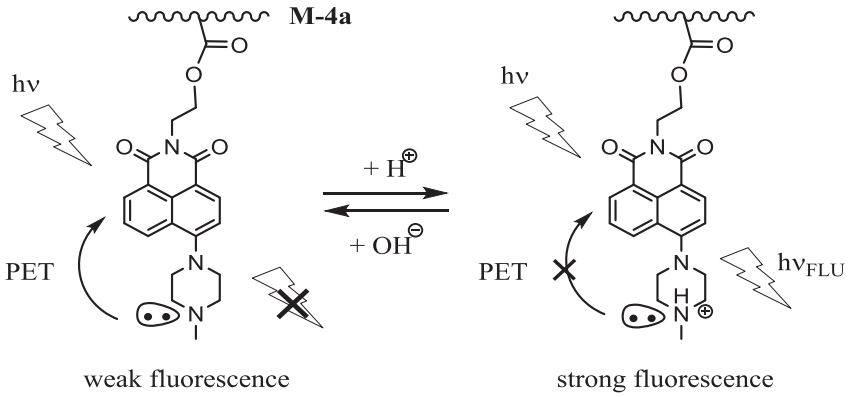

Fig. 4. Fluorescence response of piperazine-naphthalimide structure to pH though PET mechanism.

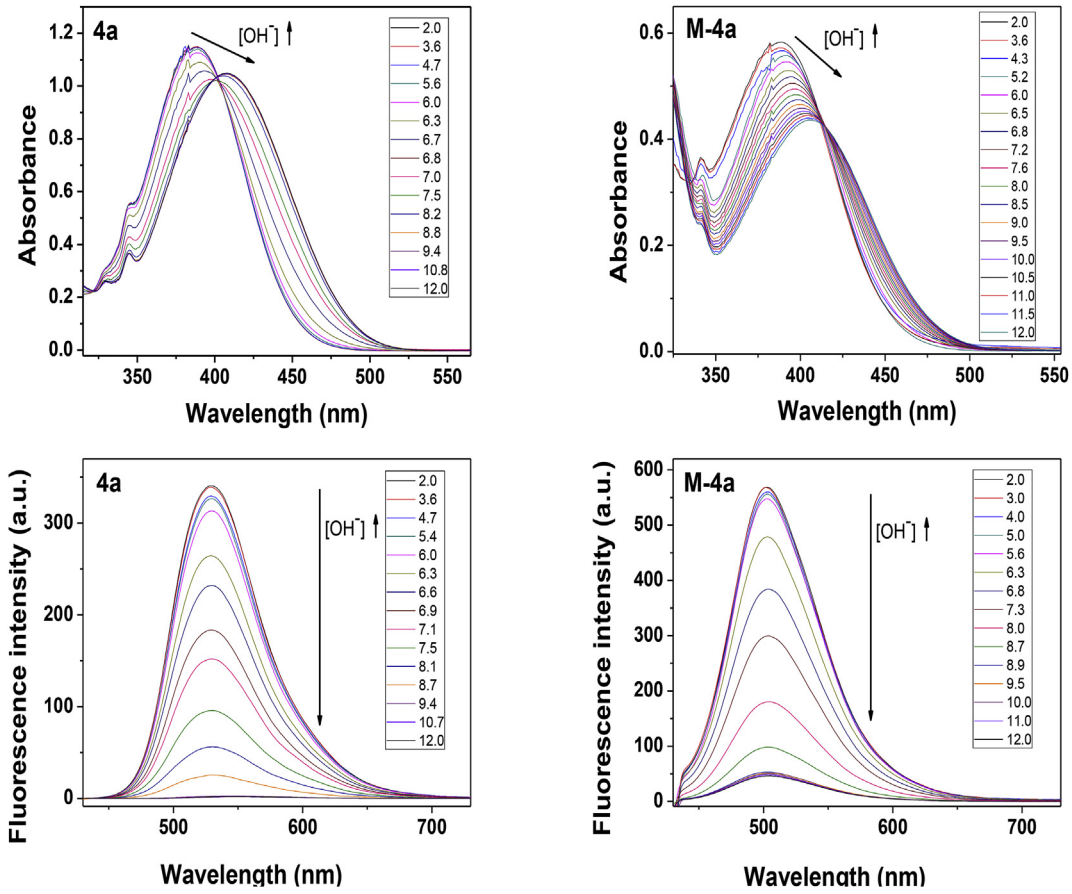

Fig. 5. Spectroscopic characteristics as a function of pH (2.0–12.0) of absorption and fluorescence of naphthalimide derivative 4a and M-4a membrane.

obtained by other authors [23], where an enhancement of 4.7 was reported with a membrane obtained by copolymerization of *N*-allyl-4-(4′-methyl-piperazinyl)-1,8-naphthalimide with 2-hydroxyethyl methacrylate and acrylamide.

The presence of hydroxyl groups in the naphthalimide derivatives studied here and the ester functionality as a linking group of the naphthalimides in the membranes reduced the factor of enhancement of fluorescence in acid media with respect to that for other similar structures having only N-alkyl substituents [21,22]. Even though FE values obtained with the membranes confirm their interesting proton "off–on" switch behaviour as an optical pH solid sensor.

The pK_a values of naphthalimide derivatives and the functionalized membranes were calculated [31] from the curves of absorption changes in the presence of increasing acidity (from pH = 12.0 to 2.0) and the obtained values are compiled in Table 3.

The smaller substituents on the amine groups (structures 3 with hydrogen or 4 with methyl as substituents) enabled a higher pK_a as they are more easily protonated than the bigger substituents (structures 5 and 6). The pK_a values obtained for the functionalized membranes are close to those values measured for the corresponding piperazine derivatives (Table 3) confirming a similar sensitivity to acid media. The pK_a of the functionalized membranes is close to the pH of 7.0 which makes it adequate for sensors in

biological and environmental applications [19].

The fluorescence response of the piperazine derivatives and the functionalized membranes at different pH was compared and the results are plotted in Fig. 6.

All the synthesized naphthalimides (Fig. 6A) exhibited a sensitive fluorescence change towards pH but with different intervals and slopes of changes depending of the size of the amino substituents. For the functionalized membranes (Fig. 6B) the fluorescence intensity increased as the pH values decreased from 9.0 to 5.0 for M-4a and from 8.5 to 4.0 for the membranes obtained by linking the naphthalimides to the substituent of the piperazine structure, M-5b and M-6b. In the acidic pH range, especially for pH lower than 4.0, the fluorescence intensity attained its maximum and kept unchanged as well as in the basic pH range up to 9.0 where the fluorescence intensity reached its minimum. The pK_a^* values (Table 3) for the excited state do not differ strongly from the corresponding pK_a for the ground state except for the structures 3a and 3b where the substituent of the piperazine is a hydrogen. For the rest of the structures and membranes the position of the inflection points in the fluorometric titration is similar to those obtained from the absorbance changes with pH.

The fluorescence quantum yields of the naphthalimides derivatives studied here are relatively low in polar solvents (water, ethanol) in comparison to those values obtained in non-polar solvents such us hexane (Table 3). This fact is probably due to the photo-induced electron transfer from the piperazine to the fluorophore and the fact that in polar solvents the orbit energy of HOMO becomes lower facilitating the PET process. The polarity effect on the photophysical properties of the naphthalimide derivatives was studied by measuring their absorption and fluorescence spectra in solvents of increasing solvent polarity parameter E_T (30). All the naphthalimide derivatives exhibited similar solvathochromic UV-Vis and emission spectra. As an illustrative example in Fig. 7, the values of absorption and emission maxima are plotted for different solvents.

The maximum wavelengths of the absorption and fluorescence emissions are slightly red shifted with increasing solvent polarity except for the H-bonding solvents in the case of naphthalimide 5b. This is due to the presence of hydroxyl groups in the structure that provoke specific solute-solvent interaction. In general, the absorption maxima are less sensitive to the influence of solvent polarity than the fluorescence maximum. In the membranes, as shown in Fig. 6 for M-5b, the low bathochromic shifts in the fluorescence maximum with an increase of solvent polarity are consistent with small differences between the dipole moments of the ground and excited states.

3.4. Response time to pH of the functionalized membranes

The reversibility of the pH induced fluorescence signal was evaluated by determining the absorbance and fluorescence of the membranes by alterning their immersion in solutions of pH 2.0 and pH 12.0. Several cycles of successfull enhancement/quenching of fluorescence were carried out with each membrane without loss of fluorescent emission. The protonation of the aliphatic amine group involved seems quite reversible and no noticeable hysteresis effect was observed in the solid sensors.

The pH response of the membranes is dependent upon the proton permeability into the photocrosslinked material. Hence, the response time of the absorption and fluorescence spectra of the functionalized membranes was studied and the obtained results are plotted in Fig. 8.

The pH response of the membranes is dependent upon the proton permeability into the crosslinked matrix and the three membranes exhibited a high sensitivity to pH in water. The absorbance and fluorescence of the membranes to acidic media (Fig. 8A and D respectively) reached the equilibrium in less than 15 min. The sensitivity to the basic medium of the membranes (Fig. 8B and E) is lower than that observed in acid media showing a slow response of around 20 min. Hence, the protonation process of the aliphatic piperazine group involved seems to be slower than the deprotonation process.

The time response of the membrane M-4a is shorter that those of the membrane b type. In the membrane M-4a the naphthalimide sensing functionality is linked to the polymer matrix through the imide group and the piperazine group is far from the polymer main chain. Hence, the interaction of the amino group of the piperazine with a proton is much easier than those of M-5b and M-6b where the piperazine is closer to the polymer main chain that can impair the mobility and hence the interactions of the sensing moiety.

The sensitivity of the solid sensor is directly related to the thickness of the pH sensitive membrane. To see the influence of the membrane thickness in the time response to the pH of the sensor, we prepared a membrane under the same experimental conditions but with 90 μm of thickness that was also an easily handled material and with good physical properties. As expected, the time response of this M-6b 90 μm-membrane (Fig. 8C and F) was notably shorter than that of the corresponding M-6b 180 μm-membrane.

In this study, we have described a useful procedure to obtain a water-swollen photocrosslinked membrane containing acid chloride groups capable of reacting with sensing molecules containing adequate functionalities, such as hydroxyl groups. The functionalization of M-Cl membrane was carried out using three derivatives

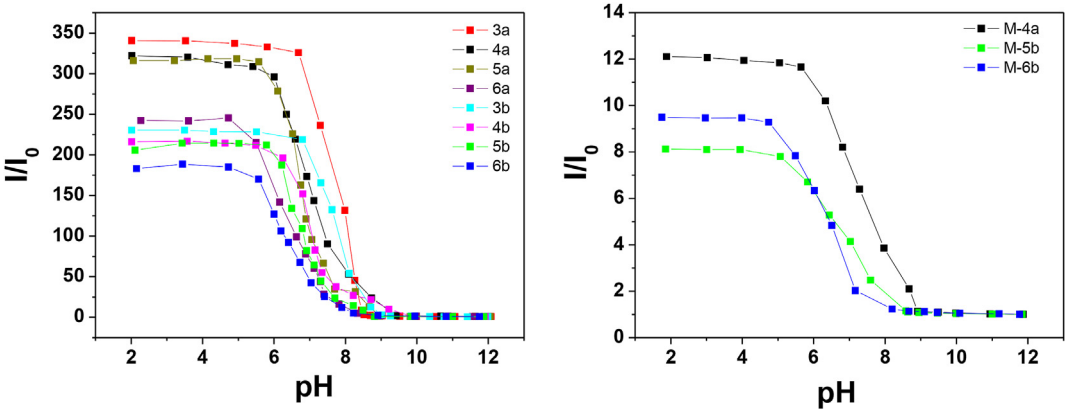

Fig. 6. Comparison of the fluorescence intensity changes (I/I_o) with pH (2.0–12.0) for the piperazine-naphthalimide derivatives in solution (A) and for functionalized membranes (B). (I_0 and I are the fluorescence intensities of initial (pH = 12.0) and that after acidification respectively).

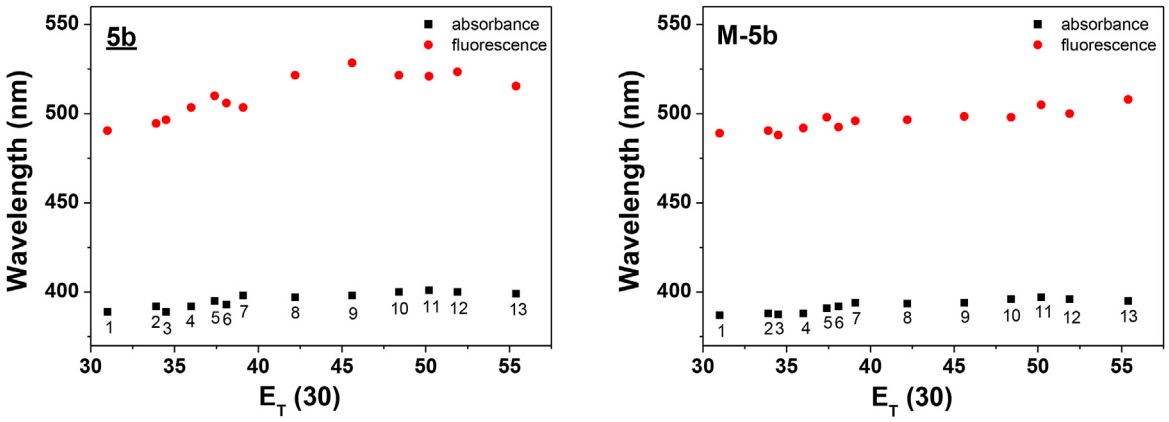

Fig. 7. Dependence of absorbance and Fluorescence emission wavelengths maxima of naphthalimide derivative 5b and the membrane M-5b on the empirical solvent polarity parameter, E_T (30). Solvents: 1. Hexane, 2. Toluene, 3. Diethyl ether, 4. Dioxane, 5. THF, 6. Ethyl acetate, 7. Chloroform, 8. Acetone, 9. Acetonitrile, 10.2-propanol, 11. Butanol, 12. Ethanol, 13. Methanol.

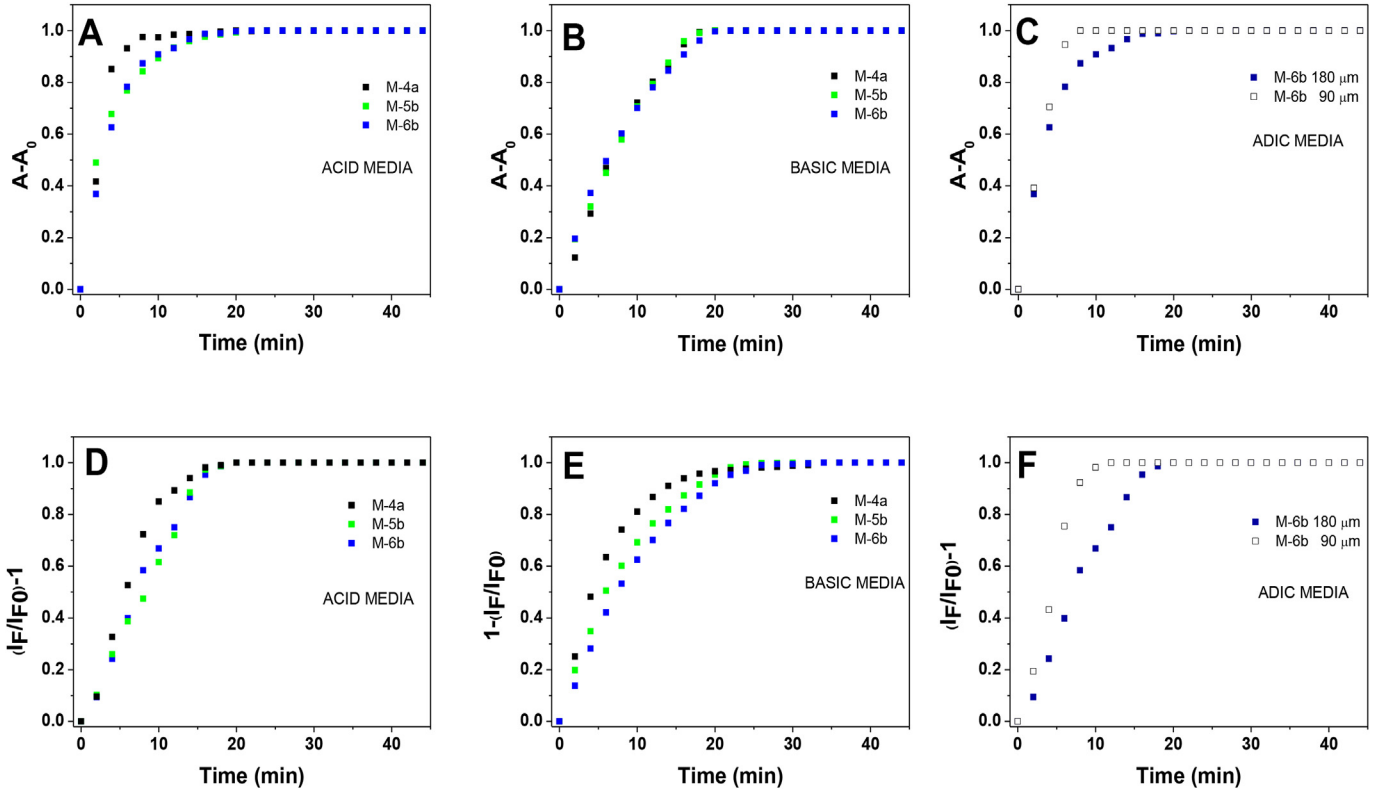

Fig. 8. Time response to pH of the functionalized membranes: Absorbance (A) and fluorescence (D) to acid media (pH = 2.0), absorbance (B) and fluorescence (E) to basic media (pH = 12.0) and effect of the membrane thickness in time response to acid media in absorbance (C) and fluorescence (F).

of piperazine naphthalimide selected from a series of compounds that had been previously synthetized and spectrophotometrically characterized as a function of pH variations. The dependence of the pH sensitivity was related to the size and structure of the piperazine-naphthalimide substituents linked to the membrane. The solid sensors functionalized with naphthalimides acted as an acid sensor with interesting ranges of sensitivity to pH changes, from 9.0 to 4.0, which are adequate for medical and environmental sensing applications.

4. Conclusions

In summary, we have developed a procedure to obtain, using a photopolymerization reaction, water-swollen membranes capable of functionalization with naphthalimide fluorescence sensors and with a pH response.

The obtained results in the synthesis of the series of substituted piperazine naphthalimide derivatives carried out in this work suggested that microwave-assisted syntheses led to higher yields within very short reaction times in comparison to the conventional methods.

The new solid sensors exhibited controlled swelling in water (30%) and sensitive fluorescence changes towards pH between 9.0 and 4.0, and showed a very strong fluorescence at pH < 5.0.

The time response of the functionalized membranes to pH is dependent on the thickness of the membrane, the size of the

substituents and the naphthalimide position of linkage to the membrane. The pH induced fluorescence signal of the solid sensors is reversible and several cycles of enhancement/quenching of fluorescence were successfully carried out without a noticeable hysteresis effect.

The present functionalized membranes could be applied as "Off-On" pH-fluorescence sensor in medical and environmental applications with satisfactory results.

Acknowledgments

This study was supported by MINECO (Project Ref. MAT2012-31709). S. Fernández-Alonso thanks MINECO for a pre-doctoral fellowship linked to the project.

References

[1] C. McDonagh, C.S. Burke, B.D. MacCraith, Optical chemical sensors, Chem. Rev. 108 (2008) 400–422.
[2] H.H. Qazi, A.B.B. Mohammad, M. Akram, Recent progress in optical chemical sensors, Sensors 12 (2012) 16522–16556.
[3] S.M. Borisov, O.S. Wolfbeis, Optical biosensors, Chem. Rev. 108 (2008) 423–461.
[4] A.S. Jeevarajan, S. Vani, T.D. Taylor, M.M. Anderson, Continuous pH monitoring in a perfused bioreactor system using an optical pH sensor, Biotechnol. Bioeng. 78 (2002) 467–472.
[5] I. Grabchev, P. Bosch, M. McKenna, A. Nedelcheva, Synthesis and spectral properties of new green fluorescent poly(propyleneimine) dendrimers modified with 1,8-naphthalimide as sensors for metal cations, Polymer 48 (2007) 6755–6762.
[6] H.N. Kim, Z. Guo, W. Zhu, J. Yoon, H. Tian, Recent progress on polymer-based fluorescent and colorimetric chemosensors, Chem. Soc. Rev. 40 (2011) 79–93.
[7] D. Staneva, I. Grabchev, P. Bosch, Fluorescent hydrogel–textile composite material synthesized by photopolymerization, Int. J. Polym. Mater. Polym. Biomater. 64 (2015) 838–847.
[8] J. Xie, Y.H. Chen, W. Yang, D.M. Xu, K.D. Zhang, Water soluble 1,8-naphthalimide fluorescent pH probes and their application to bioimagings, J. Photochem. Photobiol. A Chem. 223 (2011) 11–118.
[9] J. Qi, D. Liu, X. Liu, S. Guan, F. Shi, H. Chang, H. He, G. Yang, Fluorescent pH sensors for broad-range pH measurement based on a single fluorophore, Anal. Chem. 87 (2015) 5897–5904.
[10] S. Lee, J.H. Lee, T. Pradhan, C.S. Lim, B.R. Cho, S. Bhuniya, S. Kim, J.S. Kim, Fluorescent turn-on Zn^{2+} sensing in aqueous and cellular media, Sens. Actuators B 160 (2011) 1489–1493.
[11] C. Hou, A.M. Urbanec, H. Cao, A rapid Hg^{2+} sensor based on aza-15-crown-5 ether functionalized 1,8-naphthalimide, Tetrahedron Lett. 52 (2011) 4903–4905.
[12] L.P. Duan, Y.F. Xu, X.H. Qian, Highly sensitive and selective Pd^{2+} sensor of naphthalimide derivative based on complexation with alkynes and thio-heterocycle, Chem. Commun. (2008) 6339–6341.
[13] Y. Wang, H.-Q. Chang, W.-N. Wu, X.-J. Mao, X.-L. Zhao, Y. Yang, Z.-Q. Xu, Z.-H. Xu, L. Jia, A highly sensitive and selective colorimetric and off–on fluorescent chemosensor for Cu^{2+} based on rhodamine 6G hydrazide bearing thiosemicarbazide moiety, J. Photochem. Photobiol. A Chem. 335 (2017) 10–15.
[14] Y. Li, L. Cao, H. Tian, Fluoride ion-triggered dual fluorescence switch based on naphthalimides winged zinc porphyrin, J. Org. Chem. 71 (2006) 8279–8282.
[15] J. Jiamg, B. Leng, X. Xiao, P. Zhao, H. Tian, Off-On-Off" fluorescent proton switch synthesized by RAFT polymerization, Polymer 50 (2009) 5681–5684.
[16] I. Grabchev, X. Qian, Y. Xiao, R. Zhang, Novel heterogeneous PET fluorescent sensors selective for transition metal ions or protons: polymers regularly labelled with naphthalimide, New J. Chem. 26 (2002) 920–925.
[17] I. Grabchev, J.-M. Chovelon, New blue fluorescent sensors for metal cations, and protons based on 1,8-naphthalimide, Dyes Pigments 77 (2008) 1–6.
[18] L. Shen, X. Lu, H. Tian, W. Zhu, A long wavelength fluorescent hydrophilic copolymer based on naphthalenediimide as pH sensor with broad linear response range, Macromolecules 44 (2011) 5612–5618.
[19] Y. Tian, F. Su, W. Weber, V. Nandakumar, B.R. Shumway, Y. Jin, X. Zhou, M.R. Holl, R.H. Johnson, D.R. Meldrum, A series of naphthalimide derivatives as intra and extracellular pH sensors, Biomaterials 31 (2010) 7411–7422.
[20] J. Jiang, X. Xiao, P. Zhao, H. Tian, Colorimetric naked-eye recognizable anion sensors synthesized via RAFT polymerization, J. Polym. Sci. Part A Polym. Chem. 48 (2010) 1551–1556.
[21] J. Gan, K. Chen, C.-P. Chang, H. Tian, Luminescent properties and photo-induced electron transfer of naphthalimides with piperazine substituent, Dyes Pigments 57 (2003) 21–28.
[22] S. Zheng, P.L.M. Lynch, T.E. Rice, T.S. Moody, H.Q.N. Gunaratne, A.P. De Silva, Structural effects on the pH-dependent fluorescence of naphthalenic derivatives and consequences for sensing/switching, Photochem. Photobiol. Sci. 11 (2012) 1675–1681.
[23] Ch-G. Niu, G.-M. Zeng, L.-X. Chen, G.-L. Shen, R.-Q. Yu, Proton "off-on" behaviour of methylpiperazinyl derivative of naphthalimide: a pH sensor based on fluorescence enhancement, Analyst 129 (2004) 20–24.
[24] S. Fernández-Alonso, T. Corrales, J.L. Pablos, F. Catalina, Surface modification of poly(ethylene-butyl acrylate) copolymers by microwave methodology and functionalization with 4-dimethylamino-N-(2-hydroxyethyl)-1,8-naphthalimide for acidity sensing, React. Funct. Polym. 107 (2016) 78–86.
[25] B. Redondo-Foj, M. Carsí, P. Ortiz-Serna, M.J. Sanchis, S. Vallejos, F. García, J.M. García, Effect of the Dipole–Dipole interactions in the molecular dynamics of poly(vinylpyrrolidone)-based copolymers, Macromolecules 47 (2014) 5334–5346.
[26] V. Bühler, Polyvinylpyrrolidone Excipients for Pharmaceuticals:Povidone, Crospovidone and Copovidone, Springer, Berlin, 2005.
[27] G.A. Reynolds, K.H. Drexhage, New coumarin dyes with rigidized structure for flashlamp-pumped dye lasers, Opt. Commun. 13 (1975) 222–225.
[28] D.K. Owens, R.C. Wendt, Estimation of the surface free energy of polymers, J. Appl. Polym. Sci. 13 (1969) 1741–1747.
[29] H. Tian, J. Gan, K. Chen, J. He, Q.L. Song, X.Y. Hou, Positive and negative fluorescent imaging induced by naphthalimide polymers, J. Mater. Chem. 12 (2002) 1262–1267.
[30] Y. Tian, B.R. Shumway, A.C. Youngbull, Y. Li, A.K.-Y. Jen, R.H. Johnson, D.R. Meldrum, Dually fluorescent sensing of pH and dissolved oxygen using a membrane made from polymerizable sensing monomers, Sens. Actuators B Chem. 147 (2010) 714–722.
[31] J. Reijenga, A. van Hoof, A. van Loon, B. Teunissen, Review: development of methods for the determination of pKa values, Anal. Chem. Insights 8 (2013) 53–71.

Sensors & Actuators: B. Chemical 270 (2018) 256–262

Contents lists available at ScienceDirect

Sensors and Actuators B: Chemical

journal homepage: www.elsevier.com/locate/snb

A Switchable fluorescence solid sensor for Hg^{2+} detection in aqueous media based on a photocrosslinked membrane functionalized with (benzimidazolyl)methyl-piperazine derivative of 1,8-naphthalimide

S. Fernández-Alonso, T. Corrales, J.L. Pablos, F. Catalina*

Departamento de Química Macromolecular Aplicada, Instituto de Ciencia y Tecnología de Polímeros (CSIC), C/Juan de la Cierva, 3, 28006, Madrid, Spain

ARTICLE INFO

Keywords:
Solid sensor
Hg^{2+} recognition
Turn-on fluorescence
Naphthalimide derivative
Fluorescence probe

ABSTRACT

A Selective fluorescence solid sensor for Hg^{2+} detection in aqueous solution (M-MBZN) has been developed by grafting N-(2-hydroxyethyl)-4-(4-(1H-benzo[d]imidazol-2-yl)methyl) piperazine-1-yl)-1,8-naphthalimide (MBZN) to a photo-crosslinked M-Cl membrane reaction through the acid chloride groups. The resulting fluorescence sensor undergoes fluorescence enhancement upon binding mercuric ions which provokes a photo-induced electron transfer (PET) inhibition process from the piperazine to the naphthalimide moiety. Various photochemical parameters were determined by using pH-dependent absorption and fluorescence spectroscopies as well as the selective detection of Hg^{2+}. The sensing membrane possesses a switchable "turn-on" fluorescence response to Hg^{2+} in pure water; it is easy to use and reusable and shows high selectivity and sensitivity.

1. Introduction

The selective and sensitive detection of low concentrations of Mercury (II) in aqueous media is essential because it is a highly toxic and dangerous heavy metal with a lethal effect on the environment and living organisms [1,2]. Thus, a convenient, rapid, highly sensitive and in-situ detection of Hg^{2+} is highly desirable.

There are several classical mercury quantitative analytical methods for water samples including colorimetry [3], inductively coupled plasma mass spectrometry (ICP-MS) [4], atomic fluorescence spectroscopy (AFS) [5], atomic absorption spectroscopy [6], X-ray absorption spectroscopy [7,8] and electrochemical techniques [9]. Even though these techniques are sensitive, selective, and accurate for Hg^{2+} detection, most of them are time-consuming, require sophisticated instruments and are inappropriate for on-line or field monitoring.

Relative to the mentioned methods, the fluorescence technique has the advantages of higher sensitivity, simplicity and lower cost for the monitoring of metal ions. Chemical sensing of Hg^{2+} with all types of fluorescent probes, via Hg^{2+}-induced changes in fluorescence, has attracted much attention and has become a very active field of research [10]. Fluorescent probes for Hg^{2+} described in the literature are mainly based on the effective quenching of a fluorescence "turn-off" by Hg^{2+} ions [11–13], even though the quenching of the fluorescence signal is not as sensitive as a fluorescence enhancement signal. Therefore, much attention had been paid recently to the development of Hg^{2+} "off-on" fluorescent probes [14–17].

Derivatives of 1,8-naphthalimide have numerous applications in a variety of different areas as fluorescent probes because they have been recognized for excellent photophysical properties with excellent stability, visible excitation and emission exhibiting high fluorescence quantum yields and large Stokes' shift that minimize the effects of the background fluorescence. Among most of the reported naphthalimide derivatives as fluorescent probes for Hg^{2+}, the recognition group was linked to the 4-position of the naphthalene ring [14,17–19]. In this study we designed a sensor MBZN (Fig. 1) by incorporating a (benzimidazolyl)methyl-piperazine substituent in the position 4 of N-(2-hydroxyethyl)-1,8-naphthalimide, in which this benzimidazol structure linked to an piperazine by a methylene spacer is responsible for the specific recognition of Hg^{2+} ions by forming a stable complex structure of the Hg-MBZN that resulted in strong fluorescence in the presence of Hg^{2+}.

The use of polymeric solid supports containing organic structures capable of acting as sensors against the presence of metals [20–22] in the medium are very useful in the applied point of view and, in particular, on-site detection of Hg^{2+} ions. However, only very few sensors for Hg^{2+} based on covalently bonded probes onto the support matrixes have been reported [18,23–26]. In a recent publication [27] we prepared a photo-crosslinked membrane containing acid chloride groups (M-Cl) capable of functionalization with hydroxy derivatives of naphthalimides in a second step. In this work, we designed a novel

* Corresponding author.
E-mail address: fcatalina@ictp.csic.es (F. Catalina).

https://doi.org/10.1016/j.snb.2018.05.030
Received 20 December 2017; Received in revised form 20 April 2018; Accepted 8 May 2018
Available online 09 May 2018

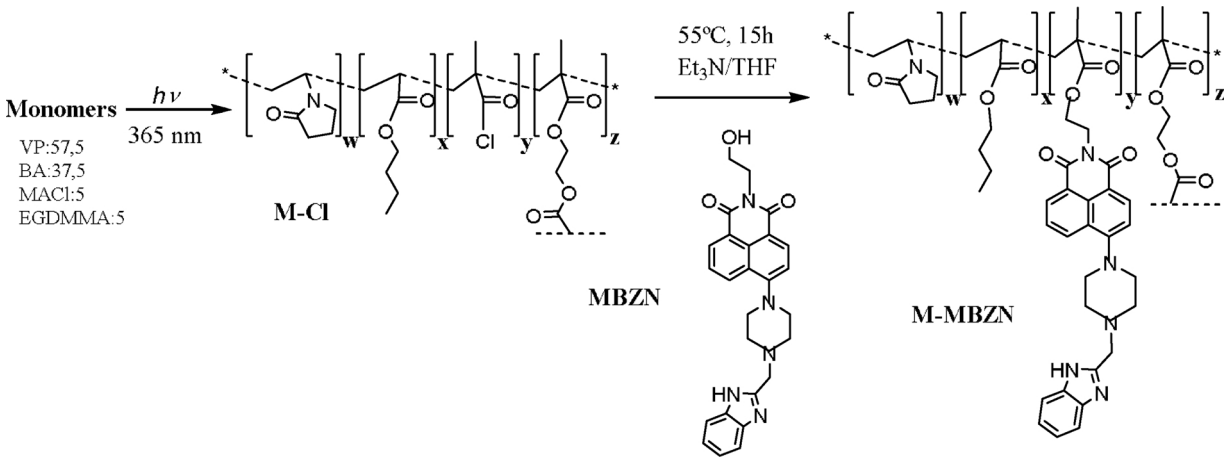

Fig. 1. Synthesis of the photo-crosslinked membrane containing acid chloride groups (M-Cl) and functionalization with N-(2-hydroxyethyl)-4-(4-(1H-benzo[d] imidazol-2-yl)methyl)piperazine-1-yl)-1,8-naphthalimide (M-MBZN).

functionalized membrane (Fig. 1) with the proposed naphthalimide graphed to the structure M-MBZN for one-step fluorescence assay to detect Hg^{2+} ions in environmental water samples.

2. Experimental

2.1. Materials and reagents

All materials and solvents were commercially available and used as received, unless otherwise indicated. The materials included: sodium hydroxide (Panreac, 98–100.5%), hydrochloric acid (VWR Chemicals, 37%), ultrapure MilliQ water (Millipore), 4-bromo-1,8-naphthalic anhydride (Aldrich, 95%), 2-aminoethanol (Aldrich, 99%), 2-(chloromethyl)benzimidazole (Aldrich, 98%), piperazine (Aldrich, 98%), Irgacure 2959 photoinitiator (BASF), triethylamine (Aldrich, ≥99%), coumarin-6 (Aldrich, 98%) and dimethylsulfoxide-D6 (Euriso-top, 99.8%-D). All metal salts and solvents employed in this work were purchased from Aldrich. Also, monomers, 1-vinyl-2-pyrrolidone, butyl acrylate and ethylene glycol dimethacrylate and methacryloyl chloride were supplied by Aldrich and distilled under vacuum prior to use.

2.2. Spectroscopic characterization and thermal analysis

Attenuated Total Reflectance/FT-Infrared Spectroscopy (ATR-FTIR) were obtained using a PERKIN ELMER BX-FTIR Spectrometer coupled with a MIRacle™ATR accessory, from PIKE Technologies.

UV spectroscopy was carried out in a PERKIN ELMER Lambda 35 spectrometer. The assessment of naphthalimide content was made in quintuplicate for each material.

Fluorescence spectroscopy was measured on a Perkin Elmer LS-55 Fluorescence Spectrometer. Fluorescence emission spectra of the probe were recorded by excitation at the isosbestic wavelength of 405 nm (Table 1). All the spectra were corrected using the response curve of the photomultiplier. The fluorescence quantum yields (ϕ_F) were measured relatively to Coumarin 6 (ϕ_F = 0.78 in ethanol) [28].

In the case of the M-MBZN membrane, films were cut into strips of 1 × 4 cm and fixed in a homemade support that can also be slotted into the cell holder of the spectrophotometers. Film strips were immersed in previously prepared vials containing solutions of fixed concentrations of Hg^{2+} or other metal ions (Na^+, K^+, Mg^{2+}, Ca^{2+}, Mn^{2+}, Fe^{3+}, Co^{2+}, Ni^{2+}, Zn^{2+}, Al^{2+}, Pb^{2+}, Ag^+, Cu^{2+}). The UV/Vis and fluorescence spectra for each Hg^{2+} concentration were taken after 20 min of conditioning time in order to obtain a stable fluorescence signal.

Nuclear magnetic resonance, ^{1}H- and ^{13}C NMR spectra were recorded on a Varian-Mercury 400 MHz and a Bruker 300 MHz Nuclear Magnetic Resonance Spectrometers using DMSO-d_6 as the solvent. ^{1}H

Table 1
Parameters determined by UV-VIS absorption and fluorescence spectroscopies[a] related to titration of Hg^{2+} cations and pH-dependence for MBZN naphthalimide in solution and M-MBZN membrane sensor[b].

Parameter	MBZN	M-MBZN
$\lambda_{ABS\text{-}neutral}$[c]	407 nm	407 nm
Log $\varepsilon_{neutral}$[d]	3.98	–
$\lambda_{ABS\text{-}acid}$[c]	390 nm	390 nm
Log ε_{acid}[d]	4.0	–
$\lambda_{Isobestic}$	405 nm	405 nm
$\lambda_{FLU\text{-}neutral}$[e]	535 nm	512 nm
$\lambda_{FLU\text{-}acid}$	530 nm	510 nm
pK_a[f]	5.3	5.3
$\phi_{FLU\text{-}neutral}$[g]	0.01	–
$\phi_{FLU\text{-}acid}$	0.18	–
$\phi_{FLUethanol}$	0.03	water:ethanol (4:1,v/
$\phi_{FLUhexane}$	0.20	v) ≪ Ethanol ≪ hexane
pK_a^*[e]	5.0	4.8
$\Delta\nu$[h]	6000	5160
Hg^{2+}: Working range of pH	–	5.5–8.0
Hg^{2+}: LOD- Detect. limit (M)[i]	7.3×10^{-8}	2.5×10^{-6}
Hg^{2+}: FE[j]	6	3
Hg^{2+}: response time (membrane thickness μm)[k]	–	10 min (40 μm); 18 min (80 μm); 25 min (180 μm)

[a] Measured at 10^{-5} M in water-ethanol (4:1, v/v) unless specifically stated otherwise.

[b] Membrane thickness 80 μm and content of MBZN:1.6×10^{-4} M.

[c] The subscripts "acid" and "neutral" refer to the limiting value of a given parameter in strong acid (pH = 2.0) or neutral (pH = 7.0) media, respectively.

[d] ε, molar absorptivity in $M^{-1}\,cm^{-1}$.

[e] Fluorescence emission spectra were obtained by excitation at $\lambda_{Isobestic}$ = 405 nm.

[f] Obtained [31] by analyzing the pH dependence of the absorbance (A) or emission intensity (I) at a given wavelength according to the equation $\log[(A_{acid} - A)/(A - A_{base})] = pH - pK_a$ or $\log[(I_{FLU\text{-}acid} - I)/(I - I_{FLU\text{-}base})] = pH - pK_a^*$.

[g] Relatively to Coumarin 6 (ϕ_F = 0.78 in ethanol).

[h] Stokes shift (ν_{FLU}-ν_{ABS}) in frequency (cm^{-1}).

[i] LOD = 3SD/s, where SD is the standard deviation of 10 measurements of the blank sample and s is the slope of the calibration curve in the region of low analyte content.

[j] Hg^{2+}-induced fluorescence enhancement of naphthalimide, factor $FE = A_{FLU\text{-}Hg(max.)}/A_{FLUabsenceHg}$.

[k] Data from Fig. 6B.

NMR and ^{13}C NMR chemical shifts were referenced to DMSO-d_6 (2.5 and 39.52 ppm, respectively) as standard.

Mass Spectra (MS) were recorded under electron impact (EI) condition on a HP 5973-MSD spectrometer.

Thermogravimetric Analysis (TGA) was carried out in a TGA Q-500 TA Instruments coupled to a Pfeiffer Vacuum ThermoStar™ mass spectrometer.

Elemental analysis (EA) was carried out on a Carlo Erba EA1108 elemental analyzer (% of C, H, N).

2.3. Swelling ratio and pH measurements

Swelling degree (SD) in water and THF of the crosslinked membranes were measured by immersing dried and weighed sample films (W_d) into deionized water or THF at 30 °C for 24 h. The SD were calculated as follows: SD (%) = $((W_s–W_d)/W_d) \times 100$, where W_s and W_d are the weight of the swollen and dry sample, respectively.

The pH of the solutions were measured with a Mettler Toledo SevenGo Duo Pro meter coupled with an InLab Expert Pro ISM-ID67 electrode at room temperature (23 °C) and previously calibrated with standard buffers.

2.4. Microwave and UV irradiation equipment

The microwave equipment used in this work was an Anton Paar Monowave™ 300 microwave synthesis reactor provided with an infrared sensor (IR pyrometer). All reactions were performed in pressure-resistant 30-mL test tubes sealed with silicon septum and using a magnetic stirring bar.

The photopolymerization reactions were carried out in a Biolink™ BLX-365 type Bio-link apparatus (Vilbert Lourmat™).

2.5. Synthesis

The synthesis procedure for the fluorescence probe N-(2-hydroxyethyl)-4-(4-(1H-benzo[d]imidazol-2-yl)methyl)piperazine-1-yl)-1,8-naphthalimide (MBZN) is shown in Fig. 2.

Synthesis of N-(2-hydroxyethyl)-4-(4-(1H-benzo[d]imidazol-2-yl) methyl) piperazine-1-yl)-1,8-naphthalimide (MBZN)

Compound 2 and 3 were synthesized from 4-bromo-1,8-naphthalic anhydride (compound 1) following the procedures (Fig. 2) described previously in the bibliography [24,29]. MBZN was synthetized in a pressure-resistant microwave test tube where compound 3 (0.20 g, 0.624 mmol), 2-(chloromethyl)benzimidazole (0.104 g, 0.624 mmol) and triethylamine (88 µL, 0.624 mmol) were mixed in 2-methoxyethanol (10 mL) and heated at 130 °C in argon atmosphere under stirring (600 rpm) for 1 h. The mixture was poured into diethyl ether and the unreacted precipitated product was filtered. The solvent was evaporated under reduced pressure, and 200 mL of water was added. The mixture was stirred 15 min and the residue filtered and identified as the desired product. Yield: 66%. M.p.: 152.60 ± 2 °C. ^1H NMR (400 MHz, DMSO-d_6) δ 12.37 (s, 1H), 8.44 (d, J = 7.3 Hz, 1H), 8.41 (d, J = 8.5 Hz, 1H), 8.37 (d, J = 8.1 Hz, 1H), 7.78 (t, J = 7.9 Hz, 1H), 7.58 (d, J = 7.4 Hz, 1H), 7.47 (d, J = 7.4 Hz, 1H), 7.32 (d, J = 8.2 Hz, 1H), 7.15 (t, J = 7.7 Hz, 2H), 4.79 (s, 1H), 4.13 (t, J = 6.5 Hz, 2H), 3.89 (s, 2H), 3.67–3.56 (m, 2H), 3.27 (s, 4H), 2.82 (s, 4H). ^{13}C NMR (101 MHz, DMSO) δ: 163.65, 163.12, 155.48, 151.47, 143.07, 134.39, 132.07, 130.54, 130.39, 129.13, 125.98, 125.24, 122.65, 121.82, 121.00, 118.54, 115.70, 114.95, 111.20, 57.85, 55.57, 52.74, 52.57, 41.62. FT-IR (wavenumbers, cm^{-1}): ν_{NH},ν_{OH} 3255 cm^{-1}; ν_{C-H} 2949, 2823 cm^{-1} aromatic stretch vibration; $\nu_{C=O}$ 1691, 1644 cm^{-1}; $\nu_{N-C=O}$ 1614 cm^{-1}; ν_{C-C} 1586 cm^{-1} aromatic ring chain vibrations; ν_{NH} 1514 cm^{-1} flexion. EA: theoretical values: %C 68.56; %H 5.53; %N 15.37; experimental values: %C 68.36; %H 5.59; %N 15.29. EI-MS m/z calculated for $C_{26}H_{25}N_5O_3$: (M + H^+) 456.2; found 456.2 (M^+).

2.6. Membrane preparation by photopolymerization (M-Cl) and functionalization with N-(2-hydroxyethyl)-4-(4-(1H-benzo[d]imidazol-2-yl)methyl)piperazine-1-yl)-1,8-naphthalimide (M-MBZN)

As shown in Fig. 1, a crosslinked membrane (M-Cl) was obtained in a first step by the bulk photopolymerization of a mixture of monomers: N-vinylpyrrolidone (VP), butyl acrylate (BA), ethylene glycol dimethacrylate (EGDMMA) as the crosslinking agent and methacryloyl chloride (MACl) as the reactive monomer following the procedure described in a recent publication [24]. In this work, the monomer molar ratio of the feed mixture was VP:57.5/BA:37.5/MACl:5/EGDMMA:5 and the photoinitiator (Irgacure 2959) was added to the mixture at 1% (w/w). After 40 min of irradiation at 365 nm (dose 20 J cm^{-2}), the transparent crosslinked membrane was demoulded, conditioned (12 h) at room temperature under argon atmosphere, washed several times with ethanol and dried under vacuum at 40 °C to remove the un-reacted monomers. The presence of acid chloride was confirmed by ATR-FTIR (wavenumbers, cm^{-1}), $\nu_{C=O}$ acyl chloride 1795 cm^{-1}; ν_{C-Cl} 898 cm^{-1} together with the characteristic co-monomers bands of VP $\nu_{C=O}$ lactam, amide-I 1675 cm^{-1} and BA, $\nu_{C=O}$ ester 1725 cm^{-1}; ν_{C-O} (O−CH_2-) ester 1161 cm^{-1}. The quantitative determination of chlorine in the M-Cl membrane was carried out by TGA-MS. A content of 1.4% was determined by MS analysis of evolved gas at 175 °C as chlorine (EI-MS m/z: 36 (Cl)), as it is shown in Fig. S1, (Supporting Information).

In a second step [24], the M-Cl film was cut into strips (1 × 4 cm) and functionalized in heterogeneous phase with MBZN (Fig. 1). The M-Cl membrane was placed in an ace round-bottom pressure flask with 20 mL of THF. 10 mg of MBZN were added under argon atmosphere. The mixture was heated at 55 °C for 15 h. After this reaction time, the corresponding modified membrane (M-MBZN) was washed with cold

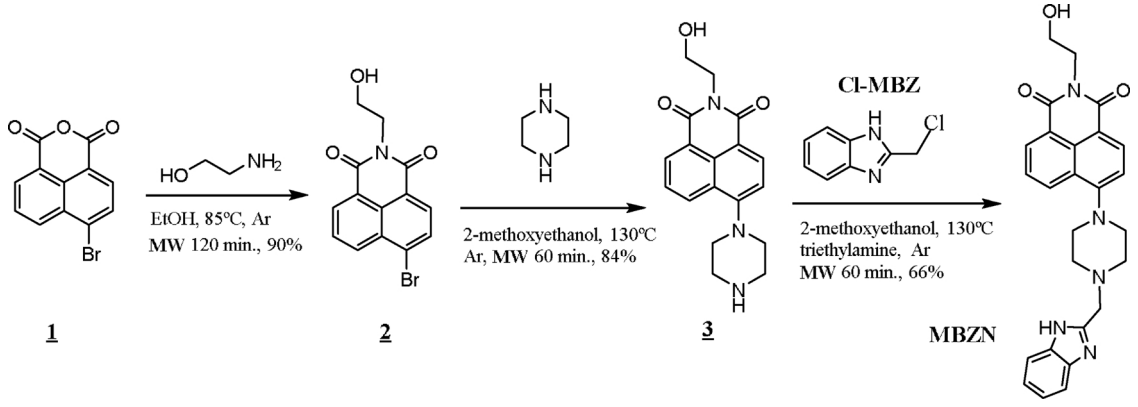

Fig. 2. Reaction pathway for the microwave (MW) synthesis of N-(2-hydroxyethyl)-4-(4-(1H-benzo[d]imidazol-2-yl)methyl) piperazine-1-yl)-1,8-naphthalimide (**MBZN**).

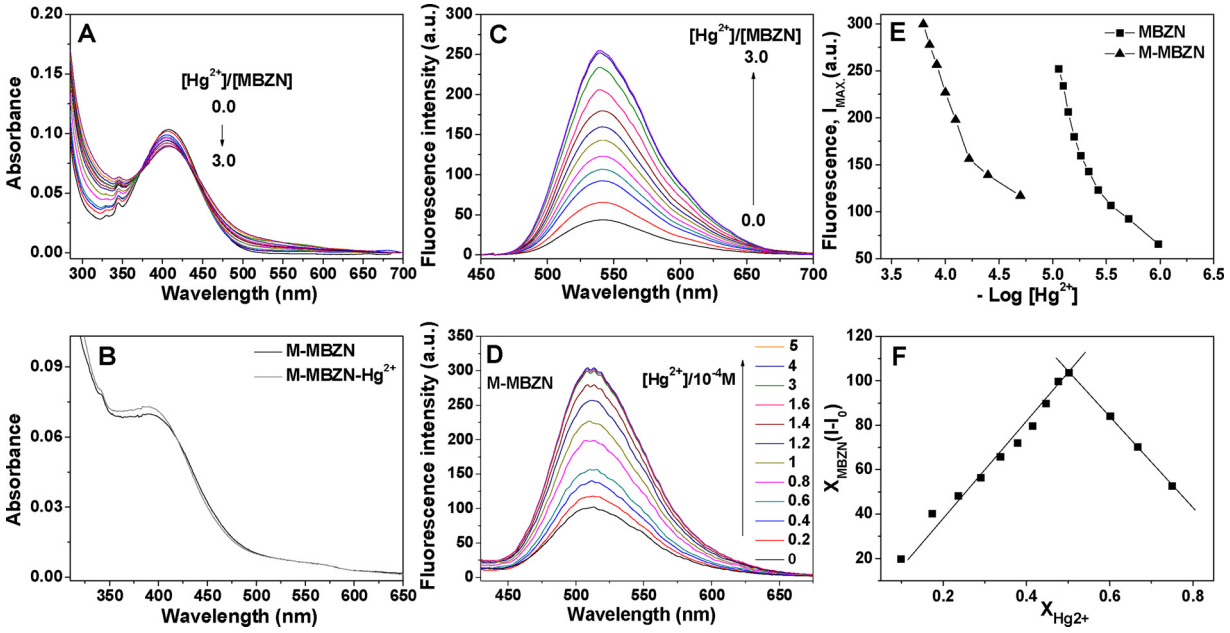

Fig. 3. Absorption and fluorescence spectra of MBZN (A,C) at a concentration of 10^{-5} M in water:ethanol 4:1 (v/v) and M-MBZN (B,D) containing 1.6×10^{-4}M of bonded naphthalimide in buffered water (pH = 7.0) in the presence of increasing concentrations of Hg^{2+} 0–3 equiv. (E) Fluorescence emission intensity change with $-\log[Hg^{2+}]$. (F) Jobs plot showing the stoichiometry of MBZN-Hg complex in buffered water.

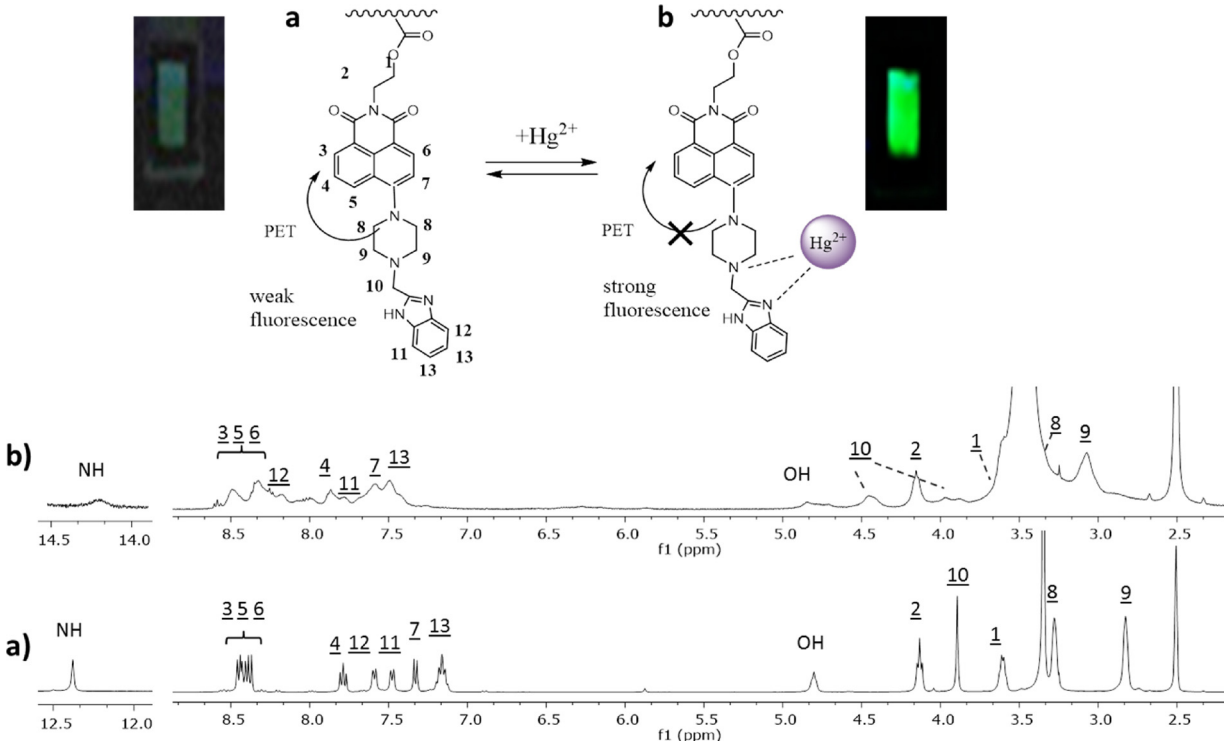

Fig. 4. Proposed reversible binding mode with Hg^{2+} together with partial ^{1}H NMR of MBZN in DMSO at 25 °C: (a) in the absence and (b) after addition of 1 equiv. of Hg^{2+}.

ethanol and with water thrice in order to remove the unreacted acid chloride groups and the unreacted naphthalimide. The hydrolysis reaction of unreacted acid chloride groups was confirmed by ATR-FTIR and by TGA-MS by the disappearance of the characteristic peaks of acid chloride (Fig. S1). The content of naphthalimide was quantitatively determined by UV–vis spectroscopy.

3. Results and discussion

3.1. Synthesis of MBZN, preparation of M-MBZN membrane and characterization

The synthetic route to obtain N-(2-hydroxyethyl)-4-(4-(1H-benzo[d] imidazol-2-yl)methyl)piperazine-1-yl)-1,8-naphthalimide (M-MBZN) is shown in Fig. 2. Compounds 2 and 3 were formed in 90% and 64%

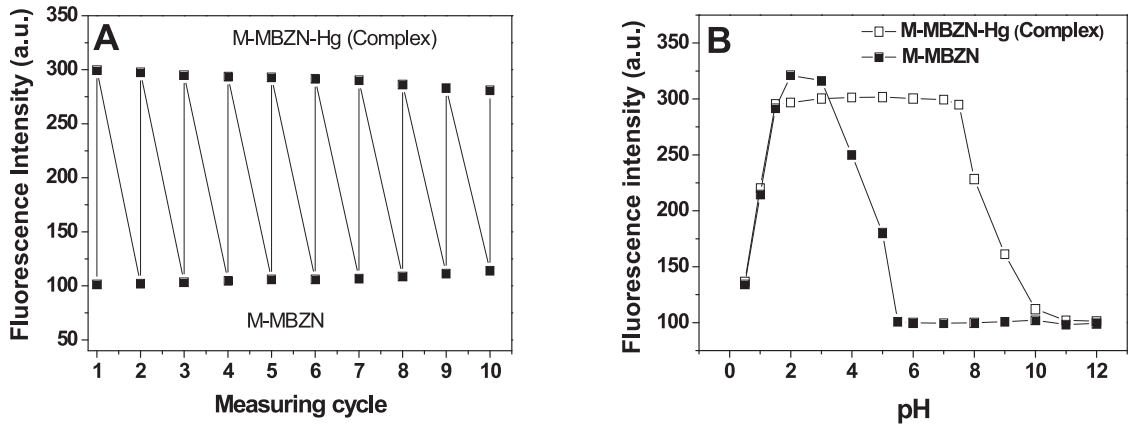

Fig. 5. (A) Reversibility for the M-MBZN membrane sensor. (B) pH-effect on the fluorescence intensity of M-MBZN and M-MBZN-Hg complex in water.

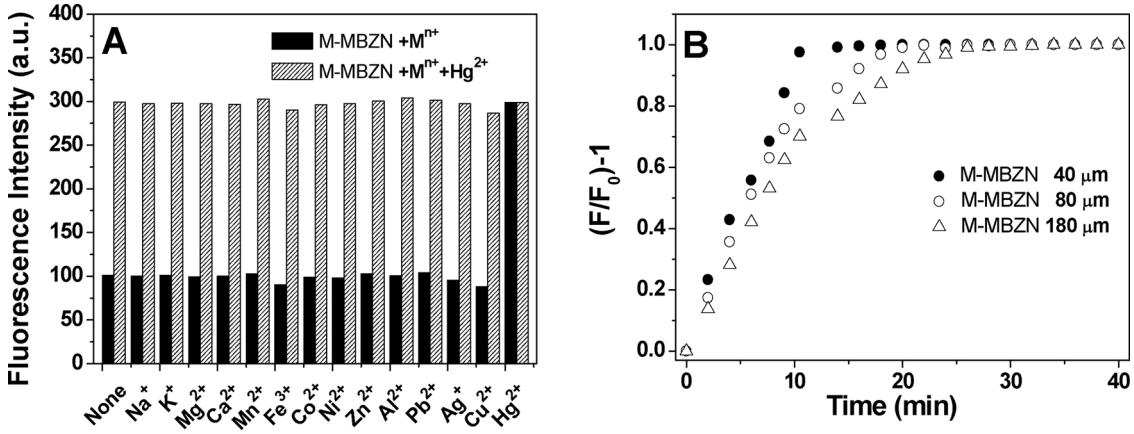

Fig. 6. Metal ion selectivity of the M-MBZN membrane (A) containing 1.6×10^{-4}M of bonded MBZN. (B) Time response for the fluorescence emission to Hg^{2+} for M-MBZN membranes of different thickness. F_0 and F are the fluorescence intensities in the absence of Hg^{2+} and that after the addition of 1 equiv. of Hg^{2+}, respectively.

yields in 2 and 1 h, respectively, using literature procedures [18,27,29] modified to carry out the reactions under microwave radiation from the 4-bromo-1,8-naphthalic anhydride (1). Compound 3 was then reacted under MW with 2-(chloromethyl)benzimidazole in basic medium in the presence of triethylamine at 130 °C as described before (see Experimental section 2.5). After 60 min of reaction time under MW, MBZN as a yellow precipitate was obtained in 66% yield. An acrylic membrane containing acid chloride functionalities (M-Cl) was obtained by photopolymerization as described previously [24] by thorough mixing of the hydrophilic monomer VP (57.5%) with the hydrophobic nature of BA (37.5%) and adding MACl (5%) as the reactive monomer for functionalization. After the bulk photopolymerization (conversion > 98%), a reversible water-swollen crosslinked acrylic membrane was produced (Fig. 1) with a 1.4% of chlorine content in the structure as expected by the composition feed and confirmed by TGA-MS (Fig. S1, Supplementary data). Finally, the M-Cl membrane was successfully functionalized [24] with the naphthalimide derivative MBZN (Fig. 1) by conventional heating in THF at 55 °C for 15 h. The amount of naphthalimide bonded to the M-MBZN membrane was determined spectrophotometrically (1.6×10^{-4} M) at the peak maximum of the absorption band (407 nm) and using the absorption coefficient of MBZN in water:ethanol (4:1 w/w) ($\varepsilon_{407} = 9.55 \times 10^3\,mol^{-1}l\,cm^{-1}$) previously calculated (Table 1).

The thermal stability of the M-Cl and M-MBZN membranes were evaluated using TGA and Table S1 (Supplementary data) shows characteristic weight loss temperatures (T_5 and T_{10}, respectively). For both membranes two peaks were observed (Fig. S1). The highest weight loss rate that was observed at 411 °C corresponds to the degradation of acrylic components of the membrane and the second one observed at 438 °C has been attributed [30] to the lactam subgroup degradation.

Also, the degree of swelling in water of both membranes (Table S1) was approx. SD = 31% confirming the hydrophilic character of the membranes and the adequate swelling for solid sensors in water. The SD value of the M-MBZN in THF (61.5%) is higher than that of the M-Cl membrane (47.1%) indicating the strong influence of the naphthalimide derivative in the SD in organic solvents, even at this low naphthalimide content in the membrane.

The cross-linked hydrophilic membrane M-MBZN obtained in this work was capable of swelling or de-swelling reversibly in water and retaining a controlled and reproducible volume of liquid in the swollen state. This behaviour, as will be seen in the next section, allowed controllable responses to external concentrations of Hg^{2+} cations.

3.2. Spectroscopic characteristics of MBZN and M-MBZN. Effect of pH

Table 1 presents the spectral characteristics of MBZN and the corresponding functionalized membrane M-MBZN in water-ethanol (4:1, v/v) such as, absorption (λ_{ABS}) and fluorescence (λ_{FLU}) maxima in acid (pH = 2.0) and neutral media (pH = 7.0), the corresponding absorption coefficient (logε), Stokes shift ($\Delta\nu$), and quantum yields of fluorescence (ϕ_{FLU}).

The spectral characteristic of MBZN and M-MBZN displayed similar pH-dependence in all the studied media as can be seen from the values listed in Table 1. The low fluorescence emission of MBZN and M-MBZN in all the studied solvents can be attributed to an efficient PET process (Fig. 3) that takes place between the photoexcited 1,8-naphthalimide and the lone-pair electrons of the nitrogen of the piperazine substituent.

The pKa values of MBZN and the functionalized membrane M-MBZN were calculated [31] from the curves of absorption changes (Fig.S2) in

the presence of increasing pH from 2.0 to 12.0. The protonation of the benzimidazole structure of MBZN (pK_a = 5.3) takes place at a lower pH than the 2-methyl benzimidazole structure [32], pK_a = 6.1, allowing the use of this structure as a sensor for Hg^{2+} cations in neutral of basic water media as we will see in the next section.

3.3. Sensitivity of MBZN and M-MBZN in Hg^{2+} sensing

Fig. 3 shows the absorption and fluorescence spectra of the MBZN (water:ethanol 4:1,v/v) (A and C) and M-MBZN (B and D) in buffered water (pH = 7.0) upon addition of different concentrations of Hg^{2+}. With the increase of Hg^{2+} concentration, the relative fluorescence intensities were drastically enhanced caused by Hg^{2+} interaction and the formation of a MBZN-Hg complex, which constituted the basis for the determination of Hg^{2+} concentrations with the MBZN-sensor.

The comparative increase of fluorescence for MBZN and the membrane M-MBZN is shown in Fig. 3E. The binding stoichiometry 1:1 for the MBZN-Hg complex was confirmed by the Jobs plot shown in Fig. 3F in which the maximum fluorescence signal was observed at the Hg^{2+} mole fraction value of 0.5.

The association constants K_a of the MBZN-Hg and M-MBZN-Hg complexes were then calculated to be 9657 M^{-1} and 3627 M^{-1}, respectively, by the ratio intercept/slope (Fig.S3) of the corresponding linear relationship by Benesi–Hildebrand [33] equation Eq. (1).

$$\frac{1}{F-F_0} = \frac{1}{K_a(F_{max} - F_0)[Hg^{2+}]} + \frac{1}{F_{max}-F_0} \quad (1)$$

where F_{max}, F, and F_0 are fluorescence intensities of MBZN or M-MBZN in the presence of Hg^{2+} at saturation, any intermediate Hg^{2+} concentration, and free sensor, respectively.

The limit of detection (LOD) was calculated by the following equation: LOD = 3 × SD/s, where SD is the standard deviation of 10 measurements of the blank and s is the slope of plot of fluorescence intensity as a function of the Hg^{2+} concentrations in the region of low analyte content. The calculated values of LOD are shown in Table 1, 7.3×10^{-8}M and 2.5×10^{-6}M for MBZN and M-MBZN, respectively. Compared with the previously reported values of Hg^{2+}-fluorescence sensors, the LOD of M-MBZN membrane presented here is lower or in the same range [18,14].

3.4. Binding mode MBZN with Hg^{2+} ion, reversibility and pH stability of the MBZN-Hg complex

NMR studies provided direct evidence of MBZN-Hg interactions. As shown in Fig. 4, ^{1}H NMR spectra show the displacement of the (benzimidazolyl)methyl-piperazine protons Fig. 4(a) in the presence of Hg^{2+}, Fig. 4(b): the protons of the methylene bridge from 3.89 (2H-10) ppm to 4.45 (1H-10) and 3.96 (1H-10) and the protons of the piperazine from 2.82 (4H-9) to 3.07 (4H-9). Also, the Hg^{2+} complexation induced an increase of the electron density of the benzimidazolyl group resulting a downfield shift of the aromatic H-11, H-12 and H-13 protons. The NH peak of the benzimidazole ring also was displaced from 12.37 ppm to 14.21 in the complex.

The reversibility of the Hg^{2+} induced fluorescence signal of the M-MBZN membrane was evaluated by alternating its immersion in solutions of blank buffered solution (pH=7.0) until the fluorescence intensity of the membrane reached again the original low value prior to the next measurement and water buffered Hg^{2+} solution. Previously to each cycle the membrane should be washed with HCl solution (pH= 1.0) since the reversibility is probably caused by the protonation of the piperazine of the MBZN structure resulting in the release of the Hg^{2+} at higher acidity. Ten successive cycles were carried out as it is shown in Fig. 5A for the membrane sensor.

As shown in Fig. 5(B), the MBZN-Hg complex produced in the membrane sensor exhibits stability of the fluorescence emission in the range of pH 2.0–7.5. The decrease in fluorescence emission upon pH values higher than 7.5 might be attributed to the formation of Hg(OH) [34] and the rapid decrease at pH values lower than 2.0, due to the destruction of the Hg^{2+} complex by the protonation of the piperazine. These results show that the M-MBZN membrane is a fully reversible sensor for the detection of Hg2+ in water which is adequate for real environmental applications and biological samples [35].

3.5. Selectivity of M-MBZN membrane sensor to Hg^{2+} with various cations and time response to detection

To investigate the selectivity of the sensor towards Hg^{2+} ions, the fluorescence of M-MBZN (with a bonded content of MBZN of 1.6×10^{-4}M) and 1 equiv. of other metal ions were studied (Fig. 6A). The competition experiments show no significant variation in the fluorescence emission at 512 nm confirming the excellent selectivity of the membrane sensor.

Fig. 6. Fluorescence analysis indicated that the recognition interaction between MBZN and Hg^{2+} was accomplished immediately by simply shaking for a few seconds. In contrast, the M-MBZN membrane sensor exhibits a time response which is dependent upon the metal ion permeability into the photo-crosslinked material and their thickness. To see the influence of the membrane thickness in the time response to the Hg^{2+} of the M-MBZN membrane sensor (Fig. 6B), we prepared another two membranes under the same experimental conditions but with 40 and 180 μm of thickness.

4. Conclusions

The novel water-swollen photo-crosslinked membrane sensor M-MBZN with pendant highly Hg^{2+}-selective “turn-on” 1,8-naphthalimide-type probe MBZN was developed and based on a specific Hg^{2+}-interaction with the (benzimidazolyl)methyl-piperazine substituent in the 4-position. The membrane sensor exhibited a 3fold increase in fluorescence intensity towards Hg^{2+} ions over other metal ions in pure water solution over a wide pH range. Also, M-MBZN shows a reversible behaviour which is an important feature for many applications. The new solid sensor reported here meets the requirements of fluorescence detection of Hg^{2+} ions and offers great potential for the further fabrication of an economical on-site tool for the detection of Hg^{2+} in aqueous environments.

Acknowledgement

This study was supported by MINECO (Project Ref. MAT2017-88923). S. Fernández- Alonso thanks MINECO for a pre-doctoral fellowship linked to the project.

Appendix A. Supplementary data

Supplementary data associated with this article can be found, in the online version, at https://doi.org/10.1016/j.snb.2018.05.030.

References

[1] D.W. Boening, Ecological effects, transport, and fate of mercury: a general review, Chemosphere 40 (2000) 1335–1351.
[2] X. Niu, Y. Ding, C. Chen, H. Zhao, M.A. Lan, A novel electrochemical biosensor for Hg^{2+} determination based on Hg^{2+}-induced DNA hybridization, Sens. Actuators B: Chem. 158 (2011) 383–387.
[3] Z. Yan, M.-F. Yuen, L. Hu, P. Sun, Ch-S. Lee, Advances for the colorimetric detection of Hg^{2+} in aqueous solution, RSC Adv. 4 (2014) 48373–48388.
[4] H. Louie, C. Wong, Y.J. Huang, S. Fredrickson, A study of techniques for the preservation of mercury and other trace elements in water for analysis by inductively coupled plasma mass spectrometry (ICP-MS), Anal. Methods 4 (2012) 522–529.
[5] Y.W. Chen, J. Tong, A. D'Ulivo, N. Belzile, Determination of mercury by continuous flow cold vapor atomic fluorescence spectrometry using micromolar concentration of sodium tetrahydroborate as reductant solution, Analyst 127 (2002) 1541–1546.
[6] L.B. Escudero, R.A. Olsina, R.G. Wuilloud, Polymer-supported ionic liquid solid phase extraction for trace inorganic and organic mercury determination in water

samples by flow injection-cold vapor atomic absorption spectrometry, Talanta 116 (2013) 133–140.
[7] G.N. George, S.P. Singh, G.J. Myers, G.E. Watson, I.J. Pickering, The chemical forms of mercury in human hair: a study using X-ray absorption spectroscopy, J. Biol. Inorg. Chem. 15 (2010) 709–715.
[8] A. Bernaus, X. Gaona, J.M. Esbrí, P. Higueras, G. Falkenberg, M. Valiente, Microprobe techniques for speciation analysis and geochemical characterization of mine environments: the mercury district of Almadén in Spain, Environ. Sci. Technol. 40 (2006) 4090–4095.
[9] R.S. N'Dri, M. Coulibaly, A.N. Yao, D. Bamba, E.G. Zoro, An electrochemical method for the determination of trace mercury(II) by formation of complexes with Indigo Carmine food dye and its analytical application, Int. J. Electrochem. Sci. 11 (2016) 5342–5350.
[10] M. Saleem, M. Rafiq, M. Hanif, Organic material based fluorescent sensor for Hg^{2+}: a brief review on recent development, J. Fluoresc. 27 (2017) 31–58.
[11] F. Yan, Y. Zou, M. Wang, Highly photoluminescent carbon dots-based fluorescent chemosensors for sensitive and selective detection of mercury ions and application of imaging in living cells, Sens. Actuators B 192 (2014) 488–495.
[12] H. Tan, Y. Zhang, Y. Chen, Detection of mercury ions (Hg^{2+}) in urine using a terbium chelate fluorescent probe, Sens. Actuators B: Chem. 156 (2011) 120–125.
[13] O. García-Beltrán, N. Mena, T.A. Berríos, E.A. Castro, B.K. Cassels, M.T. Núñez, M.E. Aliaga, A selective fluorescent probe for the detection of mercury (II) in aqueous media and its applications in living cells, Tetrahedron Lett. 53 (2012) 6598–6601.
[14] Z. Zhang, S. Lu, C. Sha, D. Xu, A single thiourea-appended 1,8-naphthalimide chemosensor for three heavy metal ions: fe^{3+} Pb^{2+}, and Hg^{2+}, Sens. Actuators B: Chem. 208 (2015) 258–266.
[15] M. Tian, L. Liu, Y. Li, R. Hu, T. Liu, H. Liu, S. Wang, Y. Li, An unusual off-on fluorescence sensor for detecting mercury ions in aqueous media and living cells, Chem. Commun. 50 (2014) 2055–2057.
[16] L. Tanga, S. Dinga, X. Zhang, K. Zhonga, S. Houa, Y. Biana, A 2-(2(-hydroxyphenyl) quinazolin-4(3H)-one derived fluorescence 'turn on' probe for recognition of Hg^{2+} in water solution and its live cell imaging, J. Photochem. Photobiol. A: Chem. 340 (2017) 15–20.
[17] F. Lv, Y. Chen, T. Tang, Y. Chen, D. Xu, A new reactive 1,8-naphthalimide derivative for highly selective and sensitive setection of Hg2+, J. Fluoresc. 27 (2017) 1285–1292.
[18] X.-F. Wu, Q.-J. Ma, X.-J. Wei, Y.-M. Hou, X. Zhu, A selective fluorescent sensor for Hg^{2+} based on covalently immobilized naphthalimide derivative, Sens. Actuators B: Chem. 183 (2013) 565–573.
[19] Y. Li, Z. Qing, Y. Yu, T. Liu, R. Jiang, Y. Li, Synthesis and self-assembly of dihydroxyperylene bisimides for the tuning of photophysical properties, Chem. Asian J. 7 (2012) 1934–1939.
[20] I. Grabchev, J.-M. Chovelon, New blue fluorescent sensors for metal cations, and protons based on 1 8-naphthalimide, Dyes Pig. 77 (2008) 1–6.
[21] I. Grabchev, S. Yordanova, P. Bosch, E. Vasileva-Tonkova, R. Kukeva, S. Stoyanov, R. Stoyanova, Structural characterization of 1,8-naphthalimides and *in vitro* microbiological activity of their Cu(II) and Zn(II) complexes, J. Mol. Struct. 1130 (2017) 974–983.
[22] M.S. Makki, D. Staneva, T.R. Sobahi, P. Bosch, R.M. Abdel-Rahman, I. Grabchev, Design and synthesis of a new fluorescent tripod for chemosensor applications, Tetrahedron 70 (2014) 9366–9372.
[23] M. Zhu, C. Zhou, Y. Zhao, Y. Li, H. Liu, Y. Li, Synthesis of a fluorescent polymer bearing covalently linked thienylene moieties and rhodamine for efficient sensing, Macromol. Rapid Commun. 30 (2009) 1339–1344.
[24] Y. Li, T. Liu, H. Liu, M.-Z. Tian, Y. Li, Self-a ssembly of intramolecular charge-transfer compounds into functional molecular systems, Acc. Chem. Res. 47 (2014) 1186–1198.
[25] O. Güney, F. Cebeci, Molecularly imprinted fluorescent polymers as chemosensors for the detection of mercury Ions in aqueous media, J. Appl. Polym. Sci. 117 (2010) 2373–2379.
[26] X.R. Guo, B. Li, L.M. Zhang, Y.H. Wang, Selective fluorescent chemosensor for detecting Hg(II) in water based on pyrene functionalized core-shell structured mesoporous silica, J. Luminesc. 132 (2012) 1729–1734.
[27] S. Fernández-Alonso, T. Corrales, J.L. Pablos, F. Catalina, Solid fluorescence sensors obtained by functionalization of photocrosslinked water-swollen acrylic membranes with 4-piperazine naphthalimide derivatives, Polymer 124 (2017) 139–150.
[28] G.A. Reynolds, K.H. Drexhage, New coumarin dyes with rigidized structure for flashlamp-pumped dye lasers, Opt. Commun. 13 (1975) 222–225.
[29] Y.Q. Tian, B.R. Shumway, C. Youngbull, A.K.Y. Jen, R.H. Johnson, D.R. Meldrum, Dually fluorescent sensing of pH and dissolved oxygen using a membrane made from polymerizable sensing monomers, Sens. Actuators B: Chem. 147 (2010) 714–722.
[30] B. Redondo-Foj, M. Carsí, P. Ortiz-Serna, M.J. Sanchis, S. Vallejos, F. García, J.M. García, Effect of the Dipole-Dipole interactions in the molecular dynamics of poly(vinylpyrrolidone)-based copolymers, Macromolecules 47 (2014) 5334–5346.
[31] J. Reijenga, A. van Hoof, A. van Loon, B. Teunissen, Review: development of methods for the determination of pK_a values, Anal. Chem. Insights 8 (2013) 53–71.
[32] T.C. Bruice, G.L. Schmir, Imidazole catalysis. II. The reaction of substituted imidazoles with phenyl acetates in aqueous solution, J. Am. Chem. Soc. 80 (1958) 148–155.
[33] H.A. Benesi, J.H. Hildebrand, A spectrophotometric investigation of the interaction of iodine with aromatic hydrocarbons, J. Am. Chem. Soc. 71 (1949) 2703–2707.
[34] Z.X. Han, X.B. Zhang, Z. Li, G.J. Mao, Z. Jin, G.L. Shen, R.Q. Yu, X.Y. Wu, A highly sensitive quinoline-containing rhodamine-B thiohydrazide based fluorescent probe for Hg2+ in aqueous solution and living cells, Anal. Lett. 43 (2010) 2751–2761.
[35] J. Luo, S.S. Jiang, S.H. Qin, H.Q. Wu, Y. Wang, J.Q. Jiang, X.X. Liu, Highly sensitive and selective turn-on fluorescent chemosensor for Hg^{2+} in pure water based on a rhodamine containing water-soluble copolymer, Sens. Actuators B: Chem. 160 (2011) 1191–1197.

Sabela Fernández-Alonso received her MSc. in Environmental Chemistry from A Coruña University, Spain, in 2013. She is currently a predoctoral fellow at Applied Macromolecular Chemistry Department of the Institute of Polymer Science and Technology, CSIC, Spain.H er research interest is focused on developing functionalized polymers with fluorescence sensors.

Teresa Corrales received her PhD in Chemistry from University Complutense of Madrid, Spain in 1994. Currently, she is Tenured Scientist at Polymer Institute (CSIC), Spain. Her research activities are focused on the design or surface modification of functional polymers for environmental preservation, with a background in polymer degradation and stability, development of fluorescent sensor for detection of pollutants, and technologies considered environmental-friendly as photopolymerization, Microwave irradiation and Plasma treatment

Jesus L. Pablos received his PhD from Autonoma University of Madrid (UAM) in 2012, based on studies of photodegradation and biodegradation on polyethylene mulching films. Currently, he is a Postdoctoral researcher at Department of Macromolecular Chemistry (Photochemistry Group) in CSIC (ICTP). His research area includes the development of new functional fluorescent polymers as sensors of analytes of interest, synthesis of new polyelectrolytes based on ionic liquids and achievement of new biodegradable materials.

Fernando Catalina received his Ph.D. in Organic Chemistry from Complutense University of Madrid, Spain in 1984. Currently, he is Professor in Polymer Science at Department of Applied Macromolecular Chemistry, Institute of Polymer Science and Technology, CSIC in Madrid. His research area includes different topics related to Polymer Photochemistry and environmental applications.